"Pathology of Ectopic Calcification in Fetuin-A Deficient Mice: Compensatory Gene Regulation and Mineralized Matrix Metabolism"

Von der Fakultät für Mathematik, Informatik und Naturwissenschaften der
RWTH Aachen University zur Erlangung des akademischen Grades
einer Doktorin der Naturwissenschaften genehmigte Dissertation

vorgelegt von

Diplom-Biologin Marietta Herrmann
aus Berlin

Berichter: Universitätsprofessor Dr. rer. nat. Willi Jahnen-Dechent
              Universitätsprofessor Dr. rer. nat. Johannes Bohrmann

Tag der mündlichen Prüfung: 9.03.2012

Diese Dissertation ist auf den Internetseiten der Hochschulbibliothek online verfügbar.

Table of Contents

Summary

Fetuin-A is a liver-derived plasma protein involved in mineralized matrix metabolism. Biochemical studies showed that fetuin-A is essential for the formation and stabilization of protein-mineral complexes, called calciprotein particles (CPPs). CPP clearance from circulation is essential to prevent local deposition and pathological calcification. Consequently, calcification-prone DBA/2 mice deficient in fetuin-A suffer from severe ectopic calcification. In contrast, C57BL/6 fetuin-A deficient mice do not calcify spontaneously. This suggests that additional mechanisms must exist to prevent ectopic calcification in these mice. The aim of this thesis was to elucidate the role of fetuin-A stabilized CPPs in mineral matrix metabolism, to gain further insight into the pathomechanisms of soft tissue calcification in calcifying DBA/2 fetuin-A deficient mice and to identify the mechanisms preventing ectopic calcification in C57BL/6 mice.

It could be shown that in mice fetuin-A containing CPPs were rapidly cleared by the reticuloendothelial system, namely by Kupffer cells of the liver and by marginal zone macrophages of the spleen. Macrophages from scavenger receptor-A (SR-A) deficient mice cleared CPPs less efficiently than macrophages from wildtype mice suggesting that SR-A is involved in CPP binding and endocytosis. The pathology of ectopic calcification in fetuin-A deficient DBA/2 mice was analyzed by comparative genomics. A genome wide gene expression analysis showed that the soft tissue calcification in fetuin-A deficient DBA/2 mice was associated with fibrotic tissue remodeling while mineralization associated genes were not differentially regulated. Furthermore, calcified lesions were found intracellularly as well as extracellularly within the microvasculature and contained serum proteins. These results suggest that ectopic calcification in fetuin-A deficient DBA/2 mice is driven by a passive, chemical mineral precipitation. In agreement with this, in non-calcifying fetuin-A deficient C57BL/6 mice prevention of calcification was not mediated by a compensatory regulation of mineralization associated genes. However, CPP clearance by macrophages derived from DBA/2 was inferior to C57BL/6 mouse macrophage clearance. This strongly suggests that defective CPP clearance contributed to the calcifying DBA/2 mouse phenotype.

In conclusion, it could be demonstrated that fetuin-A containing CPPs mediate the clearance of mineral debris by macrophages via SR-A. Since the same receptor also contributes to the uptake of modified low-density lipoprotein particles in atherosclerosis, defective endocytosis of both types of particles may impinge on lipid as well as mineral debris clearance in calcifying atherosclerosis. In DBA/2 fetuin-A deficient mice defective mineral debris clearance, particularly the absence of fetuin-A stabilized CPPs, accelerates soft tissue calcification. Thus, molecular stabilization of mineral debris in the form of fetuin-A containing CPPs and cellular CPP clearance are both crucial in preventing pathological calcification.

1. Introduction

1.1 Fetuin-A

In 1944, fetuin-A was detected for the first time in fetal calf serum [1]. The human homolog was discovered by Heremans [2], Schmid and Bürgi [3] in 1961. The protein, which belongs to the electroporetic α_2-fraction of serum [4], was termed α_2-Heremans-Schmid-glycoprotein (Ahsg) in honor to its two co-discoverers. Homologues have been described in many vertebrates [5] and most recently in snake [6]. Fetuin-A is highly expressed during fetal life [7], after birth serum fetuin-A values decrease rapidly [8, 9]. In the adult organism fetuin-A is predominantly synthesized in the liver and the physiologic serum concentration is 0.58 mg/ml [9]. During inflammation fetuin-A levels decrease, therefore fetuin-A belongs to the negative acute phase reactants [10-12].

Fetuin-A belongs to the cystatin superfamily along with fetuin-B (FETUB), kininogen (KNG) and histidine-rich glycoprotein (HRG) [13]. Fetuin-A consists of two conserved cystatin domains (D1 and D2), and a third (D3) proline rich domain [14]. Fetuin-A undergoes several posttranslational modifications, including glycosylation [15], sulfation [16] and phosphorylation [17], its molecular weight is 56 kDa. Remarkably, an array of acidic residues in D1 was found to mediate the binding to basic calcium phosphate [14, 18]. Due to its mineral affinity fetuin-A is an abundant protein in bone [19] and teeth [20].

1.2 Function of Fetuin-A

A broad array of functions of fetuin-A have been proposed mainly based on *in vitro* studies, including proteinase interaction [21-28], lipid binding [29-31], lectin binding [32-35], a role in wound closure [36] and promotion of keratinocyte migration [37]. Furthermore, it was reported that fetuin-A may bind and antagonize transforming growth factor-beta (TGF-β) and bone morphogenic proteins (BMPs) [38]. Accordingly, fetuin-A was found to regulate osteogenesis via TGF-β/BMP signaling [39] and fetuin-A deficient mice develop alterations in bone morphology [40, 41]. The group of Josiah Ochieng studied the role of fetuin-A in cancer and reported that fetuin-A facilitates tumor growth [23, 26, 42-44]. In addition, it was shown that the rat phosphoprotein of 63kDa (pp63) [45], later identified as rat fetuin [46, 47], and human fetuin-A inhibit the human insulin receptor [48]. These findings prompted further research and clinical studies investigating the role of fetuin-A in insulin resistance and metabolic syndrome (see chapter 1.2.1). Furthermore, fetuin-A was associated with rheumatoid arthritis [49], long-term survival in patients with alcoholic liver cirrhosis [50], intrauterine growth restriction [51] and most recently with Alzheimer's disease [52].

Another function of fetuin-A studied in great detail is the immunomodulatory activity, including opsonic [53] and anti-inflammatory properties [54] (see chapter 1.2.2).

First of all, fetuin-A is a systemic inhibitor of unwanted calcification, referred to as ectopic or dystrophic calcification [55]. The involvement of fetuin-A in pathological calcification has been confirmed in a knockout (KO) mouse model [56] (chapter 1.2.4) as well as in a great number of clinical studies on patients suffering from dystrophic calcification [57] (chapter 1.2.3).

1.2.1 Fetuin-A in Metabolic Syndrome

In 1983, it was described for the first time that the phosphorylated form of pp63 inhibits the insulin receptor tyrosine kinase as well as insulin receptor autophosphorylation [45]. In 1992, the identity of pp63 and rat fetuin was published [46, 47, 58, 59]. Low insulin receptor inhibition activity was reported for the human homolog of fetuin-A, the α_2-HS-glycoprotein (Ahsg) in 1993. Srinivas and coworkers showed that Ahsg purified from human serum, specifically inhibits insulin receptor autophosphorylation [48]. Subsequently, Mathews et al. showed that also bovine fetuin was efficient in inhibition of the insulin receptor tyrosine kinase [60]. However, in relevant cells with metabolic activity no classical insulin receptor inhibition could be detected, instead an unexplained downregulation of insulin mediated Elk1-phosphorylation was observed [61]. Furthermore, it is controversial whether the initial demonstrated activity of pp63 might have been attributed to a co-purified protein [46, 47]. Analyzing fetuin-A deficient mice on a mixed genetic background of C57BL/6N (B6) and 129Sv as well as pure B6 genetic background revealed that fetuin-A deficient mice on both genetic backgrounds on a high fat diet showed improved insulin sensitivity and were protected against obesity [62, 63]. Additionally, in different patient populations serum fetuin-A was positively associated with metabolic syndrome (MetS) [64-67], insulin resistance [68, 69] and type 2 diabetes [70-73]. However, Jahnen-Dechent and colleagues questioned whether the association of high-serum fetuin-A and MetS is a cause or consequence of high-caloric feeding [55].

Recently, additional functions of fetuin-A related to obesity and MetS were shown. It was shown that fetuin-A induces pro-inflammatory cytokine expression and suppresses adiponectin production [74] and that hepatic fetuin-A expression was further increased by NFκB [75]. These findings contradict the previous identification of fetuin-A as negative acute phase reactant [10-12] as well as the anti-inflammatory activity of fetuin-A discussed below (see 1.2.2).

1.2.2 Immunomodulatory Functions of Fetuin-A

1.2.2.1 Opsonic Properties of Fetuin-A

An opsonic activity of fetuin-A was first described in 1974, when van Oss and colleagues found that the presence of human serum fetuin-A enhanced the phagocytosis of *E.coli* as well as of *S.aureus* by human neutrophils [53]. In the 1980ies Lewis and coworkers showed that co-incubation of DNA or latex particles with fetuin-A increased their uptake in mouse peritoneal macrophages [76] as well as human blood monocytes [77]. Strangely, opsonization with immunoglobulin G (IgG) did not result in an increased uptake of latex particles in these studies. Two decades later Thiele et al. reanalyzed the opsonic properties of fetuin-A. In agreement with the earlier findings, fetuin-A enhanced the uptake of most microspheres in dendritic cells. This effect was comparable to IgG opsonization [78]. At the same time, Jersmann and coworkers postulated a function of fetuin-A in the clearance of apoptotic cells by human macrophages. They demonstrated a dose-dependent enhancement of endocytosis of apoptotic cells and dextran, respectively in the presence of fetuin-A [79]. Surprisingly, co-incubation of fetuin-A and apoptotic cells during endocytosis was essential to increase the uptake. In contrast, pre-incubation of apoptotic cells with fetuin-A was not sufficient to enhance their uptake.

In 2007, a Japanese group studied the uptake of fetuin-A opsonized negatively charged nanoparticles and described a receptor mediated uptake mechanism for fetuin-A opsonized particles. They could show that the uptake of fetuin-A coated 50 nm polystyrene particles by Kupffer cells was mediated by scavenger receptor A (SR-A) [80].

1.2.2.2 Anti-Inflammatory Activity of Fetuin-A

The first evidence of an anti-inflammatory activity of fetuin-A was provided by a study showing that fetuin-A inhibits neutrophil stimulation by hydroxyapatite crystals [81]. The group of Kevin Tracey reported that fetuin-A binds spermine and mediates its anti-inflammatory acting. Spermine is an omnipresent biogenic amine, which was shown to inhibit the synthesis of pro-inflammatory cytokines in human peripheral blood mononuclear cells (PBMCs) [82]. Later on it was demonstrated that fetuin-A is essential for the inhibition of tumor necrosis factor (TNF) production either by carrying spermine or the cationic drug CNI-1493. Thus, fetuin-A acted as an opsonin for cationic molecules and enabled their uptake by macrophages [54, 83]. In agreement with these results, Dziegielewska and colleagues reported that fetuin-A reduced macrophage secretion of the pro-inflammatory compounds interleukin 1β (Il-1β), nitric monoxide and TNFα [84]. Corroborating the anti-inflammatory activity of fetuin-A, Wang and co-workers recently have shown that fetuin-A can protect against early cerebral ischemic injury [85] and has a protective role in lethal systemic inflammation [12] in mice.

1.2.3 Inhibition of Ectopic Calcification – Formation of Soluble Calciprotein Particles

In 1978, Triffitt and colleagues reported a strong hydroxyapatite binding ability of fetuin-A [86], the molecular basis of specific enrichment of fetuin-A in mineralized tissue [19, 20]. This finding was confirmed by Terkeltaub et al. who studied fetuin-A adsorption to hydroxyapatite crystals [81]. In 1996, for the first time Schinke and colleagues demonstrated that fetuin-A was able to inhibit hydroxyapatite formation in mineralizing calvaria cells [14]. To further elucidate the function of fetuin-A, fetuin-A deficient mice were generated. While fetuin-A deficient mice backcrossed on a mixed C57BL/6 (B6) and 129Sv genetic background developed soft tissue calcification only occasionally [87], fetuin-A deficient mice on DBA/2 (D2) genetic background suffered from severe ectopic calcification [56] (see chapter 1.2.4). Thus, it was shown that fetuin-A is an inhibitor of ectopic calcification *in vivo*. In 2003, Heiss and colleagues proposed a mechanism mediating calcification inhibition by fetuin-A. They could demonstrate that fetuin-A, in the presence of supersaturated calcium and phosphate solutions, is highly efficient in the formation of soluble, colloidal spheres. The so-called calciprotein particles (CPPs), 30-150 nm in diameter, were initially amorphous but transformed to a crystalline, insoluble shape with time. It was suggested that transiently soluble CPPs might provide the opportunity to transport and remove calcium precipitates in the body [18]. This concept was validated by detection of fetuin-A as a major protein in protein mineral complexes *in vivo*. Price et al. identified a fetuin-A containing high molecular weight complex in the serum of rats treated with etidronate, an inhibitor of bone metabolism [88, 89]. In 2008, Heiss and colleagues found particles reminiscent to CPPs in the peritoneal dialysate of a patient suffering from calcifying peritonitis [90]. Meanwhile, detailed studies on the composition, kinetics and stability of CPPs were published [90-92]. These studies revealed that CPP formation is a two-stage process, comprising spherical primary CPPs that rapidly transform into secondary CPPs (figure 1B, C), which are stable for at least 24h [91]. Furthermore, it was shown that fetuin-A is essential particularly for primary CPP formation, while additional acidic proteins may participate in the transformation to secondary CPPs [90]. Beside mineral ion stabilization by CPP formation, a complementary mechanism was described using small angle neutron scattering. It was shown that monomeric fetuin-A stabilized mineral ions in form of subnanometer clusters called calciprotein monomers or CPM [91].

Another important finding was the identification of fetuin-A in serum granules formed by incubation of serum containing cell culture media with calcium and phosphate [93, 94]. It was proposed that such mineralo-protein complexes are reminiscent of the highly controversial entity nanobacteria [93, 95-97]. In 1998, the phenomenon of nanobacteria was identified in cell culture media for the first time [98]. In the next few years it was variously described that nanobacteria might be associated with calcification diseases [99-102]. It is now widely accepted

that the entity formerly described as nanobacteria is virtually identical to the protein-mineral complexes described above [55, 94, 96, 97].
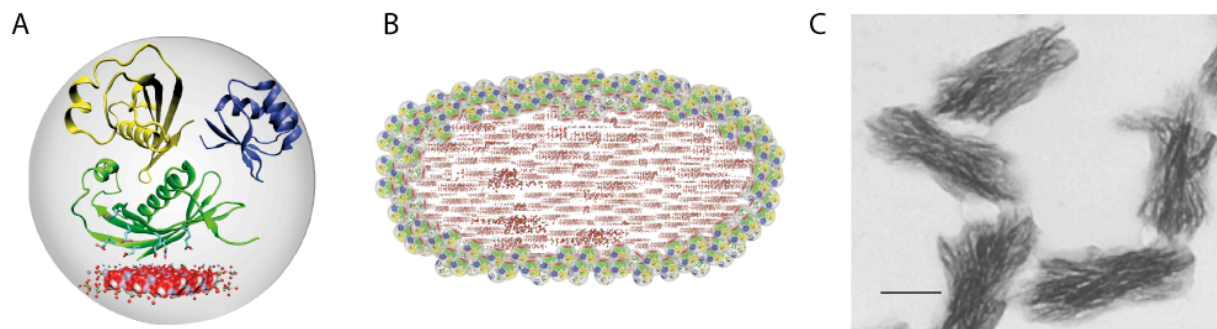
Figure 1. Fetuin-A mediates formation and stabilization of CPPs [55, 90].
A. Computer-generated homology model of fetuin-A. The cystatin-like domain 1 is depicted in green, cystatin-like domain 2 in yellow and domain 3 in green. Hydroxapatite precursors (red) interact with acidic amino acids within domain 1. **B**. Schematic view of a CPP consisting of a crystalline mineral core coated with fetuin-A. **C.** Transmission electron microscopy of CPPs. Scale bar 100 nm.

The function of fetuin-A as an inhibitor of ectopic calcification is evident since low fetuin-A serum levels were frequently associated with calcification diseases. A variety of clinical studies demonstrated that low fetuin-A concentrations were associated with vascular calcification and cardiovascular mortality in patients on dialysis [103], dystrophic calcification in patients with coronary heart disease [104], urolithiasis [105], aortic valve calcification [106], atherosclerosis [107] and peripheral artery disease in type 2 diabetes [108]. Additionally, polymorphisms in the human *Ahsg* gene were linked to aortic stiffness [109] as well as an increased risk of renal calcium oxalate stone formation [110] in recent studies. These findings suggested an important role of fetuin-A in vascular calcification, which was studied in great detail by the group of Catherine Shanahan and others (see chapter 1.4.2).

1.2.4 Fetuin-A Deficient Mice

Originally, fetuin-A KO mice were generated on a mixed genetic background of B6 and 129Sv for technical reasons. These mice did not develop any obvious phenotypic abnormalities. Occasionally, female ex-breeders showed spontaneous ectopic microcalcifications in soft tissues [87]. When the mice were fed a mineral and vitamin D-rich diet calcified lesions were observed in several tissues [56]. To clarify the role of fetuin-A *in vivo,* fetuin-A deficient mice were backcrossed on two defined genetic backgrounds, on pure B6 genetic background and on the calcification sensitive D2 genetic background [111, 112]. D2 fetuin-A deficient mice suffer from severe spontaneous soft tissue calcification. The exacerbated calcification phenotype caused a decreased breeding performance as well as increased mortality of KO mice in comparison to wildtype (WT) littermates. Calcified lesions affected almost all major organs (figure 2). The severe calcification and consequent damage of the kidney caused a secondary hyperparathyroidism and an increased accumulation of

parathyroid hormone (see also chapter 1.4.1) [56]. Myocardial calcification was associated with fibrosis and diastolic dysfunction [113]. In contrast to D2 fetuin-A deficient mice, B6 fetuin-A KO mice did not suffer from spontaneous ectopic calcification. However, in a model of chronic kidney disease (CKD), generated by nephrectomy and feeding a high phosphate diet, B6 fetuin-A deficient mice developed extraosseous calcification [114].

The influence of fetuin-A on atherosclerosis has been studied in a mouse model of CKD. Nephrectomized B6 apolipoprotein E (ApoE) deficient mice on a high phosphate diet served as a model of calcifying atherosclerosis. Double deficient mice lacking ApoE and fetuin-A showed a worsend phenotype of vascular calcification in comparison to ApoE single KOs [115].
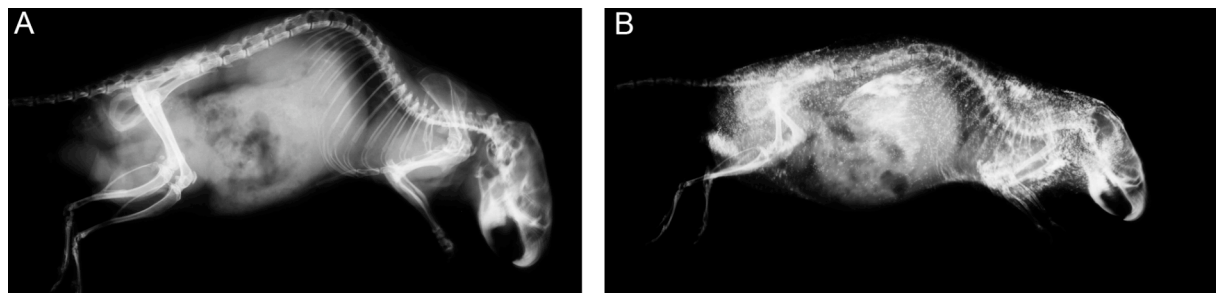
Figure 2. Severe soft tissue calcification in D2 fetuin-A deficient mice [56].
Radiological analysis of 9-month-old D2 fetuin-A KO and WT mice. KO mice develop severe ectopic calcification of thorax, neck, kidney, and testis.

In conclusion, the generation of fetuin-A deficient mice on different genetic backgrounds has clearly demonstrated the calcification inhibitory potential of fetuin-A. Nevertheless, fetuin-A deficient mice on B6 genetic background were resistant to spontaneous pathological mineralization. This suggested the existence of additional inhibitors of unwanted calcification (see chapter 1.4.2).

1.3 Fetuin-A Receptor Binding

1.3.1 The Asialoglycoprotein Receptor

Uptake of chemically or enzymatically desialylated fetuin-A, referred to as asialofetuin, was studied in great detail by Tolleshaug and co-workers. In 1977, they demonstrated that asialofetuin was taken up by hepatocytes in a saturable process *in vitro* and *in vivo* [116]. This was in accordance to previous studies showing that asialoglycoproteins are taken up by liver parenchymal cells [117]. Furthermore, Tolleshaug et al. could show that asialofetuin uptake was distinct from uptake of native fetuin-A as no competition occurred and native fetuin-A was not taken up by hepatocytes [116]. While studying the fate of internalized asialofetuin Tolleshaug demonstrated that asialofetuin is enriched in endocytic vesicles and transported to the lysosmes where it is rapidly degraded [118]. Starting in the 1980ies asialofetuin was used as a

control in diverse publications studying the uptake route via the asialoglycoprotein receptor (ASGP-R) [119]. The ASGP-R comprises of two subunits, hepatic lectin 1 (HL1) and hepatic lectin 2 (HL2), forming a hetero-oligomer [120]. Mice deficient in the major subunit HL1 showed significant impaired uptake of asialofetuin, confirming the function of the ASGP-R *in vivo* [121].

1.3.2 Uptake of Fetuin-A

Fetuin-A is a circulating serum protein. Thus, native fetuin-A is protected against hepatic uptake and is not able to bind the ASGP-R [116].

Fetuin-A is critically involved in vascular calcification ([122], chapter 1.4.3). This action is dependent on the uptake of the serum protein fetuin-A in vascular smooth muscle cells (VSMCs). Chen and colleagues showed that fetuin-A uptake in bovine VSMCs was calcium-dependent and mediated by annexins. In particular, they demonstrated that fetuin-A could bind to annexin 2 at the cell surface. [123]

1.4 Calcification

1.4.1 Maintenance of the Calcium x Phosphate Product

The calcium x phosphate product is of critical importance in maintaining mineral homeostasis. Even under physiological conditions blood is considered a metastable solution sustaining mineral precipitation once crystals are nucleated [124]. William Neuman stated that our bodies are constantly at risk of turning into a pillar of salt [125]. Thus, inhibitors are required to avoid spontaneous calcification.

In healthy man the serum total calcium concentration ranges between 2.1 and 2.6 mM. The ionized serum calcium level is tightly regulated by parathyroid hormone (PTH). PTH is secreted by the parathyroid gland at low serum calcium concentrations. It triggers calcium reabsorption in the kidney and indirectly induces bone resorption by osteoclasts and thus the mobilization of calcium from bone. Simultaneously, PTH inhibits phosphate reabsorption in the kidney to lower the serum phosphate level and to keep the calcium phosphate product constant. In case of a persistent hypocalcaemia PTH triggers calcitriol synthesis [126]. Calcitriol is the physiologically active metabolite of vitamin D3 and induces calcium reabsorption in the gut as well as bone resorption [127].

As mentioned above, the serum phosphate concentration is partially affected by serum calcium regulation via PTH and calcitriol. Recently, a Fibroblastic Growth Factor 23 (FGF-23) dependent mechanism was discovered, which directly regulates serum phosphate levels. FGF23 is predominantly expressed by osteocytes and osteoblasts [128], its synthesis is regulated by dietary phosphate and calcitriol [129-132]. The main function of FGF-23 takes place in the kidney, therefore it was suggested that phosphate homeostasis is regulated via a

bone-kidney axis [133]. In the kidney FGF-23 targets a complex of the FGF receptor and the co-receptor Klotho [134] and evokes the inhibition of phosphate uptake and calcitriol synthesis [135, 136]. Consequently, FGF-23 deficient mice suffer from hyperphospatemia, elevated calcitriol and soft tissue calcification [137-139].

1.4.2 Pathologic Calcification

Ectopic mineralization is a well-known phenomenon, occurring in many variants and associated with several diseases. Case reports described ectopic calcified lesions in patients suffering from the autoimmune disease systemic lupus erythematosus [140], different kinds of tumors and metastasis [141-143] and sarcoidosis, a rare granulomatous disease [144]. One of the most severe cases of ectopic calcifications is the *fibrodysplasia ossificans progressiva*, where connective tissue is transformed into bone [145, 146]. Most prominent diseases associated with ectopic mineralization are kidney stones, calcification associated with CKD and vascular calcification. In severe cases CKD is associated with calciphylaxis, also called calcific uremic arteriolopathy (CUA), which is a disease caused by inflammation, endovascular fibrosis and vascular smooth muscle cell apoptosis leading to calcification of small blood vessels [147].

Apart from the association with various diseases, ectopic calcification is a common adverse event in implantation of artificial prostheses, in particular heart valve replacements [148].

The mechanisms in ectopic calcification are diverse and not fully understood. Most studied is the pathology of vascular calcification as a major risk factor for cardiovascular mortality [149].

Basically, regulation of calcification is driven by the maintenance of extracellular calcium and phosphate concentrations and the control by inhibitors, including low molecular weight inhibitors as well as proteins, proteoglycans and hyaluronans (figure 3, [124]). Block and colleagues reported that elevated serum phosphate levels as well as an elevated calcium x phosphate product was associated with calcification and mortility in patients of end-stage renal disease (ESRD) [150, 151]. Low molecular weight inhibitors include magnesium and pyrophosphate; bisphosphonates may also inhibit mineralization. Dietary magnesium supplementation was shown to be of therapeutic value in high phosphate induced aortic calcification [152] and connective tissue calcification in a mouse model of pseudoxanthoma elasticum (PXE) [153, 154]. Pyrophosphate (PP) is an effective inhibitor of biological calcification [155] and served as a lead compound for synthetic bisphosphonates [124]. As PP is a potent inhibitor of mineralization, several proteins involved in PP metabolism are involved in calcification inhibition, too. Knockout of those proteins in mice resulted in various calcification phenotypes [156-159]. A strong tissue-specific inhibitor of calcification is the matrix GLA protein (MGP). MGP deficient mice develop lethal mineralization of the aortic trunk [160]. Another important modulator of unwanted calcification is osteopontin (OPN). OPN belongs to the fraction of non-collageneous bone proteins [161] and fulfills a multifunctional role in bone and the immune system [162]. During inflammation OPN is secreted by macrophages and

stimulates cytokine synthesis [163]. Originally, inhibition of ectopic calcification by OPN was shown *in vitro* [164]. *In vivo* calcification inhibition by OPN could be shown in mice deficient in OPN and MGP. These mice developed an exacerbated calcification phenotype in comparison to MGP KO animals [165]. In contrast, single deficient OPN KO mice did not show spontaneous calcification [166]. However, OPN accumulation was also detected in calcified lesions [167]. It was described that inhibition of calcification by OPN was mediated on the one hand by blocking the crystal growth and on the other hand by solubilizing mineral precipitates. In doing so, OPN induces expression of carbonic anhydrase 2 in monocytic cells, which consequently triggers dissolution of mineral by acidification of the extracellular milieu [168]. Another interesting function of OPN was demonstrated in an *in vitro* study showing that OPN may opsonize hydroxyapatite microspheres [169]. Recently, conflicting studies were published on the role of intact OPN and thrombin-cleaved OPN fragments in the progression of atherosclerosis [170, 171].

Several more protein inhibitors of ectopic calcification have been described and confirmed in KO mouse models [124, 172, 173]. However, none of the discussed inhibitors acts on the systemic level, emphasizing the important role of fetuin-A as a *bona fide* systemic inhibitor of ectopic calcification.
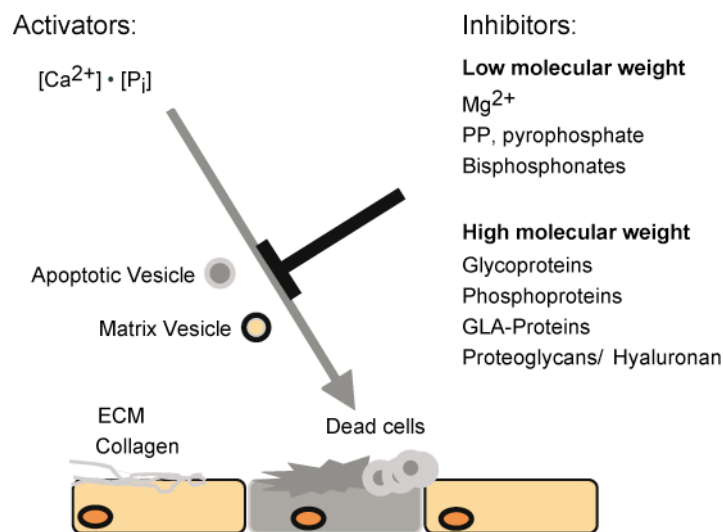
Figure 3. Regulation of calcification [124].
Elevated serum calcium and phosphate level facilitate mineralization. Apoptotic vesicle or matrix vesicle released by VSMCs may contain BCP and cause mineral precipitation. Presence of adequate amounts of inhibitors prevents ectopic calcification.

1.4.3 Mechanisms of Vascular Calcification

Chronic kidney disease is frequently associated with vascular calcification. Calcified lesions occur as intimal calcification of atherosclerotic plaques or within the media arteries. Media calcification is known as *Mönckeberg sclerosis* and occurs in calciphylaxis (chapter 1.4.2). As mentioned above prevention of unwanted calcification is a matter of accurate regulation of

calcification inhibitors as well as of maintenance of the calcium x phosphate product. Nowadays, vascular calcification is also widely considered an active process, associated with the transdifferentiation of VSMCs to an osteogenic/chondrocytic phenotype, which consequently triggers mineral formation [174]. The expression of osteogenic markers by VSMCs was shown in numerous *in vitro* and *in vivo* studies e.g. [175-177]. In particular the induction of the osteoblastic transription factor Cbfa-1/Runx2 [178] is crucial in triggering transdifferentiation of VSMCs [179]. Expression of Cbfa-1 may be induced by various conditions, including elevated inorganic phosphate levels [180], elastin degradation [181], oxidative stress [182], leptin accumulation [183] or glucocorticoides [175]. Osteogenic VSMCs release vesicles reminiscent to matrix vesicles [184], which drive bone mineralization. Whether such basic calcium phosphate (BCP) containing vesicles [185] lead to mineral deposition depends on many factors. Effective phagocytosis of vesicles may prevent calcification [186]. In addition, the presence of inhibitors like fetuin-A or γ-carboxylated MGP, which both were enriched in vesicles, might prevent mineral deposition [122, 185]. Besides vesicles released from vital VSMCs apoptotic vesicle and fragments of damaged VSMCs may further drive mineral precipitation [187]. Thus, calcification occurs also independently from osteogenic reprogramming. For instance calcification of heart valves was attributed to vascular ossification only in 13 % of all cases studied [188]. So far, it is unclear whether osteogenic transdifferentiation is a cause or a consequence of calcification [124].

1.4.4 Dyscalc1 – A Gene Locus Causative for Dystrophic Calcification

While vascular calcification was extensively studied, mechanisms in soft tissue calcification are not well understood. Certain mouse strains are prone to dystrophic calcification. It was shown that D2 mice suffer from spontaneous calcifications in myocardium [111, 189] and tongue [190, 191]. Eaton and colleagues analyzed five inbred mouse strains with respect to dystrophic cardiac calcinosis and found cardiac lesions in D2, C3H, C3Hf and BALB/c mice, while B6 mice never had any calcification [192]. Brunnert studied cardiac calcification associated with skeletal muscle necrosis induced by freeze-thaw injury and found that D2 mice as well as C3H mice were prone to ectopic mineralization while B6 mice were resistant [112]. The same model of dystrophic calcification was used in a genomic approach to identify a causative gene locus of dystrophic calcification. In this work Ivandic and coworkers identified a major locus on proximal chromosome 7, which was called *Dyscalc1,* using a linkage map approach and quantitative trait locus analysis (QTL) [193]. The same chromosomal region was identified by van den Broek and colleagues studying a D2 x and D2B6F1 backcross [194]. At the time the histidine rich calcium binding protein (Hrc) was proposed as a promising candidate gene causative for dystrophic calcification [194, 195]. In 2001, Ivandic described 3 more gene loci on chromosome 4, 12 and 14 involved in dystrophic calcification [196], additionally the *Dyscalc1* locus was shortened to a 10 cM interval. Fine mapping of *Dyscalc1* to a region of 0.76 Mbp

excluded the previous candidate Hrc, but led to the suggestion of the gene encoding the *ATP-binding cassette C6* (Abcc6) [197]. Ultrafine mapping performed by another team of researchers resulted in an interval of 80 Kb containing the genes *EMP-3*, *BC013491*, and *Abcc6* (partially) and identified *EMP-3* as a new candidate gene [198]. However, a third workgroup confirmed *Abcc6* as the causative gene for dystrophic calcification and reported on differential expression of *Abbc6* in mice susceptible and resistant for dystrophic calcification [199]. Later, a differential splice variant of *Abcc6* was identified and Abcc6 protein deficiency in calcification prone mice was attributed to a truncated protein encoded by a splice variant [200]. Today *Abcc6* is widely considered the gene causative for dystrophic calcification, which was confirmed by the fact that *Abcc6* deficient mice suffer from ectopic calcification associated with pseudoxanthoma elasticum (PXE) [201]. *Abcc6* deficient mice developed a mild calcification phenotype, where calcified lesions were detected in elastic fibers of blood vessels, Bruch's membrane in the eye [201] and strikingly in vibrissae [202]. In agreement with the phenotype of *Abcc6* KO mice, mutations of *Abcc6* were likewise associated with PXE [203].

In the current thesis, fetuin-A deficient mice on D2 genetic background were used as a model of ectopic calcification. The dramatic calcification phenotype in this particular genetic background mice may be attributed to differential expression of *Abcc6* or rather a truncated protein product of *Abcc6*.

1.5 Mononuclear Phagocyte System

Many efforts were made to group phagocytic active cells into subpopulations or a system. Two categories of phagocytes, namely mononuclear and polymorphonuclear phagocytes may be easily distinguished by the morphology of their nuclei. In 1924, Ludwig Aschoff defined the term reticulo-endothelial system (RES). He proposed that reticular cells of spleen and lymph nods, reticular cells of lymph and blood sinusoids, Kupfer cells, histiocytes, splenocytes and monocytes should fall into this category, while he excluded endothelial cells and fibrocytes because of their poor phagocytic activity [204]. The term RES has been frequently criticized, consequently during a conference on mononuclear phagocytes in 1969 a new classification was adopted [205]. Highly phagocytic active mononuclear cells were grouped to the mononuclear phagocyte system (MPS). These cells originate from bone marrow, are transported into the bloodstream and are localized in tissues as resident macrophages [206]. Depending on their localization resident macrophages display a characteristic morphology. Resident macrophages were identified in spleen, lymph nodes, bone marrow, liver (Kupfer cells), pleural and peritoneal fluids, brain (microglia), bone (osteoclasts), lung (alveolar macrophages), skin, gut and endocrine organs [206, 207].

1.5.1 Macrophages

Macrophages show a high level of heterogeneity depending on their localization as well as their activation state. Four different states of macrophage activation were described, namely innate activation, classical activation, alternative activation and deactivation. The activation pathway is regulated by the particular stimulus of activation, e.g. lipopolysaccharide (LPS) triggers innate or classical activation, while presence of IL-4 leads to alternative activation. In each case a specific program of cytokine release and modification of surface receptors is initiated [208].

Cells of the innate immune system recognize pathogen-associated molecular patterns (PAMPs) through highly conserved pattern recognition receptors (PRRs). Macrophages express a broad range of receptors involved in immune recognition of PAMPs, apoptotic cells as well as particular matter. These receptors include scavenger receptors (chapter 1.5.2), glycosylphosphatidylinositol (GPI)-anchored receptors, integrins, receptors belonging to the immunoglobulin (Ig) superfamily, seven transmembrane receptors, natural killer (NK)-like C-type lectin-like receptors, C-type lectins, toll-like receptors and the mannose receptor. In particular, complement mediated phagocytosis is mediated by the complement receptor 3 (CR3) grouped with the integrins, antibody-dependent phagocytosis is mediated by Fc receptors and fungal antigens are mainly endocytosed in a dectin-1 dependent manner [209]. Each macrophage subpopulation expresses a distinct pattern of receptors. This specific profile of surface receptors should be considered when macrophage model systems, either primary macrophages or macrophage cell lines, are studied.

1.5.2 Scavenger Receptors

The growing family of scavenger receptors (SRs) is characterized by scavenging modified forms of LDL [210]. In 1987, scavenger receptor ligands were identified *in vivo* for the first time, when the clearance of oxidized forms of LDL was studied [211]. In 1990, the first scavenger receptors were purified, the bovine scavenger receptors SR-AI and SR-AII [212]. Both subtypes have a very similar structure (figure 4), where SR-AII is lacking a c-terminal cysteine-rich domain as consequence of alternative splicing [213]. Macrophages from mice deficient in the murine scavenger receptor-A (MSR-A) gene showed a significantly decreased uptake of acetylated LDL (acLDL) *in vitro. In vivo* clearance of acLDL was normal suggesting the existence of additional scavenger receptors [214]. Later it was shown that SR-AI/II may recognize several PAMPs and are essential for immune recognition of various pathogens, e.g. *S. pyogenes* [215, 216].

Today, about 15 SRs have been described, most of them have a dual role in the recognition of modified self and pathogenic patterns [217]. Redundancy of SRs was demonstrated in macrophages from SR-A/CD36 double deficient mice, which showed significantly less efficient endocytosis of modified LDLs than corresponding single KO mice [218].

With respect to the role of SRs in the clearance of modified LDLs, their role in atherogenesis was studied in ApoE deficient mice. While decreased formation of atherosclerotic lesions was observed in ApoE/CD36 double deficient mice in comparison to ApoE single KO mice, no improvement in the atherosclerotic phenotype of ApoE/SR-AI/II deficient mice was seen [219]. These findings confirmed a pro-atherogenic role for CD36, whereas the function of SR-AI/II in atherogenesis remained unclear.
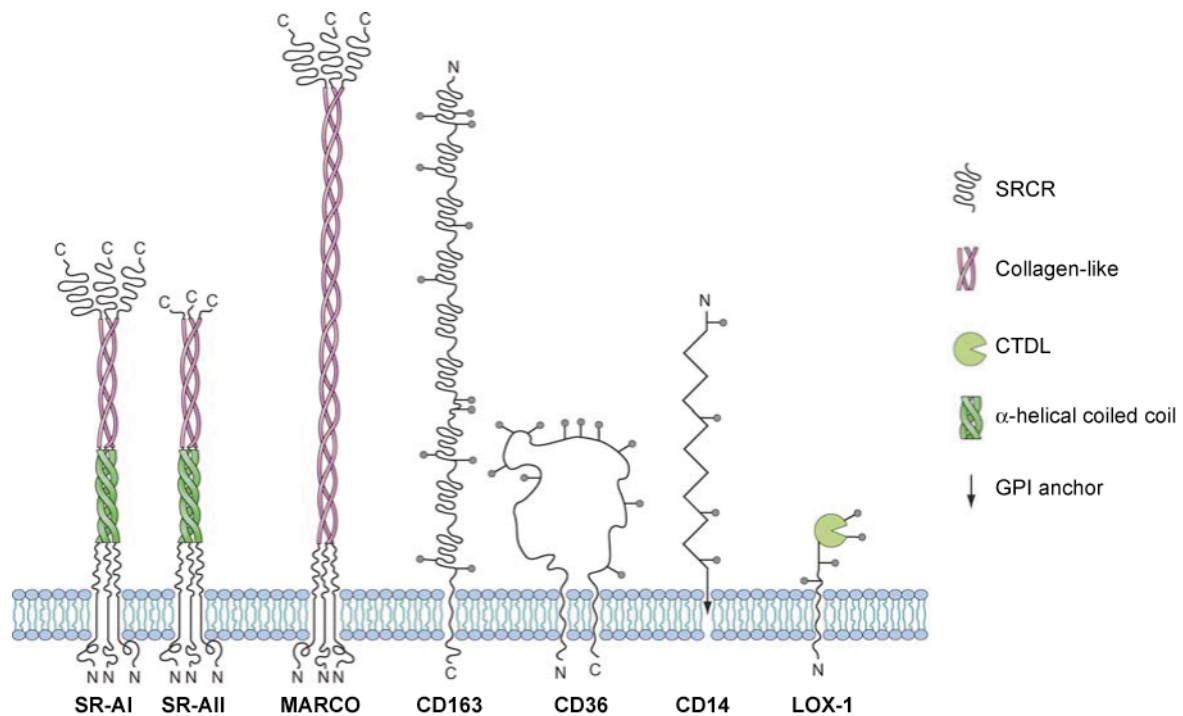
Figure 4. Scavenger receptor family [209].
Schematic view of a selection of scavenger receptors espressed by macrophages. MARCO, macrophage receptor with collagenous structure, a scavenger receptor type A; LOX-1, lectin-like oxidized low density lipoprotein receptor 1; SRCR, scavenger receptor cysteine-rich domain; CTDL, C-type lectin carbohydrate-binding domain; GPI, glycosylphosphatidylinositol.

1.6 Clearance of Particular Matter

Micro- and nanoparticles have been intensively studied in relation to targeted delivery of drugs and antigens. The uptake route of particular matter strongly depends on particle size, geometry, charge as well as on protein absorption. Studies in beagle dogs demonstrated that intravenously injected polystyrene spheres accumulated in liver, spleen and lung tissue. Increasing particle diameters (up to 12 µM) directed the spheres to the lung, while smaller microspheres (5-7 µM) were detected predominantly in liver and spleen [220]. A similar biodistribution was obtained with polystyrene particle of nanometer size [221]. Particle size influences not only the target organ but also the target cell type. For instance, Ogawara and colleagues showed a size dependent intrahepatic distribution of polystyrene particles. 500 nm particles were exclusively taken up by non-parenchymal cells, whereas 50 nm particles were also taken up by liver hepatocytes [222]. Moghimi and colleagues showed that hydrophilic

coating reduced liver particle uptake in rats but facilitated their uptake in spleen [223]. These data suggested an impact of particle surface characteristics on their biodistribution.

Apart from the targeting of particles to specific tissues and cells, the efficiency of their uptake is of particular interest. Interestingly, mechanical properties regulate phagocytosis. It was shown, that Fc-receptor mediated uptake of rigid particles was much more efficient than uptake of soft particles of identical chemical properties [224]. Thiele et al. studied the influence of plasma protein absorption to polystyrene spheres in dendritic cells *in vitro.* In particular the effects of serum albumin, immunoglobulins and fetuin-A applied as single proteins or mixtures were examined. In agreement with earlier findings (chapter 1.2.2), they showed that fetuin-A enhanced the uptake of most of the particles, the effect was comparable to IgG opsonization. In contrast albumin coating inhibited phagocytosis [78]. Champion and Mitragotri studied the influence of particle geometry on endocytosis. They pointed out that the influence of particle shape overruled particle size. This was attributed to the fact that local shape determines the complexity of the actin structure [225].

Finally, targeting of particulate matter depends on receptor recognition. Particles may be opsonized by immunoglobulins, complement or plasma proteins. Endocytosis of immunoglobulin opsonized particles is mediated by Fc receptors and complement opsonized particles are taken up via complement receptor. Furthermore, two proteins of the pentraxin family have been shown to have opsonic properties, namely serum amyloid P (SAP) and C-reactive protein (CRP). Also endocytosis of SAP and CRP-coated particles is mediated by Fc receptors [226, 227]. As described before, there is strong evidence that fetuin-A has likewise opsonic properties [78, 79]. However, no receptor responsible for fetuin-A binding was identified in these studies. Nagayama and colleagues proposed a SR-A mediated uptake of fetuin-A opsonized particles [80]. It is reasonable to assume that unopsonized particles might bind to PRRs, which have a broad ligand specifity. For instance, silica particles were taken up by macrophage receptor with collagenous structure (MARCO), a class A scavenger receptor [228].

1.6.1 Endocytosis and Immune Response of Hydroxyapatite Particles

Hydroxyapatite (HAP) crystals are associated with various inflammatory diseases, e.g. rheumatoid arthritis [229]. Endocytosis by cells of the MPS [230] and inflammatory properties of HAP have been shown *in vitro* [81] and by injection of HAPs into the foot pads of rats [231]. However, neither an uptake mechanism nor a specific signaling pathway has been discovered to this date. In 2004, Kandori and colleagues demonstrated absorption of IgG to HAP [232], which might have an impact on the immunomodulatory function of HAP. IgG opsonization of HAP was confirmed in another study. In addition to these studies OPN was suggested as an opsonin for HAP [169].

Nadra and coworkers showed uptake of BCP crystals, consisting mainly of HAP by macrophages. In addition, induction of pro-inflammatory cytokine secretion in particular of

TNFα was detected [233]. Subsequently, participation of toll-like receptor 4 (TLR4) in the pro-inflammatory response was reported [234]. Fellah et al. showed a pro-inflammatory reaction following BCP injection *in vivo* [235]. In 2008, Nadra and colleagues refined their previous analysis. They found that TNFα induction was mediated by NFκB and was critically dependent on particle size, where the smallest HAP particles were most reactive [236]. Recently, induction of IL-1β through NLRP3 inflammasome activation was shown [237].

1.7 Experimental Aims

Ectopic calcification is a common pathological event associated with chronic kidney disease as well as atherosclerosis. To this date in particular soft tissue calcification is poorly understood. D2 fetuin-A deficient mice suffer from severe soft tissue calcification and provide a suitable model for calcification diseases like calciphylaxis [56]. In the current thesis, D2 fetuin-A deficient mice were studied to investigate mechanisms involved in the formation of calcified lesions, which might serve as a basis for new therapeutic strategies of calcification diseases. Moreover, additional principles of calcification inhibition should be identified. To this end, calcification resistant B6 fetuin-A deficient mice and calcification prone D2 fetuin-A deficient mice were compared regarding their gene expression profiles and endocytic properties. Uptake of protein-mineral particles might be critically involved in the clearance of mineral debris and thus in the prevention of calcification.

The molecular basis of calcification inhibition by fetuin-A was studied in great detail by Heiss and colleagues [18, 90, 92]. In brief, fetuin-A mediates the formation and stabilization of CPPs. CPPs may form spontaneously in body fluids, in particular in situations with elevated calcium and phosphate levels. To prevent mineral precipitation removal of CPPs from circulation is of critical value. In the current thesis, the fate of CPPs was examined *in vivo.* Furthermore, the target organs, cell types and the uptake mechanism of CPPs were analyzed.

2. Methods

2.1 Animals

Wildtype and fetuin-A deficient mice on either C57BL/6N or DBA/2N genetic background were maintained in a temperature-controlled room on a 12-hour light/dark cycle. Standard diet (Ssniff, Soest, Germany) and water were given ad libitum. Mice were kept at the animal facility of Universitätsklinikum Aachen, Pauwelsstr. 30. All animal experiments were conducted in agreement with German animal protection law and were approved by the state animal welfare committee.

2.2 Necropsy

Mice were sacrificed with an overdose of isofluran (Forene, Abbott, Wiesbaden, Germany). The abdomen was opened and the skin was removed. Organs were subsequently harvested. Photomicrographs were taken using a Canon EOS D1000 XS SLR digital camera and a Canon EF 100 mm 2,8 L IS USM macro objective (Canon, Tokyo, Japan).

2.3 Immunofluorescence Staining

Mice were sacrificed with isofluran, exsanguinated, perfused with 20 ml ice-cold PBS (PBS Dulbecco, Biochrom AG, Berlin, Germany) and organs were collected. The tissues were embedded in Tissue-Tek O.C.T. compound (Sakura, Alphen aan den Rijn, Netherlands) frozen in liquid nitrogen and kept at -20 °C until usage. Cryosections 6 µm thick were cut and fixed with Bouin's fixative if not stated otherwise. Calcified tissue was decalcified with 0.5 M EDTA over night. PBS washed sections were blocked with 3 – 10 % goat serum (Dako, Hamburg, Germany) prior to primary antibody incubation. Dilution factors as well as incubation time of all primary antibodies are summarized in table 1. In case of double staining primary antibodies derived from different species were used and applied simultaneously. Primary antibodies were detected by secondary antibodies coupled with Alexa Fluor 488 or Alexa Fluor 546 (all secondary antibodies were purchased from Molecular Probes, Life Technologies, Carlsbad, CA, USA). DAPI (Sigma, Taufkirchen, Germany) was adopted as nuclear stain. Stained sections were examined using a Leica DMRX fluorescence microscope (Leica Microsystems GmbH, Wetzlar, Germany) and DISKUS software (Carl H. Hilgers, Technisches Büro, Königswinter, Germany). Pictures were processed with Adobe Photoshop (Adobe Systems GmbH, München, Germany).

2.4 Fetuin-A Imaging

Fetuin-A was used to image calcified lesions [238]. Purified bovine fetuin-A was prepared as previously described [18] and injected *intraperitoneal* one day before dissection of mice, a dose of 100 µl of a 7 mg/ml protein solution was applied. Fetuin-A was detected on Bouin's stabilized cryosections using a homemade rabbit polyclonal anti-fetuin-A antibody (AS 237) and a secondary Alexa Fluor 546 goat anti rabbit antibody (Molecular Probes).

Table 1. Antibodies for immunofluorescence staining.

antigen	company (ordering number)	dilution factor	incubation time
CD31	BD Pharmingen (550274)	10	1 h
CD68	AbD Serotec (MCA 1957)	500	1 h
F4/80	Abcam (ab6640)	1000	1 h
bovine fetuin-A	homemade, AS 237	1000	over night
Lyve-1	Acris Antibodies GmbH (DP3513P)	1000	1 h
Madcam	BD Pharmingen (550556)	10	over night
MARCO	AbD Serotec (MCA 1849)	10	over night
Moma-1	BMA Biomedicals (T-2011)	10	1 h
OPN	Assay Designs, Inc. (915-021)	100	1 h
OPN	R&D Systems (AF808)	1000	1 h

The table summarizes all primary antibodies used within this thesis. For each antibody the ordering information as well as the experimental conditions are given. Antibodies were purchased from Acris Antibodies GmbH (Herford, Germany), BD Pharmingen (Franklin Lakes, NJ, USA), Serotec (Düsseldorf, Germany), Abcam (Cambridge, UK), BMA Biomedicals (Augst, Switzerland), Assay Designs (belongs to Enzo Life Science, Lörrach, Germany).

2.5 Electron Microscopy

Evaluation of calcified lesions in young mice was performed in collaboration with Marc D. McKee, McGill University, Montreal, Canada. Mice were sacrificed with an overdose of isofluran, exsanguinated, perfused with 20 ml cold PBS and organs were collected. Tissues were fixed in 4% paraformaldehyd and sent to Canada for tissue embedding, sectioning and electron microscopy.

For examination of injected CPPs mice were sacrificed with an overdose of isofluran, exsanguinated, and perfused with 20 ml cold PBS at 30 min after injection of fluorescence labeled CPPs. Tissue samples were fixed in 3 % glutaraldehyde (in 0.1 M Soerensen's phosphate buffer (pH 7.4, 13 mM NaH_2PO_4 x H_2O, 87 mM Na_2HPO_4 x $2H_2O$)) for 24 hours and handed over to Jörg Bornemann, Electron Microscopy Facility, RWTH Aachen University, Germany for further sample preparation and evaluation.

2.6 Gene Expression Analysis

2.6.1 Sample Preparation

2.6.1.1 Microarray Analysis of Calcified Brown Adipose Tissue

Wildtype and fetuin-A deficient DBA/2 mice at 6 week of age were used, 3 female and 3 male mice. Mice were sacrificed with an overdose of isofluran, exsanguinated and perfused with 20 ml cold PBS. Brown adipose tissue was dissected from the kidney pelvis region. Tissue samples were homogenized and stored in peqGOLD RNAPure reagent (PEQLAB Biotechnologie GMBH, Erlangen, Germany). RNA extraction was performed using the RNeasy Lipid Tissue Mini Kit (Qiagen, Hilden, Germany) according to the manufacturer's protocol. Gene expression profile was analyzed with Affymetrix Mouse Genome 430 2.0 Arrays (Affymetrix, Santa Clara, CA, USA). RNA preparation and microarray handling was performed by Beate Kratz, Chip Facility, IZKF Aachen, Germany.

2.6.1.2 Microarray Analysis of Kidney and Liver

Wildtype and fetuin-A deficient DBA/2 mice and C57BL/6 mice were 36 days of age, 6 mice of each genotype were used, whereof 3 were female and 3 were male (except DBA/2 wildtype mice where 4 mice, 2 of each sex, were used). Mice were sacrificed with an overdose of isofluran, exsanguinated and perfused with 20 ml cold PBS. Liver and kidneys were collected. Tissue samples were homogenized and stored in peqGOLD RNAPure reagent (PEQLAB Biotechnologie GMBH, Erlangen, Germany). Phenol-Chloroform extraction was applied to purify RNA. Gene expression profile was analyzed with Affymetrix Mouse Genome 430 2.0 Arrays (Affymetrix, Santa Clara, CA, USA). RNA preparation and microarray handling was performed by Beate Kratz, Chip Facility, IZKF Aachen, Germany.

2.6.2 Microarray Data Analysis

Gene data analysis was carried out using Bioconductor [239] packages under R1. Differential expression between groups was examined following the workflow shown in figure 5.

2.6.2.1 Import of Files in Bioconductor and Introduction of Phenotype Information

Cel files were read into Bioconductor using the Affy package [240]. Phenotype information for each file was introduced as a table. Phenotype information included gender and genotype of the mice corresponding to the arrays.

2.6.2.2 Quality Assessment

Quality of microarrays was assessed using the ArrayQualityMetrics package [241]. The arrays were analyzed with the outlier detection algorithm within the package. Arrays with two or

more outlier calls were considered insuflient quality and were excluded from further normalization and data analysis.

Bioconductor package	Work Flow	Output

CEL files of arrays

Affy → Reading of CEL files into Bioconductor

Building of PhenoData → Table: phenotypic data

ArrayQualityMetrics → Qualitiy assessment of arrays → Report summary file

Exclusion of outliers

Affybatch object of remaining arrays

Normalization

Expression set with normalized data → Excel file with expression data

Genefilter → Filter 1: Nonspecific filtering (removing of probe sets without EntrezID and of Affymetrix controls)

Filter 2: Removal of genes with standard deviation smaller than mean standard deviation → Histogramm of p-values before and after filtering

Expression set with reduced probe sets

Limma → Detection of differential expression

Multtest → Multiple testing

List of significant probe sets

Annaffy, Annotate, Mouse4302.db → Annotation

List of significant genes → Excel and HTML Files

Volcano plot demonstration → Volcano plot

Figure 5. Microarray data analysis.
Hierarchical scheme of the microarray data analysis using Bioconductor under R1. A general work flow of data analysis is given (central column), the left column contains information about the applied Bioconductor package, the right column summarizes the type of files which can be obtained at the different stages of the analysis.

2.6.2.3 Normalization and Nonspecific Filtering

Background adjustment, normalization and summarization were applied using the RMA algorithm within the Affy package under Bioconductor [239, 240]. Afterwards the processed data was stored in a so-called expression set containing a value for each probe sets proportional to its expression strength. Next probe sets, which could not be annotated to any gene were removed from the expression set, e.g. technical controls. Finally, a mean standard deviation of all probe sets was calculated. All probe sets, which had a lower standard deviation than the mean standard deviation were excluded. Both filtering methods were performed using the Genefilter package [242].

2.6.2.4 Detection and Visualization of Differential Expression

Differential expression was probed using Bayesian statistics and Limma package [233]. Differences between genotype, sex as well as a possible interaction of both were calculated. Multiple testing correction was performed using the procedure of Benjamini Hochberg implemented in the Multtest package [243]. Probe sets with a p-value below 0.05 were considered as differentially expressed. Annotation of probe sets was applied with Annaffy, Annotate and Mouse4302.db packages [244-246] under Bioconductor. Volcano plot representation was used to visualize differential expression.

2.6.2.5 Pathway Analysis

Differential expressed probe sets were tested for overrepresentation of KEGG gene sets. The analysis was performed using the GSEABase package [247] under Bioconductor.

2.6.3 Quantitative PCR

RNA was prepared as described before (chapter 2.6.1.2). Reverse transcription was performed with the Reverse Transcription Core Kit (Eurogentec, Köln, Germany) according to the manufacturer's protocol. Primers were synthesized by Eurofins MWG Operon (Ebersberg, Germany). Primer sequences were chosen with the Primer-Blast tool (NCBI, Bethesda, MD, USA), primer sequences are given in table 2. Quantitative PCR was performed with the Maxima SYBR Green/Rox qPCR Master Mix (Fermentas GmbH, St. Leon-Rot, Germany). Eukaryotic 18S rRNA Endogenous Control (Applied Biosystems, Life Technologies) was used for standardization. PCRs were performed using an ABI 7500 System (Applied Biosystems) and a 3-step program (according to the master mix protocol). PCR amplicons were resolved on 2 % agarose gels using the Bio-Rad Sub-Cell system (Bio-Rad Laboratories GmbH, München, Germany). As size marker Gene RulerTM 100 bp DNA Ladder (Fermentas) was used.

Table 2. Primer sequences.

name	forward primer	reverse primer	product size [bp]
1453145_at	TGCACCAGGTCTGTTTCTGT	GGTGGCTGTTTCTCAGAAGG	196
1429452_x_at	GAAGCTTCTCGATTGGAAGC	CACTGCTCCAGTTGTTGGTG	257

2.6.4 Blast

Nucleotide sequences of probe sets corresponding to the transcribed sequence of *4933439C20Rik* were obtained from the NettAffx Analysis Center (Affymerix). Sequences were blasted against the mouse genomic and transcript database using the nucleotide blast tool on http://www.ncbi.nlm.nih.gov/ (NCBI).

2.7 Protein Analysis

Mice were sacrificed with an overdose of isofluran, exsanguinated and perfused with 20 ml cold PBS. Interscapular brown adipose tissue, skin (interscapular region) and heart were dissected. Calcified lesions were scraped out under a dissection microscope (Leica MZ6). Calcification-free tissue was collected as control tissue. Samples were frozen in liquid nitrogen and stored at -70 °C. Samples were thawed, transferred to 2 ml reaction tubes and incubated with SDS sample buffer (0.25 M TRIS (AppliChem GmbH, Darmstadt, Germany), 8.2 % SDS (AppliChem GmbH), 20 % glycerin (Fluka, St. Louis, MO, USA), 10 % β-mercaptoethanol (AppliChem GmbH), bromophenol blue (SERVA, Heidelberg, Germany)) containing 40 mM EDTA (ICN Biomedicals, Frankfurt, Germany) at 96 °C for 5 min. Approximately 10 µl of SDS sample buffer per 1 mg sample weight were used. The supernatant was removed and tissue pellets were homogenized for 2.5 min at 25 Hz in a mixer mill (Tissue Lyser II, Qiagen, Hilden, Germany). Afterwards samples were boiled 5 minutes in SDS sample buffer containing EDTA.

2.7.1 SDS-PAGE

Protein extracts were separated in 12.5 % polyacrylamid gels using SDS-PAGE [248]. Gels were washed in ultra-pure water and proteins were stained with Imperial Protein Stain (Thermo Fisher Scientific, Rockford, IL, USA) for 2 hours. Excessive stain was removed by washing in ultra-pure water over night. Pictures of gels were taken using a Canon DS126191 EOS Rebel XS SLR digital camera (Canon, Tokyo, Japan).

2.7.2 Mass Spectrometry Analysis

Protein bands of interest were cut out and vacuum dried in a Savant DNA SpeedVac DNA110 concentrator (Thermo Fisher Scientific). Tandem mass spectrometry analysis including sample digestion was performed by Ulrike Kusebauch, Institute For System

Biology, Seattle, WA, USA. Data analysis was conducted using Mascot algorithms [249]. The ion score cut-off was set to 30, representing a probability of 10^{-3}. Major proteins within a protein band were determined according to the exponentially modified protein abundance index (emPAI) [250].

2.8 CPP Preparation

2.8.1 Protein Purification

Bovine fetuin-A, asialofetuin and albumin (Sigma, Taufkirchen, Germany), respectively, were purified by gel filtration using a TRIS buffered HiLoad 16/60 Superdex 200 column (GE Healthcare, Freiburg, Germany) equilibrated in PBS and pumped at 1 ml/min according to a protein purification standard operation procedure (SOP) (supplemental protocol 1). The concentration of the pooled fetuin-A monomer and asialofetuin fractions was assessed photometrically ($E^{1\%}$ = 5.3 at 280 nm [115]). The concentration of the pooled albumin fractions was assessed using a Bradford-Assay (Roti-Nanoquant from Roth, Karlsruhe, Germany). Proteins were labeled with Alexa488 carboxylic acid, succinimidyl ester according to the labeling kit protocol (Invitrogen). Free label was removed using Zeba spin desalting columns (Thermo Scientific, Dreieich, Germany). Protein fractions were snap-frozen in liquid nitrogen and stored at –20 °C until use.

2.8.2 CPP Formation

Protein solutions were cleared by centrifugation (10,000 g, 10 min, 4 °C). CPPs were prepared by mixing stock solutions filtered through a 0.22 µm filter, to give a final concentration of 1.0 mg/ml fetuin-A, 10 mM $CaCl_2$, 6mM Na_2HPO_4, 140 mM NaCl, 50 mM Tris-HCl pH7.4 [14, 18]. CPP formation was performed according to a SOP (supplemental protocol 2). The precipitation mix was incubated for one hour at 37 °C and CPPs were separated from the monomer and concentrated by membrane filtration cartridges with a 300 kDa cut-off (Centrisart, Sartorius Stedim Biotech GmbH, Goettingen, Germany). Protein concentration in preparations was determined using a BCA-Assay (Thermo Scientific).

2.9 *In Vivo* Clearance of CPPs

Mice were injected *i.v.* with a maximum of 200 µl phosphate buffer solutions containing 160 µg fetuin-A, asialofetuin in form of monomeric protein or complexed as CPPs, respectively, with bovine serum albumin or with fluorescence labeled polystyrene beads of 0.17 µm or 0.055 µm diameter (Bangs Laboratories, Inc., Fishers, USA). Mice were sacrificed at 2, 10, 30, 60 and 180 minutes after injection to establish the serum clearing and organ distribution

of the different preparations. Serum samples taken immediately after injection (< 1 min) were assigned 100 % injected dose. To prepare organ extracts, mice were sacrificed with an overdose of isoflurane, exsanguinated, perfused with 20 ml cold PBS and tissues were collected.

2.9.1 Preparation of Serum and Tissue Samples

Tissues (liver, spleen, kidney, lung, heart, aorta, muscle, thymus, pancreas, gonads, skin, bone marrow, bone and brain) were split in half. One part was used for protein extraction. Organ pieces were weighed and washed in cold buffer A (50 mM TRIS/HCl (pH 7.4), 2 mM EDTA, 150 mM NaCl). Afterwards the tissue samples were homogenized in 10 parts (v/w) cold buffer B (50 mM Tris/HCl (pH 7.4), 10 % v/v glycerol, 5 mM magnesium acetate, 50 mM EDTA, 0.5 mM DTT (AppliChem GmbH), protease inhibitor cocktail (Complete (Roche, Mannheim, Germany)) in a Retsch MM300 Mixer Mill (for liver, kidney and pancreas samples 20 parts (v/w) were used). Samples were cleared by centrifugation at 10,000 g, 4 °C for 10 min. The supernatant was transferred into a fresh tube and the protein concentration was determined with a dye assay (Roti-Quant, Roth, Karlsruhe, Germany). Equal amounts of diluted tissue extracts as well as from diluted serum samples were separated using SDS-PAGE and the fluorescence signal was scanned with a Typhoon 9410 imager (GE Healthcare). The images were quantified by densitometry with the ImageJ software [251]. The remaining tissue was used for immunofluorescence staining (see chapter 2.3).

2.10 Cell Culture

All cells were cultured at 37 °C and 5 Vol.-% CO_2 in a humidified atmosphere (MCO-2OAIC CO2 incubator, Sanyo Biomedical, Bad Nenndorf, Germany). All cell handling was performed in a flow hood (Herasafe KSP 15, Thermo Fisher Scientific).

2.10.1 Cell Lines

Raw and J774A.1 macrophages, Hela cells, Cos1 and Cos7 cells and L929 cells were grown on tissue grade cell culture plates (Sarstedt, Nümbrecht, Germany) in Dulbecco´s Modified Eagle´s Medium (DMEM, Gibco, Life Technologies) or Roswell Park Memorial Institute (RPMI-1640, Gibco, Life Technologies) each containing 10 % FBS (Gibco, Life Technologies) and antibiotics, respectively. Detachment of cells was achieved by trypsin (Gibco, Life Technologies) treatment or by scraping with a rubber policeman (macrophages).

2.10.2 Production of M-CSF containing L929-Cell Conditioned Medium (LCM)

L929 cells were grown in DMEM medium containing 4.5 g/l glucose, 10 % fetal bovine serum (FBS), 29.2 mg/ml L-glutamin, 100 U penicillin and 100 µg streptomycin (media as well as

supplements were purchased from Gibco) on T-75 cell culture plates (Sartstedt) until 80-90% confluency. Cells were detached and transferred to T-175 flasks (Sarstedt) and grown for two more days. After that, cells were kept in media containing 5 % FBS and supernatant was harvested after day 2 and day 4. Collected supernatant was centrifuged at 3000 rpm, filtered through a 0.22 µm filter and aliquots were frozen at -20 °C.

2.10.3 Bone Marrow Derived Macrophage (BMM) Differentiation and Culture

Mice were sacrificed with an overdose of isofluran. Femur and tibiae of adult mice were dissected. The epiphyses were removed and bones were flushed with 20 ml of RPMI-1640 medium. The cell suspension was centrifuged at 250 x g for 5 min and resuspended in 2 ml of RPMI-1640 medium containing 10 % FBS, 20 % LCM, 29.2 mg/ml L-glutamin, 100 U penicillin and 100 µg streptomycin. Cells were seeded on two bacterial plastic dishes with a diameter of 15 cm (BD Pharmingen) containing 24 ml culture media each. At day 3 after seeding, cells were fed with 15 ml culture media. After 6 days cells were adherent and a medium change was performed. After that, medium was changed every three days. As cells were fully differentiated at this stage medium without LCM supplement was used. Experiments were carried out between day 9 and day 13 post bone marrow harvesting.

2.11 Binding Assay
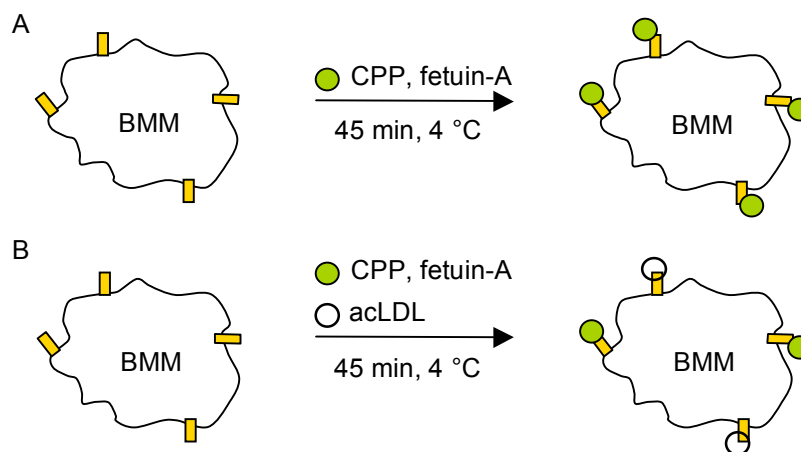
Figure 6. Schematic demonstration of CPP binding assays.
A. Binding assays performed on WT and KO macrophages (see table 3). Cells were incubated on ice with different concentrations of fetuin-A monomer or fetuin-A containing CPPs ranging from 0.01 mg/ml to 0.175 mg/ml. **B.** Competitive binding with acLDL. Macrophages were incubated on ice with CPPs in varying concentrations, ranging from 0.05 to 0.2 mg/ml fetuin-A contained in the medium in the presence or absence of 10 µg/ml acetylated LDL (acLDL).

Receptor binding was studied in cell lines or bone marrow derived macrophages harvested from mice deficient in different kind of clearing receptors. Table 3 lists all used mouse strains. BMMs were harvested and differentiated as described in chapter 2.10.3. Cell lines were used at approximately 80 % confluency and cells were detached as described in chapter 2.10.1,

BMMs were pre-treated with 10 mM EDTA for 10 min and scraped with a rubber policeman. Receptor binding assays were performed in reaction tubes with 500,000 cells (in 500 µl) + 500 µl dil-labeled acLDL (Molecular Probes), Alexa488-labeled CPPs or fetuin-A monomer containing serum-free medium for 45 minutes on ice. Cells were washed twice with medium and PBS at 4 °C, fixed with para-formaldehyde and cell-associated fluorescence was measured by flow cytometry (chapter 2.13).

2.12 Endocytosis Assay
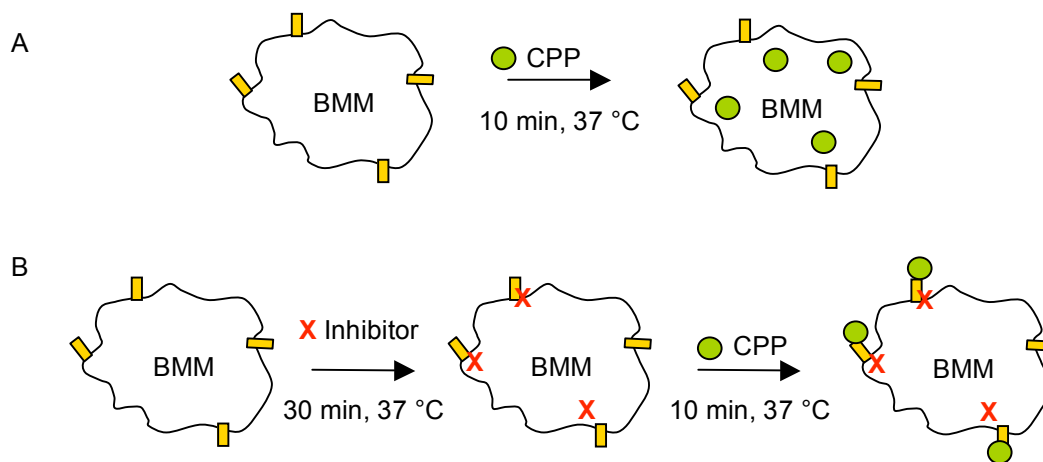
Figure 7. Schematic demonstration of CPP endocytosis assays.
A. Endocytosis assays performed on WT and KO macrophages (see table 3). Cells were incubated at 37 °C with different concentrations of fetuin-A containing CPPs ranging from 0.01 mg/ml to 0.175 mg/ml. **B.** Inhibition assays: Macrophages were pre-incubated with different endocytosis inhibitors. After that cells were incubated at 37 °C with CPPs in varying concentrations, ranging from 0.01 to 0.2 mg/ml fetuin-A contained in the medium.

2.12.1 Endocytosis Assay

The murine macrophage cell line Raw 246.7 or BMMs harvested from mice deficient in specific clearing receptors were used to study cellular uptake of fetuin-A and CPPs. Cells were seeded on 24-well cell culture plates (TPP, Trasadingen, Switzerland) with 250,000 cells per well over night. The cells were incubated for up to three hours with fluorescence labeled fetuin-A monomer or CPPs in fresh serum-free RPMI at different protein concentrations. In blocking experiment (all inhibitors were purchased from Sigma) cells were incubated for 30 min in the presence of cytochalasin D (10 - 40 µM), Ly294002 (10 – 100 µM) or polyinosinic acid (1 – 5 ng/µl, polyinosinic acid was removed for addition of CPPs) before 10 min incubation with CPPs. Cells were washed twice with PBS, fixed with para-formaldehyde and cell-associated fluorescence was measured by flow cytometry (chapter 2.13).

2.12.2 Modified Endocytosis Assay to Analyze the Role of Galectins

BMMs harvested from Galectin 1 or Galectin 3 deficient mice and wildtype mice were used to study cellular uptake of fetuin-A and CPPs in presence and absence of galectins. Cells were seeded on 24-well cell culture plates (TPP, Trasadingen, Switzerland) with 250,000 cells per well over night. Half of the wells were incubated with 1 µg/ml LPS (Sigma). For endocytosis assays the one half of the supernatant was removed and replaced by fresh serum-free RPMI containing fluorescence labeled fetuin-A monomer or CPPs at different protein concentrations. Macrophages were incubated 10 min at 37 °C. After that, cells were washed twice with PBS, fixed with para-formaldehyde and cell-associated fluorescence was measured by flow cytometry (chapter 2.13).

Table 3. Overview of clearance receptor-deficient bone-marrow derived macrophages studied in binding- and endocytosis assays.

deficiency	function in endocytosis	source
C57BL/6		
Annexin 5	phagocytosis of dead cells	Martin Herrmann (Erlangen, Germany)
Annexin 6	stimulation of LDL particle endocytosis	Martin Herrmann (Erlangen, Germany)
CD36	clearing of modified LDL particle	Peter Voshol (Leiden, Netherlands)
Dectin-1	binding of β-glucan and various unidentified bacterial and endogenous ligands	Gordon Brown (Aberdeen, UK)
FcγR	clearing of immune complexes and of SAP- and CRP- opsonized particles	Falk Nimmerjahn (Erlangen, Germany)
Galectin 1	inhibition of phagocytosis via FcγR	Martin Herrmann (Erlangen, Germany)
Galectin 3	enhancing clearance of apoptotic neutrophils	Martin Herrmann (Erlangen, Germany)
SR-A	clearing of modified LDL particle	Siamon Gordon (Oxford, UK)
Fetuin-A	enhancing clearance of apoptotic neutrophils	own breeding
WT	-	corresponding to KO or own breeding
DBA/2		
Fetuin-A	enhancing clearance of apoptotic neutrophils	own breeding
WT	-	own breeding

Note that CD36 macrophages were studied in collaboration with Laura Helming (München, Germany).
[79, 218, 227, 252-256]

2.13 Flow Cytometry

Cell-associated fluorescence was measured by flow cytometry using a FACSCalibur system (Becton Dickinson, Heidelberg, Germany), excitation optics: 15 mW 488 nm argon-ion laser; emission optics: photomultiplier with band-pass filter: 530/30 nm; detection channel: green

channel (FL-1H). 5,000 – 10,000 cells were evaluated per sample. The analysis was performed using CellQuestPro software (Becton Dickinson).

2.14 Statistics

Statistical analysis was performed using Prism 4 software (Graphpad, La Jolla, CA, USA). One-way ANOVA with Tukey's multiple comparison test was used to test for overall differences in non-size matched experimental groups. Experiments containing two factors were analyzed with two-way ANOVA with Bonferroni post test. Curve fitting was performed assuming linear or nonlinear regression.

3. Results

3.1 The Pathology of Ectopic Calcification in Fetuin-A Deficient Mice

Fetuin-A is a well-studied systemic inhibitor of ectopic calcification [55]. Consequently, fetuin-A deficient mice develop pathological mineralization. Whereas fetuin-A deficient mice backcrossed on the calcification sensitive genetic background DBA/2 (D2) showed widespread soft tissue calcifications [56], mice combined with C57BL/6 (B6) background were resistant to spontaneous ectopic mineralization. Nonetheless, uremic B6 fetuin-A deficient mice on a high phosphate diet also developed extraosseous calcification [114].

In this thesis, soft tissue calcification in D2 fetuin-A deficient mice was examined. A detailed analysis of the pathology of ectopic calcification should contribute to a better understanding of the underlying mechanism leading to the severe phenotype in D2 fetuin-A deficient mice.

3.1.1 Severe Soft Tissue Calcification in Adult D2 Fetuin-A Deficient Mice

The phenotype of D2 fetuin-A deficient mice was studied before by Schäfer et al. It was shown that mice develop soft tissue calcification in heart, lung, testis, skin, tongue and kidney [56]. Here the severe ectopic calcification is demonstrated by photographs of a representative necropsy (figure 8). The observed mouse was a female ex-breeder and 42 weeks of age. Soft tissue calcification was observed in interscapular brown adipose tissue (figure 8D-E), heart (figure 8B, F), lung (figure 8G), spleen (figure 8H), pancreas (figure 8I), kidneys (figure 8C, J), ovaries (figure 8C, K) and skin (not shown). Calcification in interscapular brown adipose tissue appeared as macroscopically visible spherical lesions (arrowheads in figure 8D, E). The heart had a heavily enlarged left atrium (figure 8B, F), calcified lesions spread throughout the myocardium and were of millimeter size (exemplary lesions are marked by arrowheads in figure 8F). Lesions in lung were spherical but considerably smaller than lesions in brown adipose tissue; in the photomicrograph they are observable as evenly distributed white spheres (figure 8G). In spleen lesions were randomly spread through the red pulp. The lesions appeared as white spheres, the size of the lesions was diverse. In average spleen lesions exceeded the size of lesions found in lung (figure 8H). Lesions in pancreas were reminiscent of those in interscapular brown adipose tissue (figure 8E, I). The kidneys showed severe ectopic calcification: a great number of white spherical lesions occurred in the cortex (figure 8J).
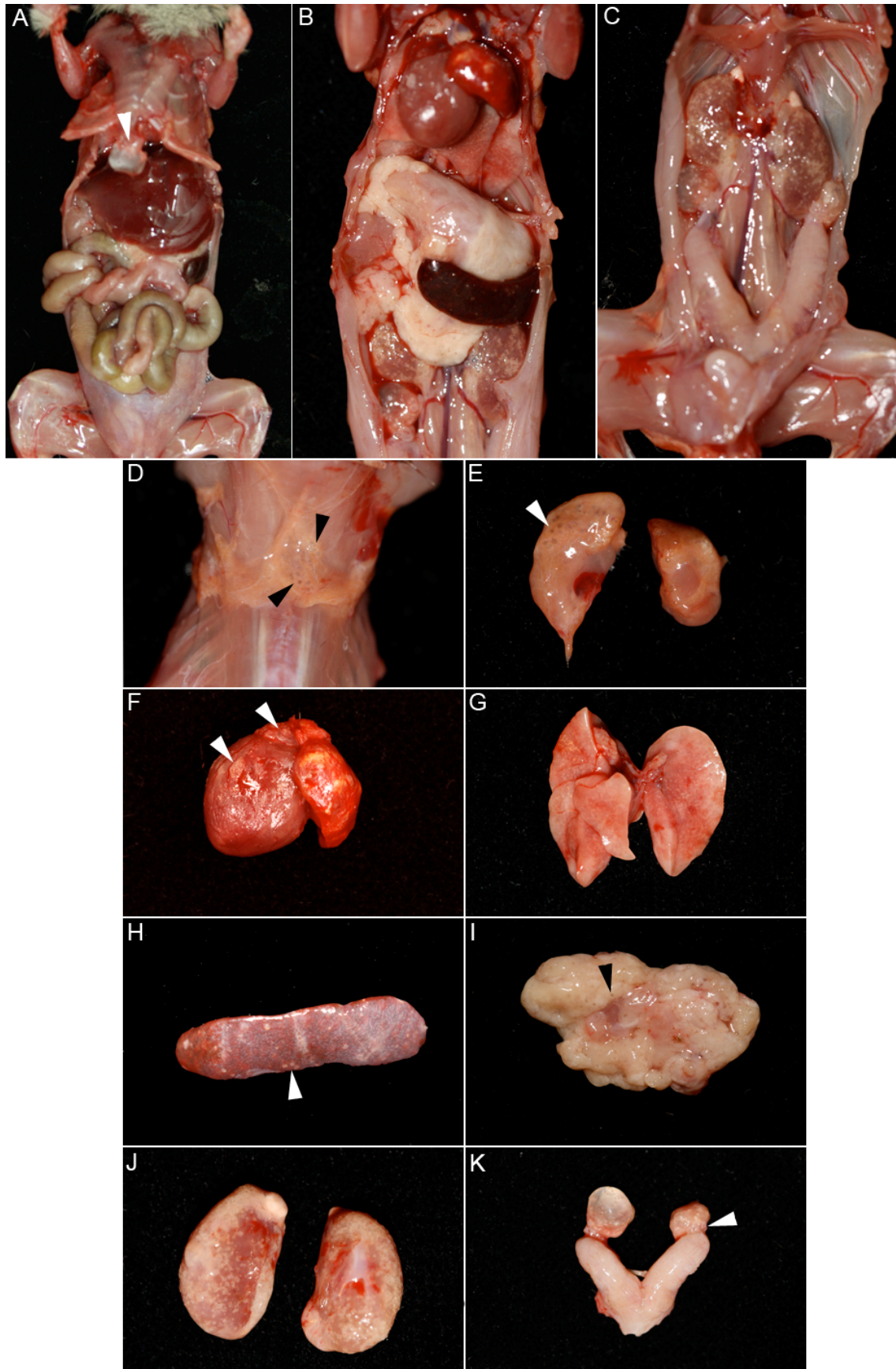
Figure 8. Necropsy of a female D2 fetuin-A deficient mouse.
The abdomen was opened and organs were subsequently removed (A-C). Severe ectopic calcification was observed in interscapular brown adipose tissue (D-E), heart (B, F), lung (G), spleen (H), pancreas (I), kidneys (C, J) and ovaries (C, K). The left ovary showed a cystoid shape. Arrowheads indicate exemplary calcified lesions (B-K) and the enlarged sternum (A).

Finally, gonads were observed. The uterus horns appeared normal, ovaries showed severe calcification (the arrowhead in figure 8K indicates an exemplary calcification). The left ovary was cystic (figure 8K). Beside the ectopic calcification the mouse had a heavily enlarged sternum (figure 8A).

In conclusion, several month old D2 fetuin-A deficient mice showed severe soft tissue calcification. Lesion morphology was dependent on the affected tissue. However, in most tissues lesions were spherical and appeared transparent to white. In all organs observed lesions were detectable macroscopically. Eventually, abnormalities including formation of cysts in ovaries (figure 8K) and kidneys (not shown) were observed.

3.1.2 Early-stage Calcified Lesions Colocalize with the Microvasculature

Formation of calcified lesions was studied in young D2 fetuin-A deficient mice. First a technique suitable to detect early stage lesions of micrometer scale even in immunofluorescence staining had to be developed. On the one hand a recently patented method was used [238]. It was shown that fetuin-A injected *intraperitoneal* into fetuin-A deficient mice accumulated at calcification sites [257]. Thus, immunofluorescence staining on cryosections from fetuin-A injected mice with a fetuin-A specific antibody was performed to detect calcified lesions. It was also previously published that osteopontin (OPN) accumulates in calcified lesions [258]. Therefore, antibody staining of OPN was used to identify calcified lesions. Both fetuin-A and OPN detected calcified lesions with high sensitivity even at early small stages (2 weeks age, figures 9A, E) that were invisible in histology and X-ray analysis.

To draw a conclusion on the mechanisms of lesion formation it was of great interest to study whether the lesion formation occurred intra- or extracellular and whether lesion formation might take place within the vasculature. Consequently, double staining of OPN or fetuin-A stained calcified lesions and either an endothelial marker, namely CD31, or the lymph duct marker lyve-1 was performed. Figure 9A and 9E shows early-stage lesions clearly localized inside capillaries. Even at late stage lesions CD31-positive vessels were found in tight proximity to the lesions (figures 9B, D, F). In contrast, double staining with lyve-1 revealed that there was no colocalization with lymphatic vessels (figures 9C, D).

In summary, early-stage calcified lesions in lung and brown adipose tissue could be identified and readily stained by fetuin-A and OPN, respectively. These lesions as well as late-stage lesions in myocardium were in tight association with the microvasculature, but not with lymph ducts.
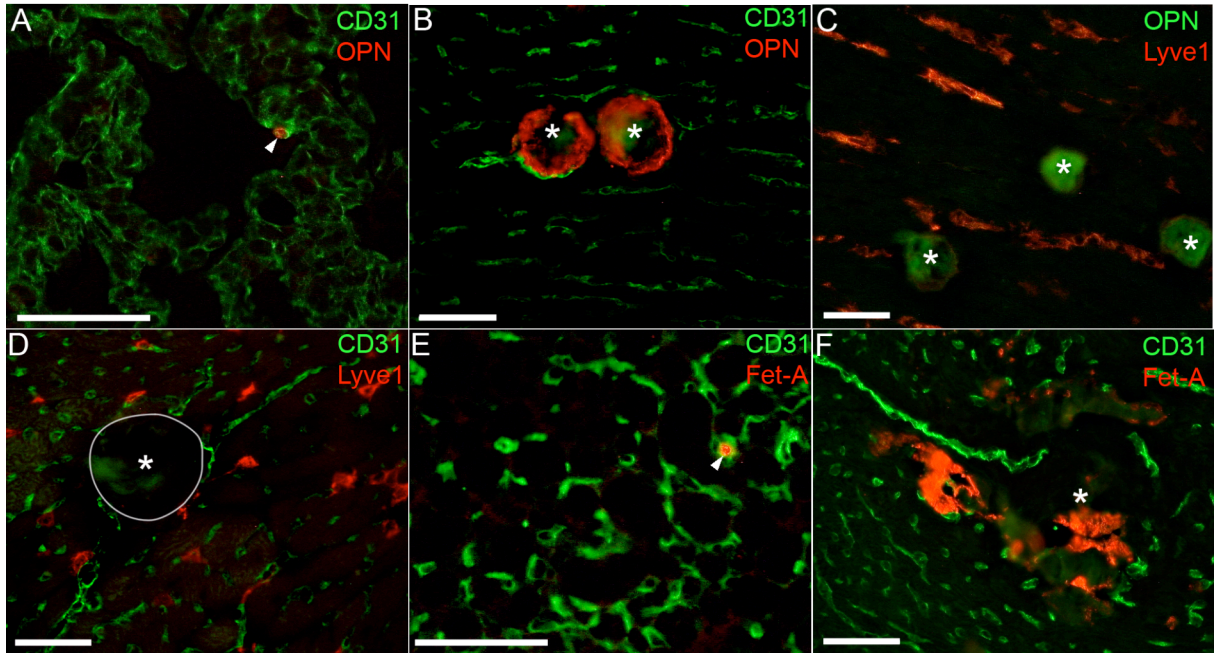
Figure 9. Colocalization of early stage calcified lesions and vascular markers.
Immunohistochemistry of cryosections prepared from brown adipose tissue (E), lung (A) or myocard (B-D, F) of D2 fetuin-A deficient mice. Calcified lesions stained positive for OPN (A, B) and were demarcated by CD31, an endothelial marker (B, D) but not by Lyve-1 a lymph duct marker (C, D). Injected fetuin-A bound to calcified lesions and was readily detected using fetuin-A antibody (E, F). Even at early small stages (2 weeks age A, E) fetuin-A like OPN staining detected calcified lesions with high sensitivity that were invisible in histology and X-ray analysis. The fetuin-A stained lesion in E was enclosed by CD31-positive endothelial cells. Asterisks and arrowheads indicate calcified lesions. Scale bars 50 µm.

3.1.3 Transmission Electron Microscopy of Calcified Lesions

Transmission Electron Microscopy (TEM) was applied to study the micro-architecture of calcified lesions in 2-week-old D2 fetuin-A deficient mice. Ectopic calcification in D2 fetuin-A deficient mice occurred in most soft tissue types [56]. However, as shown before (chapter 3.1.1) the morphology of soft tissue calcification was tissue dependent. Here, interscapular brown adipose tissue was studied because in this tissue (i) recent findings suggested that calcification is initiated very early and (ii) soft tissue calcification is severe.

In fact, TEM of early-stage calcified lesions in interscapular brown adipose tissue demonstrated a broad spectrum of lesion morphologies. Nonetheless, it was possible to classify the lesions into three categories:

Type 1: Lesions with concentric rings of alternating high and low electron density (figure 10).

Type 2: Diffuse lesions within the microvasculature (figure 11).

Type 3: Electron dense lesions (figure 12).
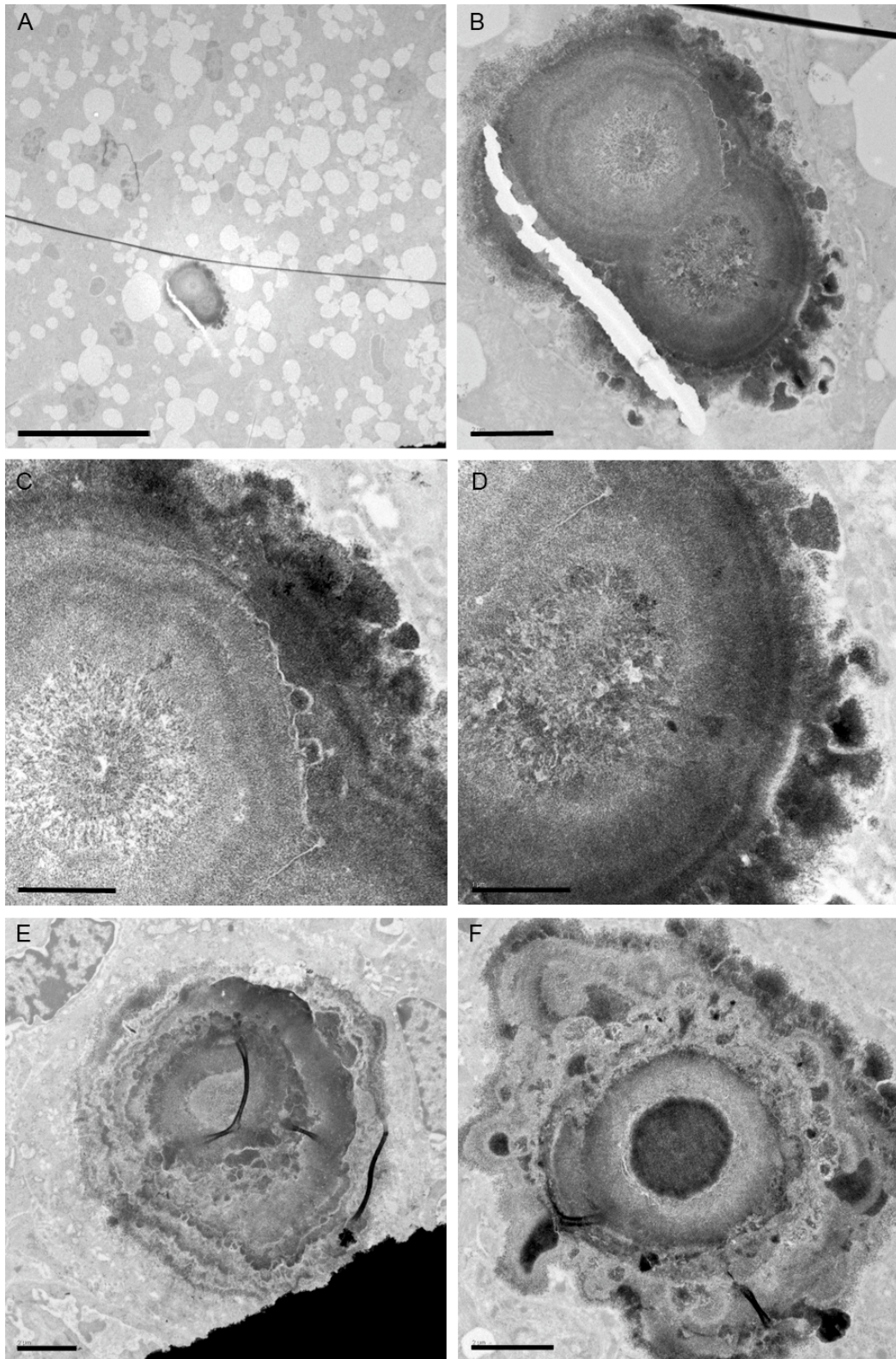
Figure 10. Lesions with concentric rings of alternating high and low electron density.
TEM of calcified lesions in brown adipose tissue dissected from a 2-week-old D2 fetuin-A deficient mice suffering from severe soft tissue calcification. Various spherical mineral precipitates with alternating layers of high and low electron densities were observed. Three different morphologies of calcified lesions are shown. Spheres had a diameter ranging from 6 to 9 µm. A: Calcified lesion embedded in brown adipose tissue, rich in lipid vacuoles. B: Inset of A. Calcified lesion built of two spheres attached to each other. Spheres displayed "tree-aging-ring-like" structures of layers with varying electron density. The outer layer of lesions was not clearly defined and included several roundish extensions. C, D: Inset of B. E: Round calcified lesion built of multiple concentric layers. F: Lesion consisting of an electron dense core surrounded by a broad layer with lower electron density. This core is enclosed by a diffuse layer consisting of several electron dense spots. Scale bars: 20 µm (A); 2 µm (B, E, F); 1 µm (C, D).
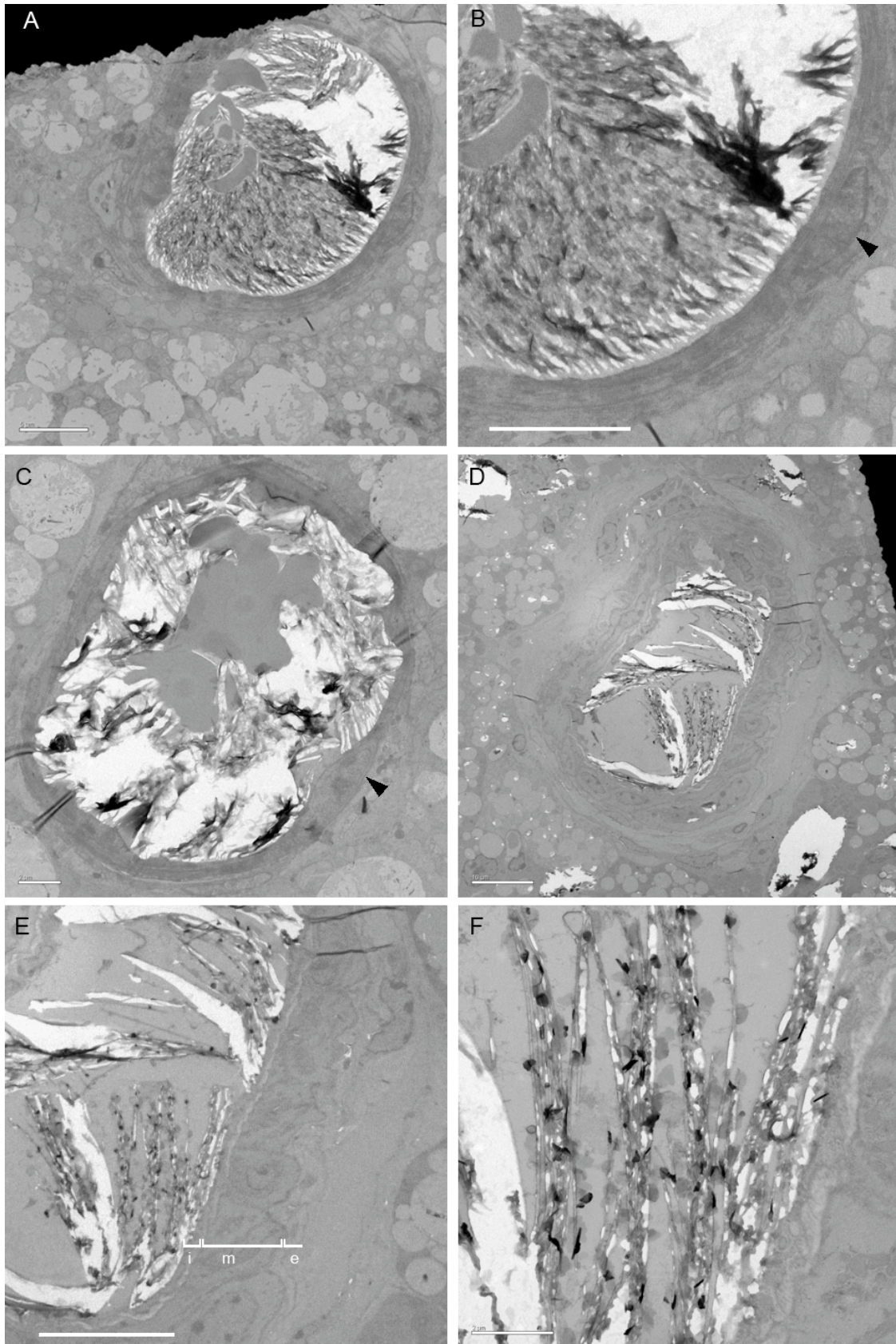
Figure 11. Difuse lesions within the microvasculature.
TEM of calcified lesions in brown adipose tissue dissected from a 2-week-old D2 fetuin-A deficient mice suffering from severe soft tissue calcification. Lesions were observed within the microvasculature. All lesions consisted of electron dense filamentous mineral debris and organic and cellular conglomerate with less electron density. A-C: Calcified lesion surrounded by endothelium, the arrowheads indicate nuclei of endothelial cells. B: Inset of A. D-F: Calcified lesion within an arteriole, clearly identified by the characteristic composition of its vessel wall: i = tunica intima; m = tunica media; e = tunica externa. E, F: Magnification of D. Scale bars: 10 µm (D-E); 5 µm (A, B); 2 µm (C, F).
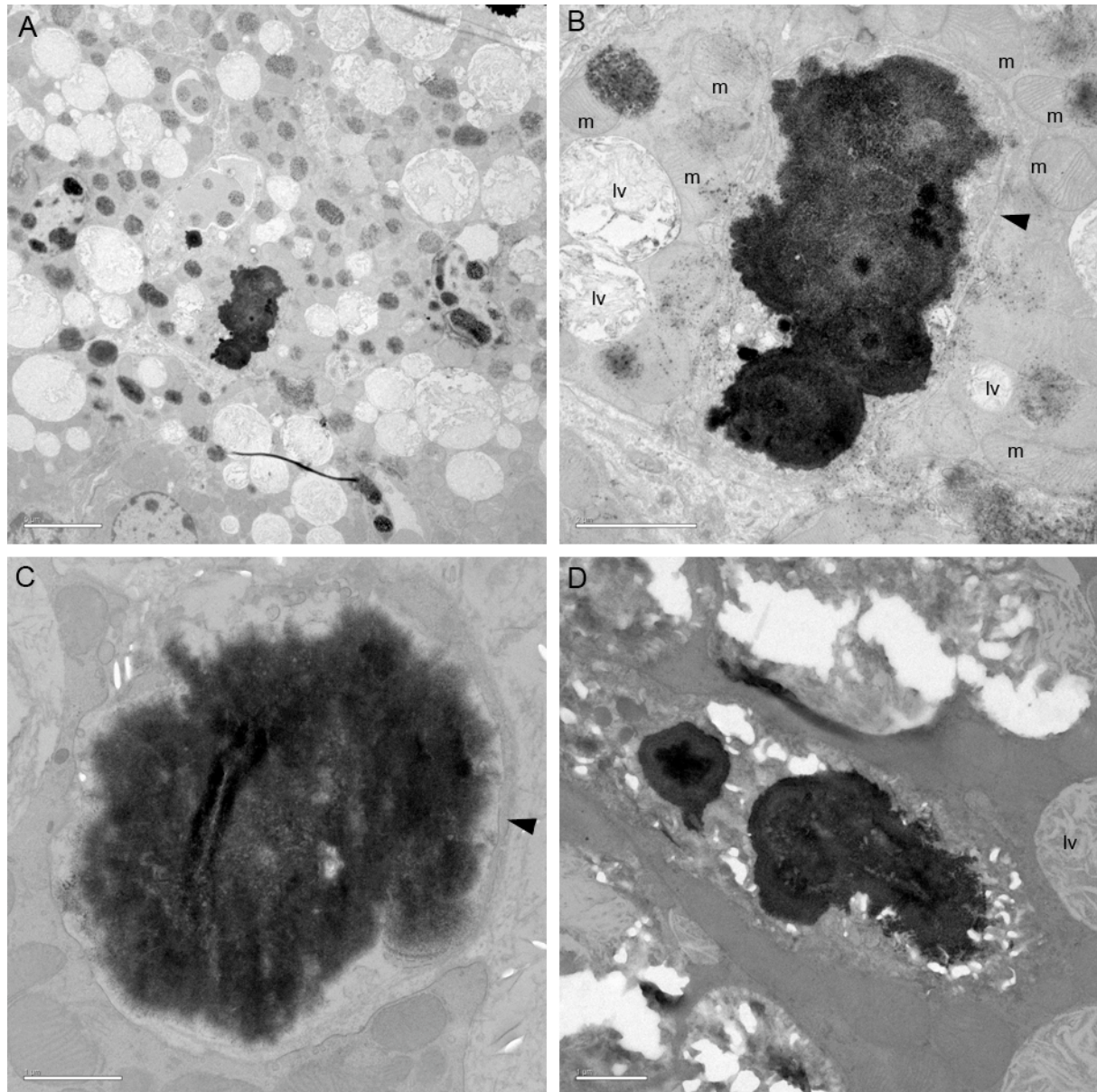
Figure 12. Electron dense lesions.
TEM of calcified lesions in brown adipose tissue dissected from a 2-week-old D2 fetuin-A deficient mice suffering from severe soft tissue calcification. A: Electron dense lesions embedded in brown adipose tissue rich in lipid vacuoles. B: Inset of A. Electron dense lesion, which might have developed by aggregation of several roundish lesions. Each of these round building blocks had a diameter of approximately 2 µm. The lesion was enclosed by membranous structures. C: A diffuse conglomerate of electron dense material was visible. The lesion was surrounded by membranous structures. D: Intracellular electron dense lesions. Lipid loaded vacuoles were found in proximity to the lesions indicating a brown adipocyte. m = mitochondria; lv = lipid vacuole; arrowheads indicate membranous structures. Scale bars: 5 µm (A); 2 µm (B); 1 µm (C, D).

Type 1 lesions were spherical and had a diameter ranging from 6 µm to 9 µm. They occurred either as single spheres (figure 10E-F) or as cluster of two spheres (figure 10A-B). The lesion shown in figure 10A-D was built of rings with alternating electron density resembling tree-aging-rings. This highly organized structure was found in particular in the core of the lesion whereas the outer layer was mostly unorganized and diffuse. In contrast, the lesion shown in figure 10E was not perfectly spherical, but was built of several layer with varying electron density. In this case, the "tree-aging-ring-like" structure was found as well in the outer layer of

the lesion. A third example of a type 1 lesion is shown in figure 10F. The lesion consisted of an electron dense core surrounded by a broad layer of lower electron density. The following layer was less organized and diffuse, it contained several single spots of high electron density. Type 2 lesions were found within the microvasculature. The lesions shown in figure 11A-C were surrounded by a single layer of endothelium. Nuclei of endothelial cells are indicated by arrowheads. The diameter of the vessels was about 19 µm (figure 11A) and 17 µm, respectively (figure 11C). The lesion shown in figure 11D-E was located within a small arteriole, it was surrounded by an endothelium (tunica intima) enclosed by a single layer of smooth muscle cells (tunica media) and the tunica externa. The arteriole had a diameter of approximately 35 µm (figure 11D). All type 2 lesions were composed of fibrous, electron dense mineral precipitate and organic conglomerate with less electron density. Type 3 lesions were the most diverse lesions observed, their morphologies ranged from clusters of electron dense spheres (figure 12A-B) to electron dense diffuse precipitates (figure 12D). Lesions shown in figure 12B, D were detected in tight proximity to lipid vacuoles and mitochondria, both characteristics of brown adipocytes. To some extent membranous structures enclosed the lesions (see arrowheads in figure 12B, D).

In summary, calcified lesions in D2 fetuin-A deficient mice showed diverse form, structure and localization. Despite this diverging morphology, lesions could be divided into three subtypes: lesions with concentric rings of alternating high and low electron density (type 1 lesions), diffuse lesions within the microvasculature (type 2 lesions) and electron dense lesions (type 3 lesions).

3.1.4 Gene Expression Analysis

3.1.4.1 Differential Gene Expression in Calcified Brown Adipose Tissue

In newborn mice brown adipose tissue is mainly localized between the scapulae [259], another deposit is found in the kidney pelvis region. Brown adipose tissue can be considered homogeneous with a limited number of cell types. Therefore, brown adipose tissue dissected from the kidney pelvis was chosen to compare the gene expression profile of calcified D2 fetuin-A deficient mice and wildtype controls. The quality of microarrays was assessed using the ArrayQualityMetrics package [241] under Bioconductor [239]. Figure 13 illustrates the analysis. Arrays, which scored as outliers in two or more tests were considered poor quality and were excluded from further analysis.
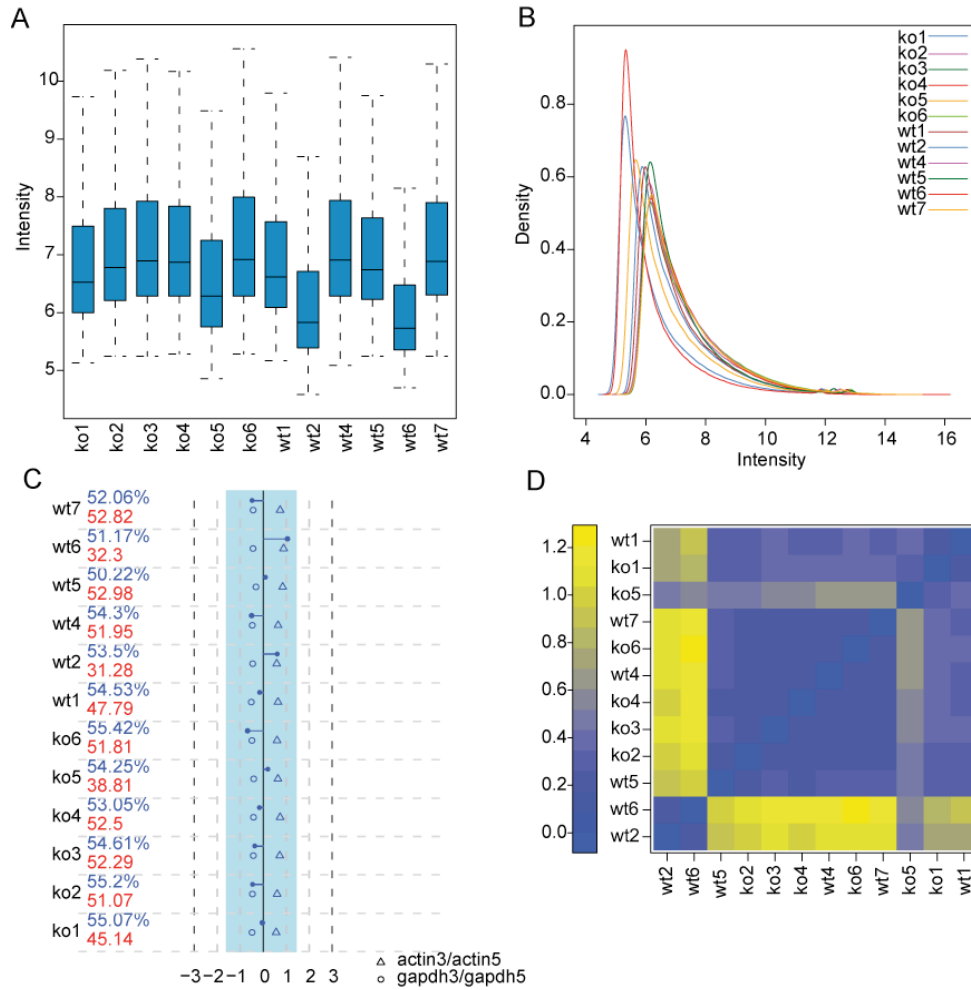
Figure 13. Quality assessment of brown adipose tissue microarrays.
Quality of microarrays was assessed using arrayQualityMetrics package under Bioconductor. **A:** Boxplot demonstration of array intensity distribution. Each box corresponds to one array. The plot summarizes the distribution of probe intensities (log₂ Intensities are plotted on the y-axis) across all arrays. Boxes should have similar size and y position (median). Sizes of boxes were in the same range, whereas the comparison of medians revealed that array ko5, wt2 and wt6 were outliers, particularly medians of wt2 and wt6 were remarkably low. **B:** Density plot illustrates the density of a given intensity within an array; one would expect a similar pattern for all arrays. The arrays wt2 and wt6 were biased towards low intensity probes, which qualified those arrays as outliers. **C:** Affymetrix quality control (QC) stats report. The percentage of "present" calls is given for each array in the left row in blue, the red numbers indicate the average background value for each array. The percentage of present calls is similar in all arrays. The background level is remarkably low for arrays wt2 and wt6 as already seen in A and B. The relation between 3' probe sets and 5' probe sets of the control genes β-actin (triangles) and GAPDH (circles) was within the recommended range (light blue box) for all arrays. **D:** Heatmap representation of the distance between arrays. The false colour heatmap indicates the mean absolute distance of the M-values for each pair of arrays, with M = log₂(intensity₁) - log₂(intensity₂), where intensity₁ is the intensity of the array studied and intensity₂ is the intensity of a "pseudo"-array, which has the median values of all the arrays. This plot confirmed wt2 and wt6 as outliers. Note that ko1-3, wt1-2 and wt7 were females and ko4-6, wt4-6 were males.

Figure 13A shows a boxplot of array intensity distribution. The mean intensity of the arrays ko5, wt2 and wt6 diverged remarkably from the other arrays. This difference of wt2 and wt6 was also observed in the density plot (figure 13B). The ratio of 3 prime and 5 prime probe sets of the constitutively expressed control genes *β-Actin* and *Gapdh* is commonly used to judge RNA quality according to an Affymetrix recommendation. The RNA quality of all arrays was good as the ratio of both control genes matched the recommended range (figure 13C). However, the Affymetrix quality control report identified the arrays wt2 and wt6 to have

remarkably low overall background intensity values. These arrays were likewise reported as outliers by distance measuring (figure 13D). Therefore, the arrays wt2 and wt6, corresponding to one female and one male wildtype animal, were removed from the data set, whereas the array ko5 was retained as it had only one outlier call. The data from the remaining ten arrays were normalized and tested for differential expression among KO and WT animals using Bayesian statistics. Volcano plot demonstration shown in figure 14 showed several genes significantly upregulated and a lower number of genes significantly downregulated in KO mice.

Figure 14. Gene expression in adipose tissue of D2 wildtype and knockout mice.
Volcano plot representatation of gene expression in brown adipose tissue dissected from the region of kidney pelvis. Examined mice had D2 genetic background and were 6 weeks old. Differential expression between fetuin-A deficient and wildtype mice is shown as log-ratio on the x-axis, negative values represent higher expression in KO mice, positive values represent higher expression in wildtype mice. The y-axis encodes the probability for differential regulation calculated by Bayesian statistics in the Limma package under Bioconductor. Each dot denotes a probe set, probe sets with highest probability score are depicted in blue and probe sets with highest log-ratio are depicted in red, marked probe sets are labeled with the appropriate gene name.

In total 395 probe sets (supplemental table 1) were found to be significantly differentially regulated (genes with a p-value < 0.05 after multiple testing correction were considered as significant). Most significant probe sets (red label) and probe sets with highest fold change (blue label) were annotated with the corresponding abbreviation of the gene name. All significant genes with a fold change above four (log-ratio >2) are summarized in table 4.

Table 4. Differential expression in adipose tissue.

probe set	symbol	p-value	log-ratio
upregulation			
RIKEN cDNA 1110032A04 gene	1110032A04Rik	0.004	-6.977
small proline-rich protein 1A	Sprr1a	0.005	-6.021
small proline-rich protein 2A	Sprr2a	0.005	-5.495
small proline-rich protein 2A	Sprr2a	0.009	-4.683
RIKEN cDNA 1110032A04 gene	1110032A04Rik	0.003	-4.369
myelin and lymphocyte protein, T-cell differentiation protein	Mal	0.001	-4.316
matrix metallopeptidase 12	Mmp12	0.001	-4.315
transmembrane protease, serine 2	Tmprss2	0.008	-4.157
secreted phosphoprotein 1	Spp1	0.024	-4.116
uroplakin 3A	Upk3a	0.014	-3.949
lymphocyte antigen 6 complex, locus D	Ly6d	0.002	-3.845
sorting nexin 31	Snx31	0.008	-3.728
forkhead box A1	Foxa1	0.001	-3.628
myelin protein zero	Mpz	0.001	-3.525
Purkinje cell protein 4	Pcp4	0.001	-3.493
prostate stem cell antigen	Psca	0.008	-3.436
carnitine palmitoyltransferase 1b, muscle	Cpt1b	0.006	-3.390
WAP four-disulfide core domain 2	Wfdc2	0.022	-3.351
cadherin 1	Cdh1	0.007	-3.256
claudin 4	Cldn4	0.002	-3.185
pyridoxal-dependent decarboxylase domain containing 1	Pdxdc1	< 0.001	-3.159
myelin basic protein	Mbp	0.001	-3.148
forkhead box Q1	Foxq1	0.001	-3.137
involucrin	Ivl	0.005	-3.078
transmembrane protease, serine 2	Tmprss2	0.016	-3.063
FXYD domain-containing ion transport regulator 3	Fxyd3	0.001	-3.056
keratin 18	Krt18	0.002	-3.046
chloride channel calcium activated 2	Clca2	0.001	-2.976
small proline-rich protein 2F	Sprr2f	0.001	-2.969
myelin basic protein	Mbp	0.001	-2.943
gasdermin C2	Gsdmc2	0.028	-2.917
chloride channel calcium activated 2	Clca2	0.010	-2.904
regulator of G-protein signaling 1	Rgs1	0.043	-2.862
grainyhead-like 2 (Drosophila)	Grhl2	0.001	-2.799
transmembrane protease, serine 2	Tmprss2	0.008	-2.798
ring finger protein 128	Rnf128	0.020	-2.792
myelin basic protein	Mbp	0.003	-2.785
otopetrin 1	Otop1	0.043	-2.784
keratin 20	Krt20	0.001	-2.775
ring finger protein 128	Rnf128	0.011	-2.772
GATA binding protein 3	Gata3	< 0.001	-2.743
myelin basic protein	Mbp	0.001	-2.702
cytochrome c oxidase, subunit VIIa 1	Cox7a1	0.030	-2.699
myelin basic protein	Mbp	0.003	-2.654
keratin 7	Krt7	0.027	-2.652
uroplakin 1A	Upk1a	0.010	-2.623
sonic hedgehog	Shh	0.012	-2.619
epiphycan	Epyc	0.001	-2.600
pyruvate dehydrogenase kinase, isoenzyme 4	Pdk4	0.005	-2.597
calponin 1	Cnn1	0.005	-2.535
RIKEN cDNA 1600029D21 gene	1600029D21Rik	0.047	-2.506
keratin 5	Krt5	0.001	-2.504
steroid 5 alpha-reductase 1	Srd5a1	0.002	-2.504
forkhead box Q1	Foxq1	0.005	-2.497
SH3-binding domain glutamic acid-rich protein	Sh3bgr	0.007	-2.492
SH3-domain GRB2-like 2	Sh3gl2	0.001	-2.454

RIKEN cDNA 1600029D21 gene	1600029D21Rik	0.006	-2.451
myosin, heavy polypeptide 11, smooth muscle	Myh11	0.003	-2.416
aquaporin 3	Aqp3	0.009	-2.409
SH3-domain GRB2-like 2	Sh3gl2	0.001	-2.406
PERP, TP53 apoptosis effector	Perp	0.029	-2.340
shisa homolog 3 (Xenopus laevis)	Shisa3	0.001	-2.324
aquaporin 3	Aqp3	0.010	-2.311
aquaporin 3	Aqp3	0.008	-2.290
interleukin 1 receptor antagonist	Il1rn	0.033	-2.255
RIKEN cDNA 2200001I15 gene	2200001I15Rik	0.007	-2.222
cathepsin E	Ctse	0.001	-2.203
tetraspanin 8	Tspan8	0.011	-2.185
claudin 7	Cldn7	0.005	-2.178
interferon regulatory factor 6	Irf6	0.044	-2.177
apolipoprotein D	Apod	0.005	-2.159
transmembrane protein 30B	Tmem30b	0.012	-2.158
myelin basic protein	Mbp	0.005	-2.140
vesicle amine transport protein 1 homolog-like (T. californica)	Vat1l	0.001	-2.137
serine protease inhibitor, Kunitz type 1	Spint1	0.033	-2.132
myocardin	Myocd	0.010	-2.110
regulating synaptic membrane exocytosis 1	Rims1	0.003	-2.087
steroid 5 alpha-reductase 1	Srd5a1	0.002	-2.070
actin, gamma 2, smooth muscle, enteric	Actg2	0.009	-2.057
claudin 23	Cldn23	0.005	-2.044
flavin containing monooxygenase 5	Fmo5	0.013	-2.030
cell death-inducing DNA fragmentation factor, alpha subunit-like effector A	Cidea	0.009	-2.022
deiodinase, iodothyronine, type II	Dio2	0.022	-2.015
RIKEN cDNA 4930550L11 gene	4930550L11Rik	0.006	-2.011
downregulation			
pyridoxal-dependent decarboxylase domain containing 1	Pdxdc1	< 0.001	4.111
cytochrome b reductase 1	Cybrd1	< 0.001	3.119
penta-EF hand domain containing 1	Pef1	< 0.001	3.108
basonuclin 1	Bnc1	0.004	2.587
glycoprotein m6a	Gpm6a	0.005	2.483
mesothelin	Msln	0.008	2.460
glycoprotein m6a	Gpm6a	0.023	2.355
fibroblast growth factor 1	Fgf1	0.007	2.091
plakophilin 2	Pkp2	0.028	2.011

The table shows probe sets, which were significant (p-value < 0.05) differentially expressed in adipose tissue dissected from 6 weeks old D2 wildtype and fetuin-A deficient mice. Bayesian statistics was used for calculation of probabilities (p-value) and log-ratio, negative log-ratio encode upregulation of the particular probe-set in fetuin-A deficient mice, positive values denote downregulation. The table shows most highly differentially regulated genes with a log-ratio above 2. Note that gene names are given for each probe set, double entries may occur in case of genes which are represented by several probe sets encoding different regions or splice variants of the gene.

In total 93 probe sets matched those criteria, 84 probe sets were upregulated in KO mice and nine were downregulated. Among the ten most highly upregulated probe sets, two members of the small proline rich (sprr) protein family were found, a protein family previously associated with various inflammatory diseases [260-262] and cellular stress response [263]. Sprr1a was 64.9 fold increased, Sprr2a was represented by two probe sets with 45.1 and 25.7 fold upregulation in KO mice respectively. The two probe sets corresponding to the transcribed sequence 1110032A05Rik with fold changes of 126 and 20.7 were further highly upregulated probe sets. They encode the small subunit of serine palmitoyltransferase B with unknown

function. The myelin and lymphocyte protein (Mal) had a fold change of 19.9. The matrix metallopeptidase 12 (Mmp12), involved in extracellular remodeling, showed a fold change of 19.9. The transmembrane protease, serin 2 (Tmprss2) had a fold change of 17.8. Uroplakin 3A showed a fold change of 15.4. Finally, the secreted phosphoprotein 1 (Spp1), with a fold change of 17.3 was detected as another highly upregulated probe set. Spp1 is also known as osteopontin, a protein with various biological functions, which was previously histologically detected at calcified deposits [258, 264, 265].

All significant probe sets, in total 395, were screened for biological function using the KEGG gene set. Table 5 lists ten gene sets, which were significantly overrepresented among the tested probe sets. Several pathways related to tissue remodeling, namely focal adhesion, ECM-receptor interaction, cell cycle, p53 signaling, cell adhesion molecules and notch signaling pathway were amongst the differentially regulated pathways.

This part of the thesis aimed to analyze changes in gene expression of calcifying brown adipose tissue in the kidney pelvis region. In summary, the gene expression analysis of brown adipose tissue revealed a strong change in gene expression pattern in response to soft tissue calcification. A program of tissue reorganization was initiated by upregulation of several genes. Most of them were found to be members of KEGG gene sets related to tissue remodeling. However, no probe sets associated with the process of deposition of calcium phosphate were found to be differentially regulated. Thus, all identified changes were likely secondary to the soft tissue calcification.

Table 5. Pathway analysis of significant regulated genes.

KEGG pathway	size	exp. count	count	p-value
Focal adhesion	174	4	11	0.001
ECM-receptor interaction	74	2	6	0.004
Cell cycle	100	2	7	0.005
p53 signaling pathway	54	1	5	0.005
Small cell lung cancer	79	6	2	0.006
Selenoamino acid metabolism	25	1	3	0.015
Aminophosphonate metabolism	13	1	3	0.03
Cell adhesion molecules (CAMs)	115	2	6	0.034
Notch signaling pathway	37	1	3	0.043
Bladder cancer	37	1	3	0.043

Differentially expressed probe sets in adipose tissue were tested of overrepresentation of KEGG gene sets. For each gene set the name of the pathway and the corresponding size is given. The expected count (exp. count) estimates the count of random hits, which depends on the size of the pathway and the number of tested probe sets. The count gives the actual number of significant probe sets matching the specific pathway. The probability of overrepresentation of the gene set is assumed by the p-value.

3.1.4.2 Differential Gene Expression in Kidney

Gene expression profile of kidneys was examined in 5-week-old D2 *Ahsg* -/- and *Ahsg* +/+ mice. Previously it was shown that ectopic calcification in D2 fetuin-A deficient mice in most tissues was detectable from an age of approximately 2 weeks, whereas soft tissue

calcification in kidneys started considerably later [264]. Therefore, in kidneys of 5-week-old mice the calcification should not exceed a few early stage calcified lesions. Thus evaluation of the gene expression pattern in these mice may provide insights into the mechanisms preceding the formation of calcified lesions.
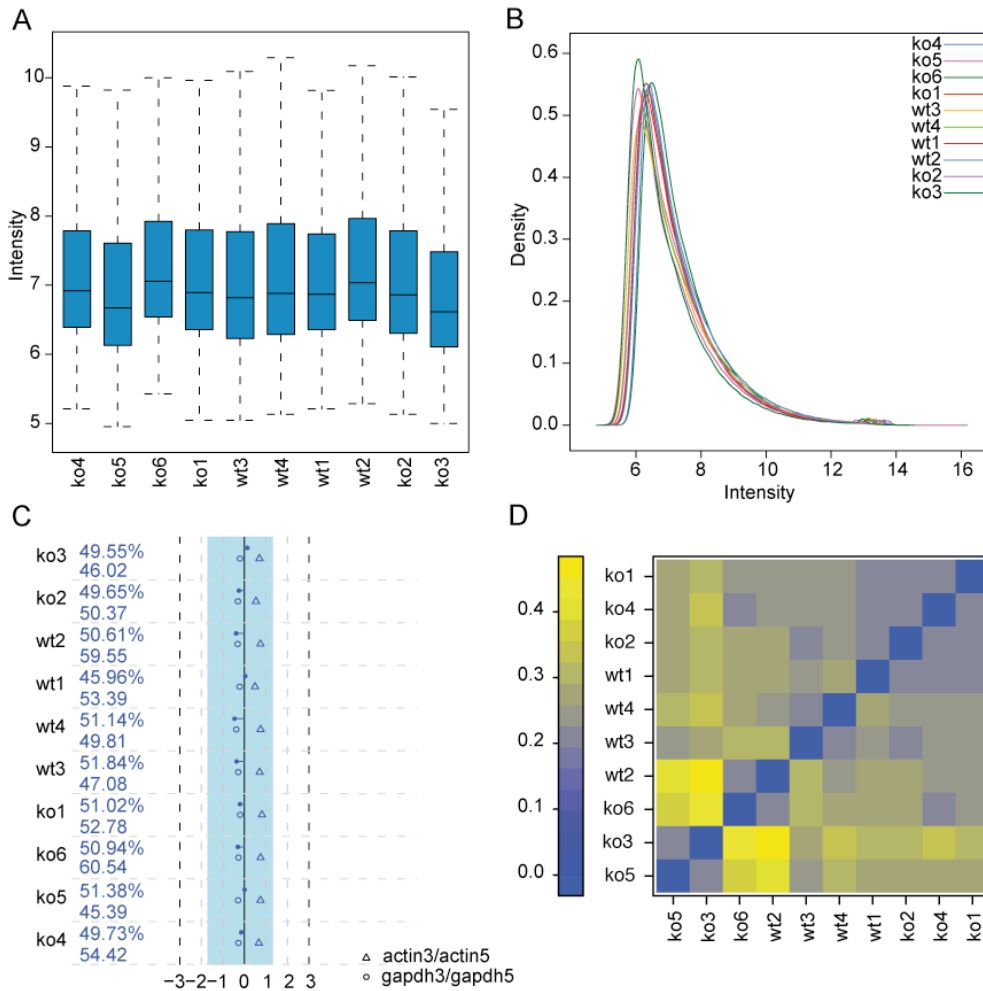
Figure 15. Quality assessment of kidney microarrays.
Quality of microarrays was assessed using arrayQualityMetrics package under bioconductor. **A.** Boxplot demonstration of array intensity distribution. Each box corresponds to one array. The plot summarizes the distribution of probe intensities ($\log_2$ intensities are plotted on the y-axis) across all arrays. Boxes had similar size and y position (median) did not show any outliers. **B.** Density plot illustrates the density of a given intensity within an array; as expected a similar pattern was found for all arrays. **C.** Affymetrix quality control (QC) stats report. The percentages of "present" calls are given for each array in the left row, upper number, the lower numbers give the average background value for the corresponding array. Both values were within the same range throughout all arrays. The relation between 3' probe sets and 5' probe sets of the control genes β-actin (triangles) and GAPDH (circles) was inside the recommended threshold (light blue box) for all arrays. **D.** Heatmap representation of the distance between arrays. The false colour heatmap depicts the mean absolute distance of the M-values for each pair of arrays, with M = $\log_2(\text{intensity}_1)$ - $\log_2(\text{intensity}_2)$, where intensity$_1$ is the intensity of the array studied and intensity$_2$ is the intensity of a "pseudo"-array, which has the median values of all the arrays. The plot demonstrats a good quality of arrays by a low distance. Note that arrays ko1-3 and wt1-2 correspond to male mice, arrays ko4-6 and wt3-4 correspond to female mice.

The quality of microarrays was evaluated using the ArrayQualityMetrics package [241] under Bioconductor [239]. Exemplary results from the quality analysis are illustrated in figure 15. All arrays were of good quality. The mean intensity of all arrays was within the same range (figure 15A-B). Moreover, the Affymetrix quality control (figure 15C) report including the measurement of the relation between 3' probe sets and 5' probe sets of the control genes β-actin and GAPDH did not identify any outlier. Last, the distance between arrays was determined confirming that array quality was homogenous (figure 15D). Thus, all arrays were retained for the analysis of differential expression among WT and KO mice. The gene expression pattern is demonstrated in a Volcano plot (figure 16), each probe set is depicted as a dot according to its p-value and ratio between WT and KO mice. The most interesting candidate genes, those with smallest p-value (red label) and highest log-ratio (blue label), are found in the upper right and upper left corner of the plot. Only few genes were found in these regions.
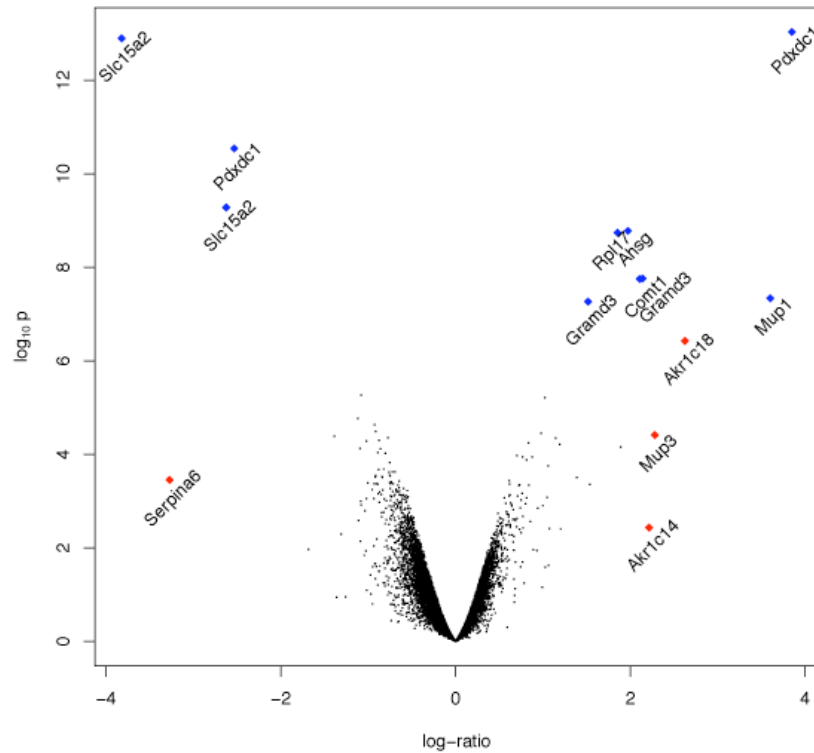
Figure 16. Gene expression in kidney of D2 wildtype and knockout mice.
Volcano plot demonstration of gene expression in kidney. Examined mice had D2 genetic background and were 5 weeks old. Differential expression between fetuin-A deficient and wildtype mice is shown as log-ratio on the x-axis, negative values represent higher expression in KO mice, positive values represent higher expression in wildtype mice. The y-axis encodes the probability for differential regulation calculated by Bayesian statistics in the limma package under bioconductor. Each dot denotes a probe set, probe sets with highest probability score are depicted in blue and probe sets with highest log-ratio are depicted in red, marked probe sets are labeled with the appropriate gene name.

In table 6 all 16 significantly differentially regulated genes are listed (genes with a p-value < 0.05 after multiple testing correction were considered as significant). Note that one gene may be represented by several probe sets, this particularly accounts to genes with long

transcripts. The two most highly upregulated probe sets encoded for solute carrier family 15 (H+/peptide transporter), member 2 (Slc15a2) and were 14.1 and 6.2 fold increased in fetuin-A deficient kidneys. Slc15a2, also known as peptide transporter 2 (PEPT2), belongs to the superfamily of proton oligopeptide transporter (POT) [266]. PEPT2 is expressed predominantly in the kidney and was shown to be a proton-dependent transporter of di- and tripeptides as well as of a variety of peptidomimetics [267, 268]. Next, three probe sets encoding the pyridoxal-dependent decarboxylase containing 1, a protein with unknown function, appeared among the differentially regulated candidates. Two of them, matching exon 14-16 and exon 24, were upregulated in D2 fetuin-A deficient mice with a fold change of 5.8 and 1.9, respectively. A third probe set matching a sequence outside the coding sequence (CDS) was 14.4 fold decreased in fetuin-A deficient animals. In total three isoforms of pyridoxal-dependent decarboxylase containing 1 are mapped in NCBI, the exons 14 to 16 are contained in all of them whereas exon 24 is uniquely expressed in isoform 3. The same differential expression pattern of the three probe sets was found in adipose tissue (see chapter 3.1.4.1) and liver of 5-week-old D2 fetuin-A deficient mice (see chapter 3.1.4.3). Further differentially upregulated probe sets were: Angiotensin I converting enzyme (peptidyl-dipeptidase A) 2, a key factor of the renin-angiotensin pathway, with a fold change of 2.2; ubiquitin specific peptidase 1 with a fold change of 2.1 and sulfotransferase family 3A, member 1 with a fold change of 1.9.

Downregulated genes were: Major urinary protein 1 with a fold change of 12.1; aldo-keto reductase family 1, member C18 with a fold change of 6.2; catechol-O-methyltransferase 1 with a fold change of 4.4; GRAM domain containing 3, represented by 2 probe sets with fold changes of 4.3 and 2.9 respectively; alpha-2-HS glycoprotein / fetuin-A with a fold change of 3.9; ribosomal protein L17 with a fold change of 3.6 and ring finger protein 41 with a fold change of 2. Given the fact that the fetuin-A gene is absent in fetuin-A deficient mice and fetuin-A is naturally expressed at very low level in wildtype kidney [269] the 3.9 fold downregulation must be interpreted as down-regulation from very low expression (< 1% of liver expression) to zero. Nevertheless, this finding demonstrated the high sensitivity of microarray based expression studies.

In summary, only few differentially regulated genes were identified in kidneys of 5-week-old D2 fetuin-A deficient and wildtype mice.

Table 6. Differential expression in kidneys from fetuin-A deficient D2 mice.

probe set	symbol	p-value	log-ratio
upregulation			
solute carrier family 15 (H+/peptide transporter), member 2	Slc15a2	< 0.001	-3.821
solute carrier family 15 (H+/peptide transporter), member 2	Slc15a2	< 0.001	-2.624
pyridoxal-dependent decarboxylase domain containing 1	Pdxdc1	< 0.001	-2.532
angiotensin I converting enzyme (peptidyl-dipeptidase A) 2	Ace2	0.030	-1.117
ubiquitin specific peptidase 1	Usp1	0.011	-1.079
pyridoxal-dependent decarboxylase domain containing 1	Pdxdc1	0.038	-0.929
sulfotransferase family 3A, member 1	Sult3a1	0.049	-0.913
downregulation			
pyridoxal-dependent decarboxylase domain containing 1	Pdxdc1	< 0.001	3.849
major urinary protein 1	Mup1	< 0.001	3.601
aldo-keto reductase family 1, member C18	Akr1c18	0.001	2.625
catechol-O-methyltransferase 1	Comt1	< 0.001	2.141
GRAM domain containing 3	Gramd3	< 0.001	2.109
alpha-2-HS-glycoprotein	Ahsg	< 0.001	1.973
ribosomal protein L17	Rpl17	< 0.001	1.854
GRAM domain containing 3	Gramd3	< 0.001	1.517
ring finger protein 41	Rnf41	0.012	1.022

The table shows probe sets, which were significantly (p-value < 0.05) differentially expressed in kidneys dissected from 5-week-old D2 wildtype and fetuin-A deficient mice. Bayesian statistics was used for calculation of probabilities (p-value) and log-ratio, negative log-ratio encode upregulation of the particular probe-set in fetuin-A deficient mice, positive values denote downregulation. Note that gene names are given for each probe set, double entries may occur in case of genes which are represented by several probe sets encoding different regions or splice variants of the gene.

3.1.4.3 Differential Gene Expression in Liver

In adult mammals fetuin-A is predominantly expressed in the liver [19, 269]. Consequently, gene expression in liver of D2 fetuin-A deficient mice and wildtype controls was studied to identify causalities of the fetuin-A deficiency in calcifying mice. Genome-wide expression was analyzed in 5-week-old D2 fetuin-A deficient mice of both sexes and matching wildtype controls using Affymetrix microarrays.

Quality of microarrays was analyzed using the ArrayQualityMetrics package [241] under bioconductor [239]. Arrays, which scored as outliers in two or more tests were considered poor quality and were excluded from further analysis. Figure 17 illustrates the analysis. Figures 17A, B point out that the mean intensity of the arrays ko4 and wt1 diverged remarkably from the other arrays. The Affymetrix quality control shown in figure 17C confirmed this finding in reporting high background levels for those two arrays. The RNA quality measured by judging the ratio of 3' and 5' probe sets of two houskeeping genes was good in all arrays. Finally, distance measuring (figure 17D) confirmed the arrays ko4 and wt1 as outliers and suggested to exclude these arrays from the data set. The remaining data was normalized and differential expression was calculated using Bayesian statistics. The gene expression profile is illustrated in a Volcano plot (figure 18), each probe set is depicted as a dot according to its p-value and ratio between WT and KO mice.
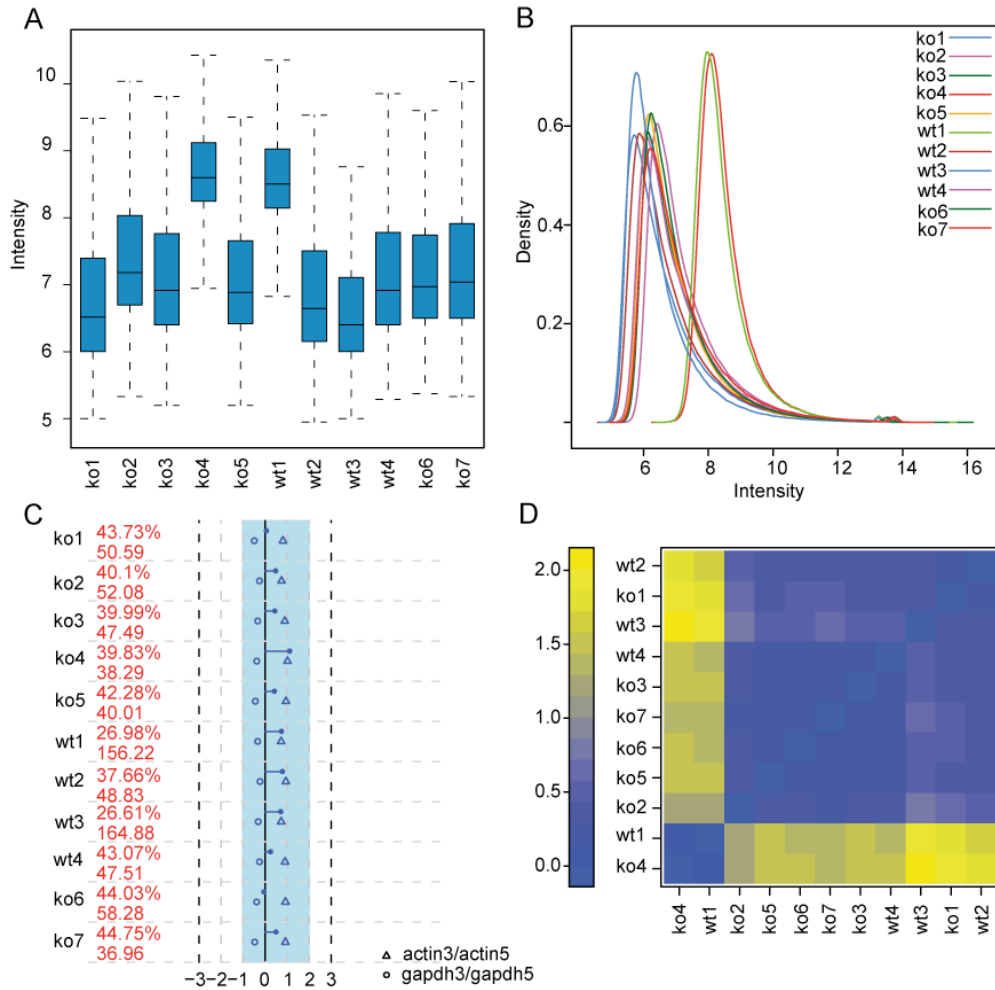
Figure 17. Quality assessment of liver microarrays.
Quality of microarrays was assessed using arrayQualityMetrics package under bioconductor. **A:** Boxplot demonstration of array intensity distribution. Each box corresponds to one array. The plot summarizes the distribution of probe intensities ($\log_2$ intensities are plotted on the y-axis) across all arrays. The boxes of the arrays ko4 and wt1 were slightly smaller in comparison to all other arrays. Along with this the median intensity of those arrays was remarkably high. **B:** Density plot illustrates the density of a given intensity within an array; one would expect a similar pattern for all arrays. The arrays ko4 and wt1 were biased towards high intensity probes, which denoted those arrays as outliers. **C:** Affymetrix quality control (QC) stats report. The percentages of "present" calls are given for each array in the left row, upper number, the lower numbers give the average background value for the corresponding array. The percentage of present calls was clearly lower for ko4 and wt1. Furthermore, the background level was remarkably high for those arrays as already seen in A and B. The relation between 3' probe sets and 5' probe sets of the control genes β-actin (triangles) and GAPDH (circles) was inside the recommended threshold (light blue box) for all arrays. **D:** Heatmap representation of the distance between arrays. The false colour heatmap depicts the mean absolute distance of the M-values for each pair of arrays, with M = $\log_2$(intensity$_1$) - $\log_2$(intensity$_2$), where intensity$_1$ is the intensity of the array studied and intensity$_2$ is the intensity of a "pseudo"-array, which has the median values of all the arrays. This plot confirmed ko4 and wt1 as outliers. Note that arrays ko1-3 and wt1-2 correspond to male mice, arrays ko4-7 and wt3-4 correspond to female mice.

In total, 142 probe sets (supplemental table 2) were significantly differentially regulated (probe sets with a p-value < 0.05 after multiple testing correction were considered as significant). Differentially regulated probe sets with a fold change above 4 (log-ratio >2) are summarized in table 7.
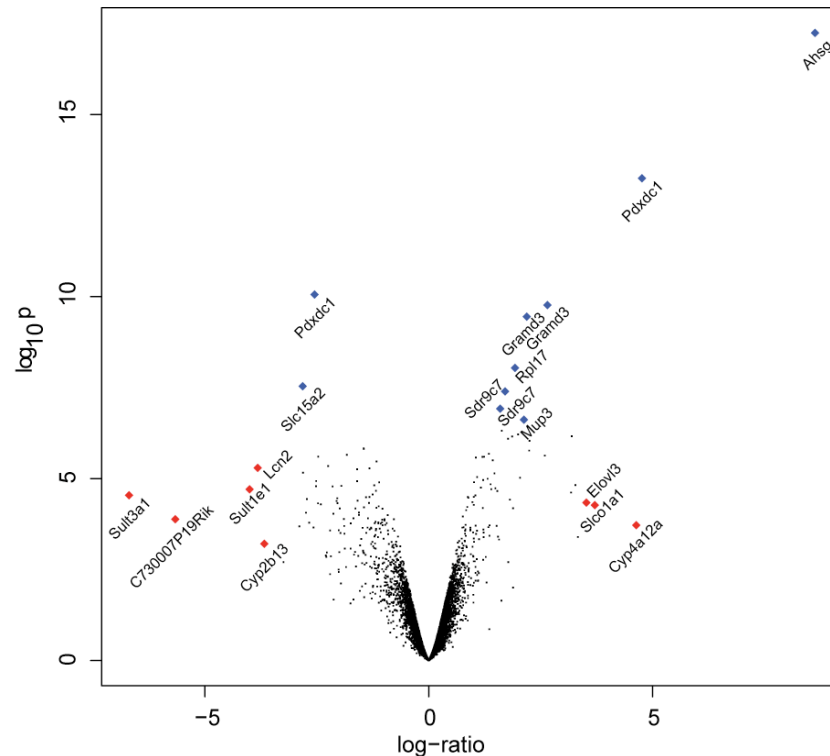
Figure 18. Gene expression in liver of D2 wildtype and fetuin-A knockout mice.
Volcano plot demonstration of gene expression in liver. Examined mice had D2 genetic background and were 5 weeks old. Differential expression between fetuin-A deficient and wildtype mice is shown as log-ratio on the x-axis, negative values represent higher expression in KO mice, positive values represent higher expression in wildtype mice. The y-axis encodes the probability for differential regulation calculated by Bayesian statistics in the limma package under bioconductor. Each dot denotes one probe set, probe sets with highest probability score are depicted in blue and probe sets with highest log-ratio are depicted in red, marked probe sets are labeled with the appropriate gene name.

Most highly upregulated genes in fetuin-A deficient liver were three sulfotransferases, enzymes of the phase II metabolism. Sulfotransferase family 3A, member1 (Sult3a1) was 103.6-fold increased in D2 fetuin-A deficient mice, sulfotransferase family 2A, member 2 (Sult2a2) was 50.7-fold upregulated and expression of sulfotransferase family 1E, member 1 (Sult1e1) was 16-fold higher in fetuin-A deficient animals than in wildtype littermates. Another highly upregulated probe set matched lipocalin 2, a carrier protein involved in the innate immune response [270], and was 14.1-fold increased in D2 fetuin-A deficient mice. Furthermore, the acute-phase reactants [271] serum amyloid A 2 (SAA-2) and serum amyloid A1 (SAA-1) were increased 7.4-fold and 6-fold, respectively. Likewise, the scavenger receptor CD36, which recently was identified as a receptor of serum amyloid A proteins [272], was upregulated 4.2-fold. Additionally, two genes already identified in the kidney expression analysis appeared among the differentially regulated genes: the probe sets of pyridoxal-dependent decarboxylase containing 1 and the peptide transporter PEPT2 showed the same expression pattern as in the kidney (compare chapter 3.1.4.2).

Table 7. Differential Expression in liver from fetuin-A deficient D2 mice.

probe set	symbol	p-value	log-ratio
upregulation			
sulfotransferase family 3A, member 1	Sult3a1	0.012	-6.695
RIKEN cDNA C730007P19 gene	C730007P19Rik	0.032	-5.665
sulfotransferase family 1E, member 1	Sult1e1	0.009	-4.002
lipocalin 2	Lcn2	0.004	-3.820
serum amyloid A 2	Saa2	0.042	-2.890
solute carrier family 15 (H+/peptide transporter), member 2	Slc15a2	< 0.001	-2.817
ribonucleotide reductase M2	Rrm2	0.005	-2.810
DNA segment, Chr 17, human D6S56E 5	D17H6S56E-5	0.024	-2.744
baculoviral IAP repeat-containing 5	Birc5	0.014	-2.721
cyclin B2	Ccnb2	0.038	-2.670
serum amyloid A 1	Saa1	0.043	-2.575
pyridoxal-dependent decarboxylase domain containing 1	Pdxdc1	< 0.001	-2.551
cDNA sequence AB056442	AB056442	0.008	-2.517
minichromosome maintenance deficient 6 (MIS5 homolog, S. pombe) (S. cerevisiae)	Mcm6	0.007	-2.516
minichromosome maintenance deficient 6 (MIS5 homolog, S. pombe) (S. cerevisiae)	Mcm6	0.016	-2.474
regulator of calcineurin 2	Rcan2	0.002	-2.470
ribonucleotide reductase M2	Rrm2	0.017	-2.411
SPARC related modular calcium binding 2	Smoc2	0.004	-2.247
PDZ binding kinase	Pbk	0.046	-2.204
SPARC related modular calcium binding 2	Smoc2	0.008	-2.148
cell division cycle associated 8	Cdca8	0.025	-2.131
CD36 antigen	Cd36	0.015	-2.059
minichromosome maintenance deficient 5, cell division cycle 46 (S. cerevisiae)	Mcm5	0.013	-2.043
histone cluster 1, H2ae	Hist1h2ae	0.016	-2.039
downregulation			
alpha-2-HS-glycoprotein	Ahsg	< 0.001	8.631
pyridoxal-dependent decarboxylase domain containing 1	Pdxdc1	< 0.001	4.762
cytochrome P450, family 4, subfamily a, polypeptide 12a	Cyp4a12a	0.041	4.635
solute carrier organic anion transporter family, member 1a1	Slco1a1	0.017	3.712
elongation of very long chain fatty acids (FEN1/Elo2, SUR4/Elo3, yeast)-like 3	Elovl3	0.016	3.522
hydroxy-delta-5-steroid dehydrogenase, 3 beta- and steroid delta-isomerase 5	Hsd3b5	0.008	3.275
kidney androgen regulated protein	Kap	0.001	3.193
RIKEN cDNA 2610016E04 gene	2610016E04Rik	0.011	3.181
GRAM domain containing 3	Gramd3	< 0.001	2.651
hydroxy-delta-5-steroid dehydrogenase, 3 beta- and steroid delta-isomerase 2	Hsd3b2	0.002	2.593
cytochrome P450, family 7, subfamily b, polypeptide 1	Cyp7b1	0.001	2.252
cytochrome P450, family 7, subfamily b, polypeptide 1	Cyp7b1	0.002	2.244
GRAM domain containing 3	Gramd3	< 0.001	2.190
major urinary protein 3	Mup3	0.001	2.125
NADPH oxidase 4	Nox4	0.006	2.039

The table shows probe sets, which were significant (p-value < 0.05) differentially expressed in liver dissected from 5-weeks-old D2 wildtype (n=3) and fetuin-A deficient mice (n=5). Bayesian statistics was used for calculation of probabilities (p-value) and log-ratio, negative log-ratio encode upregulation of the particular probe-set in fetuin-A deficient mice, positive values denote downregulation. The table shows most highly differentially regulated genes with a log-ratio above 2. Note that gene names are given for each probe set, double entries may occur in case of genes which are represented by several probe sets encoding different regions or splice variants of the gene.

As expected fetuin-A / Ahsg was identified as the most strongly downregulated gene in the liver of D2 fetuin-A deficient mice (this finding was confirmed in B6 fetuin-A deficient mice,

see 3.3.1.2), a fold change of 396.5 was observed, indicating absence of fetuin-A expression in D2 fetuin-A deficient livers. Further highly downregulated genes in the liver of D2 fetuin-A deficient mice were: Cytochrome P450, family 4, subfamily a, polypeptide 12a with a 24.9-fold decrease; solute carrier organic anion transporter family, member 1a1 with a 13.1-fold decrease and elongation of very long chain fatty acids /FEN1/Elo2, SUR4/Elo3, yeast-like 3 with a 11.5 fold change.

Interestingly, none of the upregulated genes mentioned above was significantly differentially regulated in the liver of non-calcifying B6 fetuin-A deficient mice, pointing to a role of these genes in the pathology of ectopic calcification. In contrast, all mentioned downregulated probe sets showed a similar expression pattern on B6 genetic background, therefore the downregulation was not linked to the calcification phenotype.

3.1.5 Protein Content of Calcified Lesions

Soft tissue calcification in D2 fetuin-A deficient mice was detected from an age of 10 days [264]. Early calcified lesions were nodular and of micrometer size. In the course of time the lesions grew consecutively. The lesions reached millimeter size, and progress of lesions was associated with intensive tissue remodelling. Here late stage calcified lesions were dissected and analyzed with regard to their protein content. Figure 19B demonstrates millimeter sized lesions isolated from interscapular brown adipose tissue (BAT). Proteins were extracted from calcified lesions and intact tissue and separated using SDS-PAGE. Comparison of the protein band pattern in calcified and non-calcified tissue revealed several differentially expressed bands (figure 19A). The protein content of these bands was determined with mass spectrometry (MS). The table in figure 19C lists the major proteins of each band ranked by their emPAI score. This score measures the quantitative contribution of each identified protein to the sum of proteins detected in the individual band. In skin lesions five bands were enriched or shifted in comparison to intact tissue. Band 1 and 2 were at the same height as the serum albumin band, which was also present in intact skin. Consequently, serum albumin was identified in both bands. Interestingly, band 1 also contained complement component 9 and hemoglobin subunit beta-1. Fibrinogen beta chain was also highly enriched in calcified skin tissue (figure 19A, C band 3). In band 4 carbonic anhydrase 3, Ig kappa chain C region, histone H2B type 1-C/E/G and serum amyloid P-component (SAP) were detected. Apolipoprotein A-I (ApoA1) was identified in band 5 as well as in protein extracts from calcified lesions in the heart and BAT (band 6 and 7).

In summary, MS could identify several serum proteins tightly associated or bound to calcified lesions. The enzyme carbonic anhydrase 3, which catalyzes the formation of bicarbonate was also enriched in calcified lesions of the skin. The most proteins were found in skin lesions, whereas in lesions of heart and BAT exclusively ApoA1 was identified.
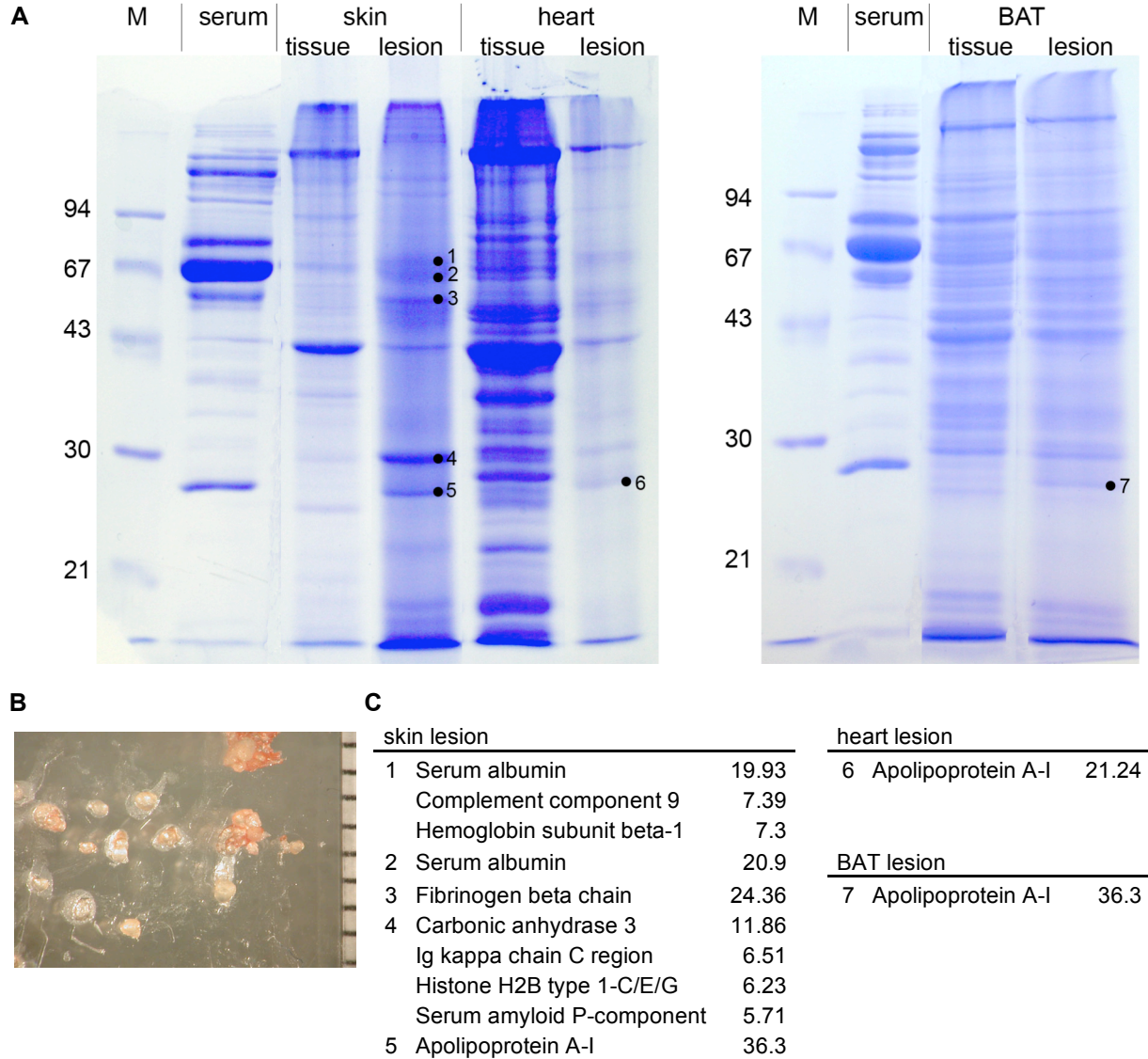
Figure 19. Proteomic analysis of calcified lesions.
Calcified lesions as well as non-calcified tissue samples were dissected from D2 fetuin-A deficient mice with severe ectopic calcification. Proteins were extracted using SDS sample buffer containing EDTA and homogenized using a mixer mill. **A:** SDS-PAGE of samples prepared from serum, intact tissue and calcified lesions of skin, heart and brown adipose tissue (BAT). Numbered protein bands were enriched in calcified lesions. M = marker. **B:** Millimeter-sized nodular calcified lesions scraped from interscapular BAT. **C:** Proteins identified by LC-MS in bands marked in A. Proteins that were most frequently detected in the MS-based peptide fragment analysis are shown. Analysis of MS results was performed under Mascot [249], the ion score cut-off was set to 30 and exponentially modified protein abundance index (emPAI) was used to identify the major proteins. EmPAI score for each identified protein is given. Proteins which contributed at least 50% to the entity of proteins within the examined band are shown.

3.2 Clearance of Calciprotein Particles

Various biochemical studies have shown that fetuin-A is essential for the formation of high molecular weight protein-mineral complexes, called calciprotein particles (CPPs) [18, 90-92]. To prevent local deposition and pathological calcification CPPs must be cleared from circulation once they have formed. Thus, the *in vivo* clearance of CPPs was studied to identify the target

organ and cell type responsible for CPP uptake. Finally, the specific uptake route and a candidate receptor will be examined.

3.2.1 Clearance of Protein-Mineral Complexes from the Circulation is Fast and Efficient

To study the clearance of CPPs *in vivo*, CPPs were generated as described before [18] and injected intravenously into mice. All protein and particle preparations were purified before use. For comparison labeled monomeric fetuin-A (F-A), asialofetuin (AsF) and bovine serum albumin (BSA) were injected. It is known that AsF is rapidly cleared by the asialoglycoprotein receptor (ASGP-R), which binds terminal galactose residues on desialylated plasma proteins [273, 274]. BSA has a long half-life in serum [275].

Figure 20 illustrates the clearance of various fluorescence-labeled proteins and CPP preparations from blood. Blood was collected at different time points and clearance calculated from densitometry of the fluorescence signal of serum samples separated in SDS-PAGE.
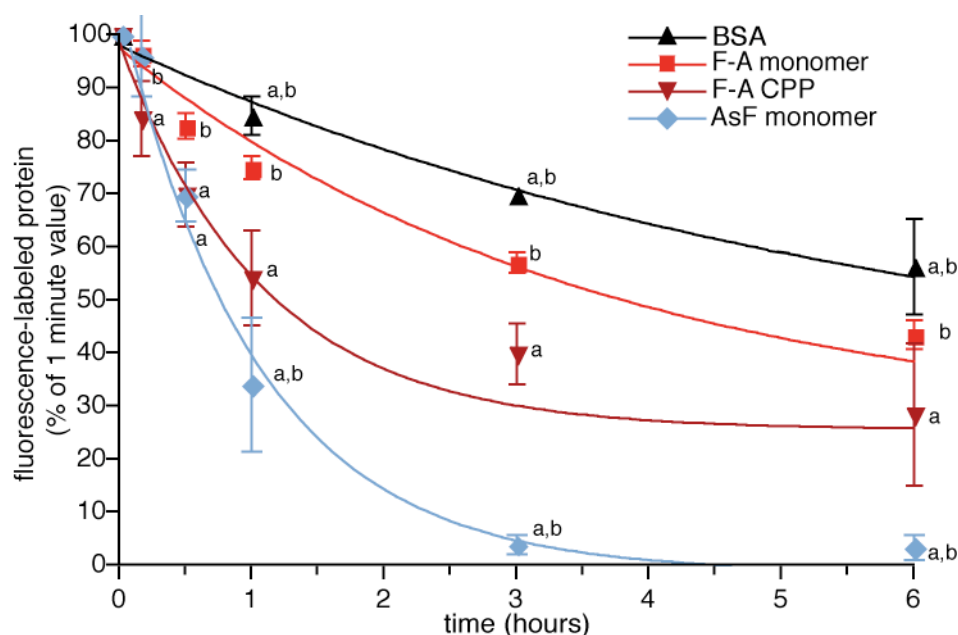
Figure 20. Clearance of fluorescence-labeled protein from mouse serum.
Fluorescence-labeled proteins (160 µg) were injected intravenously into mice and blood was drawn at indicated time points to determine the amount of remaining circulating protein. Shown are the fluorescence signals as percentage of the value measured one minute after injection. BSA had the longest half-life ($t_{1/2}$) of all proteins tested, and in descending order: $t_{1/2}$ fetuin-A monomer > $t_{1/2}$ CPPs > $t_{1/2}$ asialofetuin. a, statistically significant different from fetuin-A monomer at the same time point, $p < 0.01$; b, statistically significant different from CPP, $p < 0.01$. $n \geq 4$

Figure 1 shows that the clearance of fetuin-A CPPs was faster than the clearance of fetuin-A monomer with serum half-lifes $t_{1/2}$ of 45 and 149 minutes, respectively. CPP clearance was also clearly faster than BSA clearance ($t_{1/2}$ 247 min) and AsF monomer was cleared even faster than both fetuin-A monomer and CPPs with $t_{1/2}$ 43 minutes. This finding corroborated the presence of a high-affinity asialoglycoprotein receptor, strongly discriminating between

fully glycosylated fetuin-A and asialofetuin (half-life 149 min vs. 43 min, respectively). In summary, faster clearance of fetuin-A containing CPPs vs. fetuin-A monomer suggested that clearance was greatly enhanced by mineral complex formation of fetuin-A and possibly by fetuin-A clustering.

3.2.2 CPPs Are Taken up by Liver Kupffer Cells

The CPP clearance from blood should be reflected by their organ accumulation. Figure 21 illustrates CPP clearance and accumulation in the liver, a major organ of the reticuloendothelial system (RES). Figure 21 shows fluorescence micrographs of liver sections and localization of fluorescent CPPs in defined cells scattered throughout the liver sinusoids (figure 21A-E). Antibody staining showed that CPPs were taken up by F4/80 and CD68 positive liver macrophages or Kupffer cells (figure 21F, G), while F4/80-negative liver sinusoidal endothelial cells did not accumulate CPPs. CD68 or macrosialin is a transmembrane glycoprotein belonging to the lysosomal-associated membrane protein (LAMP) family and is expressed specifically by tissue macrophages [276]. F4/80 antigen is a cell surface glycoprotein expressed on a wide range of mature tissue macrophages including Kupffer cells and macrophages in the red pulp of the spleen [209].

A similar distribution was observed when fluorescent polystyrene beads were injected into mice. These beads had a diameter of 170 nm and thus resembled CPP size. Like CPPs beads colocalized with F4/80 and CD68 (figure 22).
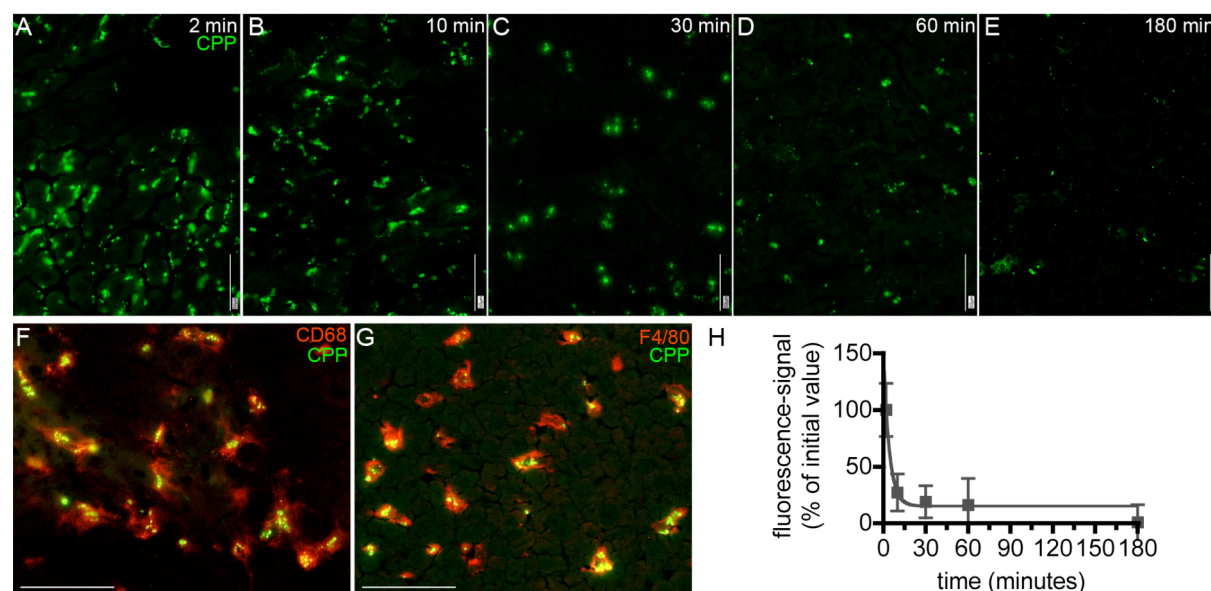
Figure 21: Localization and degradation of labeled CPPs in the liver.
A-E. The green fluorescence signal of the CPPs in liver sections diminished rapidly from 2 to 180 minutes suggesting maximum clearing within 10 min and degradation thereafter. **F., G.** Immunostaining with macrophage specific antibodies CD68 and F4/80 (red) showed colocalization (yellow) with CPPs (green) inside the macrophages. H. Decrease in fluorescence of liver sections measured by histomorphometry (black line, n ≥ 4 for each time point) as shown in A-E. Shown are the mean values ± SEM. Bars in A-G: 50 µm.

Taking fluorescence of Kupffer cells as a proxy of cellular clearance, uptake of fluorescence-labeled CPPs peaked at two minutes and decreased thereafter (figure 21A-E). Densitometry of fluorescence micrographs showed that 55 % of the fluorescent material present 2 minutes after injection had disappeared 8 minutes later indicating fast clearance and degradation of CPPs in Kupffer cells (figure 21H). The half-life of CPPs in Kupffer cells was 3 minutes. Thus, the clearance rate for CPPs was considerably faster than that determined from serum disappearance ($t_{1/2}$ 45 min) shown above (see 3.2.1). This may be attributed to the fact that CPP preparations also contain monomeric fetuin-A [92] greatly distorting the apparent serum clearance rate, but not the CPP accumulation rate in Kupffer cells.

In accordance to published data asialofetuin monomer was predominantly cleared by hepatocytes, not by macrophages (not shown) [121, 274]. Fetuin-A monomer was cleared by unspecified cells with slow kinetics typical for long circulating plasma proteins like albumin (not shown). Of note, quantification of the more or less homogenous fluorescence-signal of both monomer types was disturbed by tissue auto-fluorescence of the liver. In summary, no cell-type specific accumulation was observed in fetuin-A monomer, whereas a rapid macrophage specific uptake and clearance was observed for CPPs.
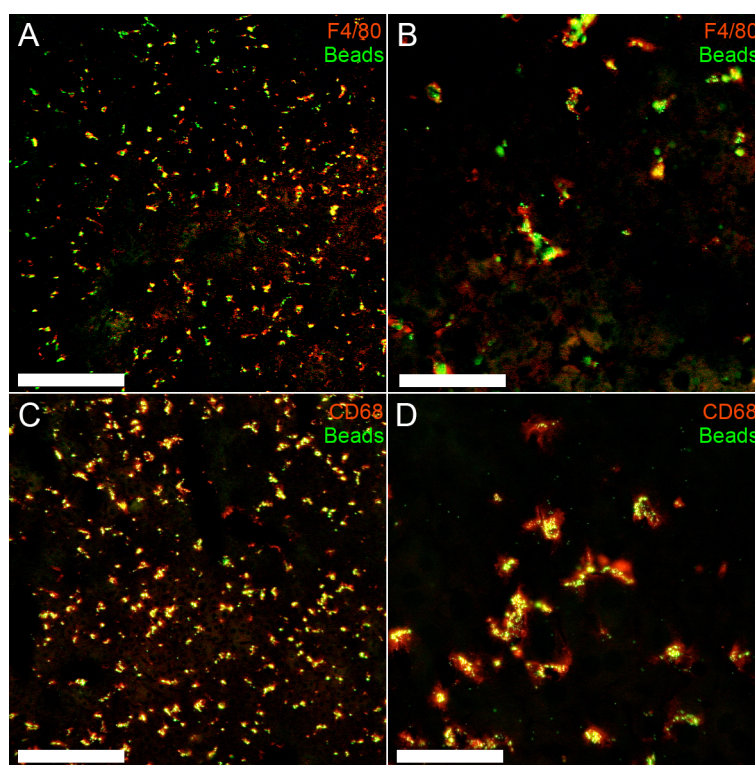
Figure 22. Localization of beads in the liver.
Beads were injected *i.v.* into mice and the liver was harvested 30 min thereafter. Shown are different magnifications of frozen sections with green fluorescent beads (diameter 170 nm) and cellular antigens detected with a secondary antibody labeled in red. Immunostaining with macrophage specific antibodies F4/80 (A, B) and CD68 (C, D) showed co-localization (yellow) with beads inside the macrophages. Size bars in A, C 200 µm; B, D 50 µm.

3.2.3 Uptake of CPPs – TEM Analysis

Next, we determined the fate of CPPs after uptake by liver macrophages. We therefore studied transmission electron micrographs of liver samples taken 30 minutes after injection of CPPs. Figure 23 shows that CPPs formed electron dense, dark small needle like crystals with a size of approximately 60 to 160 nm along the long axis, which were densely packed in vesicles in Kupffer cells. These vesicles differed in size (approximately 0.5-2 µm diameter, see figure 23C-E) and were surrounded by membranes suggesting endosomal uptake and degradation of CPPs. Lysosomes were found next to CPP containing endosomes. Eventually, endosomes and lysosomes fused and formed heterolysosomes (see figure 23D-E).
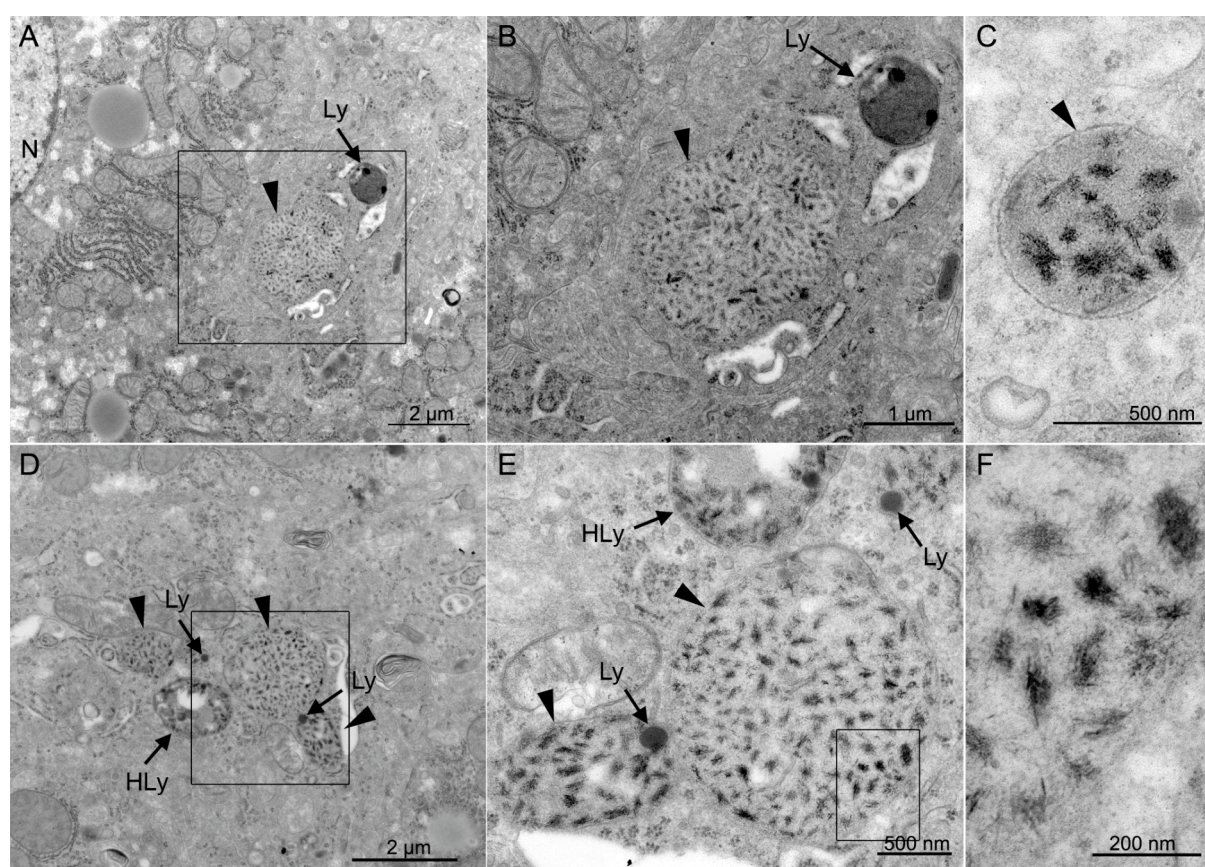
Figure 23. Intracellular localization of CPPs following Kupffer cell endocytosis.
In bright field transmission electron microscopy (TEM) of liver sections, injected CPPs appeared as electron dense, dark, nanosized crystals. A., B. CPPs accumulated in vesicles (B inset of A). In the immediate vicinity of the CPP-containing vesicles, lysosomes (Ly) were observed. C. A small vesicle with a well defined double layer membrane surrounding a dense package of CPPs is assessable. Generally, all membranes appeared intact and therefore no signs of apoptosis or cell stress could be detected by TEM. D. Several CPP-containing vesicles were located near to each other, lysosomes were tightly associated with the vesicles. A heterolysosom (HLy) was formed by fusion of a CPP-containing vesicle and a lysosome. E., F. Successive magnifications of D showing calciumphosphate crystals with a size of about 50 to 150 nm. N: nucleus; Arrowheads: CPP containing vesicles.

3.2.4 Organ Distribution of Fetuin-A, Asialofetuin and CPPs

To quantify the organ distribution of fluorescence-labeled CPPs and monomeric proteins, individual perfused organs of mice were analyzed. The amount of intact (high molecular weight) and degraded (low molecular weight) labeled fetuin-A was measured in cellular extracts by SDS-PAGE and quantified by fluorescence imaging (figure 24). The background fluorescence was arbitrarily set to the average fluorescence signal observed in extracts from those organs that scored negative by immunofluorescence (figure 25, the background level is indicated by dashed lines in each case). Any residual signal in these organs was attributed to insufficient blood removal despite organ perfusion.
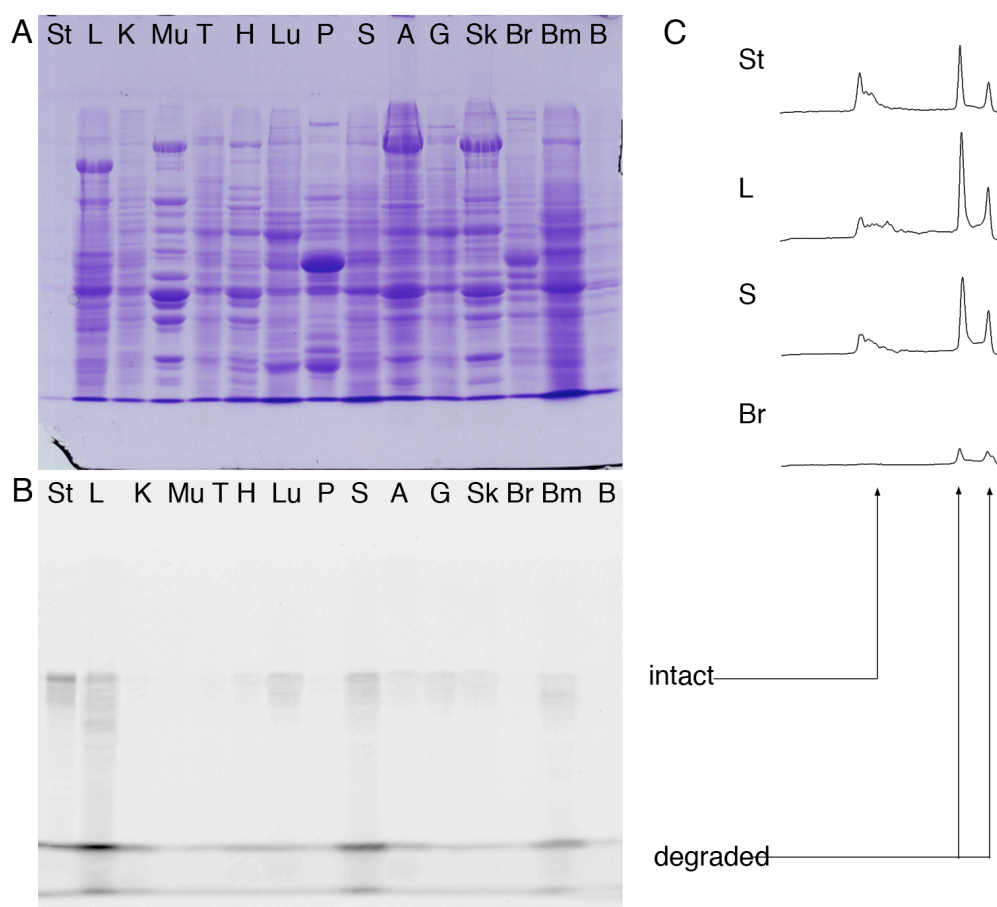
Figure 24. Densitometry of organ extracts.
Representative analysis of organ extracts 30 min after *i.v.* injection of fluorescence-labeled fetuin-A containing CPPs. **A.** Coomassie staining of organ extracts separated by SDS-PAGE. **B.** Fluorescence scan revealed accumulation of CPPs predominantly in liver and spleen. 10 ng of purified fluorescence-labeled fetuin-A served as internal standard (first lane). Intact fetuin-A was detected in high molecular weight bands, degraded fetuin-A was detected in two low molecular weight bands. **C**. Densitometry of fluorescent protein bands. Intact and degraded fetuin-A in organ extracts were measured relative to the internal protein standard. In brain no signal for intact protein was detected, therefore signals of low molecular bands were set as background and subtracted from all other samples. St, standard; L, liver; K, kidney; Mu, muscle tissue; T, thymus; H, heart; Lu, lung; P, pancreas; S, spleen; A, aorta; G, gonads; Sk, skin; Br, brain; Bm, bone marrow; B, bone.

Fetuin-A monomer accumulated to 1.5-fold background level in liver, kidney and bone marrow (figure 25A) suggesting that these organs may be involved in clearance, excretion and deposition of monomeric fetuin-A, which is highly enriched in bone mineral matrix

compared to other serum proteins [19]. This slight fluorescence accumulation was not caused by free fluorescence dye that might have dissociated from fetuin-A, because injected Alexa-488 dye was immediately excreted through the kidney and appeared in the urine within seconds without any detectable accumulation in organ extracts (not shown).

The AsF monomer showed a specific accumulation in the liver so that the hepatic content was up to 8.6-fold higher than the background (figure 25B). The AsF content in the liver peaked at 60 minutes reaching a maximum of 2.75 µg/100 mg fresh organ weight and declined thereafter. The second highest signal (up to 2.9-fold over background) was detected in kidneys showing mostly degraded asialofetuin. This suggests elimination of AsF protein from circulation in the liver and subsequent excretion through the kidney.
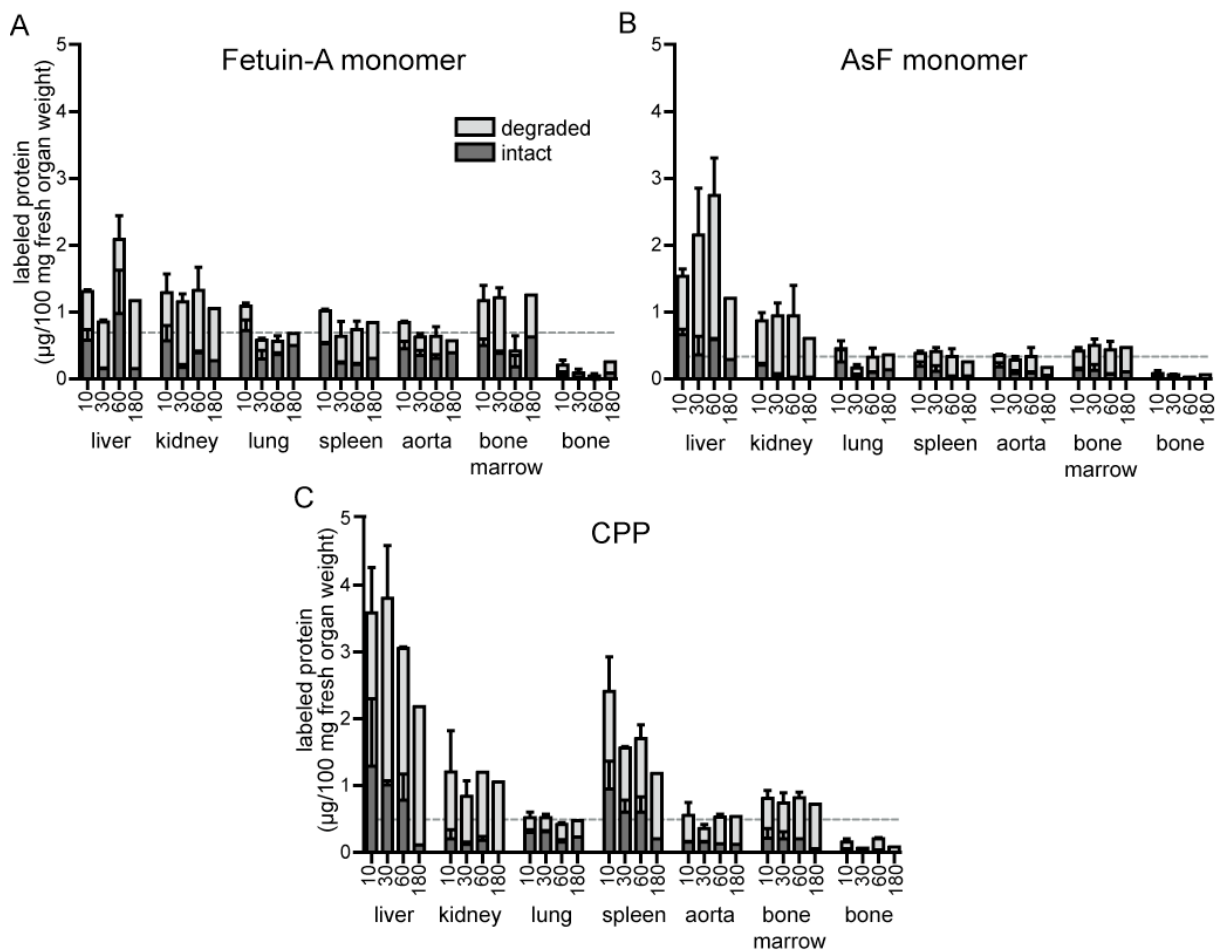
Figure 25. Organ distribution and kinetics of fluorescence-labeled proteins.
Fluorescence-labeled proteins were injected *i.v.* in mice. Mice sacrificed 10, 30, 60 and 180 minutes afterwards and organs were harvested. The tissue protein extracts were analyzed by SDS-PAGE and the content of the fluorescence-label in the tissues was evaluated by densitometry. The values shown were quantified relative to an internal standard of 10 ng labeled fetuin-A co-separated on each gel. The protein content is given as the absolute protein amount per 100 mg fresh organ weight. The dotted lines indicate the mean signal of all organs after the subtraction of the brain values considered as negative control because of the blood-brain barrier and excluding bone because of the considerably lower values. Note the significantly increased levels of labeled protein in the liver of AsF monomer and CPP compared to the mean protein content of the other organs as well as the higher levels observed in the spleen of CPP injected mice. (At least three animals per group were investigated at each time point).

Figure 25B shows that the distribution of CPPs differed strongly from fetuin-A monomer. Strong fluorescence signals were detected in liver extracts immediately after injection of CPPs (figure 25, see also figure 21A-E, H) and decreased continuously between 10 min and 3 hours. The highest amount was present at 30 minutes post injection and attained 8-fold background level. At this time CPP liver content corresponded to 31 % of the total injected dose of CPP. A decrease over time was seen for both, the intact as well as the degraded portion of CPP associated fetuin-A. A comparable pattern was seen in the spleen revealing up to 5-fold increase over background yet lower content than the liver (range 5 - 2.5-fold in spleen and 8 - 4.6-fold in liver). The initially high fluorescence continuously decreased at 60 and 180 min post injection. All other tissues showed comparatively constant fluorescence values over time and thus did not contribute to clearance and excretion of CPPs. Fluorescent protein content was also consistently low in myocardium, axillary lymph nodes, pancreas, gonads and skeletal muscle (all not shown).

In summary, the quantification of organ extracts showed that CPPs were predominantly cleared by liver and spleen. Both organs also degraded CPPs as shown by the initial rapid increase and the following steady decline in signal intensity compared to other tissues.

3.2.5 Marginal Zone Macrophages of the Spleen Clear Protein Mineral Particles

Besides the specific uptake of CPPs by Kupffer cells of the liver, quantification of organ extracts suggested the spleen as the second major organ clearing CPPs from circulation. Next to the liver, spleen is a major organ of the reticuloendothelial system involved in clearance of particles from circulation. The clearance of fluorescent CPPs in spleen was analyzed using fluorescence microscopy. The spleen comprises two compartments, the red pulp and the white pulp. The red pulp filters aged erythrocytes, the white pulp has an important role in antigen recognition and immune cell maturation. The spleen marginal zone separates these two compartments. Figure 26 demonstrates clearly that CPPs accumulated within the marginal zone. Cell-type specific markers were employed to determine the cell type responsible for CPP clearance in spleen. The spleen harbors several types of macrophages, localized in the red pulp or the marginal zone. The white pulp is mostly free of macrophages, but contains dendritic cells (DC).

Red pulp macrophages were identified by immunostaining using F4/80 antibody (figure 27), marginal metallophilic macrophages (MMM) were stained with MOMA-1/sialoadhesin antibody (figure 27A, B) and marginal zone macrophages (MZM) were stained with antibody against MARCO (macrophage receptor with collagenous structure, a scavenger receptor type A) (figure 27E, F) [277]. MMM and MZM macrophage populations in the marginal zone are separated by a layer of sinus lining cells, which stain positive for the cell adhesion molecule MAdCAM-1 (figure 27C, D). MZM are located exclusively in the outer side of the sinus lining cell layer of the marginal zone (pointing to the red pulp), the MMM are localized mainly on the inner side of the marginal sinus pointing to the white pulp and a fraction of weakly MOMA-1 positive cells is also found on the outer side pointing to the red pulp. Figure 26 shows that CPP (green color) accumulated in the marginal zone, but were absent in white pulp and red pulp. The sinus lining cell marker MAdCAM-1 (figure 27C, D) separated a few $CPP^{lo}/MOMA^{pos}$ macrophages from $CPP^{hi}/MARCO^{pos}$ macrophages (figure 27E, F) suggesting that most CPPs were taken up by $MARCO^{pos}$ MZM whereas the contribution of $MOMA\text{-}1^{pos}$ MMM was clearly lower. The same MARCO-positive cell population was shown to take up also fluorescent polystyrene beads of 170 nm diameter (figure 28E, F). In contrast, using beads of smaller size (diameter 55 nm) we could not detect a similar distribution in the marginal zone (not shown). No specific accumulation of this kind of particle could be visualized in vesicles of macrophages as seen with the CPPs or with larger beads.
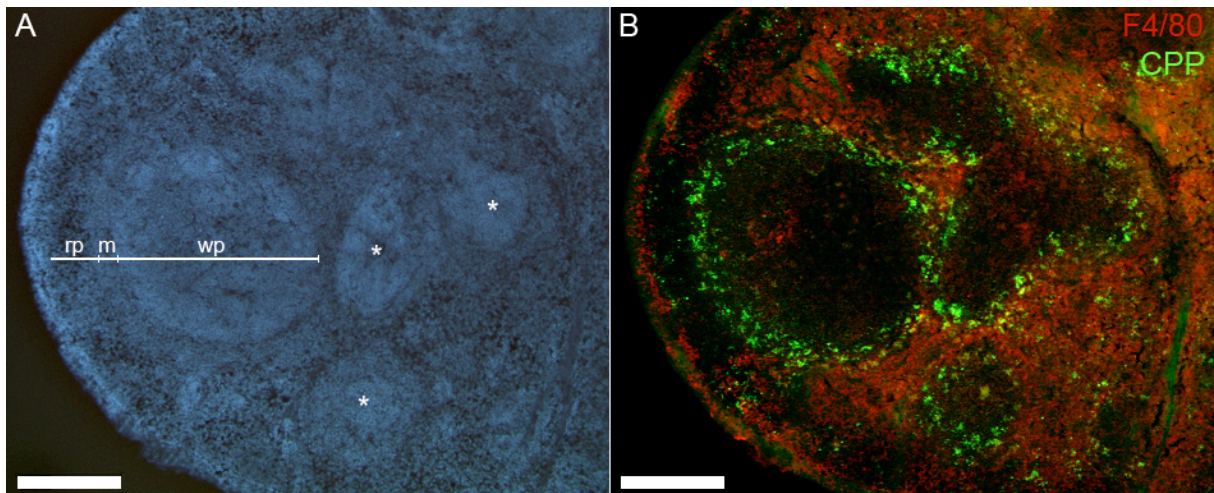
Figure 26. CPPs accumulate in the marginal zone of the spleen.
Spleen was harvested 30 min after CPP injection. Shown are different stains of spleen sections. **A.** Dapi, nuclear staining and **B.** Alexa-488 labeled CPPs in green and F4/80 staining of red pulp (rp) macrophages with a secondary antibody in red. CPPs accumulated in the marginal zone (m), which confines the white pulp (wp). Asterisks indicate white pulp segments. Scale bars 200 µm.
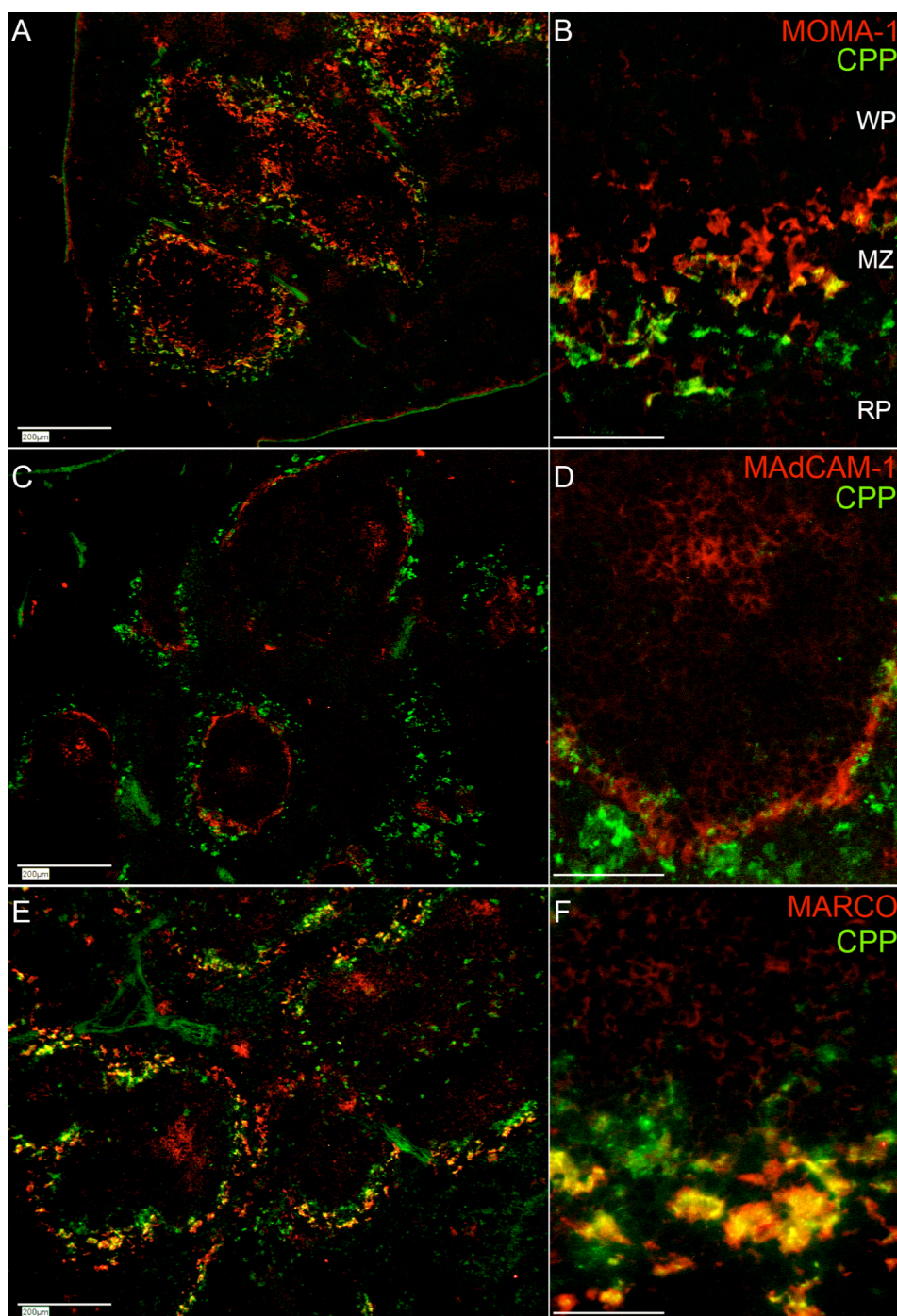
Figure 27. Colocalization of CPPs with cell-type specific markers in the marginal zone.
Spleens were harvested 30 min after CPP injection. Shown are different magnifications of spleen sections with Alexa-488 labeled CPPs in green and cell-type specific surface markers detected with a secondary antibody in red. CPPs showed partial co-localization (yellow) with the MOMA-1 antigen of the MMM (A, B), no co-localization with MAdCAM-1 as a marker for sinus lining cells (C,D), and almost complete colocalization with MARCO-positive marginal zone macrophages. WP, indicates white pulp; MZ, marginal zone and RP, red pulp. Scale bars in A, C and E: 200 μm, bars in B, D and F: 50 μm.
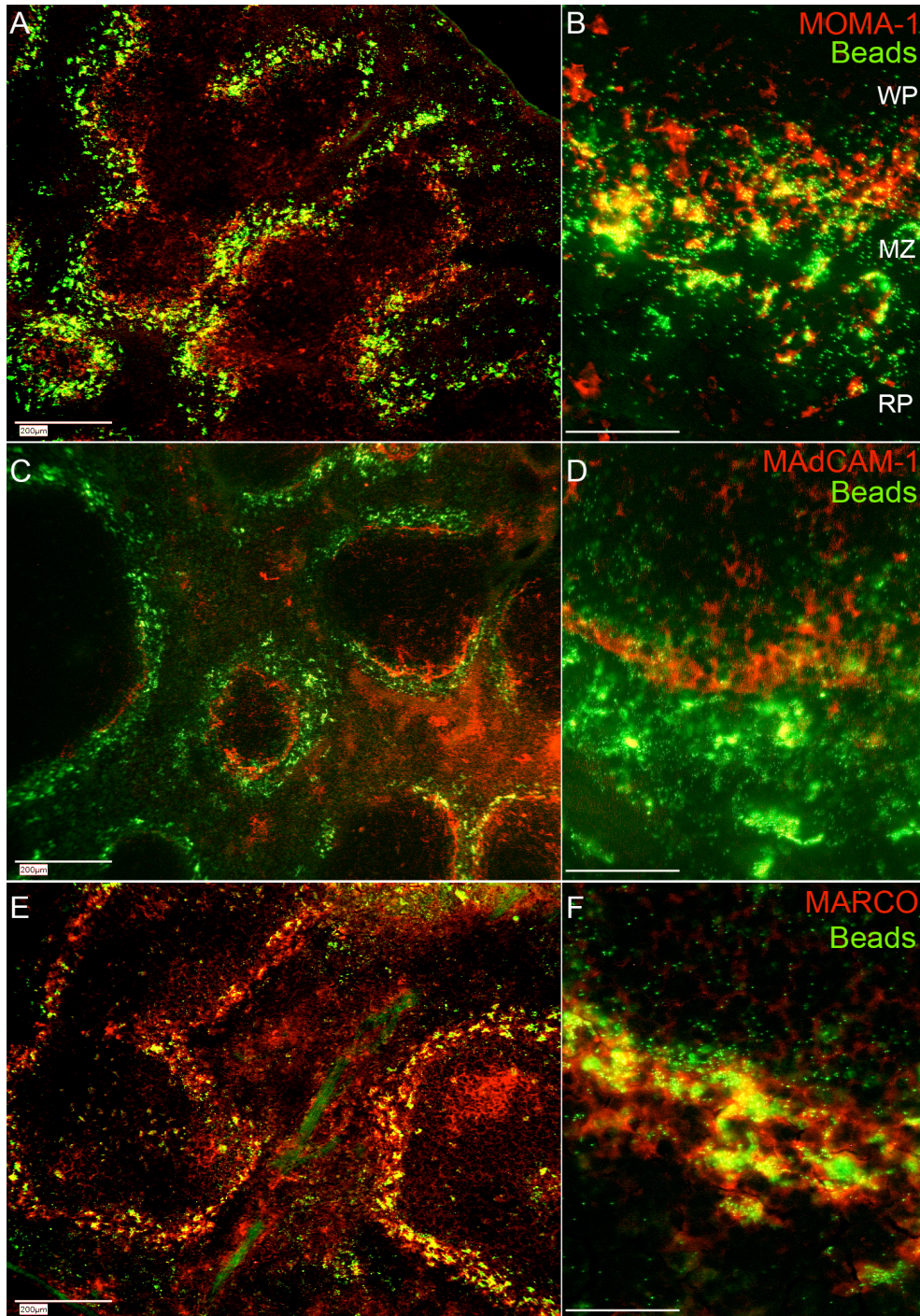
Figure 28. Colocalization of polysytrene beads with cell-type specific markers in the spleen marginal zone.
Beads were injected *i.v.* into mice and spleens were harvested 30 min thereafter. Shown are different magnifications of frozen sections with green fluorescent beads (diameter 170 nm) and cellular antigens detected with a secondary antibody labeled in red. The beads showed a similar distribution as the CPPs before: only a weak co-localization with the MOMA-1 marker for MMM (A, B), no overlap with MAdCAM-1 as a marker for sinus lining cells (C, D) but a strong colocalization with MARCO-positive marginal zone macrophages (E, F). WP, white pulp; MZ, marginal zone and RP, red pulp. Scale bars in A, C and E: 200 µm, bars in B, D and F: 50 µm.

3.2.6 Deposition of Injected Calciprotein Particles in Lung Tissue

Occasionally, spotty fluorescent aggregates were noticed in lung tissue. They were detected in nearly all samples taken from mice injected with CPPs, but were never seen in lung tissue of mice injected with fluorescent fetuin-A (figure 29) or AsF monomer (not shown).
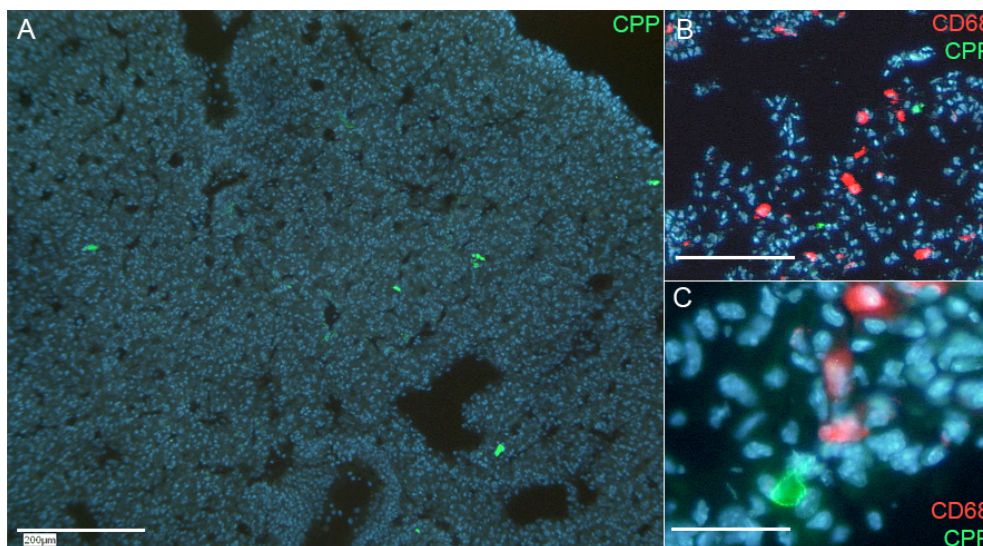
Figure 29. CPP accumulation in the lung microvasculature.
Fluorescent deposits were observed in lung tissue of mice injected with CPPs after a circulation time of 60 minutes. **A:** Distribution of green-fluorescent CPPs in lung tissue. **B, C:** Colocalization studies with the CD68 specific macrophage antibody revealed no overlap of the CPP signal with alveolar macrophages. Shown are the overlays of the DAPI nuclei staining (blue), the green fluorescence of Alexa 488 labeled fetuin-A incorporated in the injected CPPs and the red fluorescence of the CD68 staining, respectively. Scale bars: 200 μm (A, B); 50 μm (C).

The large size of these fluorescent deposits and their distribution indicated aggregation or precipitation of CPPs at predilection sites (figure 29A). Unlike the fluorescence signal of CPPs in liver sections (figure 29A), the signal in lung tissue did not decrease significantly during the observation period of 3 h (not shown). This points to continued deposition without degradation of CPPs in lung tissue. Indeed, immunohistological staining of alveolar macrophages showed that there was no colocalization of CPP aggregates with CD68-positive macrophages (figure 29B, C). The CPP deposits found were often too large to be endocytosed by a phagocytic active cell (figure 29A). Furthermore, lung alveolar macrophages are specialized to take up antigens from the alveolar space rather than from circulation.

3.2.7 *In Vitro* Clearance of CPPs by Macrophages

Liver and spleen are both part of the RES or mononuclear phagocytic system. The RES comprises phagocytes that clear endogenous cell debris, fibrin clots and particulate matter including colloidal particles and bacteria. Foremost among these phagocytes are Kupffer cells in the liver and tissue-resident macrophages in the spleen and stromal tissues (histiocytes). The immunohistological staining with macrophage-specific antibodies (figure

21, 27) showed that CPPs were cleared by macrophages. To study the clearance in detail endocytosis assays using the macrophage-like murine cell line RAW 246.7 were performed.
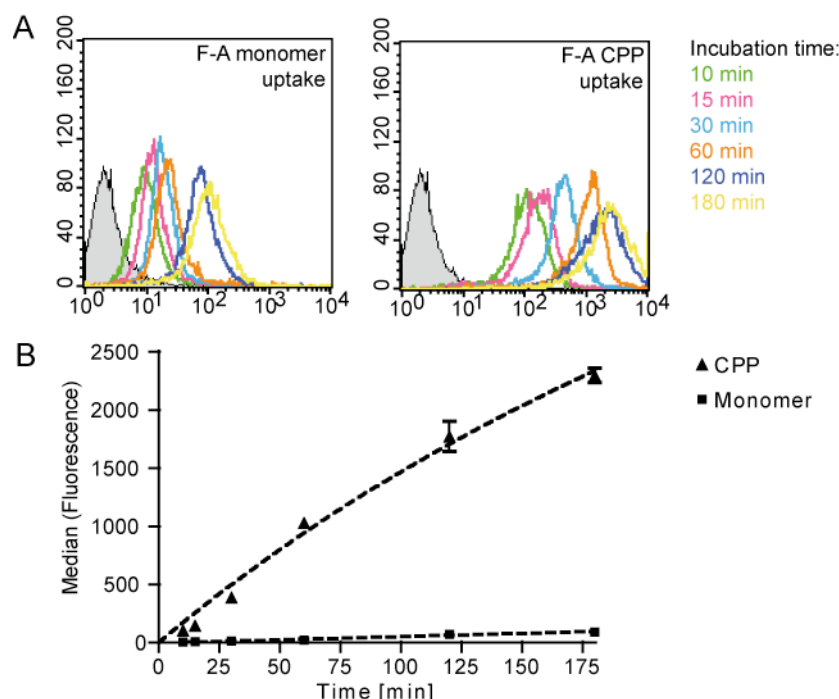
Figure 30. Raw 246.7 cells endocytose CPPs rapidly.
A. Adherent cells were incubated with fetuin-A monomer or CPPs both containing 0.1 mg/ml fluorescent fetuin-A and fluorescence was measured by flow cytometry. Cell count was plotted against cell-associated fluorescence. Each curve represents a different incubation time as indicated in the legend, the filled grey curve represents untreated cells. **B.** Uptake of fetuin-A monomer (squares) and CPPs (triangles) demonstrates highly increased uptake of CPPs in comparison to monomeric fetuin-A.

Figure 30 shows the results of a typical experiment testing endocytosis of fetuin-A monomer and CPPs at 37°C. Uptake was measured by evaluating cell-associated fluorescence using flow cytometry. Figure 29A illustrates the flow cytometry results for cell-specific fluorescence after incubation with fluorescence-labeled fetuin-A monomer (F-A monomer) or CPPs (F-A CPP), respectively. Despite similar amounts of labeled fetuin-A present in both monomer and CPP preparations offered to RAW 246.7 cells (figure 30B squares and triangles, respectively), much more CPPs than fetuin-A monomer were endocytosed. The cell-associated fluorescence signal of fetuin-A monomer ranged between 2 – 6% of the signal detected for CPPs (p < 0.001 for all time points). These results are in full agreement with the *in vivo* clearance shown in figures 20, 21, 25 and 27 that consistently showed much more efficient uptake of fetuin-A containing CPPs than monomeric fetuin-A resulting in colocalization of CPPs but not of fetuin-A monomer with macrophages.

To determine the uptake mechanism for CPPs RAW 246.7 macrophages were pre-incubated with different inhibitors of endocytosis (table 8) for 30 min. Pre-incubation of RAW 246.7 macrophages with cytochalasin D an inhibitor of actin polymerization reduced the uptake of CPPs. This effect was most prominent at the highest CPP concentration (0.1 mg/ml). The

cell-associated fluorescence of internalized CPPs decreased from 1282 to 253 and 151 when 20 µM or 40 µM cytochalasin D were added (ns for 20 µM and $p < 0.01$ for 40 µM, figure 31, table 8). Additionally, binding of CPPs to RAW macrophages in the presence of Cytochalasin D was studied at 4°C. A decrease in cell-associated fluorescence was observed for 0.1 mg/ml CPPs from 184.5 to 93.9 ($p < 0.05$) and 125.3 (n.s.) for 20 µM or 40 µM cytochalasin D, respectively. Theoretically, CPP binding should not be dependent on the cytoskeleton. Thus, the small effect of cytochalasin D at 4°C may be attributed to residual uptake activity of macrophages under these conditions.
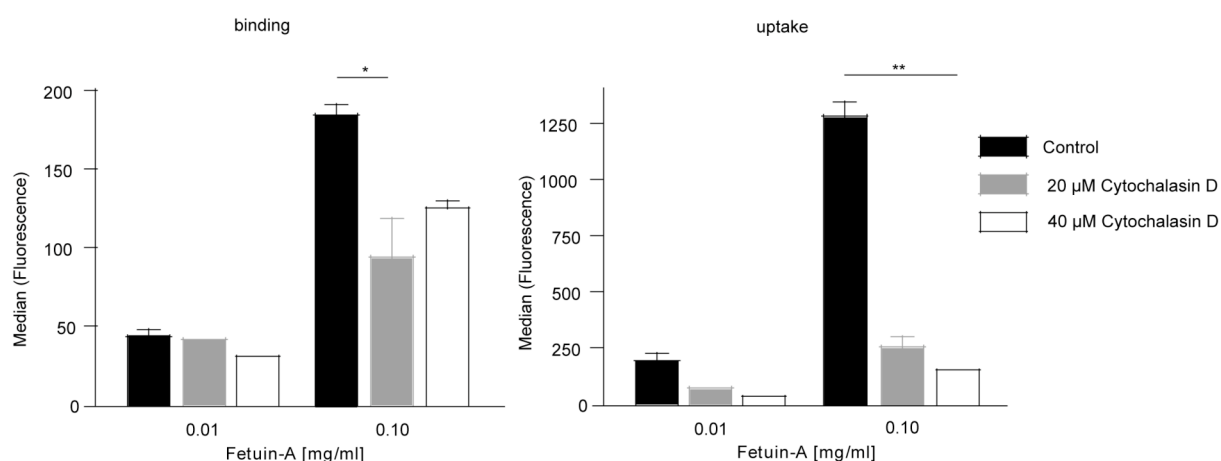
Figure 31. CPP uptake requires the cytoskeleton.
Raw macrophages were incubated with CPPs containing 0.01 or 0.1 mg/ml fluorescent labeled fetuin-A, respectively, for (A) 60min at 4°C or (B) 10 min at 37°C. Cells were pre-treated with the indicated dosage of Cytochalasin D, an inhibitor of actin polymerization, 30 min before addition of CPPs (except controls). Cell-associated fluorescence was measured by flow cytometry. Cytochalasin D slightly reduced CPP binding to macrophages and strongly inhibited the uptake of CPPs. * $p < 0.05$; ** $p < 0.01$.

3.2.8 Inhibition of the Spleen Tyrosine Kinase

The spleen tyrosine kinase (SYK) belongs to the family of non-receptor tyrosine kinases. SYK is a crucial mediator in the signal transduction cascade mediated by transmembrane proteins containing immunoreceptor tyrosine-based activation motifs (ITAMs). ITAM motifs are found associated to a broad range of immunoreceptors [278]. The influence of SYK in binding and uptake of CPPs was evaluated using Piceatannol a known inhibitor of SYK [279]. Figures 32A, B show a dose-dependent inhibition of CPP uptake in both RAW macrophages and bone marrow derived macrophages (BMMs) by pre-treatment of cells with Piceatannol. The CPP uptake was reduced to 19% and 11% of the initial cell-associated fluorescence in RAW macrophages and BMMs, respectively, when 100 µM Piceatannol were applied ($p < 0.001$). Uptake of fetuin-A monomer was low as described before (see chapter 3.2.7) and not affected by Piceatannol treatment. Binding of CPPs, evaluated by incubation of RAW macrophages at 4°C was also not affected by Piceatannol treatment (figure 32C).
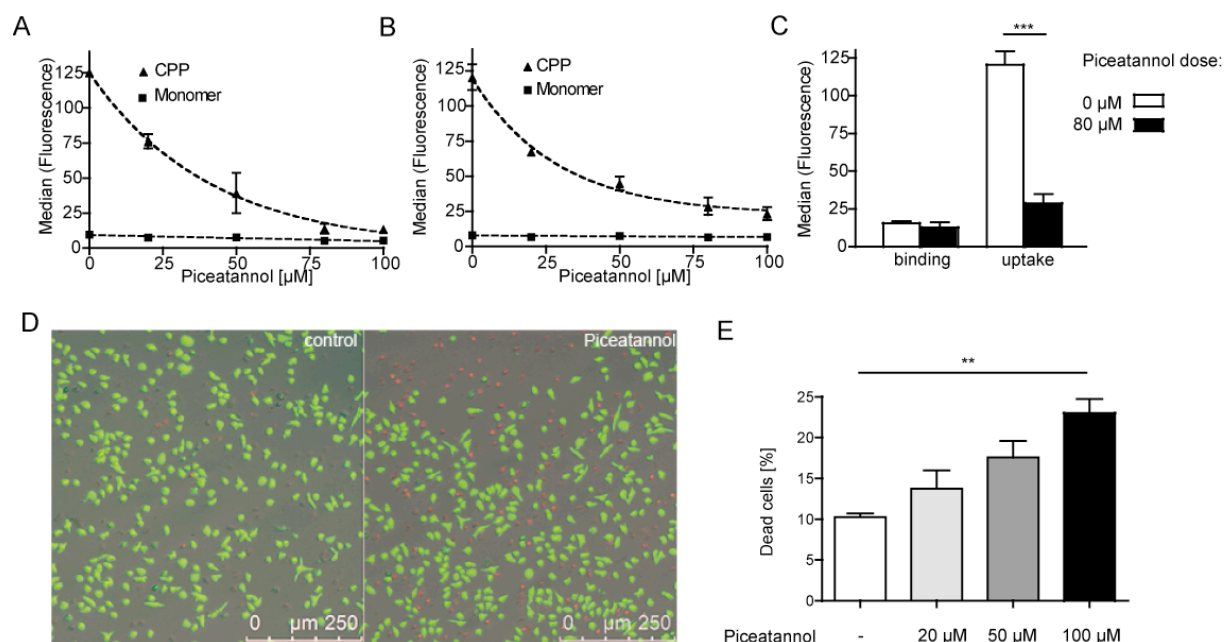
Figure 32. Influence of Piceatannol-treatment on CPP uptake and viability of cells.
A.-C. BMMs (A) or Raw Macrophages (B, C) were pre-treated with Piceatannol an inhibitor of the spleen tyrosin kinase (syk) for 30 min in serum-free medium. Cells were incubated with either fetuin-A monomer or CPPs both containing 0.1 mg/ml fluorescent fetuin-A for 10 min at 37°C (uptake, A-C) or for 60 min at 4°C (binding, C). Cell-specific fluorescence was measured by flow cytometry. **D., E.** Viability of cells after Piceatannol-treatment was evaluated. Adherent cells were incubated with Piceatannol for 30 min. Live/dead staining was performed 1h after removal of Piceatannol. Living cells were stained with FDA (green fluorescence), dead cells stained positive for PI (red fluorescence). (D) Representative picture of control cells (left) and cells treated with 100 μM Piceatannol (right). (E) Quantitative analysis of PI/FDA staining showing increased cell death of Piceatannol-treated cells. ** p < 0.01.

Piceatannol was used in various studies to inhibit SYK [226, 280, 281]. Nevertheless, specificity of this inhibitor is questionable, and inhibition of other kinases was also described [281, 282]. Therefore, the influence of Piceatannol on the uptake of additional ligands including acetylated lipoproteins (acLDLs) and polystyrene beads was evaluated. Although uptake of acLDL is mediated predominantly by a SYK independent route via scavenger receptors [216], endocytosis of acLDL as well as of polystyrene beads was strongly inhibited by Piceatannol treatment (data not shown). Therefore, a live/dead staining was performed to test if reduced particle uptake was attributed to an effect of Piceatannol on cell viability. To address this question viability of Piceatannol-treated cells was evaluated one hour after the treatment. Figure 32D shows a representative fluorescence micrograph of untreated cells and cells incubated with 100 μM Piceatannol clearly demonstrating increased numbers of dead cells. The quantitative analysis shown in figure 31E revealed a doubling in dead cells count at 100 μM Piceatannol compared to untreated cells (p < 0.01).

In summary, a severe reduction in CPP endocytosis following Piceatannol treatment was observed. However, it remains unclear whether this effect was attributed to specific SYK inhibition, to an unspecific inhibition of other kinases involved in signal-transduction or to cytotoxicity.

3.2.9 Fcγ Receptor Does not Participate in CPP Binding and Uptake

Even though a high number of dead cells was seen after Piceatannol treatment it could not be excluded that SYK may participate in CPP endocytosis as the inhibitory effect of CPP uptake overruled the cell mortality. Therefore, Fcγ receptor (FcγR) mediated endocytosis, the most prominent SYK-dependent pathway [280] was further studied. Thus, the role of the endocytosis pathway used by the classical opsonins, immunoglobulins, as well as by the opsonic serum proteins C-reactive protein and serum amyloid P [226, 283] was elucidated. Downstream of SYK phosphatidylinositol 3-kinase (PI3K) acts as a key molecule in the signal transduction pathway of the FcγR. Inhibition of PI3K was studied in RAW macrophages using Ly294002 hydrochloride. Inhibition of PI3K resulted only in a weak reduction of CPP uptake at both CPP concentrations tested (figure 33A). In addition, the role of FcγR in CPP endocytosis was studied in BMMs from FcγR deficient mice in comparison to wildtype BMMs. Cells were incubated with CPPs at 4 °C or 37 °C to study binding and endocytosis, respectively. Figures 33B, C show that neither binding nor endocytosis of CPPs was affected by FcγR deficiency.

In summary, it could be shown that CPP uptake was not mediated by FcγR. Furthermore, a participation of PI3K-dependent pathways was excluded.
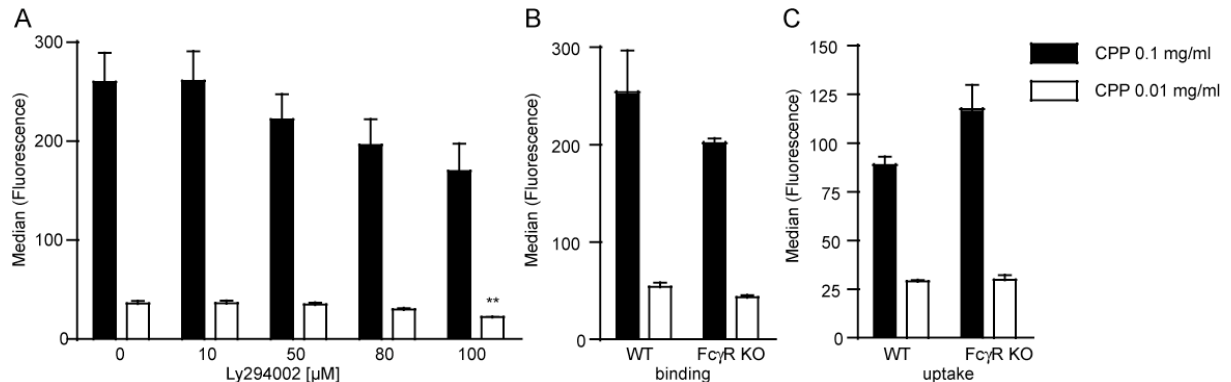
Figure 33. Fcγ receptor does not participate in CPP binding and uptake.
A. Adherent Raw macrophages were pre-treated with Ly294002, an inhibitor of the phosphoinositol-3-kinase, for 30 min in serum-free medium. After that, cells were incubated with CPPs containing 0.01 mg/ml or 0.1 mg/ml fluorescent fetuin-A, respectively, for 10 min at 37°C. Cell-specific fluorescence was measured by flow cytometry. CPP uptake was slightly diminished at the highest inhibitor concentration. ** $p < 0.01$. **B,C.** Bone marrow derived macrophages of wildtype (WT) FcγR- deficient mice were studied. **B.** Binding assay: Cells were seeded (500,000 cells per sample) and incubated on ice for 45 minutes with CPPs. Cell-associated fluorescence was measured by flow cytometry. **C.** Adherent cells (250,000 cells per sample) were incubated at 37°C for 10 minutes with 0.01 mg/ml or 0.1 mg/ml CPPs. Cell-associated fluorescence was measured by flow cytometry. FcγR deficiency did not influence CPP binding and uptake.

Table 8. Summary of CPP binding- and phagocytosis assays.

	binding	uptake
KO BMM:		
C57BL/6 SR-A KO (n=3)	↓ p < 0.001	↓ p < 0.001 (↓ p < 0.001)
C57/BL6 SR-A/MARCO KO (n=3)	↓ p < 0.001	n.d.
C57BL/6 CD36 KO (n=2)	=	n.d.
C57BL/6 Fcγ KO (n=3)	=	=
C57BL/6 AnnexinA5 KO (n=2)	n.d.	=
C57BL/6 AnnexinA6 KO (n=2)	n.d.	=
C57BL/6 Dectin KO (n=2)	n.d.	=
C57BL/6 Galectin 1 KO (n=2)	n.d.	=
C57BL/6 Galectin 3 KO (n=2)	n.d.	=
Inhibitors Raw Mφ:		
Cytochalasin D (20µM, 40 µM)	=	↓ p < 0.01
Piceatannol (10-100 µM)	↓ p < 0.05*	↓ p < 0.001 (↓ p < 0.001*)
Ly294002 (10-100 µM)	n.d.	=
Poly-I (2-40 ng/µl)	n.d.	↓ p < 0.001 (↓ p < 0.001)
Competition BMM:		
acLDL (n=3)	↓ p < 0.01	n.d.

Binding or uptake of fluorescently labeled CPPs (values in brackets refer to CPPs pre-incubated with mouse serum) was analyzed using flow cytometry. Median fluorescence of macrophages was compared to untreated or wildtype control cells with two way ANOVA statistics. Each comparison was repeated at least three times. ↓ reduced binding/uptake of CPPs; ↑ enhanced binding/uptake of CPPs; = no significant change in binding/uptake of CPPs; * only one inhibitor dose tested; n.d. not determined.

3.2.10 Scavenger Receptor-A is Involved in CPP Clearance

It was stated that CPPs resemble lipoprotein particles in many ways [55]. Therefore, the role of scavenger receptors a growing family of receptors known for scavenging modified forms of LDL [216] was studied. First, polyinosinic acid (Poly-I) a well-known ligand of these receptors was used as competitive ligand. Indeed, CPP uptake by RAW macrophages was inhibited when cells were pre-incubated with Poly-I (figure 34D). The cell-associated fluorescence was reduced from 172 to 124 (p < 0.01) and 100 (p < 0.001) when macrophages were pre-incubated with 2 ng/µl or 10 ng/µl Poly-I, respectively (figure 34D). These results confirmed a major role of scavenger receptors in the uptake of CPPs. Here SR-AI/II and the class B scavenger receptor CD36 were studied further. BMMs were prepared from CD36 and SR-AI/II knock-out mice to investigate the role of these receptors in CPP endocytosis. Figure 34A shows CPP uptake in WT (green) and SR-AI/II KO macrophages (pink). Indeed, wildtype macrophages showed higher uptake of fluorescence-labeled CPPs than macrophages from the SR-AI/II deficient mice. The cell-specific fluorescence was reduced in SR-AI/II deficient macrophages at all examined CPP concentrations and ranged from 57% to 73% of the fluorescence signal detected in wildtype macrophages (p < 0.01 for all CPP concentrations tested). To mimic *in vivo* uptake we pre-incubated CPPs with mouse serum before addition to cells. Using this approach, the role of additional serum proteins which may

adhere to CPPs and consequently may influence their uptake, was examined. In fact, studying SR-AI/II-KO BMMs compared to wildtype BMMs the difference in CPP uptake was even more pronounced when CPPs were pre-incubated with mouse serum (figure 34B). Here the fluorescence signal was reduced to 44-49% ($p < 0.001$ for all CPP concentrations tested). Remarkably, CPP uptake in SR-AI/II deficient BMMs was as low as fetuin-A monomer uptake (dashed line figure 34B).

The effect of serum pre-treatment on endocytosis in RAW macrophages incubated with Poly-I was in agreement with these results. While 10 ng/µl Poly-I reduced endocytosis of uncoated CPPs to 52%, uptake of CPPs pre-incubated with serum was reduced to 37%, 32% and 29%, respectively employing mouse, human or fetal calf serum (figure 34D). Remarkably, endocytosis of serum-coated CPPs per se was also reduced in comparison to uncoated CPPs (figure 34D).

In addition to uptake CPP binding to cells was investigated. In agreement with the results from endocytosis assays SR-AI/II deficient BMMs showed diminished CPP binding, the fluorescence signal was reduced to 63-78% compared to wildtype BMMs ($p < 0.05$ for 0.05 mg/ml and 0.175 mg/ml CPPs). The difference in binding was less pronounced than the difference in uptake. This may be explained by the general tendency of CPPs to adhere to the cell membrane, as CPPs also bound to various cell lines including non-professional phagocytic cells, HeLa, Cos1 and Cos7 cells (data not shown). Of note, under the same conditions only negligible binding of fetuin-A monomer was observed in all four macrophage types (dashed lines in figure 34C).

To support the role of SR-AI/II in CPP binding we conducted a competitive binding assay and incubated wildtype BMMs with CPPs in the presence or absence of acetylated low-density lipoprotein particles (acLDL), a known ligand of SR-AI/II. Figure 35 shows that binding of CPPs to macrophages was decreased in the presence of acLDL. The observed cell-associated fluorescence was diminished to 43-71% dependent on CPP concentrations studied ($p < 0.001$).
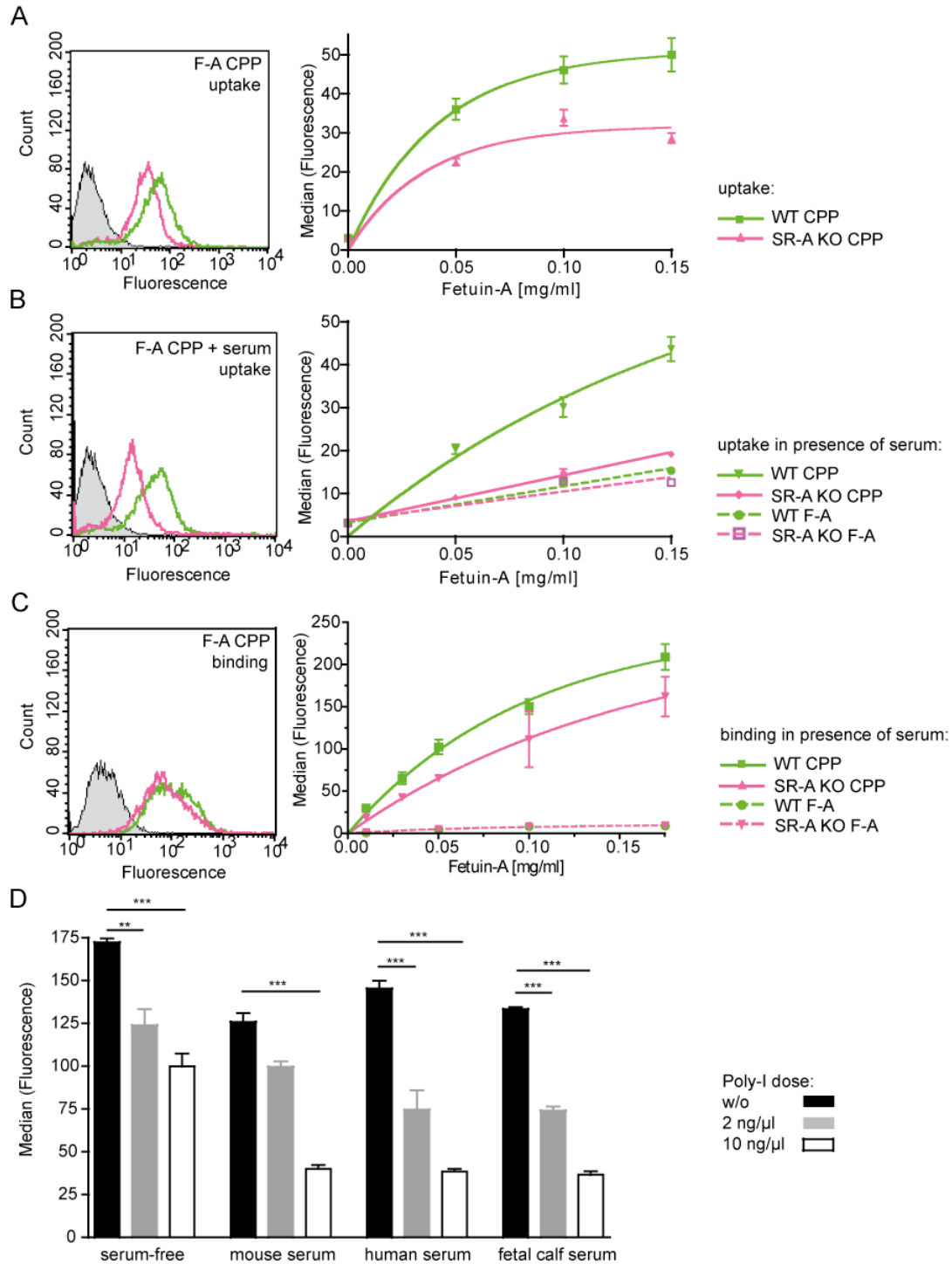
Figure 34. Scavenger receptors are involved in binding and uptake of CPPs.
A-C. BMMs of WT and SR-A KO mice were studied. **A, B.** Uptake assay: Adherent cells were incubated at 37 °C for 10 minutes with CPPs (A) or with fetuin-A monomer or with CPPs pre-treated with serum (B). Cell-associated fluorescence was measured by flow cytometry. Uptake of uncoated CPPs and serum-coated CPPs was concentration dependent and saturable. SR-A KO BMM uptake of CPPs was reduced ($p < 0.001$). Uptake of serum pre-treated fetuin-A monomer was low and did not show any difference between WT and KO. Remarkably SR-A KO macrophage uptake of serum pre-treated CPPs was as low as uptake of fetuin-A monomer. **C.** Binding assay: Cells were seeded and incubated on ice for 45 minutes with CPPs or fetuin-A monomer ranging from 0.01 to 0.175 mg/ml fetuin-A contained in the medium. Cell-associated fluorescence was measured by flow cytometry. The binding of CPPs was concentration dependent saturable. Macrophages from SR-A KO mice showed reduced binding compared to wildtype ($p < 0.001$). Binding of fetuin-A monomer to macrophages of all cell sources was minimal. **D.** Adherent raw macrophages were incubated with CPPs or CPPs pre-incubated with serum in a concentration of 0.1 mg/ml fluorescent labeled fetuin-A for 10 minutes. Cells were treated with the SR-A ligand polyinosinic acid (Poly-I) 30 min before addition of CPPs. Cell-associated fluorescence was measured by flow cytometry. Poly-I dose-dependently reduced CPP uptake. Serum absorption to CPPs slightly diminished the overall uptake of CPPs, yet caused an even greater inhibition of uptake by Poly-I. ** $p < 0.01$; *** $p < 0.001$
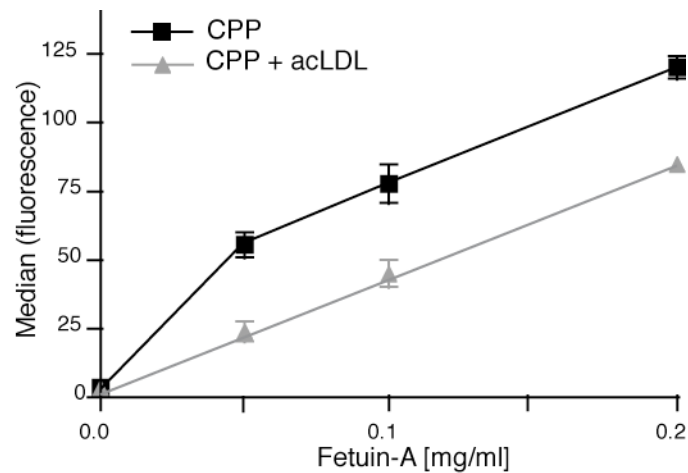
Figure 35. Competitive binding of CPPs and acetylated LDL.
Bone marrow derived macrophages from wildtype mice were seeded and incubated on ice for 45 minutes with CPPs in the presence or absence of 10 µg/ml acetylated LDL (acLDL). Cell-associated fluorescence was measured by flow cytometry. Added acLDL decreased CPP binding at all concentrations of fetuin-A. *** p < 0.001

While SR-AI/II was essential for CPP binding and endocytosis, the acLDL receptor CD36 [284], had no impact on CPP binding. Binding of CPPs to CD36 deficient BMMs was at the same level as to wildtype BMMs (data not shown, table 8). Although endocytosis of CPPs particles was strongly decreased in SR-AI/II deficient BMMs, a small proportion of CPPs was still taken up. Thus, other receptors may contribute to CPP uptake. Annexins 2, 5, and 6 have been reported to mediate fetuin-A endocytosis [123, 285], apoptotic cell clearance [252] and enhanced lipoprotein particle endocytosis [253], respectively. However, the endocytosis of CPPs either in the absence or the presence of serum was not affected by annexin A5 or annexin A6 deficiency (figure 36B, C).

Finally, the influence of the C-type lectin dectin-1 on CPP endocytosis was studied. Dectin-1 is involved in antifungal immunity and recognizes β-glucan as well as unidentified bacterial and endogenous ligands [254]. Importantly, dectin-1 signaling includes SYK [278]. Since a contribution of SYK in CPP endocytosis could not be excluded (see chapter 3.2.8), SYK-dependent receptors, e.g. dectin-1 may be critically involved in CPP uptake. This possibility was studied using the well established endocytosis assay comparing BMMs from KO mice with wildtype BMMs. Figure 36A shows that dectin-1 deficiency had no influence on CPP uptake.
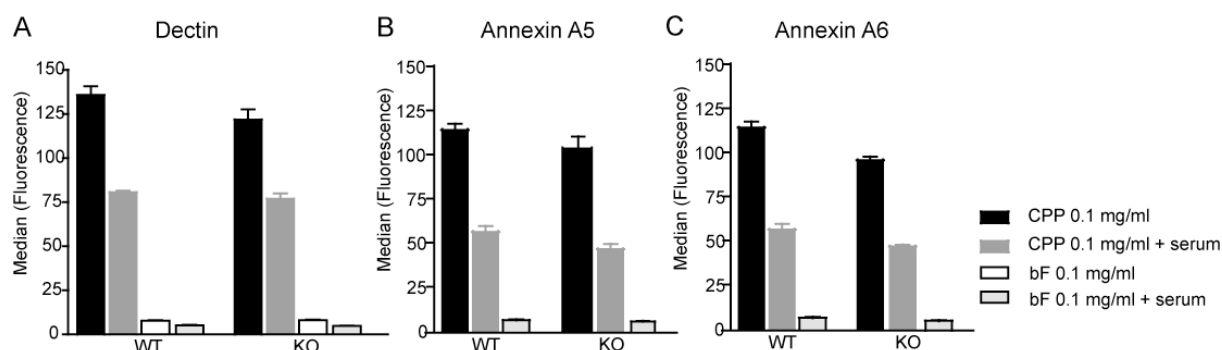
Figure 36. CPP uptake in Dectin- Annexin A5- and Annexin A6- deficient macrophages.
Bone marrow derived macrophages of wildtype (WT) and Dectin- (A), Annexin A5-(B) and Annexin A6- (C) deficient mice were studied. Adherent cells were incubated at 37°C for 10 minutes with 0.1 mg/ml CPPs or fetuin-A monomer with or without serum pre-treatment (see legend). Cell-associated fluorescence was measured by flow cytometry. Observed fluorescence was dependent on the ligand presented but none of the studied receptor deficiencies (KO) caused reduced CPP uptake.

In summary, the results suggest that CPPs are bound and taken up by macrophages via receptor-mediated endocytosis and that tissue macrophages such as marginal zone macrophages in the spleen and Kupffer cells in the liver participate in this uptake. The uptake mechanism is restricted to the fetuin-A containing CPPs, because fetuin-A monomer circulates much longer *in vivo* and distributes differently in the body when compared to CPPs. Binding and uptake of CPPs by macrophages is predominantly mediated by SR-AI/II while CD36, Fcγ, dectin-1, annexin A5 or annexin A6 are not involved.

3.2.11 Does a Galectin-Fetuin Interaction Influence CPP Uptake?

The galectin family of proteins shares an affinity for β-galactosides. In addition, all galectins contain a homologous carbohydrate recognition domain (CRD) [286]. Various functions of galectins have been described in immune cells [287]. In macrophages, it was shown that galectin-1 inhibited phagocytosis via FcγR [255] while galectin-3 was effective in enhancing clearance of apoptotic neutrophils [256]. To elucidate the role of these galectins in CPP uptake, CPP endocytosis was studied in galectin-1 and galectin-3 deficient BMMs in comparison to wildtype BMMs. Since a lipopolysaccharide (LPS)-galectin interaction was reported in particular for galectin-3 [288], the influence of LPS stimulation was examined as well. Figure 37 shows that neither galectin-1 nor galectin-3 deficiency affected endocytosis of uncoated or serum-coated CPPs or fetuin-A monomer. Even following LPS stimulation no differences among galectin genotypes were observed (figure 37B).
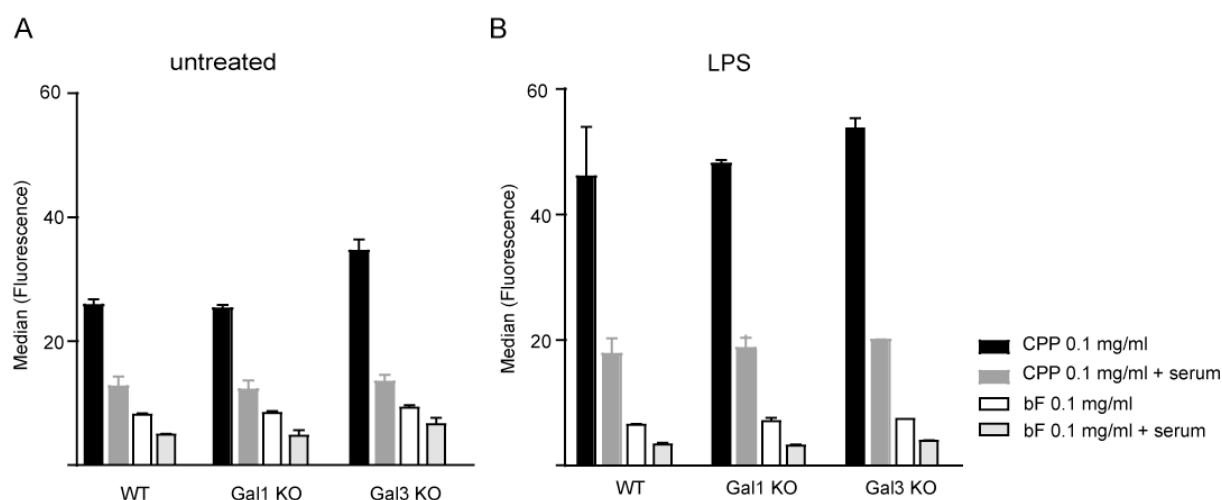
Figure 37. Does a galectin – fetuin-A interaction influence CPP uptake?
Bone marrow derived macrophages of wildtype (WT), Galectin 1 and Galectin 3 deficient mice were studied. Cells were seeded and incubated in presence of 1 µg/ml LPS (except controls), after 24h 0.1 mg/ml CPPs or fetuin-A monomer (serum-coated or serum-free, as indicated) were added and cells were incubated for 10 minutes at 37°C. Cell-associated fluorescence was measured by flow cytometry. LPS treatment increased the uptake of serum-free CPPs ($p < 0.05$) but not of the other ligands, the galectin genotype had no influence on CPP uptake.

Thus, for the first time it could be shown that fetuin-A stabilized calciprotein particles, CPPs were removed from circulation fast and efficient *in vivo*. Cells of the reticuloendothelial system, namely hepatic Kupffer cells and splenic marginal zone macrophages contributed to the clearance of CPPs but not of fetuin-A monomer. It could be shown that macrophage uptake of CPP is receptor mediated and that in particular scavenger receptor AI/II is essential for CPP endocytosis.

3.3 Prevention of Ectopic Calcification in B6 Fetuin-A Deficient Mice

While fetuin-A deficiency combined with DBA/2 (D2) genetic background led to severe soft tissue calcification (see 3.1), C57BL/6 (B6) fetuin-A deficient mice were resistant to spontaneous ectopic calcification. In this part of the thesis, mechanisms involved in the prevention of ectopic calcification in resistant B6 mice were studied.

3.3.1 Gene Expression Analysis

To identify putative candidate genes involved in the inhibition of dystrophic calcification in fetuin-A deficient B6 mice, differential gene expression in liver and kidney of fetuin-A deficient and wildtype mice was studied. The genome wide expression pattern of non-calcifying B6 mice and calcifying D2 mice were analyzed by comparative genomic and bioinformatics tools to identify compensatory genes. Gene expression in kidney was evaluated to identify local changes in gene expression induced by calcification, while gene expression in liver was examined to identify systemic changes in gene expression induced by calcification.

3.3.1.1 Gene Expression Profile of Kidney of B6 Fetuin-A Deficient Mice

Gene expression profiles of kidneys were examined in 5-week-old B6 fetuin-A deficient and wildtype mice using genome wide gene expression microarrays. The quality of microarrays was evaluated using the ArrayQualityMetrics package [241] and Bioconductor software [239]. Exemplary results from the quality analysis are illustrated in figure 38.

Figure 38. Quality assessment of B6 kidney microarrays.
Quality of microarrays was assessed using arrayQualityMetrics package under bioconductor. **A:** Boxplot demonstration of array intensity distribution. Each box corresponds to one array. The plot summarizes the distribution of probe intensities ($\log_2$ intensities are plotted on the y-axis) across all arrays. Sizes of boxes were in the same range, whereas the comparison of medians revealed fluctuation between arrays. **B:** Density plot illustrates the density of a given intensity within an array; as expected a comparable pattern was found for all arrays. **C:** Affymetrix quality control (QC) stats report. The percentages of "present" calls are given for each array in the left row, upper number, the lower numbers give the average background value for the corresponding arrays. The number of present calls was within the same range for all arrays. The background value confirmed the fluctuations seen in A. The relation between 3' probe sets and 5' probe sets of the control genes β-actin (triangles) and GAPDH (circles) was inside the recommended threshold (light blue box) for all arrays. **D:** Heatmap representation of the distance between arrays. The false color heatmap depicts the mean absolute distance of the M-values for each pair of arrays, with M = $\log_2(\text{intensity}_1)$ - $\log_2(\text{intensity}_2)$, where intensity_1 is the intensity of the array studied and intensity_2 is the intensity of a "pseudo"-array, which has the median value of all arrays. This plot confirmed the variability between arrays. Note that arrays ko1-3 and wt4-6 correspond to female mice, arrays ko4-6 and wt1-3 correspond to male mice.

The mean intensity of arrays showed slight fluctuations, but no outlier was detected (figure 38A-B). This could be confirmed via the Affymetrix quality control report (figure 38C) including the measurement of the relation between 3' probe sets and 5' probe sets of the control genes β-actin and GAPDH. The low amount of variation in mean intensities likewise suggested a good method reproducibility (figure 38D). Therefore, all arrays were included in the analysis of differential expression of WT and KO mice. The gene expression patterns are represented in a Volcano plot (figure 39). Each probe set is depicted as one dot according to its p-value and expression ratio between WT and KO mice. The most interesting candidate genes have the lowest p-value (red label) and the highest log-ratio (blue label). They are found in the upper right and upper left corner of the plot. Only few genes were found in these regions. In total, 74 probe sets (supplemental table 3) were significantly differentially regulated (probe sets with a p-value < 0.05 after multiple testing correction were considered significant).

Figure 39. Gene expression in kidney of B6 wildtype and knockout mice.
Volcano plot demonstration of gene expression in kidney. Examined mice had B6 genetic background and were 5-week-old. Differential expression between fetuin-A deficient and wildtype mice is shown as log-ratio on the x-axis, negative values represent higher expression in KO mice, positive values represent higher expression in wildtype mice. The y-axis encodes the probability for differential regulation calculated by Bayesian statistics in the Limma package under Bioconductor. Each dot denotes a probe set, probe sets with highest probability score are depicted in blue and probe sets with highest log-ratio are depicted in red, marked probe sets are labeled with the appropriate gene name.

Table 9. Differential expression in kidney of B6 fetuin-A deficient mice.

probe set	symbol	p-value	log-ratio
upregulation			
D site albumin promoter binding protein	Dbp	< 0.001	-3.169
cytochrome P450, family 24, subfamily a, polypeptide 1	Cyp24a1	0.003	-2.987
D site albumin promoter binding protein	Dbp	< 0.001	-2.890
RIKEN cDNA 4933439C20 gene	4933439C20Rik	0.001	-2.366
RIKEN cDNA 4933439C20 gene	4933439C20Rik	< 0.001	-2.010
downregulation			
aldo-keto reductase family 1, member C14	Akr1c14	< 0.001	2.928
aldo-keto reductase family 1, member C18	Akr1c18	0.001	2.519
alpha-2-HS-glycoprotein	Ahsg	< 0.001	2.466
lymphocyte antigen 6 complex, locus F	Ly6f	< 0.001	2.387
RIKEN cDNA 9130221J18 gene	9130221J18Rik	0.001	2.017

The table shows probe sets, which were significant (p-value < 0.05) differentially expressed in kidney dissected from 5-week-old B6 wildtype (n=4) and fetuin-A deficient mice (n=6). Bayesian statistic was used for calculation of probabilities (p-value) and log-ratio, negative log-ratio encodes upregulation of the particular probe-set in fetuin-A deficient mice, positive values denote downregulation. The table shows most highly differentially regulated genes with a log-ratio above 2. Note that gene names are given for each probe set, double entries may occur in case of genes which are represented by several probe sets encoding different regions or splice variants of the gene.

Differentially regulated probe sets with a fold change above 4 (log-ratio > 2) are summarized in table 9. Five probe sets matching these criteria were differentially upregulated. They correspond to the genes D site albumin promoter binding protein (*Dbp*), cytochrome P450, family 24, subfamily a, polypeptide 1 (*Cyp24a1)* and the RIKEN cDNA 4933439C20 gene (*4933439C20Rik*). *Dbp,* a transcription factor under circadian control [289], was represented by two probe sets showing 9- and 7.4-fold upregulation. *Cyp24a*1, encoding the 25-hydroxyvitamin D-24-hydroxylase enzyme (24-OHase), was 7.9-fold increased in KO mice. 24-OHase is responsible for the catabolic breakdown of 1,25-dihydroxyvitamin D, the active form of vitamin D [290]. Further highly upregulated probe sets were the two probe sets corresponding to the transcribed sequence *4933439C20Rik* showing 5.2- and 4-fold upregulation, respectively. Five probe sets were strongly downregulated (table 9, log-ratio > 2). Aldo-keto reductase family 1, member C14 was 7.6-fold decreased and expression of aldo-keto reductase family 1, member C18 was 5.7-fold reduced in fetuin-A deficient mice. Both enzymes belong to the family of hydroxysteroid dehydrogenases [291]. Fetuin-A deficiency could be detected in that the *Ahsg* gene was 5.5-fold downregulated. Further decreased probe sets were lymphocyte antigen 6 complex, locus F, showing 5.2-fold downregulation and the transcribed sequence RIKEN cDNA 9130221J18 gene showing 4.1-fold downregulation.

The following part of the thesis focused on the identification of genes having a compensatory function and thus contributing to prevention of ectopic mineralization. To detect candidate genes, differentially expressed genes in fetuin-A deficient B6 mice were chosen. Expression of these candidates was analyzed in calcifying D2 fetuin-A deficient mice as well, and genes

showing differential regulation (log-ratio > 1) were excluded. Exclusion was decided based on the fact that these genes obviously were not efficient in inhibition of pathological calcification as severe soft tissue mineralization occurred in D2 fetuin-A deficient mice. The resulting candidates are illustrated in a heatmap (figure 40).
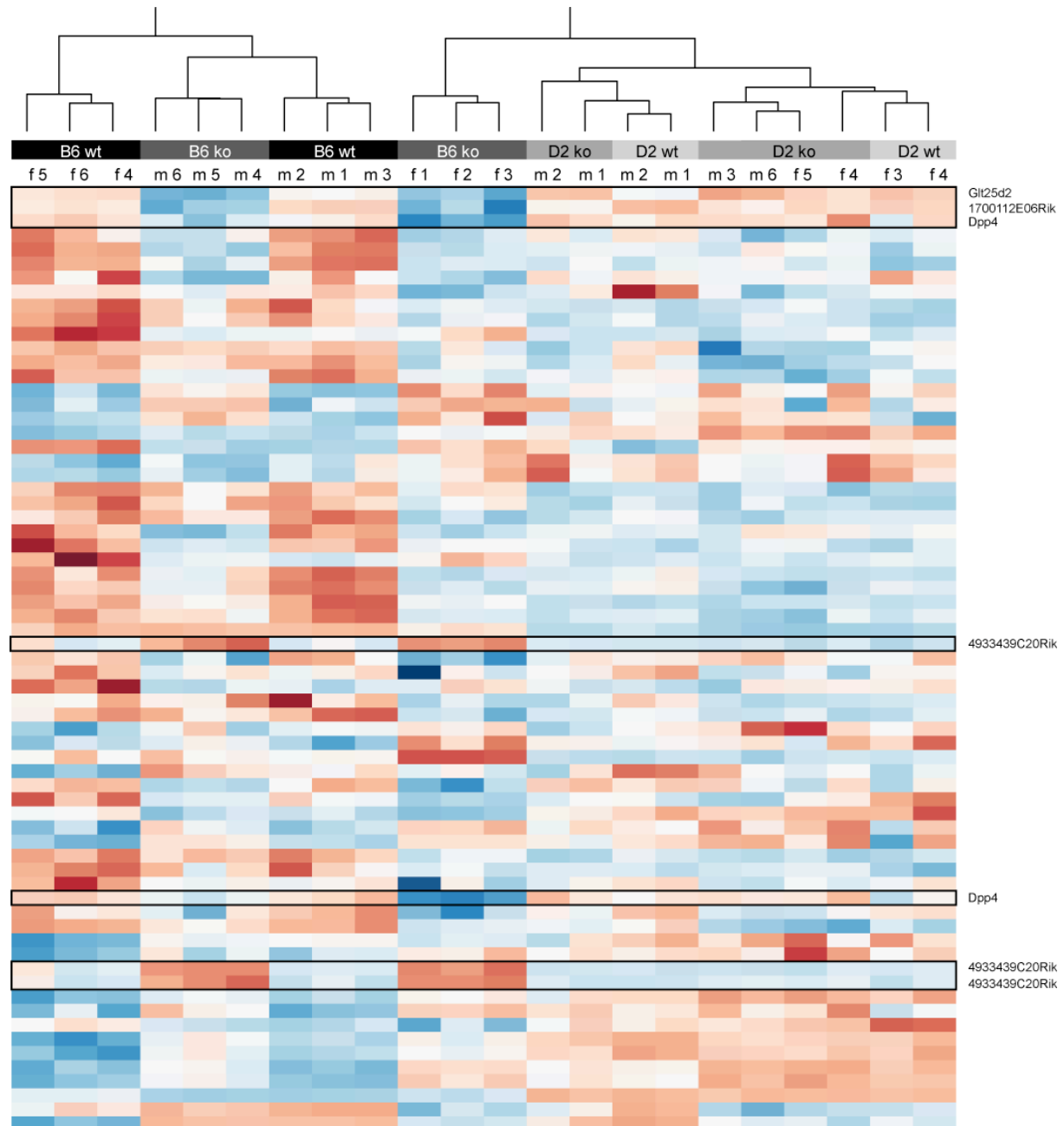
Figure 40. Heatmap representation of differentially expressed genes in kidney of B6 mice.
Differential expression in kidneys of 5-week-old fetuin-A deficient and wildtype mice was calculated using Bayesian statistics under Bioconductor. Probe sets shown were significantly (p < 0.05) differentially expressed in B6 mice; probe sets, which were altered in kidneys of D2 mice (log-ratio > 1) were excluded. Each column corresponds to one DNA array; each row represents a probe set. The color encodes the expression intensity of individual probe sets, ranging from highest expression values in dark red, medium expression values in white to lowest expression values in dark blue. Probe sets, which were altered in B6 knockout animals in comparison to all other genotypes are encircled (black boxes) as candidate genes for a compensatory effect. Hierarchical clustering of arrays according to the shown subset of genes revealed that B6 genotypes were differentiated by this subset while D2 genoytpes were partially unassigned.

Expression values in B6 fetuin-A deficient and wildtype mice as well as in mice with D2 genetic background are color-coded, lowest expression values are depicted in dark blue, medium expression values in white and highest expression values in dark red. The arrays were assigned to columns according to a hierarchical clustering algorithm of this subset of genes. Assignment of arrays matched the fetuin-A genotype in the B6 samples, whereas D2 arrays clustered only partially according to the *Ahsg* genotype. This finding confirmed the specific importance of this gene subset in fetuin-A deficient B6 mice but not in D2 mice.

Seven candidate probe sets could be identified using this heatmap representation. These candidates were of special interest because they showed (i) high expression values in B6 fetuin-A deficient mice along with low expression values in B6 and D2 wildtype and in D2 fetuin-A deficient mice or (ii) they showed remarkably low expression values in B6 fetuin-A deficient mice and high expression values in all other genotypes. Probe sets with high expression values encode for *4933439C20Rik*. Probe sets showing low expression in B6 fetuin-A deficient mice correspond to dipeptidyltransferase 4 (*Dpp4*), glycosyltransferase 25 domain containing 2 (*Glt25d2*) and the transcribed sequence RIKEN cDNA 1700112E06 gene (*1700112E06Rik*). It seems unlikely that a compensatory mechanism based on downregulation of genes prevented ectopic mineralization in B6 fetuin-A deficient mice. If such a mechanism existed the candidate gene would be inhibited in non-calcifying wildtype mice. Therefore, it was assumed that prevention of calcification in B6 fetuin-A deficient mice might be due to compensatory upregulation of candidate genes. Thus, the expression profile and function of the uniquely upregulated probe sets corresponding to *4933439C20Rik* was further studied (see chapter 3.3.1.3).

3.3.1.2 Gene Expression Profile in Liver of B6 Fetuin-A Deficient Mice

Gene expression profile of liver was examined in 5-week-old B6 *Ahsg* -/- and *Ahsg* +/+ mice using genome wide gene expression microarrays. The quality of microarrays was evaluated using the ArrayQualityMetrics package [241] under Bioconductor [239]. Exemplary results from the quality analysis are illustrated in figure 41. The mean intensity of arrays showed slight fluctuations (figure 41A-B). No outlier could be identified, which could be confirmed by the Affymetrix quality control report (figure 41C) including the measurement of the relation between 3' probe sets and 5' probe sets of the control genes β-actin and *GAPDH*. Last not least the distance in mean intensities between arrays was evaluated showing again that only little variability occurred (figure 41D). Therefore, all arrays were included in the analysis of differential expression among WT and KO mice. The gene expression pattern is illustrated in a Volcano plot (figure 42). Each probe set is depicted as a single dot according to its p-value and the ratio between WT and KO mice. The most interesting candidates have the lowest p-values (red label) and the highest log-ratios (blue label). They can be found in the upper right and upper left corner of the plot. Only few genes were found in these regions.
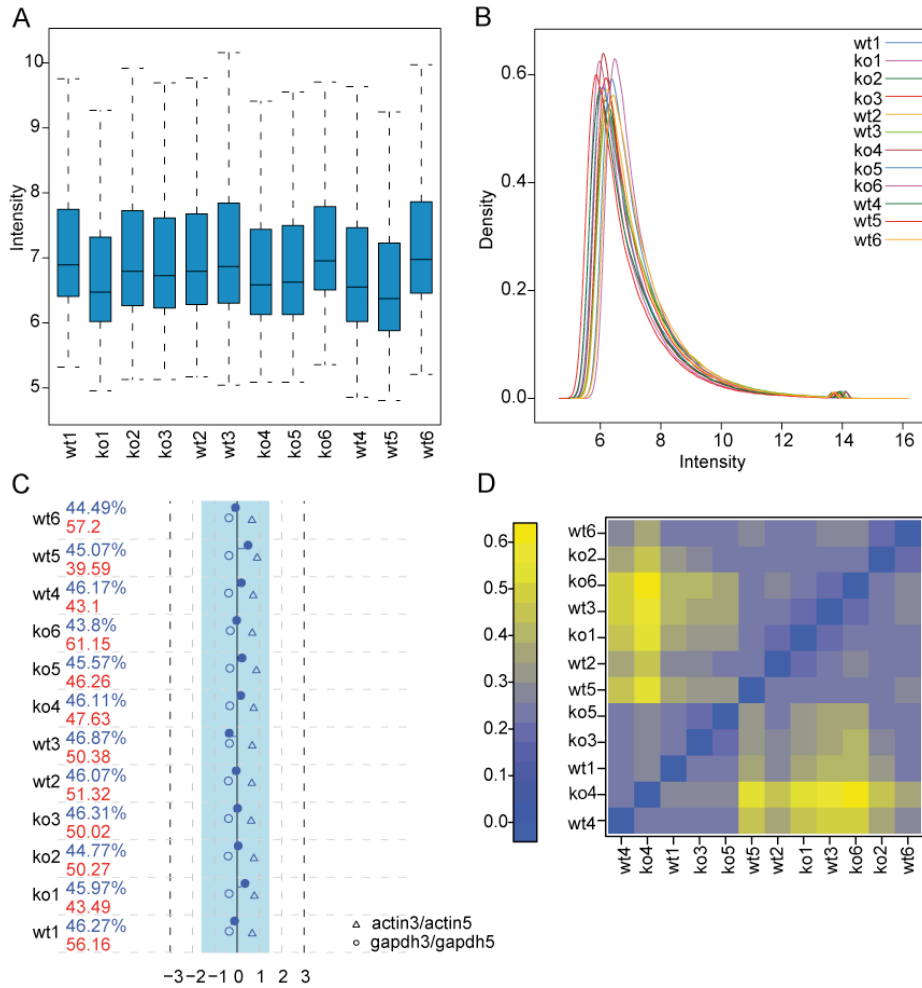
Figure 41. Quality assessment of B6 liver microarrays.
Quality of microarrays was assessed using ArrayQualityMetrics package under Bioconductor. **A:** Boxplot demonstration of array intensity distribution. Each box corresponds to one array. The plot summarizes the distribution of probe intensities ($\log_2$ intensities are plotted on the y-axis) across all arrays. Sizes of boxes were in the same range, comparison of medians revealed slight variations between arrays. **B:** Density plot illustrates the density of a given intensity within an array; as expected a comparable pattern was found for all arrays. **C:** Affymetrix quality control (QC) stats report. The number of present calls (left row, upper number) was within the same range for all arrays. The background value (left row, lower numbers) confirmed slight fluctuations as seen in A. The relation between 3' probe sets and 5' probe sets of the control genes β-actin (triangles) and GAPDH (circles) was inside the recommended threshold (light blue box) for all arrays. **D:** Heatmap representation of distance between arrays. The false color heatmap depicts the mean absolute distance of M-values for each pair of arrays, with M = $\log_2$(intensity$_1$) - $\log_2$(intensity$_2$), where intensity$_1$ is the intensity of the array studied and intensity$_2$ is the intensity of a "pseudo"-array, which has the median values of all arrays. This plot confirmed slight variability between arrays. Note that arrays ko1-3 and wt4-6 correspond to female mice, arrays ko4-6 and wt1-3 correspond to male mice.

In total, 273 probe sets (supplemental table 4) were significantly differentially regulated (probe sets with a p-value < 0.05 after multiple testing correction were considered as significant). Differentially regulated probe sets with a fold change above 4 (log-ratio >2) are summarized in table 10. Two probe sets corresponding to *Dbp* were highly upregulated with a fold change of 28.3 and 12.8, a comparable uregulation of *Dbp* was already detected in kidney (see 3.3.1.1). The non-lysosomal protease cathepsin E, implicated in several physiological and pathological processes [292], was 13.6-fold increased in B6 fetuin-A deficient mice. Another upregulated probe set was the non-coding H19 fetal liver mRNA with a fold change of 7.9. Two probe sets matching period homolog 3 (*Per3*) were 7.4-fold and 4.2-fold

upregulated. *Per3* and *Dbp* are transcription factors under circadian control [293]. Renin 1, constitutively expressed in the kidney and counter regulating angiotensin, was 4.9-fold increased in the liver of B6 fetuin-A deficient mice. Furthermore, regulator of G-protein signaling 16 (*Rgs 16*) showed a 4.2-fold upregulation. Like *Per3* and *Dbp, Rgs 15* is involved in the maintenance of circadian rhythm [294].
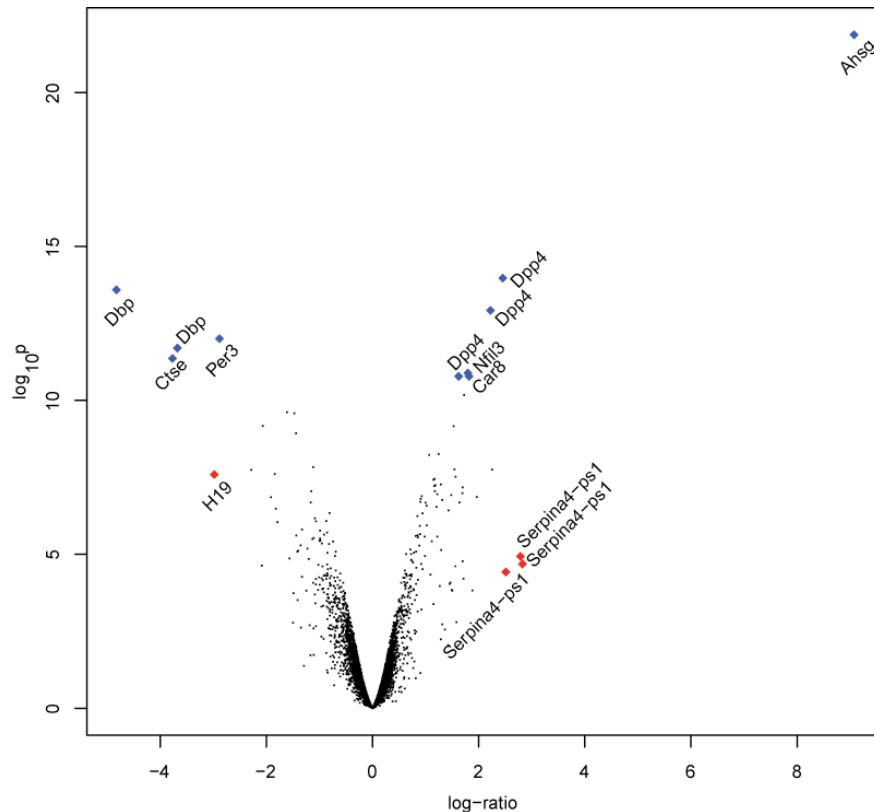
Figure 42. Gene expression in liver of B6 wildtype and knockout mice.
Volcano plot demonstration of gene expression in liver. Examined mice had B6 genetic background and were 5-week-old. Differential expression between fetuin-A deficient and wildtype mice is shown as log-ratio on the x-axis, negative values represent higher expression in KO mice, positive values represent higher expression in wildtype mice. The y-axis encodes the probability for differential regulation calculated by Bayesian statistics in the Limma package under Bioconductor. Each dot denotes a probe set, probe sets with highest probability score are depicted in blue and probe sets with highest log-ratio are depicted in red, marked probe sets are labeled with the appropriate gene name.

The most highly downregulated probe set (fold-change 538.6) represents fetuin-A, which is constitutively expressed in the liver. This finding confirmed the knockout of *Ahsg*. Additionally, 3 probe sets matching the serine (or cysteine) peptidase inhibitor, clade A, member 4, pseudogene 1 were 7.1-fold, 6.9-fold and 5.7-fold decreased, respectively. Downregulation of two probe sets encoding for *Dpp4* and showing 5.5-fold and 4.7-fold reduction, respectively, resembled the expression pattern in the kidney. Another highly downregulated probe set was the transcribed sequence A4630005I04Rik with a fold-change of 4.8.

Table 10. Differential expression in liver of B6 fetuin-A deficient mice.

probe set	symbol	p-value	log-ratio
upregulation			
D site albumin promoter binding protein	Dbp	< 0.001	-4.823
cathepsin E	Ctse	< 0.001	-3.768
D site albumin promoter binding protein	Dbp	< 0.001	-3.676
H19 fetal liver mRNA	H19	< 0.001	-2.980
period homolog 3 (Drosophila)	Per3	< 0.001	-2.882
renin 1 structural	Ren1	< 0.001	-2.282
regulator of G-protein signaling 16	Rgs16	0.005	-2.084
period homolog 3 (Drosophila)	Per3	< 0.001	-2.070
downregulation			
alpha-2-HS-glycoprotein	Ahsg	< 0.001	9.073
serine (or cysteine) peptidase inhibitor, clade A, member 4, pseudogene 1	Serpina4-ps1	0.005	2.826
serine (or cysteine) peptidase inhibitor, clade A, member 4, pseudogene 1	Serpina4-ps1	0.003	2.787
serine (or cysteine) peptidase inhibitor, clade A, member 4, pseudogene 1	Serpina4-ps1	0.008	2.513
dipeptidylpeptidase 4	Dpp4	< 0.001	2.454
RIKEN cDNA A630005I04 gene	A630005I04Rik	< 0.001	2.254
dipeptidylpeptidase 4	Dpp4	< 0.001	2.222

The table shows probe sets, which were significantly (p-value < 0.05) differentially expressed in liver dissected from 5-week-old B6 wildtype (n=4) and fetuin-A deficient mice (n=6). Bayesian statistic was used for calculation of probabilities (p-value) and log-ratio, negative log-ratio encodes upregulation of the particular probe-set in fetuin-A deficient mice, positive values denote downregulation. The table shows most highly differentially regulated genes with a log-ratio above 2. Note that gene names are given for each probe set, double entries may occur in case of genes which are represented by several probe sets encoding different regions or splice variants of the gene.

The most interesting compensatory candidate genes in non-calcifying B6 fetuin-A deficient mice should be the ones showing differential expression in B6 *Ahsg* -/- mice but not in calcifying D2 *Ahsg* -/- mice. Figure 43 shows a heatmap demonstration of the candidate genes. The expression values of probe sets are encoded by color. Probe sets with low expression value are depicted in dark blue, probe sets with medium expression value are depicted in white and high expression is shown in dark red. Assignment of arrays by hierarchical clustering showed a pattern reminiscent of kidney arrays (see chapter 3.3.1.1), where arrays were clustered according to the fetuin-A genotype in the case of B6 derived samples, but not in the case of D2 derived samples.

The most interesting candidate genes were characterized by their color pattern in the heatmap representation and were marked by black boxes. Using this approach, 10 candidate probe sets could be identified. Three probe sets matched the transcribed sequence *4933439C20Rik* that were also detected in the kidney. Further candidates were transcribed sequence *64307056D22 Rik* (two probe sets), response to metastatic cancer 5 (*Rmcs5*), histocompatibility antigen *H2-A1*, serine peptidase inhibitor, clade A, member 7 (*Serpina7*) and nuclear receptor subfamily 5, group A, member 2 *(Nr5a2).*
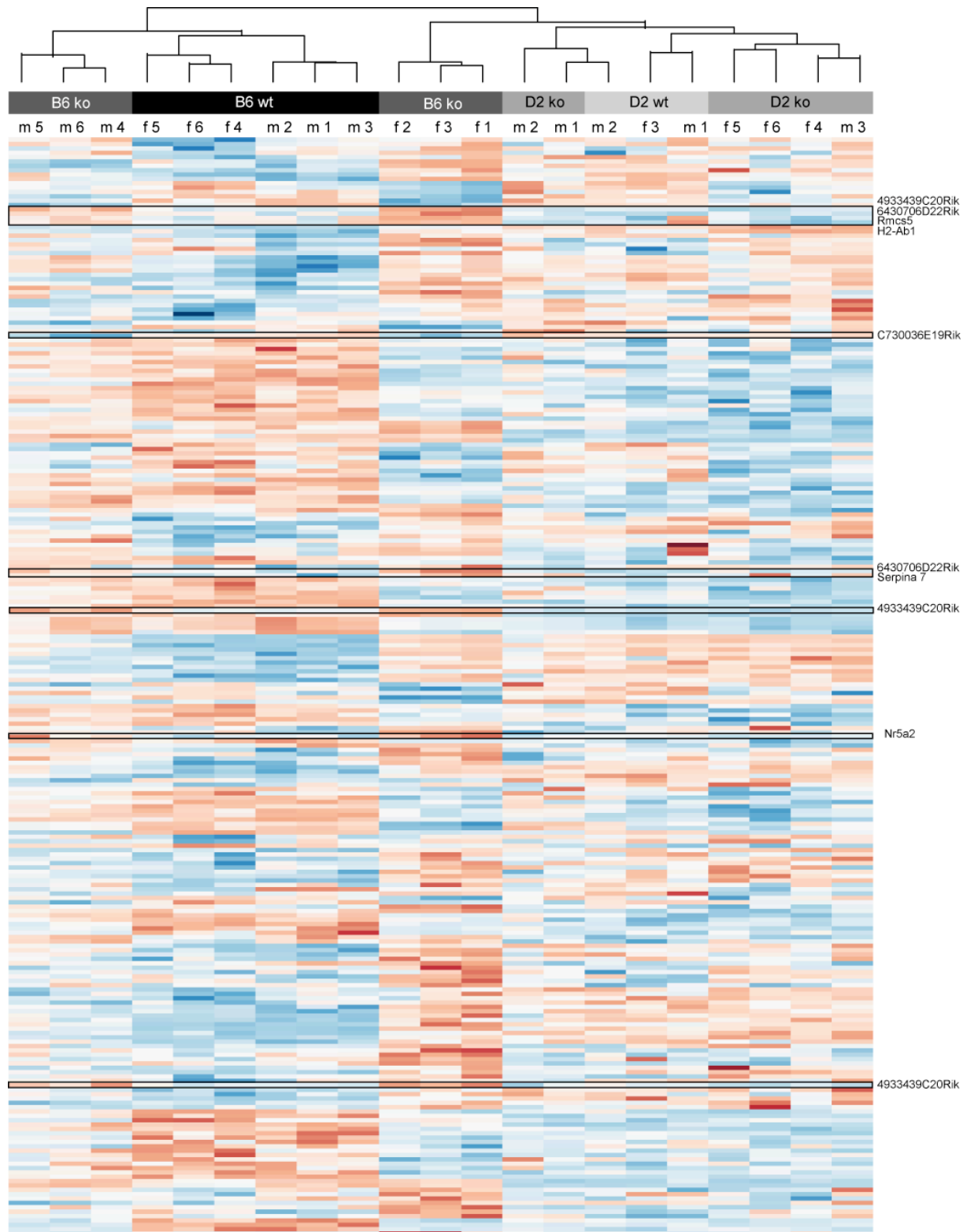
Figure 43. Heatmap representation of differentially expressed genes in liver of B6 mice.
Differential expression in liver of 5-week-old fetuin-A deficient and wildtype mice was calculated using Bayesian statistics under Bioconductor. Probe sets shown were significantly (p < 0.05) differentially expressed in B6 mice; probe sets, which were altered in kidney of D2 mice (log-ratio > 1), were excluded. Each column corresponds to one array; each row represents a probe set. The color encodes the expression intensity of individual probe sets, ranging from highest expression values in dark red, medium expression values in white to lowest expression values in dark blue. Probe sets, which were altered in B6 knockout animals in comparison to all other genotypes are encircled (black boxes) as candidate genes for a compensatory effect. Hierarchical clustering of arrays according to the shown subset of genes revealed that B6 genotypes were differentiated by this subset while D2 genoytpes were nearly randomly distributed.

All candidates mentioned before were differentially upregulated in B6 fetuin-A deficient mice, while transcribed sequences *C730036E19Rik* was downregulated. As discussed before, it is reasonable to assume that candidate genes for the inhibition of ectopic calcification in B6 fetuin-A deficient mice are increased not decreased. Thus, *4933439C20Rik* was studied further as this candidate was detected in both kidney and liver.

3.3.1.3 Expression Profile of *4933439C20Rik*

The transcribed sequence *4933439C20Rik* was differentially upregulated in kidney and liver of B6 fetuin-A deficient mice (see chapters 3.3.1.2 and 3.3.1.3), but not in D2 fetuin-A deficient mice.

The transcribed sequence 4933439C20Rik was represented by three probe sets (figures 44A-C). Two of the probe sets showed an overlap in their sequences (blue label figures 44A, B). The probe sets shown in figure 44A and figure 44C were blasted against the NCBI mouse genomic and transcript database. The blast of the sequence shown in figure 44A revealed consensus with the sequences of phosphatidylserine decarboxylase pseudogene 1 and phosphatidylserine decarboxylase pseudogene 2 (figure 44D). The search query covered 60 % of the phosphatidylserine decarboxylase pseudogene 1 with 96 % identities and 66 % of the phosphatidylserine decarboxylase pseudogene 2 with 93 % identities. The blast of the probe set shown in figure 43C did not return any hit in the mouse transcript database.

To confirm the differential regulation of *4933439C20Rik* a quantitative PCR was performed. The primer sequences are underlined in figures 44A and C. The PCR supported the findings of the microarray approach. The two probe sets showed differential upregulation in B6 fetuin-A deficient mice (figures 44E, F).

In summary, the comparative microarray approach led to the identification of the transcribed sequence *4933439C20Rik* as a putative candidate gene for inhibition of calcification in B6 fetuin-A deficient mice. In liver, further candidates were identified but still need to be verified.

A   probe set: 1429452_x_at

cagctgagctgcatgtccagacctgctctgaatctgcgctcctggctgntgaccatactcnantacctcctgcccttccgt
gtgctcgggcccacagccaggtgggatggaggccnntgagcaggtttgacagagccggaattatttagaaagag
gaactctcaactgtganattgcctccatctgactggcctgcaggaagtggagaagcttctcgattggaagccgctgccg
tcaatnatancnnngcngnccgnnnntnccnnacaanccctccagantctntntnnntgccggancaagctcanc
tntcccggggaccacagattggaagcaggcagtcactggtcttggacaggaagactctntccggccttntcagctgtg
ntcctctaacctgtgcctgtgagccaccaagagtgaacggaaactagaagcattgccaccaacaactggagcagtg
accaca

B   probe set: 1453144_at

ctcgggccccacagccaggtgggatggaggccnntgagcaggtttgacagagccggaattatttagaaagaggaa
ctctcaactgtganattgcctccatctgactggcctgcaggaagtg

C   probe set: 1453145_at

ctcttggtggtctttcaagcttgcaccaggtctgtttctgtcctcatcttccatttgtaagaaccaaggctatacagcccagtc
tccacctctgggattaaggcagctgctctttgacctttgtgtgctatagcaaaaatgatacaggctacatgtatatccagc
cttgttttgagtatttggtgagcagtctggttccttctgagaaacagccacctcacaaaccagcctgaacacttgggccttc
gtggtggcgtctgtagagtttctttctc
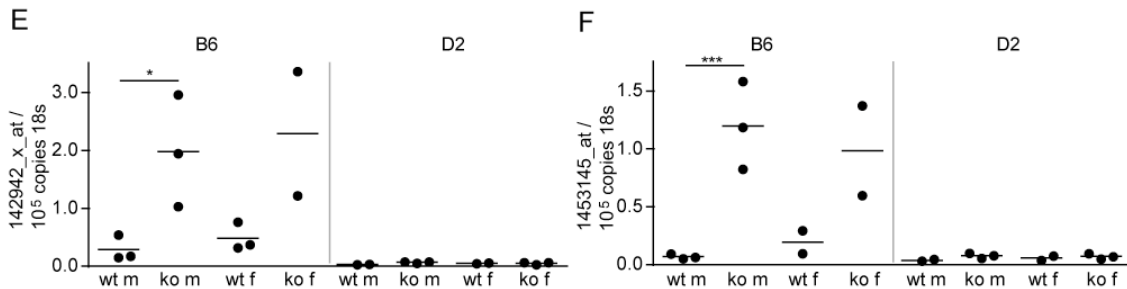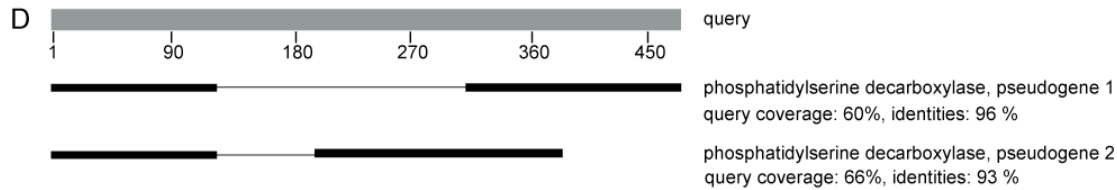
Figure 44. Differential expression of 4933439C20Rik.
A-C. Nucleotide sequences of probe sets corresponding to 4933439C20Rik. The sequence of B is contained in A (blue label). **D.** Blast: The gene sequence of A was searched against the mouse genomic and transcript database on NCBI. Two matching transcripts were identified; overlap of hits with the query sequences is demonstrated as black box. **E-F.** Quantitative PCR of the probe set shown in A and C, primer sequences are underlined. Gene expression of ribosomal 18s RNA was used as internal correction. Both probe sets were specifically upregulated in kidneys of B6 fetuin-A deficient mice but not in D2 fetuin-A deficient mice. * $p < 0.05$, *** $p < 0.001$.

3.3.2 Impaired Clearance of Calciprotein-Particles in BMMs Derived from D2 Mice

Fetuin-A is highly effective in the formation and stabilization of calciprotein-particles (CPPs) [18, 90-92]. In the current thesis, the fate of CPPs *in vivo* was elucidated (see chapter 3.2) and it could be shown that CPP clearance was fast and efficient. Thus, fetuin-A mediated removal of mineral debris plays a critical role in prevention of unwanted precipitation of excess calcium phosphate and prevention of pathological mineralization. Therefore, effectiveness of CPP clearance may contribute to the different calcification phenotypes observed in fetuin-A deficient mice on B6 and D2 genetic background. This hypothesis was tested using the well-

established flow cytometry assays to evaluate CPP binding and endocytosis in bone marrow derived macrophages (BMMs) (see chapter 3.2). CPP binding was studied in BMMs derived from B6 and D2 fetuin-A deficient and wildtype mice. Binding of CPPs was clearly dependent on the mouse strain but not on the fetuin-A genotype (figure 45A).
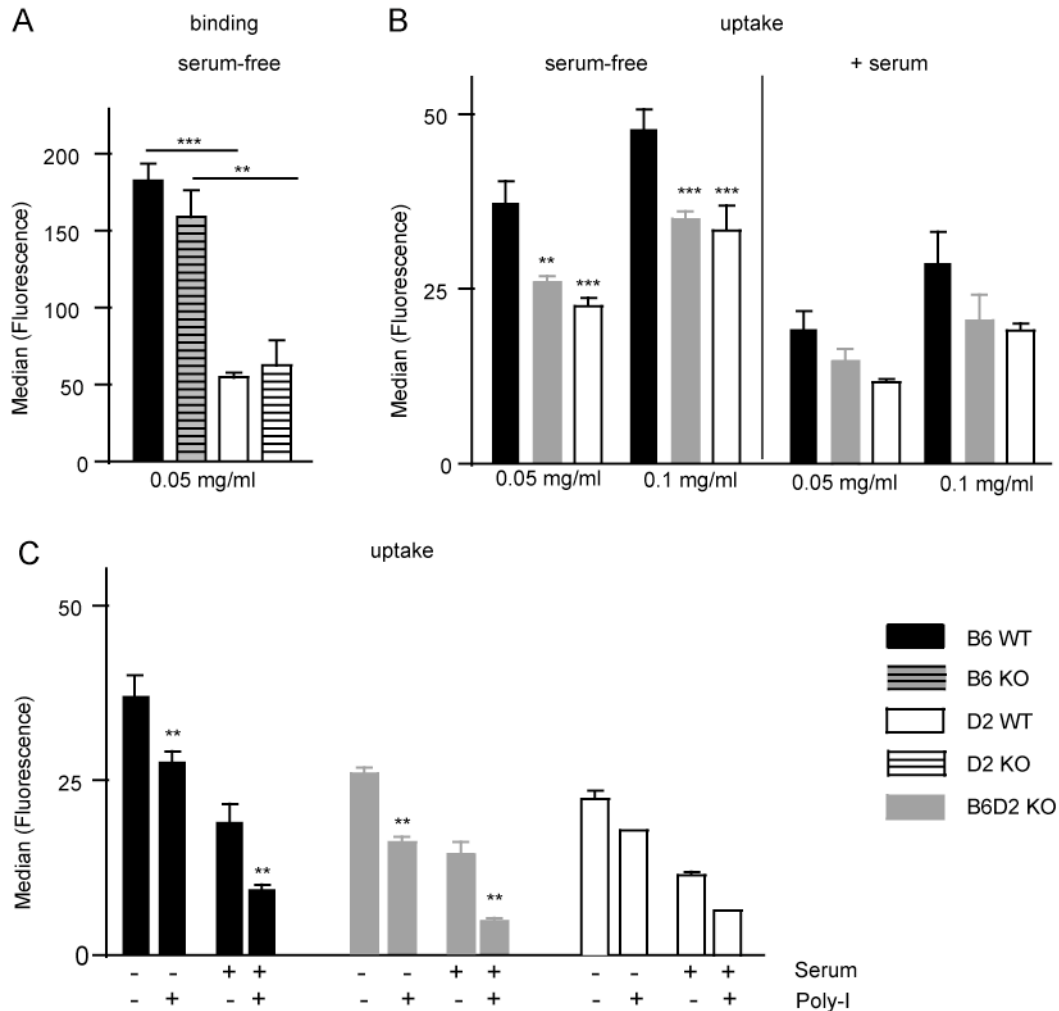
Figure 45. Impaired binding and endocytosis of CPPs in bone marrow macrophages derived from D2 mice.
Bone marrow derived macrophages from wildtype (WT) and fetuin-A knockout (KO) mice on B6 and D2 genetic background were studied, additionally macrophages derived from the offspring of B6 x D2 fetuin-A KO mice (B6D2 KO) breeding were examined. To evaluate binding of CPPs, cells were seeded (500,000 cells per sample) and incubated on ice for 45 minutes with 0.05 mg/ml CPPs (A). Endocytosis assays were performed on adherent cells (250,000 cells per sample) incubated with indicated concentrations of CPPs with or without serum pre-treatment at 37°C for 10 minutes (B, C). Scavenger receptor mediated CPP uptake was inhibited by Poly-I pre-treatment before addition of 0.05 mg/ml CPPs with or without serum pre-treatment (see legend) (C). Cell-associated fluorescence was measured by flow cytometry. CPP binding and uptake was reduced in BMMs derived from D2 and B6D2 KO mice. ** $p < 0.01$ *** $p < 0.001$.

The cell-associated fluorescence in BMMs derived from B6 mice was 223 and 194, for WT and KO cells, respectively in comparison to 66 and 75 in BMMs derived from D2 WT and KO mice (WT, $p < 0.001$ and KO, $p < 0.01$). Likewise, endocytosis of CPPs was diminished in D2 BMMs compared to B6 BMMs (figure 45B). Uptake of uncoated CPPs was reduced from 37 to 22 ($p < 0.001$) and from 48 to 33 ($p < 0.001$), when macrophages were incubated either

with 0.05 mg/ml or 0.1 mg/ml fetuin-A containing CPPs. As observed before (see chapter 3.2.9) uptake of serum-coated CPPs was less efficient than endocytosis of uncoated CPPs. The comparison of endocytosis of serum-coated CPPs between D2 and B6 BMMs revealed the same tendency as for uncoated CPPs but was not statistically significant (figure 45B). In addition, CPP endocytosis was studied in BMMs derived from F1 hybrid mice, generated from B6 and D2 fetuin-A deficient mice (B6D2 KO). CPP uptake in these macrophages resembled the endocytosis of D2 BMMs (figure 45B).

It was shown that CPP uptake is mediated by scavenger receptors (see chapter 3.2.10). Thus, the possibility of an impaired CPP uptake in D2 BMMs as a consequence of decreased expression or defects of scavenger receptors was tested. However, pre-incubation of cells with the scavenger receptor ligand Poly-I inhibited CPP uptake in all types of BMMs to the same extent (figure 45C).

In conclusion, CPP binding and endocytosis was remarkably decreased in BMMs derived from D2 mice. Thus, impaired CPP clearance may play a key role in development of severe soft tissue calcification in D2 fetuin-a deficient mice.

4. Discussion

4.1 The Pathology of Ectopic Calcification in Fetuin-A Deficient Mice

Sensitivity of DBA/2 (D2) mice to ectopic calcification is well known. Spontaneous myocardial calcification [111, 189, 295] and focal calcification in the tongue [190, 191] was observed starting at day 20-25 in mice. Thereafter a rapid increase in lesion size was noticed. Ultrastructural analysis revealed that calcification foci were mostly found in degenerated mitochondria [296, 297]. Large lesions in the right ventricular surface were surrounded by fibrous tissue [189, 295]. Furthermore, it was shown that D2 mice are prone to calcification in response to freeze-thaw injury [112 1999]. The dramatic calcification phenotype of 2 fetuin-A deficient mice was published by Schäfer et al in 2003. Severe soft tissue calcification in 7-9 month old mice affected almost every organ, although it was most prominent in skin, kidney, myocardium and testis. This dramatic calcification was associated with an increased mortality [56].

Here, ectopic calcification in D2 fetuin-A deficient mice was examined using TEM, immunofluorescence staining, gene expression analysis as well as proteomic analysis. In particular early stage calcified lesions were studied in order to reveal the mechanisms involved in lesion formation in fetuin-A deficient D2 mice.

The necropsy of a 42-week-old D2 fetuin-A deficient mice (figure 8) was in full agreement with the findings from Schäfer et al [56]. However, it could be shown for the first time that brown adipose tissue is affected by ectopic calcification. The severity of ectopic calcification exceeded those lesions found in D2 wildtype mice by far and thus demonstrated the importance of fetuin-A as an inhibitor of ectopic calcification.

4.1.1 Structure of Calcified Lesions

At D2 fetuin-A deficient mice older than 3-month calcified lesions were visible macroscopically. Lesions appeared as transparent to white spherules in most tissues. In the heart a large, diffuse calcified area was observed on the surface of the right ventricle. Calcification in the myocardium was similar to the findings in D2 wildtype mice [111, 189, 295-298], whereas soft tissue calcification in most major organs was unique to fetuin-A deficient D2 mice.

TEM of calcified lesions in brown adipose tissue showed a broad spectrum of lesion morphologies. Nonetheless, lesions could be classified in three subtypes: lesions with concentric rings of alternating low and high electron density (type 1 lesions), diffuse lesions within the microvasculature (type 2 lesions) and electron dense lesions (type 3 lesions). Despite their diverse morphologies, early-stage lesions were mostly spherical, occasionally other shapes were derived from clustering of initially spherical lesions.

The laminated structure of calcified lesion was not unique to brown adipose tissue. Often the characteristic tree-aging-ring-like structures appeared even in immunohistological staining, e.g. in lung, pancreas and testis of D2 fetuin-A deficient mice [258]. Spherical mineral structures, containing various kinds of tree-aging-ring-like structures, are a common phenomenon throughout phylogeny. Ryall presented a panel of TEM pictures from a wide variety of mineral granules in her outstanding review about the future of stone research [299]. She pointed out that a large diversity in shape, size and morphology exists. In his review on calcification seen with the electron microscope [300] Ghadially also reported on laminated structures. Such morphologies were found in so-called Michaelis-Gutmann bodies, associated with Malakoplakia, a rare inflammatory disease affecting the urinary tract, and in tumor associated calcification, where laminated structures derived from collagen fiber calcification, named Psammoma bodies were found. Moreover, similar structures were found for serum granules [94], previously also described as nanobacteria [98] or nanons [96]. Thus, at least the appearance of type 1 lesions was in agreement with other well-known mineral granulations. However, serum granules as well as nanons are much smaller than all lesions observed here. All these granules were of nanometer size and rarely exceeded a size of 0.5 µm whereas type 1 calcified lesions in brown adipose tissue of D2 fetuin-A deficient mice ranged between 6 and 9 µm. Nonetheless, not only the structure of calcified lesions but also the proteomic content was in part reminiscent of the serum granules described by Young et al. [94]. This will be discussed in detail in chapter 4.1.4.

Mechanisms of mineral formation, in particular the nucleation mechanisms involved in laminated mineral structure formation are largely unknown. Thus, at this point it was unfeasible to draw a conclusion on the mineral formation mechanism of type 1 lesions in D2 fetuin-A deficient mice.

Type 2 lesions were identified within the microvasculature as will be discussed in detail in the next chapter (4.1.2). However, the structure of these lesions was completely different when compared with the highly organized type 1 lesions. The mineral appeared as fibrous precipitate and lesions contained organic material with lower electron density. As those lesions without a doubt occurred in the lumen of vessels, it is reasonable to assume that these distinct regions of low electron density were proteinaceous or of anuclear cellular origin, e.g. erythrocytes or platelets. To the best of my knowledge no comparable ectopic calcification phenotype has been described so far. The structure of these lesions might be determined by (i) the nucleation mechanism and (ii) the environment. However, the TEM observation could not reveal any evidence concerning the starting point of mineral precipitation.

The third subtype of lesions identified in brown adipose tissue of D2 fetuin-A deficient mice was amorphous; lesions were electron dense and occasionally associated or surrounded by

membranes. These lesions did not show an organized structure and resembled the lesions identified in the myocardium of D2 wildtype mice [111, 189, 295, 296, 298]. It was proposed that these lesions develop from mitochondria calcification [296, 297]. Electron dense granules within degenerating mitochondria are considered precursors of mitochondria calcification [297, 300]. Here, type 3 lesions were found in tight proximity of mitochondria, but neither electron dense granules nor degenerated mitochondria could be observed. However, brown adipose tissue is highly effective in generating body heat and thus extremely rich in mitochondria. Thus, it is reasonable to assume that type 3 lesions may be a result of mitochondria calcification. In fact, it is likely that type 3 lesions as well as similar calcified lesions in the heart of D2 fetuin-A deficient mice may not be directly related to the fetuin-A deficiency, but to the pre-disposition of the D2 strain to calcify. It would be of great interest to examine whether type 3 calcified lesions also occur in D2 wildtype mice. As brown adipose tissue calcification is described here for the first time, it is reasonable to assume that brown adipose tissue has not been examined in previous studies on D2 mice.

In conclusion, a broad spectrum of morphologies of calcified lesions has been detected. This was on the one hand dependent on the tissue studied, but on the other hand occurred also within one type of tissue, e.g. brown adipose tissue, which was analyzed in TEM. Structural diversity of calcified lesions is a common observation and was described in various other studies [94, 299, 300]. It can be assumed that at least partly the different morphologies may be attributed to different mechanisms of lesion formation. For instance type 3 lesions in D2 fetuin-A deficient mice may be related to mitochondrial calcification characteristic of the D2 genetic background. As type 1 and type 2 lesions were remarkably different in structure as well as in terms of localization, it is likely that a different mechanism of lesion formation was involved. However, the mechanisms of ectopic calcification in D2 fetuin-A deficient mice, in particular the mechanisms of nucleation, remain to be determined.

4.1.2 Localization of Calcified Lesions

The structure of calcified lesions in D2 fetuin-A deficient mice was pleomorphic, and so was their localization. Colocalization of calcified lesions with either blood vessels or lymphatic ducts was examined using double immunofluorescence staining (figure 9). Calcified lesions were frequently observed in close proximity with the endothelial marker CD31, but never with lymphatic ducts. Calcified blood vessels were clearly identified as microvasculature by their small diameter as well as by lack of auto-fluorescence, which is characteristic of elastic fibers in larger arteries. However, even though a colocalization of calcified lesions with microvessels could be shown in different tissues as well as in different stages of the calcification progress, calcified lesions may still develop outside the microvasculature.

TEM analysis of calcified lesions was performed to overcome the limitations of immuno-fluorescence staining. Generally it was observed that there is a rapid increase in number and

size of calcified lesions once initiation of calcification has started. This was observed for spontaneous calcification in D2 wildtype mice [189] as well as for severe soft tissue calcification in D2 fetuin-A deficient mice [264]. Therefore, brown adipose tissue (BAT) of a 2 week-old D2 fetuin-A deficient mice was studied, as a pilot study had suggested that calcification in BAT is initiated during the first weeks of life.

Indeed, a large number of calcified lesions was observed in TEM. Type 2 lesions, localized within the microvasculature, confirmed the findings from immunofluorescence. This finding was also in agreement with the identification of serum proteins bound to calcified lesions (see chapter 3.1.5) and this was probably not restricted to type 2 lesions, because the lesions employed for proteomic analysis had been dissected macroscopically without distinction of vasculature. However, as discussed before calcified lesions were pleomorphic. There was no evidence that type 1 or type 3 lesions were located within the microvasculature. In fact, one can hypothesize that type 3 lesions, resembling mitochondria calcification in their structure (see chapter 4.1.1), were initially always intracellular, within brown adipocytes. This was shown by their proximity to lipid vacuoles and intact mitochondria in the 2 week-old D2 fetuin-A deficient mice studied.

In conclusion, it could be shown for the first time, that calcification in D2 fetuin-A deficient mice occurred within the microvasculature. Even though it is not clear how nucleation of mineral precipitates commences, the occurrence of micrometer-sized lesions within the vasculature reflects once again the important role of fetuin-A as a systemic inhibitor of ectopic calcification.

Structure as well as localization of calcified lesions was extremly variable. In addition to the extracellular calcification there was also evidence for intracellular calcification, possibly derived from calcifying mitochondria. Thus, even though calcification in D2 fetuin-A deficient mice appeared macroscopically uniform it might be driven by distinct mechanisms. Finally, the analysis of the mechanisms involved in ectopic mineral formation is severely limited in that the observation of early-stage lesions is very rare, because calcification progresses rapidly once started. High sensitivity *in vivo* imaging methods in small rodents may help to further delineate the underlying mechanisms of polymorphic calcification.

4.1.3 Gene Expression Analysis

4.1.3.1 Differential Gene Expression in Adipose Tissue

Differential gene expression was studied in brown adipose tissue in the kidney pelvis region of 6-week-old D2 fetuin-A deficient and wildtype mice. Soft tissue calcification in this tissue was detectable from an age of 3 weeks. Thus, 6-week-old mice should have developed early stage soft tissue calcification [264]. Histological examination of the tissue showed that progression of calcification was associated with development of fibrosis [264]. Fibrotic tissue

remodeling requires an induction of genes involved in tissue reorganization. The current microarray analysis identified a total number of 395 differentially regulated genes, most of which were upregulated in KO mice. Probing the differentially expressed probe sets against the KEGG data base of biological pathways revealed mostly signaling and remodeling processes, namely focal adhesion, ECM-receptor interaction, cell cycle regulation, p53 signaling pathway, cell adhesion molecules and notch signaling pathway. Among the most highly upregulated genes were two members of the small proline-rich protein family, Sprr1a and Sprr2a. The function of these proteins is currently unknown, but they have been associated with various inflammatory diseases including inflammatory skin diseases [260], allergic inflammation [261] and fibrosis [262]. Pradervand and colleagues demonstrated a stress-related induction of Sprr1a in cardiomyocytes and a protective effect against ischemic injury [263]. Thus, increased expression of Sprr1a in calcified brown adipose tissue may be secondary to the pro-fibrotic stimulus of calcification. In addition a 17.3-fold increase of OPN expression was detected in calcifying brown adipose tissue. OPN is known for its calcification inhibitory function and was previously detected at calcification sites in uremic B6 fetuin-A deficient mice [114], in histology of D2 fetuin-A deficient mice [258, 301] and in calcified human coronary arteries [265, 302]. Calcification-associated OPN is secreted by macrophages, which commonly accumulate at calcified lesions [258]. Various functions of OPN have been proposed. In ectopic calcification OPN prevented mineral growth and partially dissolved mineral deposits. Steitz and colleagues reported that OPN physiologically blocked crystal growth by induction of carbonic anhydrase 2 and thus by acidification of the extracellular milieu [168]. This finding was confirmed in MGP-deficient mice where genetic ablation of OPN further enhanced the calcification phenotype [165]. OPN accumulation was however not associated with reduced levels of calcification in D2 fetuin-A deficient mice. On the contrary, OPN was always associated with calcified tissue, but not with calcification-free tissue. Thus, OPN expression seemed to be reactive rather than preventive. Recent publications suggested a bifunctional role of OPN. While intact phosphorylated OPN is an effective inhibitor of mineralization as previously described, a fragment of OPN derived from thrombin cleavage was shown to be pro-inflammatory [170] and to promote ectopic mineralization in aortic calcification of LDLR deficient mice [171]. Beside its role in calcification OPN was described in association with a broad spectrum of immunomodulatory functions. Among others it was shown to function as a chemotactic stimulus for macrophage infiltration [162, 303]. Thus, OPN expression in calcified brown adipose tissue may reflect the recruitment of macrophages and leukocytes.

Another highly upregulated gene in calcified brown adipose tissue was MMP12. Dean et al. reported that MMP12 effectively cleaved a group of CXC chemokines and may therefore play a key role in regulation of active inflammatory responses by terminating the influx of

polymorphonuclear leukocytes [304]. In calcified lesions of D2 fetuin-A deficient mice an increased MMP12 expression may explain the previously described moderate progress of inflammation [264]. While macrophage accumulation was observed in most cases, polymorphonuclear leukocytes were only detected occasionally. Also macrophage enrichment was primarily detected in calcifying tissues containing resident macrophages. Possibly MMP12 counteracted the chemotactic function of OPN as well as of serum amyloid P, another opsonic protein, which was shown to accumulate at calcified lesions of D2 fetuin-A deficient mice [301].

In conclusion, gene expression analysis of brown adipose tissue in a state of early soft tissue calcification revealed an activation of genes involved in tissue remodeling and inflammation. This was in agreement with earlier findings showing a steady progression of calcification in D2 fetuin-A deficient mice. In early stages small globular lesions were occasionally covered by macrophages, whereas the surrounding tissue appeared completely normal. With increasing age of the D2 fetuin-A deficient mice the lesions progressed and fibrotic remodeling was observed [264].

Ectopic calcification was studied in great detail in association with atherosclerosis and vascular calcification. Originally vascular calcification was considered to be a passive process, mainly regulated by chemical equilibrium of mineral ions. However, the identification of matrix vesicles in calcified vasculature [305-307] and the detection of bone-associated proteins such as OPN, MGP and BMP2 in human atherosclerotic plaques [265, 308] changed this view. The overexpression of several mineralization-associated transcription factors, namely Msx1, Msx2 and Cbfa1, was shown in cultured calcifying vascular smooth muscle cells *in vitro* [176, 184] as well as in mouse models [176, 179] and calcified human arterial biopsies [177] *in vivo*. Ever since vascular calcification is considered an active biological process including an osteochondrocytic transdifferentiation of vascular smooth muscle cells. A similar mechanism was suggested for valvular calcification [309], yet the principle of osteogenic differentiation remains controversial. Anger and colleagues published a DNA microarray analysis reporting the gene expression profile of human calcified aortic valves. In comparison with non-calcified control samples they found elevated inflammatory markers but no upregulation of osteoblastic markers [310]. Recently Villa-Bellosta and colleagues showed that the deposition of calcium phosphate was passive and the osteogenic differentiation of VSMCs happened after the initial calcification [311]. A recent DNA microarray study compared mesenchymal cell derived osteoblasts with calcifying VSMCs and likewise showed that CVC predominantly retained their VSMC profile and only partially overlapped with the osteoblastic gene expression profile [312]. The DNA microarray analysis presented here also suggested that calcification in fetuin-A deficient mice does not involve osteochondrogenic conversion of cells. As discussed before no osteogenic genes were upregulated in these mice.

Furthermore, the pathway analysis did not reveal any pathway associated with bone or cartilage formation within the significant differentially regulated genes. Thus the underlying mechanism of soft tissue calcification in D2 fetuin-A deficient mice may be distinct from the one of vascular calcification.

4.1.3.2 Gene Expression Analysis of Fetuin-A Deficient Kidney

Differential gene expression in kidneys of 5-week-old D2 fetuin-A deficient and wildtype mice was studied to identify genes involved in precipitation of calcium phosphate as well as in lesion formation. The analysis revealed only 12 differentially regulated genes. The expression of 5 genes was increased in fetuin-A deficient kidneys whereas 7 genes were downregulated. The upregulation of angiotensin I converting enzyme (petidyl-dipeptidase) 2 (Ace2), a key factor of the renin-angiotensin system, may point to alterations in the mineral balance of fetuin-A deficient mice. This is in agreement with all previous findings. It was shown that fetuin-A is effective in stabilizing calcium phosphate by forming transient soluble calciprotein particles [18, 90-92, 313], which enable the clearing of excess calcium phosphate from the circulation (see chapter 3.2). Thus, lack of fetuin-A in D2 fetuin-A deficient mice may cause changes in the mineral homeostasis, finally leading to progressive soft tissue calcification. It was shown that calcified lesions were detectable from an age of 2 weeks in most tissues but remarkably later in kidneys (slight calcification was observed in 1-month-old mice) [264]. Therefore, in the 5-week-old mice analyzed ectopic calcification might have been initiated. Nevertheless, none of the differentially regulated genes in kidney was directly related to mineralization. Furthermore, no genes involved in tissue remodelling as seen in calcified adipose tissue were differentially regulated. This reflected that kidneys of 5-week-old mice were indeed not yet calcified severly.

As discussed before, osteochondrocytic transdifferentiation of vascular smooth muscle cells was proposed by serveral groups as the underlying mechanism of vascular calcification. Some recent publications suggest a passive process that does not primarily involve osteochondrocytic transdifferentiation. The absence of any differentially regulated genes related to mineralization or osteogenic differentiation in kidney likewise suggests that calcification in D2 fetuin-A deficient mice is not osteogenic. Osteochondrogenic gene expression may happen at later stages of calcification, but kidneys of 5-week-old D2 fetuin-A deficient mice showed neither calcification nor osteochondrogenic cell conversion.

4.1.3.3 Gene Expression Profile of the Liver

The liver gene expression in D2 fetuin-A deficient mice was studied for three reasons. First, in adult mice fetuin-A is constitutively expressed in the liver. Thus, fetuin-A deficiency may cause alterations in the gene expression pattern. Such changes may influence the calcification phenotype. In this case they would be exclusively detected in calcifying D2

fetuin-A deficient mice, but not in resistant B6 fetuin-A deficient mice. Secondly, it is reasonable to assume that lack of fetuin-A, a major plasma protein caused changes in gene expression independent of the calcification phenotype. These effects should be detectable on both genetic backgrounds. The third reason to study the liver gene expression is the key function of liver in metabolism. Massive defects in peripherical organs afflicted by ectopic calcification should be reflected in a modified gene expression pattern in the liver.

In fact genome-wide expression analysis identified 142 significantly differentially regulated genes in the liver of D2 fetuin-A deficient mice. Strikingly, three genes of the phase II metabolic pathway including the sulfotransferase family members Sult3A1, Sult2a2 and Sult1e1 were dramatically upregulated in fetuin-A deficient liver. Remarkably, these genes were not upregulated in non-calcifying fetuin-A deficient mice on B6 genetic background (see chapter 3.3.2). Thus, increased expression of the sulfotransferases may be related to the phenotype of massive soft tissue calcification in D2 fetuin-A deficient mice. The correlation of these metabolic changes and ectopic mineralization remains to be clarified.

Increased expression of the acute-phase reactants [271] and apolipoproteins [314] serum amyloid A1 (SAA-1) and serum amyloid A2 (SAA-2) may be caused by inflammatory stimuli. In 5-week-old D2 fetuin-A deficient mice several organs exhibited calcified lesions, occasionally associated with macrophages as well as granulocytes [264]. Even though inflammation was moderate in calcified D2 fetuin-A deficient mice it is reasonable to assume that a mild acute-phase response was initiated. Typically the expression of serum amyloid proteins rises up to 1000-fold during the acute phase of inflammation [271]. Here a comparatively slight increase of 7.4- and 6-fold for SAA-2 and SAA-1, respectively, was observed. The mild if any induction of acute phase reactants is underscored by the absence of differential expression of other major acute phase reactants like C-reactive protein.

The most highly upregulated probe sets were invariably identified in D2 fetuin-A deficient mice but not in B6 fetuin-A deficient mice. Therefore, the upregulation was likely related to the calcification phenotype, even though none of these proteins were directly related to mineralization or tissue remodelling.

As expected fetuin-A was the most highly downregulated gene. Few other probe sets were more than 10-fold decreased in D2 fetuin-A deficient mice. Most of these genes could also be detected in B6 fetuin-A deficient mice, suggesting that the downregulation was associated with gene regulatory effects caused by the knockout of fetuin-A but not by the calcification phenotype.

In conclusion, gene expression analysis confirmed that ectopic calcification in D2 fetuin-A deficient mice was associated with fibrotic tissue remodelling. Differentially regulated genes related to osteochondrogenic mineral formation could be identified neither in fetuin-A

deficient kidneys before initiation of calcification nor in calcified adipose tissue nor in liver. These findings pointed to dystrophic rather than osteochondrogenic mineralization and lesion formation. However, the failure of the gene expression analysis to identify genes related to calcification may also be attributed to technical reasons. RNA was extracted from whole organ samples. Particularly, kidney and liver are heterogeneous tissues, which may lead to large variability between replicates. Furthermore, the number of replicates in the current gene expression analysis was low, the wildtype control groups comprised only 3-4 mice. Previously Pavlidis and colleagues studied the effect of replication on gene expression microarray experiments and came to the conclusion that at least 5 biological replicates are needed to obtain stable results [315]. Thus, the current microarray approach may not be sufficient to identify all alterations in gene expression with high reproducibility. Thus, further validation should be sought for any given candidate gene using independent gene expression measurements.

4.1.4 Proteomic Analysis

Protein content in calcified lesions was studied by comparison of the protein expression in intact, calcification-free tissue and in calcified lesions of mice suffering from severe ectopic calcification. Using this approach, differentially expressed proteins could be identified. Most detected proteins were serum proteins, including serum albumin, apolipoprotein A1 (ApoA1), hemoglobin subunit beta-1, fibrinogen beta chain, serum amyloid P (SAP), Ig kappa chain C region and complement component 9 (C9). The identification of serum proteins in calcified lesions suggests that precipitation of calcium phosphate happened in the presence of serum and thus extracellularly. This hypothesis is supported by results of Young and colleagues who studied serum granulations derived from human or bovine serum mixed with calcium, phosphate or both [93, 94, 316]. The granules contained various serum proteins, with serum albumin, ApoA1 and hemoglobin fetal subunit beta, as well as components of the complement systems comprising the most abundant proteins [94]. The striking similarity in protein content of serum granules and calcified lesions studied here suggest similar mechanisms of mineral formation, preferentially in the presence of serum. An earlier study of proteins contained in fetuin-mineral complexes isolated from serum of etidronate-treated rats further confirmed this hypothesis. Price et al. detected matrix Gla protein, secreted phosphoprotein 24, SAP, prothrombin, platelet factor 4 and occasionally hemoglobin along with fetuin-A in fetuin-mineral complexes [89]. At this time it is not clear whether the protein composition in calcified lesion merely reflected the relative abundance of proteins in the given environment as previously discussed by Young et al. [94], or if there was a selective enrichment of the identified proteins. In the case of SAP both may be true. SAP was shown to have opsonic properties [227] and binds to a broad spectrum of pathogen-related substances, e.g. lipopolysaccharide [317]. Furthermore, SAP accumulats in atherosclerotic

plaques [318, 319]. Thus, it is reasonable to assume that SAP accumulation in pathological calcification (i) reflects its abundance in serum and (ii) that SAP binds to mineral debris due to its opsonic binding capacity.

The non-serum protein, carbonic anhydrase 3 (Ca3), an intracellular protein, was identified in calcified lesions isolated from skin of D2 fetuin-A deficient mice. Carbonic anhydrases catalyze the conversion of carbon dioxide and water to bicarbonate and protons. Their main function is to maintain the acid/base balance in tissue. Earlier work from our laboratory showed that calcified skin lesions of D2 fetuin-A deficient mice contained a mixed mineral of calcium phosphate and calcium carbonate liberating copious amounts of carbon dioxide when treated with acid. The detection of Ca3 in the skin, but not in other tissues suggests that the mixed calcium phosphate/carbonate mineral, which was likewise formed in the skin but not in other tissues, might be formed by the local induction of Ca3 in response to lack of fetuin-A. Alternatively, Ca3 induction might be an adaptive response following calcification, but not leading towards calcification. It is well known that carbonic anhydrases play a critical role in bone resorption [320]. Carbonic anhydrase 2 deficiency is linked to the development of osteopetrosis [321]. However, Kim et al showed that Ca3 was dispensable in mice living under standard laboratory husbandary conditions [322]. Taking all these findings into account, it remains unclear whether Ca3 enrichment in calcified lesion was linked to a mineral resorption activity, or if it was a result of a disbalance in acid/base homeostasis in the environment of calcified lesions. So far there is no evidence for either osteoclast accumulation or bone resorption activities at calcified lesions in D2 fetuin-A deficient mice. Gene expression analysis as well as histological observation of calcified tissue failed to detect such activities. The analysis of osteoclast specific tartrate-resistant acid phosphatase (TRAP) should be included in further studies to clarify the role of osteoclasts and bone resorption in ectopic calcification in fetuin-A deficient mice.

Several proteins differentially expressed in calcified lesions could be identified in the current proteomic analysis. Nevertheless, further studies on the protein content of ectopic calcifications in D2 fetuin-A deficient mice are needed. The comparison of protein patterns in tissue extracts was restricted to proteins, which could be stained with Coomassie blue protein stain. Moreover, differential expression was hardly detectable in protein-rich tissues, e.g. heart. Another limitation of the method used was the extraction protocol; EDTA treatment of samples might not be sufficient to detach proteins strongly bound to the hydroxyapatite mineral. To overcome this, further studies should adapt extraction procedures used for bone and teeth proteins.

4.1.5 Summary

It was previously known that D2 fetuin-A deficient mice develop spontaneous soft tissue calcification [56]. In the current thesis the pathology of ectopic calcification was studied in great

detail. For the first time it could be shown that calcification affects brown adipose tissue. Ultrastructural analysis of calcified lesions revealed a broad variety in microarchitecture of lesions. Two important findings were made. First, calcified lesions could be detected within the microvasculature. This was obvious in TEM, in immunofluorescence staining, and was further confirmed by the detection of serum proteins as part of the protein matrix of lesions. A second subtype of lesions was found intracelluarly in tight proximity to mitochondria, probably reflecting mitochondria calcification. Thus, different mechanisms of calcification contributed to the severe soft tissue calcification. Gene expression analysis of calcified tissue showed that the mineral formation process did not involve an active transdifferentiation towards bone or cartilage cells as was found in vascular calcification. Once calcified lesions had formed, changes in both local gene expression patterns as well as in systemic gene expression were activated. This conclusion is based on the upregulation of several genes involved in tissue remodelling in calcified brown adipose tissue, as well as the differential expression of several liver specific genes.

4.2 Clearance of Calciprotein Particles

Soluble colloidal protein-mineral complexes are now considered natural byproducts of general mineral homeostasis. They are variously called calciprotein particles (CPPs) in analogy to lipoprotein particles [55] or mineralo-protein complexes [94]. To prevent local deposition of such granules, especially in conditions with excess calcium and phosphate in the body, a clearance mechanism is required mediating CPP recycling or disposal by dissolution, degradation or storage. It was shown that the plasma protein fetuin-A plays a critical role in the formation and stabilization of such protein-mineral complexes [18, 55]. Accordingly, fetuin-A deficient mice develop widespread ectopic calcification [56]. Here clearance and disposal of *in vitro* generated fetuin-A containing CPPs was studied in mice, and a receptor responsible for macrophage uptake of CPPs was identified.

4.2.1 *In Vivo* Clearance of CPPs

4.2.1.1 Clearance from Circulation is Fast and Efficient

Several studies have investigated the clearance of fetuin-A monomer, and especially of its desialylated form, asialofetuin. Endocytosis of fetuin-A monomer was found to be mediated by annexins expressed on the cell surface [123, 285]. Asialofetuin, like many asiologlycoproteins, is rapidly cleared from the circulation by the hepatic asialoglycoprotein receptor ASGP-R [121, 323, 324]. To study the role of fetuin-A in the clearance of CPPs, the clearance of fetuin-A monomer, its desialylated form asialofetuin, serum albumin and fetuin-A containing CPPs were compared *in vivo*. The asialofetuin monomer was cleared from circulation within

minutes confirming the highly efficient ASGP-R mediated endocytosis of this protein (figure 20). The kinetics observed *in vivo* demonstrated slow clearance for monomeric albumin ($t_{1/2}$ ~ 4 h) and fetuin-A ($t_{1/2}$ ~ 2.5 h), and faster clearance for asialofetuin ($t_{1/2}$ ~ 43 min.). In the case of albumin and fetuin-A monomer most likely a mixture of clearance and tissue redistribution/sequestration from blood was observed as albumin and fetuin-A monomer did not accumulate in particular organs judged from tissue blots (figure 25) and fluorescent tissue sections (figure 21, 27). In contrast, accumulation of asialofetuin monomer was detected in liver tissue (not shown) the major site of ASGP-R expression. This finding confirmed the well-established activity of the ASGP-R [121] and thus validated the experimental approach. Employing CPPs a fast clearance ($t_{1/2}$ ~ 4 min) in spleen and liver was observed (figure 21, 27) pointing to an efficient clearing mechanism.

4.2.1.2 CPPs are Taken Up by Macrophages

Immunofluorescence staining revealed that CPPs accumulate in macrophages of the reticulo-endothelial system (RES), namely hepatic Kupffer cells and splenic MARCO-positive marginal zone macrophages (MZMs) (figures 21, 27). These cells are known to be involved in the clearance of aged blood cells [325] and particulate matter [326]. In contrast, liver sinusoid endothelial cells and hepatocytes, the prime sites of ASGP-R expression, did neither accumulate fetuin-A monomer nor fetuin-A containing CPPs (figure 21). Thus the particulate form of fetuin-A bound to CPPs invoked a clearance mechanism that overcame the putative clearance of fetuin-A monomer and the well established ASGP-R mediated endocytosis of asialofetuin-A monomer. An equal tissue distribution was found for polysterene beads in size reminiscent to CPPs (figures 22, 28). This finding was in full agreement with an earlier study on the biodistribution of polystyrene particles, where particles were found predominantly in liver and spleen [221].

In addition to the CPP accumulation observed in liver and spleen, aggregated forms of CPPs were detected in the lung (figure 29). These aggregates clearly exceeded the size of CPPs found in Kupffer cells and MZMs and probably were located within the microvasculature. Lung capillaries have been considered a predilection sites for microparticulate depositions because of their small diameter [327]. Accordingly, in D2 fetuin-A deficient mice, where soft tissue calcification occurred in the microvasculature to some extend (see chapter 3.1), the lung was one of the most calcification-prone organs.

Tissue distribution of CPPs, CPP aggregates as well as of polystyrene particles suggests that particle size may determine the targeting of particles. It was previously shown in beagle dogs that organ distribution of microspheres depended on particle size. Whereas 3 µm particles were found predominantly in liver and spleen, an increasing size targeted particles to the lung [220]. Beside organ distribution also the cell type of target tissues may depend on particle size. Jansen and colleagues showed that particulate preparations of formaldehyde-

treated albumin were taken up by Kupffer cells in the liver, while considerably smaller monomeric preparations accumulated predominantly in liver endothelial cells [328].

4.2.2 Identification of a CPP Receptor *In Vitro*

4.2.2.1 Receptor Mediated Endocytosis of CPPs but not of Fetuin-A Monomer

Endocytosis of fetuin-A monomer and CPPs was studied in RAW 246.7 macrophages *in vitro* (figure 30). RAW cell endocytosis of labeled fetuin-A followed linear non-saturable kintics suggesting a fluid-phase uptake (pinocytosis) rather than a receptor-mediated uptake. This is in full agreement with findings of Chen et al. [123] who showed that uptake of Cy5-labeled fetuin-A in vascular smooth muscle cells could not be inhibited by excess unlabeled fetuin-A, suggesting fluid phase uptake.

Compared to pinocytosis of fetuin-A monomer, uptake of a similar amount of fetuin-A contained in CPPs by RAW 246.7 macrophages was strongly enhanced. The inhibition of uptake by inhibition of actin polymerization with Cytochalsin D suggested that CPP uptake is an active process. Furthermore, CPP uptake in BMMs was dose-dependent saturable suggesting a receptor-mediated uptake mechanism. In conclusion, the *in vitro* assays collectively confirmed the findings *in vivo* suggesting that fetuin-A containing CPPs, but not monomeric fetuin-A are taken up in a receptor-mediated manner by macrophages.

4.2.2.2 Scavenger Receptor-A is Involved in CPP Clearance

Using a cell culture assay, blocking reagents and macrophages from clearance receptor deficient mice, it could be shown that macrophage uptake of CPPs is receptor mediated, and that in particular scavenger receptor AI/II is essential for CPP endocytosis. This was in agreement with a previous study showing that uptake of polystyrene nanospheres, 50 nm in size, coated with fetuin-A into cultured rat Kupffer cells could be partially inhibited by polyinosinic acid, as well as by anti-class A scavenger receptor antibodies. Moreover, similar results were obtained in liver perfusion studies in rats [80]. Collectively these results and the *in vivo* clearance presented in this study demonstrate that Kupffer cells and MZMs, both expressing SR-AI/II [329], most likely cleared CPPs through SR-AI/II *in vivo*.

However, the specific architecture of the RES constituting a mechanical microfilter must direct CPP clearance to Kupffer cells and MZM macrophages (see 4.2.1.2), since SR-A expression alone is insufficient for CPP clearance. For instance, SR-AI/II positive liver endothelial cells [329, 330] failed to take up CPPs (see 4.2.1.2). Similarly, particulate preparations of formaldehyde-treated albumin were taken up via scavenger receptors of Kupffer cells, but not by endothelial cells [328]. Furthermore, splenic red pulp macrophages are SR-AI/II positive [329], but did not accumulate CPPs. At least in part this may be explained by the blood flow in spleen; arterial blood passes into the marginal sinus, from where it flows

through the marginal zone into the red pulp [331]. Thus, MZMs may capture CPPs before they reach the red pulp. However, not all arterial blood takes this route. Some arterial branches end directly in the red pulp [331]. In conclusion, specific architecture of the RES as well as particle size (see chapter 4.2.1.2) likely contribute in targeting CPPs to specific SR-AI/II positive cells.

Regarding the ligand responsible for SR-AI/II binding the data suggest that additional serum proteins other than fetuin-A might confer high affinity CPP binding and clearance by macrophages, while fetuin-A is mainly responsible for the stabilization of CPPs. It is currently unknown which serum proteins contribute to the clearance of CPPs and fetuin-A stabilized mineral debris. A situation similar to the "clearance synapse" identified for the clearance of apoptotic cells containing many, yet circumscriptive factors [332] can be anticipated. The identification of albumin as a major contributor in mineralo-protein complexes [89, 90, 94, 96], suggests that albumin and the albumin receptor GP60 [333] may contribute to CPP clearance as well. Apolipoprotein A1 (ApoA1), a known SR-AI/II ligand, likewise is a candidate ligand [334], which was previously identified in mineralo-protein complexes [94] as well as in calcified lesions of fetuin-A deficient mice (see chapter 3.1.5).

4.2.2.3 Contribution of Additional Receptors and Uptake Routes

CPP uptake in SR-AI/II deficient macrophages was significantly reduced. However, some CPP endocytosis was still detectable. Participation of SR-AI/II in CPP uptake suggested an uptake route similar to that of modified lipoprotein particles. Therefore, it was reasonable to assume that other receptors involved in endocytosis of modified lipoproteins may also contribute to CPP uptake. In the current study, the focus was on CD36 whereas MARCO another member of the scavenger receptor family involved in endocytosis of acLDL was not examined. However, the lack of MARCO expression on Kupffer cells [335] suggests that MARCO might not be essential for CPP clearance *in vivo*. Furthermore, CPP uptake in CD36 deficient macrophages was not altered excluding a participation of this class B scavenger receptor as well. Thus, endocytosis pathways distinct from scavenger receptor mediated uptake routes might be involved in CPP endocytosis.

Several groups have previously reported an opsonic activity of fetuin-A enhancing the phagocytosis of *E.coli* and *S.aureus* by human neutrophils [53], increasing uptake of DNA or latex particles in mouse peritoneal macrophages [76] and neutrophils [77] and accelerated phagocytosis of fetuin-A opsonized polystyrene particles [78]. Thus, we investigated the uptake route of two well known opsonic plasma proteins, namely serum amyloid P (SAP) and C-reactive protein (CRP) [226, 336]. The endocytosis of both, SAP or CRP opsonized particles could be strongly reduced by inhibition of the Fcγ receptor pathway, e.g. through spleen tyrosin kinase (SYK) and phosphatidylinositol-3-kinase (PI3K) function. Transfection of non-phagocytic cells with distinct subtypes of the Fcγ receptor (FcγR) resulted in a gain of

function in that transfected cells could efficiently endocytose the opsonized particles [226, 337, 338]. In the current work the inhibition of uptake using inhibitors of SYK and PI3K showed inconclusive results. While inhibition of PI3K resulted in a slight non-significant decrease in CPP uptake, SYK inhibition caused a strong reduction of CPP endocytosis. However, cell viability following SYK inhibition was also much reduced. To clarify the role of FcγR-mediated endocytosis of CPPs, FcγR-deficient BMMs were tested. This experiment clearly showed that FcγR was not involved in CPP uptake and thus uptake of fetuin-A opsonized particles or of fetuin-A containing CPPs for that matter did not resemble the endocytosis of SAP, CRP or immunoglobulin opsonized particles and pathogens.

Furthermore, dectin-1, which is also associated with SYK activity, was apparently not involved in CPP endocytosis judged by the comparison of CPP uptake in dectin-1 KO BMMs in comparison to WT BMMs. However, dectin-1 expression on BMMs is weak [339, 340]. Therefore, a contribution of dectin-1 in CPP endocytosis could not be excluded with confidence using the current approach.

Annexins A2, A5, and A6 have been reported to mediate fetuin-A endocytosis [123, 285]. Here, endocytosis of CPPs was not affected by annexin A5 or annexin A6 deficiency. This result once again confirmed the finding that fetuin-A in a particulate form, such as fetuin-A containing CPP is cleared differently from fetuin-A monomer. Thus, the CPP clearance mechanism is specific for fetuin-A-mineral complexes and therefore highly efficient in preventing pathological deposition of mineral debris without touching general fetuin-A metabolism.

In conclusion, in the current thesis no additional receptors involved in CPP endocytosis could be identified. On the one hand this might be due to a specific CPP uptake exclusively by SRA-I/II. Yet, minor endocytosis of CPPs was observed in SR-AI/II-deficient BMMs and there was evidence that SYK, which is not associated with scavenger receptors, is involved in CPP uptake. The failure to detect additional receptors might be attributed to technical reasons. Subpopulations of macrophages show a high level of heterogeneity in their surface receptors [209]. Therefore, the current approach using BMM is restricted to receptors expressed by this macrophage subtype and may not completely represent CPP uptake in Kupffer cells and MZMs *in vivo*.

4.2.2.4 Does a Galectin-Fetuin Interaction Influence CPP Uptake?

Fetuin-A is a highly glycosylated protein [15]. Accordingly, it is reasonable to assume that an interaction with proteins of the galectin family might influence endocytosis of fetuin-A containing CPPs or fetuin-A monomer. Importantly, in macrophages it was shown that galectin-1 inhibited phagocytosis via FcγR [255], while galectin-3 was effective in enhancing clearance of apoptotic neutrophils [256]. However, the presence or absence of galectin-1 and

galectin-3 did not affect the uptake of fetuin-A monomer or CPPs. This is in agreement with the fact that CPPs prepared from asialofetuin showed identical tissue distribution and kinetics in organ accumulation as fetuin-A containing CPPs (supplemental figure 1).

4.2.3 Interference with Lipid Metabolism and Atherosclerosis

The data shows that SR-AI/II is responsible for the major part of endocytosis of CPPs. The finding that SR-AI/II, a well-known scavenger receptor for LDL particles [216] and lipid debris, likewise participates in the clearance of CPPs and therefore of mineral debris, may help to explain why atherosclerotic plaque frequently calcifies especially in patients with perturbed mineral homeostasis. Several studies in humans showed that fetuin-A colocalizes with atherosclerotic plaque in calcifying atherosclerosis [341-343]. In mice the combined deficiencies for fetuin-A and apolipoprotein E caused an exacerbated phenotype of calcifying atherosclerosis [115] further supporting a combined role for the clearance of lipids and mineral debris in the pathogenesis of atherosclerosis. Thus, the stimulation of SR-AI/II function in clearing macrophages may be of therapeutic value in calcifying atherosclerosis.

4.2.4 Summary

The deposition of mineral precipitates in the vasculature and in soft tissues is a common pathological event especially in dialysis patients [344]. Even under physiological conditions, blood is considered a metastable aqueous calcium-phosphate system sustaining mineral precipitation once crystals are nucleated. Thus, a mechanism is required to safeguard against the disposal of mineral nuclei from circulation to prevent pathological calcification. It was shown that fetuin-A plays a critical role in the formation and stabilization of protein-mineral complexes CPPs [18, 55].

Here it could be shown for the first time that fetuin-A containing CPPs were removed from circulation fast and efficiently. SR-AI/II dependent CPP uptake by hepatic Kupffer cells and splenic MZMs therefore prevented pathological deposition of mineral debris. Thus, CPPs interfered with the endocytosis of modified lipoprotein particles, demonstrating a protective role of fetuin-A in atherosclerosis.

4.3 Prevention of Ectopic Calcification in B6 Fetuin-A Deficient Mice

D2 fetuin-A deficient mice suffer from severe soft tissue calcification (see chapter 3.1 and [56]). In contrast, B6 fetuin-A deficient mice on a high phosphate diet developed extraosseous calcification under uremic conditions, but were resistant to spontaneous calcification [56, 114]. These findings suggest that B6 mice posses protective mechanisms preventing pathological dystrophic calcification.

The sensitivity to ectopic calcification of certain mouse strains was previously described. Using a quantitative trait locus (QTL) analysis, a major locus named *Dyscalc1* was identified

[193, 195, 345]. Subsequent ultra-fine mapping approaches led to the identification of ATP-binding cassette sub-family C member 6 (*Abbc6*) as a putative causative gene [197, 198]. Indeed, *Abbc6* mutation or deficiency was associated with pseudoxanthoma elasticum (PXE), a disorder of connective tissue linked to ectopic calcification in humans [203] and mice [201], respectively. However, a mechanism explaining the linkage of *Abbc6* and soft tissue calcification has not been described so far. In these studies, dystrophic calcification was commonly induced by myocardial cell death as a consequence of a freeze-thaw injury [195-198, 346]. Even though a stable calcification phenotype could be induced, calcification was restricted to the myocardium, whereas pathological mineralization in fetuin-A deficient D2 mice affected almost all major organs (see chapter 3.1 and [56]). Consequently, fetuin-A deficient mice should be particularly suitable for the detection of genes involved in the formation as well as the prevention of dystrophic calcification.

4.3.1 Differential Gene Expression in B6 Fetuin-A Deficient Mice

First, a DNA microarray approach was applied to detect candidate genes. Differential gene expression in kidney and liver of fetuin-A deficient mice on B6 and D2 genetic background was compared. In B6 mice fetuin-A deficiency is most apparent in bone as previously described in fetuin-A deficient mice on a mixed 129Sv x C57BL/6 genetic background [40]. In B6 mice femora were severely stunted and growth plates showed increased mineralization [55]. Apart from that, B6 fetuin-A deficient mice had no obvious alterations in phenotype. Nevertheless, a number of genes were differentially expressed in kidney and liver of B6 KO mice. One of the candidate genes, the enzyme 24-OHase, has a known function in mineralization biology. 24-OHase is responsible for the catabolic breakdown of 1,25-dihydroxyvitamin D, the active form of vitamin D [127]. Mice deficient in 24-OHase developed abnormal mineralization, which is explained by increased serum calcium levels of active vitamin D [290]. Here, 24-OHase was differentially upregulated in the kidney of female B6 fetuin-A deficient mice. In D2 mice, expression of 24-OHase was also high in two KO mice (one female and one male), whereas expression in all other D2 mice was lower but still increased in comparison to B6 WT and male KO mice. Thus, the role of 24-OHase in pathologic calcification of fetuin-A deficient mice suggests further studies on the vitamin D status.

Genes whose expression patterns corresponded to the calcification phenotype of fetuin-A deficient mice were identified in a heatmap representation. Genes, which were differentially upregulated in non calcifying B6 fetuin-A deficient, while their expression remained constant in fetuin-A deficient calcifying D2 mice were of particular interest. Those genes may be compensating fetuin-A deficiency and preventing ectopic calcification in B6 fetuin-A deficient mice. Kidneys of D2 fetuin-A deficient mice are affected by soft tissue calcification. Thus, in kidneys of calcification resistant fetuin-A deficient B6 mice local mechanisms might be

differentially upregulated to inhibit mineral deposition. In contrast, the liver of fetuin-A deficient B6 mice might express genes preventing ectopic calcification on a systemic level. However, no genes involved in mineralization biology could be detected by this approach. Instead, a transcribed sequence, mapped with high identity to phosphatidylserine decarboxylase pseudogene 1 and phosphatidylserine decarboxylase pseudogene 2 using NCBI nucleotide blast, could be identified in both organs. The differential expression of the transcripts was confirmed by quantitative PCR. Thus, differential expression of this transcript may be involved in inhibition of ectopic calcification in B6 mice. However, identification of a corresponding gene product as well as biological significant function is missing.

Interestingly, *Abcc6,* previously identified as a causative gene for dystrophic calcification (see above), was not differentially regulated. After identifying *Abcc6* as a major causal gene, Meng and colleagues demonstrated up to 100-fold higher expression of *Abbc6* in liver, heart and kidney of B6 mice in comparison to calcification susceptible C3H or D2 mice [199]. This finding could not be reproduced by the whole genome expression study presented here. However, a more recent study identified a splice variant of the *Abcc6* gene in C3H as well as in D2 mice, leading to a truncated protein and consequently to a protein deficiency [200]. Taking this finding into account, it is reasonable to assume that a difference in *Abcc6* expression might not be detectable on RNA level. Thus, to clarify the role of *Abcc6* in fetuin-A deficient mice, differential expression should be investigated on the protein level or at least on the level of specific exons.

In conclusion, the current DNA microarray analysis did not identify genes with an obvious function in calcification prevention in B6 mice. As discussed before (see chapter 4.1.3) this might be attributed to technical reasons and the number of replicates might have been insufficient to obtain valid, reproducible results. Furthermore, the time points and tissues studied might have been suboptimal. Although ectopic calcification in fetuin-A deficient D2 mice was already detected in 2-week-old mice, the initiation of calcification varied between organs; in addition, variability of initiation was observed in different animals [264]. Remarkably, calcification in kidney was detected only occasionally in young mice, which was attributed to high expression of the calcification inhibitor osteopontin in kidney tubules [166, 264]. Thus, if one assumes that predominantly local mechanisms might prevent calcification in fetuin-A deficient B6 mice, it is reasonable to assume that such mechanisms might not have been initiated in kidneys of 5-week-old mice.

4.3.2 Impaired Clearance of Calciprotein-Particles in BMMs Derived from D2 Mice

In the current thesis, it could be shown that fetuin-A plays a critical role in clearance of mineral debris *in vivo* (see chapter 3.2)*.* Even under physiological conditions, blood is considered a metastable aqueous calcium-phosphate system sustaining mineral precipitation once crystals are nucleated. William Neuman aptly stated that we all suffer "Lot's wife's

problem" the imminent danger of turning into a pillar of salt [125]. Thus, a mechanism protecting against the disposal of mineral nuclei to prevent pathological calcification is of high importance. Consequently, efficiency in clearance of mineral particles from circulation might contribute to the different phenotypes of B6 and D2 fetuin-A deficient mice. Indeed, CPP clearance by BMMs derived from D2 mice was less efficient than by BMMs derived from B6 mice. Having shown that CPP clearance was predominantly mediated by scavenger receptor AI/II (see chapter 3.2), it was tested whether impaired CPP clearance in D2 BMMs is likewise due to a decreased expression of SR-AI/II. Inhibition of SR-AI/II using the SR antagonist polyinosinic acid further reduced uptake of CPPs in D2 BMMs. However, inhibition of CPP endocytosis in both B6 and D2 BMMs reached about a 25 % reduction only for uncoated CPPs and a 50 % reduction when serum-coated CPPs were applied. Therefore, using this assay differences in SR-A expression might be difficult to detect. On the other hand, a complete absence of SR-AI/II in D2 BMMs could thus be excluded. Further analysis of SR-AI/II expression on the protein level might prove difficult, because a polymorphism in B6 mice prevents detection of SR-AI/II using the popular monoclonal antibody clone 2F8 [347].

The analysis of endocytosis of particular matter distinct from CPPs might be of interest to obtain further information of causes for an impaired CPP uptake in D2 BMMs. Furthermore, it might be interesting to evaluate whether impaired CPP clearance is restricted to BMMs or if it is a common phenomenon in different macrophage subtypes in D2 vs. B6 mice. Finally, CPP clearance should be studied in D2 mice *in vivo*.

4.3.3 Summary

This part of the thesis aimed to identify molecular mechanisms determining the different calcification phenotypes of fetuin-A deficient B6 and D2 mice. So far, no candidate genes involved in mineralization mechanisms could be identified on the gene expression level. However, it is reasonable to assume that mechanisms distinct from differential gene expression in the tissues and at the particular time studied might contribute to calcification resistance and calcification susceptibility, respectively. Here, for the first time a significant difference in clearance of mineral particles was detected *in vitro.* This difference needs yet to be validated *in vivo.*

Finally, it may be assumed that a combination of several effects may result in the calcification susceptibility of certain mouse strains. In addition to the clearance efficiency reported here, the concentration of calcification inhibitors may be of importance. For instance, it was described recently that dietary magnesium was sufficient to inhibit connective tissue calcification in *Abcc6* deficient mice [153, 154]. It was previously shown that serum magnesium levels were considerably lower in D2 mice compared to B6 mice [56, 348] suggesting a correlation of serum magnesium levels and the calcification phenotype of D2 mice.

4.4 Perspectives

Fetuin-A is effective in formation and stabilization of soluble protein mineral particles (CPPs). In the current thesis it could be shown that CPPs are rapidly removed from the circulation *in vivo.* Endocytosis of CPPs was mediated by macrophages of liver and spleen in a SR-AI/II dependent manner. Protein analysis suggested a rapid degradation of fetuin-A. However, using these methods no information on the fate of internalized calcium phosphate was obtained. Several studies suggested a pro-inflammatory effect of hydroxyapatite [233, 234, 236, 237]. Thus, future work should include the elucidation of the inflammatory potential of CPPs. Furthermore, it should be studied whether the mineral content of CPPs is resolved and restored to the calcium phosphate pool, or if the endocytosed mineral remains in the macrophages. In vascular calcification, an increased calcium accumulation in vascular smooth muscle cells mediates cell death associated with the release of calcification-prone apoptotic bodies [185]. Therefore, it is reasonable to assume that high doses of intracellular calcium in macrophages may likewise lead to cell death and consequently to mineral deposition.

In the current study, accumulation of intravenously injected CPPs was detected in spleen and liver. It was not analyzed whether CPPs were also cleared directly by blood monocytes. This might be of interest, because recently circulating calcifying cells were identified, which had a high potential to induce calcification [349]. The origin of these cells is unknown, but it was shown that they derived from myeloid precursors. Therefore, one could hypothesize that these cells might have developed from monocytes, which have taken up CPPs or mineral debris. To answer this question it should be examined whether uptake of CPPs induces expression of osteogenic markers, which is characteristic for circulating calcifying cells.

Another part of the current thesis was to study mechanisms of ectopic calcification in fetuin-A deficient mice. Gene expression analysis pointed to a passive chemical process of mineral precipitation distinct from the active cell-mediated mineralization triggering vascular calcification. For instance low serum magnesium levels, which were detected in D2 mice [56, 348] may contribute to calcification. As dietary magnesium supplementation was shown to be of therapeutic value in high phosphate induced aortic calcification [152] and connective tissue calcification in a mouse model of pseudoxanthoma elasticum (PXE) [153, 154], it should be tested if dietary magnesium is likewise of therapeutic value in calcifying D2 fetuin-A deficient mice. Furthermore, studies on the uptake of CPPs by macrophages of calcifying D2 mice in comparison to BMM derived from non-calcifying B6 mice revealed an impaired endocytosis of CPPs in D2 mice. Defective or rather ineffective clearance of mineral debris might therefore be another risk factor for calcification in D2 mice. The relevance of CPP clearance for ectopic calcification may be elucidated by studying CPP clearance in D2 mice *in vivo*. If macrophage uptake of CPPs is crucial to prevent calcification, D2 mice should have

prolonged circulation of CPPs in serum compared to B6 mice. Furthermore, extended CPP accumulation may lead to aggregation and subsequently to deposition of mineral debris.

In conclusion, an important role of fetuin-A in the clearance of mineral debris was identified *in vivo*. The finding that SR-AI/II, a well-known scavenger receptor for LDL particles and lipid debris [216], likewise participates in the clearance of CPPs and mineral debris points to a combined role for the clearance of lipids and mineral debris in the pathogenesis of atherosclerosis. Thus, the stimulation of SR-AI/II function in macrophages may be of therapeutic value in calcification diseases, in particular in calcifying atherosclerosis.

References

1. Pedersen KO. Fetuin, a new globin isolated from serum. *Nature.* 1944;154:575-570.

2. Heremans JF. *Les Globulines Sériques du Système Gamma.*; 1960.

3. Schmid K, Bürgi W. Preparation and properties of the human plasma Ba-alpha2-glycoproteins. *Biochim Biophys Acta.* 1961;47:440-453.

4. Schultze HE, Heide K, Haupt H. Charakterisierung eines niedermoleularen α2-Mukoids aus Humanserum. *Naturwiss.* 1962;49:15-17.

5. Dziegielewska KM, Bock E, Cornelis ME, Møllgard K, New H, Saunders NR. Identification of fetuin in human and rat fetuses and in other species. *Comp Biochem Physiol A Comp Physiol.* 1983;76(2):241-245.

6. Aoki N, Deshimaru M, Kihara K, Terada S. Snake fetuin: isolation and structural analysis of new fetuin family proteins from the sera of venomous snakes. *Toxicon.* 2009;54(4):481-490.

7. Terkelsen O, Jahnen-Dechent W, Nielsen H, Moos T, Fink E, Nawratil P, Müller-Esterl W, Mollgard K. Rat fetuin: distribution of protein and mRNA in embryonic and neonatal rat tissues. *Anat Embryol (Berl).* 1998;197(2):125-133.

8. Suzuki M, Shimokawa H, Takagi Y, Sasaki S. Calcium-binding properties of fetuin in fetal bovine serum. *J Exp Zool.* 1994;270(6):501-507.

9. Häusler M, Schäfer C, Osterwinter C, Jahnen-Dechent W. The physiologic development of fetuin-a serum concentrations in children. *Pediatr Res.* 2009;66(6):660-664.

10. Lebreton J, Joisel F, Raoult J, Lannuzel B, Rogez J, Humbert G. Serum concentration of human alpha 2 HS glycoprotein during the inflammatory process: evidence that alpha 2 HS glycoprotein is a negative acute-phase reactant. *J Clin Invest.* 1979;64(4):1118-1129.

11. Daveau M, Christian-Davrinche, Julen N, Hiron M, Arnaud P, Lebreton JP. The synthesis of human alpha-2-HS glycoprotein is down-regulated by cytokines in hepatoma HepG2 cells. *FEBS Lett.* 1988;241(1-2):191-194.

12. Li W, Zhu S, Li J, Huang Y, Zhou R, Fan X, Yang H, Gong X, Eissa NT, Jahnen-Dechent W, Wang P, Tracey KJ, Sama AE, Wang H. A hepatic protein, fetuin-A, occupies a protective role in lethal systemic inflammation. *PLoS ONE.* 2011;6(2):e16945.

13. Lee C, Bongcam-Rudloff E, Sollner C, Jahnen-Dechent W, Claesson-Welsh L. Type 3 cystatins; fetuins, kininogen and histidine-rich glycoprotein. *Front Biosci.* 2009;14:2911-2922.

14. Schinke T, Amendt C, Trindl A, Pöschke O, Müller-Esterl W, Jahnen-Dechent W. The serum protein alpha2-HS glycoprotein/fetuin inhibits apatite formation in vitro and in mineralizing calvaria cells. A possible role in mineralization and calcium homeostasis. *J Biol Chem.* 1996;271(34):20789-20796.

15. Spiro RG, Bhoyroo VD. Structure of the O-glycosidically linked carbohydrate units of fetuin. *J Biol Chem.* 1974;249(18):5704-5717.

16. Hortin GL, Schilling M, Graham JP. Inhibitors of the sulfation of proteins, glycoproteins, and proteoglycans. *Biochem Biophys Res Commun.* 1988;150(1):342-348.

17. Jahnen-Dechent W, Trindl A, Godovac-Zimmermann J, Müller-Esterl W. Posttranslational processing of human alpha 2-HS glycoprotein (human fetuin). Evidence for the production of a phosphorylated single-chain form by hepatoma cells. *Eur J Biochem.* 1994;226(1):59-69.

18. Heiss A, DuChesne A, Denecke B, Grötzinger J, Yamamoto K, Renné T, Jahnen-Dechent W. Structural basis of calcification inhibition by alpha 2-HS glycoprotein/fetuin-A. Formation of colloidal calciprotein particles. *J Biol Chem.* 2003;278(15):13333-13341.

19. Triffitt JT, Gebauer U, Ashton BA, Owen ME, Reynolds JJ. Origin of plasma alpha2HS-glycoprotein and its accumulation in bone. *Nature.* 1976;262(5565):226-227.

20. Takagi Y, Shimokawa H, Suzuki M, Nagai H, Sasaki S. Immunohistochemical localization of alpha 2HS glycoprotein in dentin. *Calcif Tissue Int.* 1990;47(1):40-45.

21. Fisher HW, Puck TT, Sato G. Molecular growth requirements of single mammalian cells: The action of fetuin in promoting cell attachment to glass. *Proc Natl Acad Sci USA.* 1958;44(1):4-10.

22. Tajirian T, Dennis JW, Swallow CJ. Regulation of human monocyte proMMP-9 production by fetuin, an endogenous TGF-beta antagonist. *J Cell Physiol.* 2000;185(2):174-183.

23. Leite-Browning ML, McCawley LJ, Choi OH, Matrisian LM, Ochieng J. Interactions of alpha2-HS-glycoprotein (fetuin) with MMP-3 and murine squamous cell carcinoma cells. *Int J Oncol.* 2002;21(5):965-971.

24. Ray S, Lukyanov P, Ochieng J. Members of the cystatin superfamily interact with MMP-9 and protect it from autolytic degradation without affecting its gelatinolytic activities. *Biochim Biophys Acta.* 2003;1652(2):91-102.

25. Leite-Browning ML, McCawley LJ, Jahnen-Dechent W, King LE, Matrisian LM, Ochieng J. Alpha 2-HS glycoprotein (fetuin-A) modulates murine skin tumorigenesis. *Int J Oncol.* 2004;25(2):319-324.

26. Kundranda MN, Henderson M, Carter KJ, Gorden L, Binhazim A, Ray S, Baptiste T, Shokrani M, Leite-Browning ML, Jahnen-Dechent W, Matrisian LM, Ochieng J. The serum glycoprotein fetuin-A promotes Lewis lung carcinoma tumorigenesis via adhesive-dependent and adhesive-independent mechanisms. *Cancer Res.* 2005;65(2):499-506.

27. Mellgren RL, Huang X. Fetuin A stabilizes m-calpain and facilitates plasma membrane repair. *J Biol Chem.* 2007;282(49):35868-35877.

28. Hedrich J, Lottaz D, Meyer K, Yiallouros I, Jahnen-Dechent W, Stöcker W, Becker-Pauly C. Fetuin-A and cystatin C are endogenous inhibitors of human meprin metalloproteases. *Biochemistry.* 2010;49(39):8599-8607.

29. Kumbla L, Cayatte AJ, Subbiah MT. Association of a lipoprotein-like particle with bovine fetuin. *Faseb J.* 1989;3(9):2075-2080.

30. Cayatte AJ, Kumbla L, Subbiah MT. Marked acceleration of exogenous fatty acid incorporation into cellular triglycerides by fetuin. *J Biol Chem.* 1990;265(10):5883-5888.

31. Kumbla L, Bhadra S, Subbiah M. Multifunctional role for fetuin (fetal protein) in lipid transport. *Faseb J.* 1991;5(14):2971-2975.

32. Cawley DB, Simpson DL, Herschman HR. Asialoglycoprotein receptor mediates the toxic effects of an asialofetuin-diphtheria toxin fragment A conjugate on cultured rat hepatocytes. *Proc Natl Acad Sci USA.* 1981;78(6):3383-3387.

33. Chong P, Klein M. Single-step purification of pertussis toxin and its subunits by heat-treated fetuin-sepharose affinity chromatography. *Biochem Cell Biol.* 1989;67(7):387-391.

34. Skelton SK, Wong KH. Simple, efficient purification of filamentous hemagglutinin and pertussis toxin from Bordetella pertussis by hydrophobic and affinity interaction. *J Clin Microbiol.* 1990;28(5):1062-1065.

35. Grossbard ML, Lambert JM, Goldmacher VS, Blättler WA, Nadler LM. Correlation between in vivo toxicity and preclinical in vitro parameters for the immunotoxin anti-B4-blocked ricin. *Cancer Res.* 1992;52(15):4200-4207.

36. Wang X-Q, Hayes MT, Kempf M, Fraser JF, Liu P-Y, Cuttle L, Friend LRR, Rothnagel JA, Saunders NA, Kimble RM. Fetuin-A: a major fetal serum protein that promotes "wound closure" and scarless healing. *J Invest Dermatol.* 2008;128(3):753-757.

37. Wang X-Q, Hung BS, Kempf M, Liu P-Y, Dalley AJ, Saunders NA, Kimble RM. Fetuin-A promotes primary keratinocyte migration: independent of epidermal growth factor receptor signalling. *Experimental Dermatology.* 2010;19(8):e289-292.

38. Demetriou M, Binkert C, Sukhu B, Tenenbaum H, Dennis J. Fetuin/alpha2-HS glycoprotein is a transforming growth factor-beta type II receptor mimic and cytokine antagonist. *J Biol Chem.* 1996;271(22):12755-12761.

39. Binkert C, Demetriou M, Sukhu B, Szweras M, Tenenbaum HC, Dennis JW. Regulation of osteogenesis by fetuin. *J Biol Chem.* 1999;274(40):28514-28520.

40. Szweras M, Liu D, Partridge EA, Pawling J, Sukhu B, Clokie C, Jahnen-Dechent W, Tenenbaum HC, Swallow CJ, Grynpas MD, Dennis JW. alpha 2-HS glycoprotein/fetuin, a transforming growth factor-beta/bone morphogenetic protein antagonist, regulates postnatal bone growth and remodeling. *J Biol Chem.* 2002;277(22):19991-19997.

41. Rittenberg B, Partridge E, Baker G, Clokie C, Zohar R, Dennis JW, Tenenbaum HC. Regulation of BMP-induced ectopic bone formation by Ahsg. *J Orthop Res.* 2005;23(3):653-662.

42. Zhu WQ, Ochieng J. Rapid release of intracellular galectin-3 from breast carcinoma cells by fetuin. *Cancer Res.* 2001;61(5):1869-1873.

43. Sakwe AM, Koumangoye R, Goodwin SJ, Ochieng J. Fetuin-A ({alpha}2HS-glycoprotein) is a major serum adhesive protein that mediates growth signaling in breast tumor cells. *Journal of Biological Chemistry.* 2010;285(53):41827-41835.

44. Guillory B, Sakwe AM, Saria M, Thompson P, Adhiambo C, Koumangoye R, Ballard B, Binhazim A, Cone C, Jahanen-Dechent W, Ochieng J. Lack of fetuin-A (alpha2-HS-glycoprotein) reduces mammary tumor incidence and prolongs tumor latency via the transforming growth factor-beta signaling pathway in a mouse model of breast cancer. *Am J Pathol.* 2010;177(5):2635-2644.

45. Auberger P, Falquerho L, Contreres JO, Pages G, Le Cam G, Rossi B, Le Cam A. Characterization of a natural inhibitor of the insulin receptor tyrosine kinase: cDNA cloning, purification, and anti-mitogenic activity. *Cell.* 1989;58(4):631-640.

46. Le Cam G, Auberger P, Falquerho L, Contreres J, Pages G, Rossi B. pp63 is very likely the rat fetuin. *Cell.* 1992;68(1):8.

47. Brown WM, Christie DL, Dziegielewska KM, Saunders NR, Yang F. The rat protein encoded by clone pp63 is a fetuin/alpha 2-HS glycoprotein-like molecule, but is it the tyrosine kinase inhibitor pp63? *Cell.* 1992;68(1):7-8.

48. Srinivas P, Wagner A, Reddy L, Deutsch D, Leon M, Goustin A, Grunberger G. Serum alpha 2-HS-glycoprotein is an inhibitor of the human insulin receptor at the tyrosine kinase level. *Mol Endocrinol.* 1993;7(11):1445-1455.

49. Sato H, Kazama JJ, Wada Y, Kuroda T, Narita I, Gejyo F, Gao P, Yamashita H. Decreased levels of circulating alpha2-Heremans-Schmid glycoprotein/Fetuin-A (AHSG) in patients with rheumatoid arthritis. *Intern Med.* 2007;46(20):1685-1691.

50. Kalabay L, Gráf L, Vörös K, Jakab L, Benkő Z, Telegdy L, Fekete B, Prohászka Z, Füst G. Human serum fetuin A/α2HS-glycoprotein level is associated with long-term survival in patients with alcoholic liver cirrhosis, comparison with the Child-Pugh and MELD scores. *BMC Gastroenterol.* 2007;7(1):15.

51. Karamessinis PM, Malamitsi-Puchner A, Boutsikou T, Makridakis M, Vougas K, Fountoulakis M, Vlahou A, Chrousos G. Marked defects in the expression and glycosylation of alpha2-HS glycoprotein/fetuin-A in plasma from neonates with intrauterine growth restriction: proteomics screening and potential clinical implications. *Mol Cell Proteomics.* 2008;7(3):591-599.

52. Smith ER, Nilforooshan R, Weaving G, Tabet N. Plasma fetuin-A is associated with the severity of cognitive impairment in mild-to-moderate Alzheimer's disease. *J Alzheimers Dis.* 2011;24(2):327-333.

53. van Oss CJ, Gillman CF, Bronson PM, Border JR. Opsonic properties of human serum alpha-2 hs glycoprotein. *Immunol Commun.* 1974;3(4):329-335.

54. Wang H, Zhang M, Soda K, Sama A, Tracey KJ. Fetuin protects the fetus from TNF. *Lancet.* 1997;350(9081):861-862.

55. Jahnen-Dechent W, Heiss A, Schäfer C, Ketteler M. Fetuin-A regulation of calcified matrix metabolism. *Circ Res.* 2011;108(12):1494-1509.

56. Schäfer C, Heiss A, Schwarz A, Westenfeld R, Ketteler M, Floege J, Müller-Esterl W, Schinke T, Jahnen-Dechent W. The serum protein alpha 2-Heremans-Schmid glycoprotein/fetuin-A is a systemically acting inhibitor of ectopic calcification. *J Clin Invest.* 2003;112(3):357-366.

57. Burke AP, Kolodgie FD, Virmani R. Fetuin-A, Valve Calcification, and Diabetes: What Do We Understand? *Circulation.* 2007;115(19):2464-2467.

58. Haasemann M, Nawratil P, Müller-Esterl W. Rat tyrosine kinase inhibitor shows sequence similarity to human alpha 2-HS glycoprotein and bovine fetuin. *Biochem J.* 1991;274 (Pt 3):899-902.

59. Rauth G, Pöschke O, Fink E, Eulitz M, Tippmer S, Kellerer M, Häring HU, Nawratil P, Haasemann M, Jahnen-Dechent W. The nucleotide and partial amino acid sequences of rat fetuin. Identity with the natural tyrosine kinase inhibitor of the rat insulin receptor. *Eur J Biochem.* 1992;204(2):523-529.

60. Mathews ST, Srinivas PR, Leon MA, Grunberger G. Bovine fetuin is an inhibitor of insulin receptor tyrosine kinase. *Life Sci.* 1997;61(16):1583-1592.

61. Chen H, Srinivas PR, Cong LN, Li Y, Grunberger G, Quon MJ. Alpha2-Heremans Schmid glycoprotein inhibits insulin-stimulated Elk-1 phosphorylation, but not glucose transport, in rat adipose cells. *Endocrinology.* 1998;139(10):4147-4154.

62. Mathews ST, Singh GP, Ranalletta M, Cintron VJ, Qiang X, Goustin AS, Jen K-LC, Charron MJ, Jahnen-Dechent W, Grunberger G. Improved insulin sensitivity and resistance to weight gain in mice null for the Ahsg gene. *Diabetes.* 2002;51(8):2450-2458.

63. Mathews ST, Rakhade S, Zhou X, Parker GC, Coscina DV, Grunberger G. Fetuin-null mice are protected against obesity and insulin resistance associated with aging. *Biochem Biophys Res Commun.* 2006;350(2):437-443.

64. Ix JH, Shlipak MG, Brandenburg VM, Ali S, Ketteler M, Whooley MA. Association between human fetuin-A and the metabolic syndrome: data from the Heart and Soul Study. *Circulation.* 2006;113(14):1760-1767.

65. Axelsson J, Wang X, Ketteler M, Qureshi AR, Heimbürger O, Bárány P, Lindholm B, Nordfors L, Stenvinkel P. Is fetuin-A/alpha2-Heremans-Schmid glycoprotein associated with the metabolic syndrome in patients with chronic kidney disease? *Am J Nephrol.* 2008;28(4):669-676.

66. Brix JM, Stingl H, Höllerl F, Schernthaner GH, Kopp H-P, Schernthaner G. Elevated Fetuin-A concentrations in morbid obesity decrease after dramatic weight loss. *J Clin Endocrinol Metab.* 2010;95(11):4877-4881.

67. Xu Y, Xu M, Bi Y, Song A, Huang Y, Liu Y, Wu Y, Chen Y, Wang W, Li X, Ning G. Serum fetuin-A is correlated with metabolic syndrome in middle-aged and elderly Chinese. *Atherosclerosis.* 2011;216(1):180-186.

68. Stefan N, Hennige AM, Staiger H, Machann J, Schick F, Kröber SM, Machicao F, Fritsche A, Häring H-U. Alpha2-Heremans-Schmid glycoprotein/fetuin-A is associated with insulin resistance and fat accumulation in the liver in humans. *Diabetes Care.* 2006;29(4):853-857.

69. Ishibashi A, Ikeda Y, Ohguro T, Kumon Y, Yamanaka S, Takata H, Inoue M, Suehiro T, Terada Y. Serum fetuin-A is an independent marker of insulin resistance in Japanese men. *J Atheroscler Thromb.* 2010;17(9):925-933.

70. Andersen G, Burgdorf KS, Sparsø T, Borch-Johnsen K, Jørgensen T, Hansen T, Pedersen O. AHSG tag single nucleotide polymorphisms associate with type 2 diabetes and dyslipidemia: studies of metabolic traits in 7,683 white Danish subjects. *Diabetes.* 2008;57(5):1427-1432.

71. Stefan N, Fritsche A, Weikert C, Boeing H, Joost H-G, Häring H-U, Schulze MB. Plasma fetuin-A levels and the risk of type 2 diabetes. *Diabetes.* 2008;57(10):2762-2767.

72. Song A, Xu M, Bi Y, Xu Y, Huang Y, Li M, Wang T, Wu Y, Liu Y, Li X, Chen Y, Wang W, Ning G. Serum Fetuin-A Associates with Type 2 Diabetes and Insulin Resistance in Chinese Adults. *PLoS ONE.* 2011;6(4):e19228.

73. Ou H-Y, Yang Y-C, Wu H-T, Wu J-S, Lu F-H, Chang C-J. Serum fetuin-A concentrations are elevated in subjects with impaired glucose tolerance and newly diagnosed type 2 diabetes. *Clin Endocrinol (Oxf).* 2011;75(4):450-455.

74. Hennige AM, Staiger H, Wicke C, Machicao F, Fritsche A, Häring H-U, Stefan N. Fetuin-A induces cytokine expression and suppresses adiponectin production. *PLoS ONE.* 2008;3(3):e1765.

75. Dasgupta S, Bhattacharya S, Biswas A, Majumdar SS, Mukhopadhyay S, Ray S, Bhattacharya S. NF-kappaB mediates lipid-induced fetuin-A expression in hepatocytes that impairs adipocyte function effecting insulin resistance. *Biochem J.* 2010;429(3):451-462.

76. Lewis JG, André CM. Effect of human alpha 2HS glycoprotein on mouse macrophage function. *Immunology.* 1980;39(3):317-322.

77. Lewis JG, André CM. Enhancement of human monocyte phagocytic function by alpha 2HS glycoprotein. *Immunology.* 1981;42(3):481-487.

78. Thiele L, Diederichs JE, Reszka R, Merkle HP, Walter E. Competitive adsorption of serum proteins at microparticles affects phagocytosis by dendritic cells. *Biomaterials.* 2003;24(8):1409-1418.

79. Jersmann HPA, Dransfield I, Hart SP. Fetuin/alpha2-HS glycoprotein enhances phagocytosis of apoptotic cells and macropinocytosis by human macrophages. *Clin Sci.* 2003;105(3):273-278.

80. Nagayama S, Ogawara K-i, Minato K, Fukuoka Y, Takakura Y, Hashida M, Higaki K, Kimura T. Fetuin mediates hepatic uptake of negatively charged nanoparticles via scavenger receptor. *International Journal of Pharmaceutics.* 2007;329(1-2):192-198.

81. Terkeltaub RA, Santoro DA, Mandel G, Mandel N. Serum and plasma inhibit neutrophil stimulation by hydroxyapatite crystals. Evidence that serum alpha 2-HS glycoprotein is a potent and specific crystal-bound inhibitor. *Arthritis Rheum.* 1988;31(9):1081-1089.

82. Zhang M, Caragine T, Wang H, Cohen PS, Botchkina G, Soda K, Bianchi M, Ulrich P, Cerami A, Sherry B, Tracey KJ. Spermine inhibits proinflammatory cytokine synthesis in human mononuclear cells: a counterregulatory mechanism that restrains the immune response. *J Exp Med.* 1997;185(10):1759-1768.

83. Wang H, Zhang M, Bianchi M, Sherry B, Sama A, Tracey KJ. Fetuin (alpha2-HS-glycoprotein) opsonizes cationic macrophage-deactivating molecules. *Proc Natl Acad Sci USA.* 1998;95(24):14429-14434.

84. Dziegielewska KM, Andersen NA, Saunders NR. Modification of macrophage response to lipopolysaccharide by fetuin. *Immunol Lett.* 1998;60(1):31-35.

85. Wang H, Li W, Zhu S, Li J, D'Amore J, Ward MF, Yang H, Wu R, Jahnen-Dechent W, Tracey KJ, Wang P, Sama AE. Peripheral administration of fetuin-A attenuates early cerebral ischemic injury in rats. *J Cereb Blood Flow Metab.* 2010;30(3):493-504.

86. Triffitt J, Owen M, Ashton B, Wilson J. Plasma disappearance of rabbit alpha2HS-glycoprotein and its uptake by bone tissue. *Calcif Tissue Res.* 1978;26(2):155-161.

87. Jahnen-Dechent W, Schinke T, Trindl A, Müller-Esterl W, Sablitzky F, Kaiser S, Blessing M. Cloning and targeted deletion of the mouse fetuin gene. *J Biol Chem.* 1997;272(50):31496-31503.

88. Price PA, Thomas GR, Pardini AW, Figueira WF, Caputo JM, Williamson MK. Discovery of a high molecular weight complex of calcium, phosphate, fetuin, and matrix gamma-carboxyglutamic acid protein in the serum of etidronate-treated rats. *J Biol Chem.* 2002;277(6):3926-3934.

89. Price PA, Nguyen TMT, Williamson MK. Biochemical characterization of the serum fetuin-mineral complex. *J Biol Chem.* 2003;278(24):22153-22160.

90. Heiss A, Eckert T, Aretz A, Richtering W, Van Dorp W, Schafer C, Jahnen-Dechent W. Hierarchical Role of Fetuin-A and Acidic Serum Proteins in the Formation and Stabilization of Calcium Phosphate Particles. *Journal of Biological Chemistry.* 2008;283(21):14815-14825.

91. Heiss A, Jahnen-Dechent W, Endo H, Schwahn D. Structural dynamics of a colloidal protein-mineral complex bestowing on calcium phosphate a high solubility in biological fluids. *Biointerphases.* 2007;2(1):16-20.

92. Wald J, Wiese S, Eckert T, Jahnen-Dechent W, Richtering W, Heiss A. Formation and stability kinetics of calcium phosphate–fetuin-A colloidal particles probed by time-resolved dynamic light scattering. *Soft Matter.* 2011;7:2869-2874.

93. Young J, Martel J, Young L, Wu C, Young A, Young D. Putative nanobacteria represent physiological remnants and culture by-products of normal calcium homeostasis. *PLoS ONE.* 2009;4(2):e4417.

94. Young JD, Martel J, Young D, Young A, Hung C-M, Young L, Chao Y-J, Young J, Wu C-Y. Characterization of granulations of calcium and apatite in serum as pleomorphic mineralo-protein complexes and as precursors of putative nanobacteria. *PLoS ONE.* 2009;4(5):e5421.

95. Cisar J, Xu D, Thompson J, Swaim W, Hu L, Kopecko D. An alternative interpretation of nanobacteria-induced biomineralization. *Proc Natl Acad Sci U S A.* 2000;97(21):11511-11515.

96. Raoult D, Drancourt M, Azza S, Nappez C, Guieu R, Rolain J-M, Fourquet P, Campagna B, La Scola B, Mege J-L, Mansuelle P, Lechevalier E, Berland Y, Gorvel

J-P, Renesto P. Nanobacteria are mineralo fetuin complexes. *PLoS Pathog.* 2008;4(2):e41.

97. Young JD, Martel J. The rise and fall of nanobacteria. *Sci Am.* 2010;302(1):52-59.

98. Kajander EO, Ciftçioglu N. Nanobacteria: an alternative mechanism for pathogenic intra- and extracellular calcification and stone formation. *Proc Natl Acad Sci USA.* 1998;95(14):8274-8279.

99. Ciftçioglu N, Björklund M, Kuorikoski K, Bergström K, Kajander EO. Nanobacteria: an infectious cause for kidney stone formation. *Kidney Int.* 1999;56(5):1893-1898.

100. Hjelle JT, Miller-Hjelle MA, Poxton IR, Kajander EO, Ciftcioglu N, Jones ML, Caughey RC, Brown R, Millikin PD, Darras FS. Endotoxin and nanobacteria in polycystic kidney disease. *Kidney Int.* 2000;57(6):2360-2374.

101. Sedivy R, Battistutti WB. Nanobacteria promote crystallization of psammoma bodies in ovarian cancer. *APMIS.* 2003;111(10):951-954.

102. Miller VM, Rodgers G, Charlesworth JA, Kirkland B, Severson SR, Rasmussen TE, Yagubyan M, Rodgers JC, Cockerill FR, Folk RL, Rzewuska-Lech E, Kumar V, Farell-Baril G, Lieske JC. Evidence of nanobacterial-like structures in calcified human arteries and cardiac valves. *Am J Physiol Heart Circ Physiol.* 2004;287(3):H1115-1124.

103. Ketteler M, Bongartz P, Westenfeld R, Wildberger J, Mahnken A, Bohm R, Metzger T, Wanner C, Jahnen-Dechent W, Floege J. Association of low fetuin-A (AHSG) concentrations in serum with cardiovascular mortality in patients on dialysis: a cross-sectional study. *Lancet.* 2003;361(9360):827-833.

104. Ix JH, Chertow GM, Shlipak MG, Brandenburg VM, Ketteler M, Whooley MA. Association of fetuin-A with mitral annular calcification and aortic stenosis among persons with coronary heart disease: data from the Heart and Soul Study. *Circulation.* 2007;115(19):2533-2539.

105. Stejskal D, Karpisek M, Vrtal R, Student V, Solichova P, Fiala R, Stejskal P. Urine fetuin-A values in relation to the presence of urolithiasis. *BJU Int.* 2008;101(9):1151-1154.

106. Koos R, Brandenburg V, Mahnken AH, Mühlenbruch G, Stanzel S, Günther RW, Floege J, Jahnen-Dechent W, Kelm M, Kühl HP. Association of fetuin-A levels with the progression of aortic valve calcification in non-dialyzed patients. *Eur Heart J.* 2009;30(16):2054-2061.

107. Bilgir O, Kebapcilar L, Bilgir F, Bozkaya G, Yildiz Y, Pinar P, Tastan A. Decreased serum fetuin-A levels are associated with coronary artery diseases. *Intern Med.* 2010;49(13):1281-1285.

108. Eraso LH, Ginwala N, Qasim AN, Mehta NN, Dlugash R, Kapoor S, Schwartz S, Schutta M, Iqbal N, Mohler ER, Reilly MP. Association of lower plasma fetuin-a levels with peripheral arterial disease in type 2 diabetes. *Diabetes Care.* 2010;33(2):408-410.

109. Jung JY, Hwang Y-H, Lee H, Ro H, Lee H, Chung W, Chae D-W, Joo KW, Ahn C, Oh K-H. Association of AHSG gene polymorphisms and aortic stiffness in peritoneal dialysis patients. *Am J Nephrol.* 2010;31(6):510-517.

110. Aksoy H, Aksoy Y, Ozturk N, Aydin HR, Yildirim AK, Akçay F. Fetuin-A gene polymorphism in patients with calcium oxalate stone disease. *Urology.* 2010;75(4):928-932.

111. Ball CR, Williams WL. Spontaneous and dietary-induced cardiovascular lesions in DBA mice. *Anat Rec.* 1965;152(2):199-209.

112. Brunnert SR. Morphologic response of myocardium to freeze-thaw injury in mouse strains with dystrophic cardiac calcification. *Lab Anim Sci.* 1997;47(1):11-18.

113. Merx MW, Schäfer C, Westenfeld R, Brandenburg V, Hidajat S, Weber C, Ketteler M, Jahnen-Dechent W. Myocardial stiffness, cardiac remodeling, and diastolic dysfunction in calcification-prone fetuin-A-deficient mice. *J Am Soc Nephrol.* 2005;16(11):3357-3364.

114. Westenfeld R, Schäfer C, Smeets R, Brandenburg VM, Floege J, Ketteler M, Jahnen-Dechent W. Fetuin-A (AHSG) prevents extraosseous calcification induced by uraemia and phosphate challenge in mice. *Nephrol Dial Transplant.* 2007;22(6):1537-1546.

115. Westenfeld R, Schäfer C, Krüger T, Haarmann C, Schurgers LJ, Reutelingsperger C, Ivanovski O, Drueke T, Massy ZA, Ketteler M, Floege J, Jahnen-Dechent W. Fetuin-A protects against atherosclerotic calcification in CKD. *J Am Soc Nephrol.* 2009;20(6):1264-1274.

116. Tolleshaug H, Berg T, Nilsson M, Norum KR. Uptake and degradation of 125I-labelled asialo-fetuin by isolated rat hepatocytes. *Biochim Biophys Acta.* 1977;499(1):73-84.

117. Ashwell G, Morell AG. The role of surface carbohydrates in the hepatic recognition and transport of circulating glycoproteins. *Adv Enzymol Relat Areas Mol Biol.* 1974;41(0):99-128.

118. Tolleshaug H, Berg T, Frölich W, Norum KR. Intracellular localization and degradation of asialofetuin in isolated rat hepatocytes. *Biochim Biophys Acta.* 1979;585(1):71-84.

119. Thornburg RW, Day JF, Baynes JW, Thorpe SR. Carbohydrate-mediated clearance of immune complexes from the circulation. A role for galactose residues in the hepatic uptake of IgG-antigen complexes. *J Biol Chem.* 1980;255(14):6820-6825.

120. Lodish HF. Recognition of complex oligosaccharides by the multi-subunit asialoglycoprotein receptor. *Trends Biochem Sci.* 1991;16(10):374-377.

121. Tozawa R, Ishibashi S, Osuga J, Yamamoto K, Yagyu H, Ohashi K, Tamura Y, Yahagi N, Iizuka Y, Okazaki H, Harada K, Gotoda T, Shimano H, Kimura S, Nagai R, Yamada N. Asialoglycoprotein receptor deficiency in mice lacking the major receptor subunit. Its obligate requirement for the stable expression of oligomeric receptor. *J Biol Chem.* 2001;276(16):12624-12628.

122. Reynolds JL, Skepper JN, McNair R, Kasama T, Gupta K, Weissberg PL, Jahnen-Dechent W, Shanahan CM. Multifunctional roles for serum protein fetuin-a in inhibition of human vascular smooth muscle cell calcification. *J Am Soc Nephrol.* 2005;16(10):2920-2930.

123. Chen NX, O'Neill KD, Chen X, Duan D, Wang E, Sturek MS, Edwards JM, Moe SM. Fetuin-A uptake in bovine vascular smooth muscle cells is calcium dependent and mediated by annexins. *Am J Physiol Renal Physiol.* 2007;292(2):F599-606.

124. Jahnen-Dechent W, Baeuerlein E. Lot's wife's problem revisited: how we prevent pathological calcification. *Biomineralization Progress in Biology, Molecular Biology and Application*; 2004:243-267.

125. Neuman WF, Urist MR. Bone material and calcification mechanisms. *Fundamental and Clinical Bone Physiology*; 1980:83-107.

126. Brown E. Extracellular Ca2+ sensing, regulation of parathyroid cell function, and role of Ca2+ and other ions as extracellular (first) messengers. *Physiol Rev.* 1991;71(2):371-411.

127. Dusso AS, Brown AJ, Slatopolsky E. Vitamin D. *Am J Physiol Renal Physiol.* 2005;289(1):F8-28.

128. Liu S, Guo R, Simpson LG, Xiao Z-S, Burnham CE, Quarles LD. Regulation of fibroblastic growth factor 23 expression but not degradation by PHEX. *J Biol Chem.* 2003;278(39):37419-37426.

129. Kolek OI, Hines ER, Jones MD, LeSueur LK, Lipko MA, Kiela PR, Collins JF, Haussler MR, Ghishan FK. 1alpha,25-Dihydroxyvitamin D3 upregulates FGF23 gene expression in bone: the final link in a renal-gastrointestinal-skeletal axis that controls phosphate transport. *Am J Physiol Gastrointest Liver Physiol.* 2005;289(6):G1036-1042.

130. Ferrari SL, Bonjour J-P, Rizzoli R. Fibroblast growth factor-23 relationship to dietary phosphate and renal phosphate handling in healthy young men. *J Clin Endocrinol Metab.* 2005;90(3):1519-1524.

131. Burnett S-AM, Gunawardene SC, Bringhurst FR, Jüppner H, Lee H, Finkelstein JS. Regulation of C-terminal and intact FGF-23 by dietary phosphate in men and women. *J Bone Miner Res.* 2006;21(8):1187-1196.

132. Perwad F, Azam N, Zhang MYH, Yamashita T, Tenenhouse HS, Portale AA. Dietary and serum phosphorus regulate fibroblast growth factor 23 expression and 1,25-dihydroxyvitamin D metabolism in mice. *Endocrinology.* 2005;146(12):5358-5364.

133. Quarles LD. Evidence for a bone-kidney axis regulating phosphate homeostasis. *J Clin Invest.* 2003;112(5):642-646.

134. Kurosu H, Ogawa Y, Miyoshi M, Yamamoto M, Nandi A, Rosenblatt KP, Baum MG, Schiavi S, Hu M-C, Moe OW, Kuro-o M. Regulation of fibroblast growth factor-23 signaling by klotho. *J Biol Chem.* 2006;281(10):6120-6123.

135. Shimada T, Hasegawa H, Yamazaki Y, Muto T, Hino R, Takeuchi Y, Fujita T, Nakahara K, Fukumoto S, Yamashita T. FGF-23 is a potent regulator of vitamin D metabolism and phosphate homeostasis. *J Bone Miner Res.* 2004;19(3):429-435.

136. Liu S, Quarles LD. How fibroblast growth factor 23 works. *J Am Soc Nephrol.* 2007;18(6):1637-1647.

137. Shimada T, Kakitani M, Yamazaki Y, Hasegawa H, Takeuchi Y, Fujita T, Fukumoto S, Tomizuka K, Yamashita T. Targeted ablation of Fgf23 demonstrates an essential physiological role of FGF23 in phosphate and vitamin D metabolism. *J Clin Invest.* 2004;113(4):561-568.

138. Sitara D, Razzaque MS, Hesse M, Yoganathan S, Taguchi T, Erben RG, Jüppner H, Lanske B. Homozygous ablation of fibroblast growth factor-23 results in hyperphosphatemia and impaired skeletogenesis, and reverses hypophosphatemia in Phex-deficient mice. *Matrix Biol.* 2004;23(7):421-432.

139. Liu S, Zhou J, Tang W, Jiang X, Rowe DW, Quarles LD. Pathogenic role of Fgf23 in Hyp mice. *Am J Physiol Endocrinol Metab.* 2006;291(1):E38-49.

140. Savin JA, Wallace HJ. Systemic lupus erythematosus with ectopic calcification. *Br J Dermatol.* 1971;84(2):191-192.

141. Williamson BR, Carey RM, Innes DJ, Teates CD, Bray ST, Lees RF, Sturgill BC. Poorly differentiated lymphocytic lymphoma with ectopic parathormone production: visulization of metastatic calcification by bone scan. *Clin Nucl Med.* 1978;3(10):382-384.

142. Balachandran S, Abbud Y, Prince MJ, Chausmer AB. Tumoral calcinosis: scintigraphic studies of an affected family. *Br J Radiol.* 1980;53(634):960-964.

143. Hatori M, Oomamiuda K, Kokubun S. Hydroxyapatite crystals in tumoral calcinosis: a case report. *Tohoku J Exp Med.* 1996;180(4):359-364.

144. Fujita N, Torres A, Sharma OP. Letter: Ectopic calcification in sarcoidosis. *JAMA.* 1974;227(5):556.

145. Smith R, Russell RG, Woods CG. Myositis ossificans progressiva. Clinical features of eight patients and their response to treatment. *J Bone Joint Surg Br.* 1976;58(1):48-57.

146. Shafritz AB, Shore EM, Gannon FH, Zasloff MA, Taub R, Muenke M, Kaplan FS. Overexpression of an osteogenic morphogen in fibrodysplasia ossificans progressiva. *N Engl J Med.* 1996;335(8):555-561.

147. Sowers KM, Hayden MR. Calcific uremic arteriolopathy: pathophysiology, reactive oxygen species and therapeutic approaches. *Oxid Med Cell Longev.* 2010;3(2):109-121.

148. Schoen FJ, Levy RJ. Calcification of tissue heart valve substitutes: progress toward understanding and prevention. *Ann Thorac Surg.* 2005;79(3):1072-1080.

149. Wilson PW, Kauppila LI, O'Donnell CJ, Kiel DP, Hannan M, Polak JM, Cupples LA. Abdominal aortic calcific deposits are an important predictor of vascular morbidity and mortality. *Circulation.* 2001;103(11):1529-1534.

150. Block G, Hulbert-Shearon T, Levin N, Port F. Association of serum phosphorus and calcium x phosphate product with mortality risk in chronic hemodialysis patients: a national study. *Am J Kidney Dis.* 1998;31(4):607-617.

151. O'neill WC. The fallacy of the calcium-phosphorus product. *Kidney Int.* 2007;72(7):792-796.

152. Luoma H, Nuuja T, Collan Y, Nummikoski P. The effect of magnesium and fluoride on nephrocalcinosis and aortic calcification in rats given high sucrose diets with added phosphates. *Calcif Tissue Res.* 1976;20(3):291-302.

153. Larusso J, Li Q, Jiang Q, Uitto J. Elevated dietary magnesium prevents connective tissue mineralization in a mouse model of pseudoxanthoma elasticum (Abcc6(-/-)). *J Investig Dermatol.* 2009;129(6):1388-1394.

154. Gorgels TGMF, Waarsing JH, de Wolf A, ten Brink JB, Loves WJP, Bergen AAB. Dietary magnesium, not calcium, prevents vascular calcification in a mouse model for pseudoxanthoma elasticum. *J Mol Med.* 2010;88(5):467-475.

155. Meyer JL. Can biological calcification occur in the presence of pyrophosphate? *Arch Biochem Biophys.* 1984;231(1):1-8.

156. Okawa A, Nakamura I, Goto S, Moriya H, Nakamura Y, Ikegawa S. Mutation in Npps in a mouse model of ossification of the posterior longitudinal ligament of the spine. *Nat Genet.* 1998;19(3):271-273.

157. Fedde KN, Blair L, Silverstein J, Coburn SP, Ryan LM, Weinstein RS, Waymire K, Narisawa S, Millán JL, MacGregor GR, Whyte MP. Alkaline phosphatase knock-out

mice recapitulate the metabolic and skeletal defects of infantile hypophosphatasia. *J Bone Miner Res.* 1999;14(12):2015-2026.

158. Ho AM, Johnson MD, Kingsley DM. Role of the mouse ank gene in control of tissue calcification and arthritis. *Science.* 2000;289(5477):265-270.

159. Tesch W, Vandenbos T, Roschgr P, Fratzl-Zelman N, Klaushofer K, Beertsen W, Fratzl P. Orientation of mineral crystallites and mineral density during skeletal development in mice deficient in tissue nonspecific alkaline phosphatase. *J Bone Miner Res.* 2003;18(1):117-125.

160. Luo G, Ducy P, McKee MD, Pinero GJ, Loyer E, Behringer RR, Karsenty G. Spontaneous calcification of arteries and cartilage in mice lacking matrix GLA protein. *Nature.* 1997;386(6620):78-81.

161. Hunter GK, Kyle CL, Goldberg HA. Modulation of crystal formation by bone phosphoproteins: structural specificity of the osteopontin-mediated inhibition of hydroxyapatite formation. *Biochem J.* 1994;300 (Pt 3):723-728.

162. Gravallese EM. Osteopontin: a bridge between bone and the immune system. *J Clin Invest.* 2003;112(2):147-149.

163. Weber G, Cantor H. The immunology of Eta-1/osteopontin. *Cytokine Growth Factor Rev.* 1996;7(3):241-248.

164. Boskey A, Maresca M, Ullrich W, Doty S, Butler W, Prince C. Osteopontin-hydroxyapatite interactions in vitro: inhibition of hydroxyapatite formation and growth in a gelatin-gel. *Bone Miner.* 1993;22(2):147-159.

165. Speer MY, McKee MD, Guldberg RE, Liaw L, Yang H-Y, Tung E, Karsenty G, Giachelli CM. Inactivation of the osteopontin gene enhances vascular calcification of matrix Gla protein-deficient mice: evidence for osteopontin as an inducible inhibitor of vascular calcification in vivo. *J Exp Med.* 2002;196(8):1047-1055.

166. Rittling SR, Denhardt DT. Osteopontin function in pathology: lessons from osteopontin-deficient mice. *Exp Nephrol.* 1999;7(2):103-113.

167. Mohler ER, Adam LP, McClelland P, Graham L, Hathaway DR. Detection of osteopontin in calcified human aortic valves. *Arteriosclerosis, Thrombosis, and Vascular Biology.* 1997;17(3):547-552.

168. Steitz SA, Speer MY, McKee MD, Liaw L, Almeida M, Yang H, Giachelli CM. Osteopontin inhibits mineral deposition and promotes regression of ectopic calcification. *Am J Pathol.* 2002;161(6):2035-2046.

169. Pedraza CE, Nikolcheva LG, Kaartinen MT, Barralet JE, McKee MD. Osteopontin functions as an opsonin and facilitates phagocytosis by macrophages of hydroxyapatite-coated microspheres: implications for bone wound healing. *Bone.* 2008;43(4):708-716.

170. Breyne J, Juthier F, Corseaux D, Marechaux S, Zawadzki C, Jeanpierre E, Ung A, Ennezat P-V, Susen S, Van Belle E, Le Marec H, Vincentelli A, Le Tourneau T, Jude B. Atherosclerotic-like process in aortic stenosis: activation of the tissue factor-thrombin pathway and potential role through osteopontin alteration. *Atherosclerosis.* 2010;213(2):369-376.

171. Shao J-S, Sierra OL, Cohen R, Mecham RP, Kovacs A, Wang J, Distelhorst K, Behrmann A, Halstead LR, Towler DA. Vascular Calcification and Aortic Fibrosis: A Bifunctional Role for Osteopontin in Diabetic Arteriosclerosis. *Arteriosclerosis, Thrombosis, and Vascular Biology.* 2011.

172. Hsu JJ, Tintut Y, Demer LL. Murine models of atherosclerotic calcification. *Curr Drug Targets.* 2008;9(3):224-228.

173. Mizobuchi M, Towler D, Slatopolsky E. Vascular calcification: the killer of patients with chronic kidney disease. *J Am Soc Nephrol.* 2009;20(7):1453-1464.

174. New SEP, Aikawa E. Cardiovascular Calcification. *Circulation journal : official journal of the Japanese Circulation Society.* 2011.

175. Mori K, Shioi A, Jono S, Nishizawa Y, Morii H. Dexamethasone enhances In vitro vascular calcification by promoting osteoblastic differentiation of vascular smooth muscle cells. *Arteriosclerosis, Thrombosis, and Vascular Biology.* 1999;19(9):2112-2118.

176. Steitz SA, Speer MY, Curinga G, Yang HY, Haynes P, Aebersold R, Schinke T, Karsenty G, Giachelli CM. Smooth muscle cell phenotypic transition associated with calcification: upregulation of Cbfa1 and downregulation of smooth muscle lineage markers. *Circ Res.* 2001;89(12):1147-1154.

177. Tyson KL, Reynolds JL, McNair R, Zhang Q, Weissberg PL, Shanahan CM. Osteo/chondrocytic transcription factors and their target genes exhibit distinct patterns of expression in human arterial calcification. *Arteriosclerosis, Thrombosis, and Vascular Biology.* 2003;23(3):489-494.

178. Otto F, Thornell AP, Crompton T, Denzel A, Gilmour KC, Rosewell IR, Stamp GW, Beddington RS, Mundlos S, Olsen BR, Selby PB, Owen MJ. Cbfa1, a candidate gene for cleidocranial dysplasia syndrome, is essential for osteoblast differentiation and bone development. *Cell.* 1997;89(5):765-771.

179. Towler DA, Bidder M, Latifi T, Coleman T, Semenkovich CF. Diet-induced diabetes activates an osteogenic gene regulatory program in the aortas of low density lipoprotein receptor-deficient mice. *J Biol Chem.* 1998;273(46):30427-30434.

180. Jono S, McKee MD, Murry CE, Shioi A, Nishizawa Y, Mori K, Morii H, Giachelli CM. Phosphate regulation of vascular smooth muscle cell calcification. *Circ Res.* 2000;87(7):E10-17.

181. Basalyga DM, Simionescu DT, Xiong W, Baxter BT, Starcher BC, Vyavahare NR. Elastin degradation and calcification in an abdominal aorta injury model: role of matrix metalloproteinases. *Circulation.* 2004;110(22):3480-3487.

182. Byon CH, Javed A, Dai Q, Kappes JC, Clemens TL, Darley-Usmar VM, McDonald JM, Chen Y. Oxidative stress induces vascular calcification through modulation of the osteogenic transcription factor Runx2 by AKT signaling. *J Biol Chem.* 2008;283(22):15319-15327.

183. Parhami F, Tintut Y, Ballard A, Fogelman AM, Demer LL. Leptin enhances the calcification of vascular cells: artery wall as a target of leptin. *Circ Res.* 2001;88(9):954-960.

184. Shioi A, Mori K, Jono S, Wakikawa T, Hiura Y, Koyama H, Okuno Y, Nishizawa Y, Morii H. Mechanism of atherosclerotic calcification. *Z Kardiol.* 2000;89 Suppl 2:75-79.

185. Reynolds JL, Joannides AJ, Skepper JN, McNair R, Schurgers LJ, Proudfoot D, Jahnen-Dechent W, Weissberg PL, Shanahan CM. Human vascular smooth muscle cells undergo vesicle-mediated calcification in response to changes in extracellular calcium and phosphate concentrations: a potential mechanism for accelerated vascular calcification in ESRD. *J Am Soc Nephrol.* 2004;15(11):2857-2867.

186. Proudfoot D, Davies JD, Skepper JN, Weissberg PL, Shanahan CM. Acetylated low-density lipoprotein stimulates human vascular smooth muscle cell calcification by promoting osteoblastic differentiation and inhibiting phagocytosis. *Circulation.* 2002;106(24):3044-3050.

187. Proudfoot D, Skepper JN, Hegyi L, Bennett MR, Shanahan CM, Weissberg PL. Apoptosis regulates human vascular calcification in vitro: evidence for initiation of vascular calcification by apoptotic bodies. *Circ Res.* 2000;87(11):1055-1062.

188. Mohler ER, Gannon F, Reynolds C, Zimmerman R, Keane MG, Kaplan FS. Bone formation and inflammation in cardiac valves. *Circulation.* 2001;103(11):1522-1528.

189. Nabors CE, Ball CR. Spontaneous calcification in hearts of DBA mice. *Anat Rec.* 1969;164(2):153-161.

190. Matsushima Y, Imai T, Watanabe O, Kawahara H, Ohne M, Takai H. Spontaneous calcified tongue lesions in DBA mice. *Jikken Dobutsu.* 1984;33(4):539-542.

191. Imaoka K, Honjo K, Doi K, Mitsuoka T. Development of spontaneous tongue calcification and polypoid lesions in DBA/2NCrj mice. *Lab Anim.* 1986;20(1):1-4.

192. Eaton GJ, Custer RP, Johnson FN, Stabenow KT. Dystrophic cardiac calcinosis in mice: genetic, hormonal, and dietary influences. *Am J Pathol.* 1978;90(1):173-186.

193. Ivandic BT, Qiao JH, Machleder D, Liao F, Drake TA, Lusis AJ. A locus on chromosome 7 determines myocardial cell necrosis and calcification (dystrophic cardiac calcinosis) in mice. *Proc Natl Acad Sci USA.* 1996;93(11):5483-5488.

194. van den Broek FA, Bakker R, den Bieman M, Fielmich-Bouwman AX, Lemmens AG, van Lith HA, Nissen I, Ritskes-Hoitinga JM, van Tintelen G, van Zutphen LF. Genetic analysis of dystrophic cardiac calcification in DBA/2 mice. *Biochem Biophys Res Commun.* 1998;253(2):204-208.

195. Brunnert SR, Shi S, Chang B. Chromosomal localization of the loci responsible for dystrophic cardiac calcinosis in DBA/2 mice. *Genomics.* 1999;59(1):105-107.

196. Ivandic BT, Utz HF, Kaczmarek PM, Aherrahrou Z, Axtner SB, Klepsch C, Lusis AJ, Katus HA. New Dyscalc loci for myocardial cell necrosis and calcification (dystrophic cardiac calcinosis) in mice. *Physiological Genomics.* 2001;6(3):137-144.

197. Korff S, Schoensiegel F, Riechert N, Weichenhan D, Katus HA, Ivandic BT. Fine mapping of Dyscalc1, the major genetic determinant of dystrophic cardiac calcification in mice. *Physiological Genomics.* 2006;25(3):387-392.

198. Aherrahrou Z, Doehring LC, Kaczmarek PM, Liptau H, Ehlers E-M, Pomarino A, Wrobel S, Götz A, Mayer B, Erdmann J, Schunkert H. Ultrafine mapping of Dyscalc1 to an 80-kb chromosomal segment on chromosome 7 in mice susceptible for dystrophic calcification. *Physiological Genomics.* 2007;28(2):203-212.

199. Meng H, Vera I, Che N, Wang X, Wang SS, Ingram-Drake L, Schadt EE, Drake TA, Lusis AJ. Identification of Abcc6 as the major causal gene for dystrophic cardiac calcification in mice through integrative genomics. *Proc Natl Acad Sci USA.* 2007;104(11):4530-4535.

200. Aherrahrou Z, Doehring LC, Ehlers E-M, Liptau H, Depping R, Linsel-Nitschke P, Kaczmarek PM, Erdmann J, Schunkert H. An alternative splice variant in Abcc6, the gene causing dystrophic calcification, leads to protein deficiency in C3H/He mice. *J Biol Chem.* 2008;283(12):7608-7615.

201. Gorgels TGMF, Hu X, Scheffer GL, van der Wal AC, Toonstra J, de Jong PTVM, van Kuppevelt TH, Levelt CN, de Wolf A, Loves WJP, Scheper RJ, Peek R, Bergen AAB. Disruption of Abcc6 in the mouse: novel insight in the pathogenesis of pseudoxanthoma elasticum. *Human Molecular Genetics.* 2005;14(13):1763-1773.

202. Klement JF, Matsuzaki Y, Jiang Q-J, Terlizzi J, Choi HY, Fujimoto N, Li K, Pulkkinen L, Birk DE, Sundberg JP, Uitto J. Targeted ablation of the abcc6 gene results in ectopic mineralization of connective tissues. *Mol Cell Biol.* 2005;25(18):8299-8310.

203. Bergen AA, Plomp AS, Schuurman EJ, Terry S, Breuning M, Dauwerse H, Swart J, Kool M, van Soest S, Baas F, ten Brink JB, de Jong PT. Mutations in ABCC6 cause pseudoxanthoma elasticum. *Nat Genet.* 2000;25(2):228-231.

204. Aschoff L. Das reticulo-endotheliale System. *Ergebnisse Innere Medizin Kinderheilkunde.* 1924;26:1.

205. van Furth R, Cohn ZA, Hirsch JG, Humphrey JH, Spector WG, Langevoort HL. The mononuclear phagocyte system: a new classification of macrophages, monocytes, and their precursor cells. *Bull World Health Organ.* 1972;46(6):845-852.

206. Lasser A. The mononuclear phagocytic system: a review. *Hum Pathol.* 1983;14(2):108-126.

207. Gordon S, Keshav S, Chung LP. Mononuclear phagocytes: tissue distribution and functional heterogeneity. *Curr Opin Immunol.* 1988;1(1):26-35.

208. Gordon S, Taylor PR. Monocyte and macrophage heterogeneity. *Nat Rev Immunol.* 2005;5(12):953-964.

209. Taylor PR, Martinez-Pomares L, Stacey M, Lin H-H, Brown GD, Gordon S. Macrophage receptors and immune recognition. *Annu. Rev. Immunol.* 2005;23:901-944.

210. Goldstein JL, Ho YK, Basu SK, Brown MS. Binding site on macrophages that mediates uptake and degradation of acetylated low density lipoprotein, producing massive cholesterol deposition. *Proc Natl Acad Sci USA.* 1979;76(1):333-337.

211. Quinn MT, Parthasarathy S, Fong LG, Steinberg D. Oxidatively modified low density lipoproteins: a potential role in recruitment and retention of monocyte/macrophages during atherogenesis. *Proc Natl Acad Sci USA.* 1987;84(9):2995-2998.

212. Kodama T, Freeman M, Rohrer L, Zabrecky J, Matsudaira P, Krieger M. Type I macrophage scavenger receptor contains alpha-helical and collagen-like coiled coils. *Nature.* 1990;343(6258):531-535.

213. Emi M, Asaoka H, Matsumoto A, Itakura H, Kurihara Y, Wada Y, Kanamori H, Yazaki Y, Takahashi E, Lepert M. Structure, organization, and chromosomal mapping of the human macrophage scavenger receptor gene. *J Biol Chem.* 1993;268(3):2120-2125.

214. Suzuki H, Kurihara Y, Takeya M, Kamada N, Kataoka M, Jishage K, Ueda O, Sakaguchi H, Higashi T, Suzuki T, Takashima Y, Kawabe Y, Cynshi O, Wada Y, Honda M, Kurihara H, Aburatani H, Doi T, Matsumoto A, Azuma S, Noda T, Toyoda Y, Itakura H, Yazaki Y, Kodama T. A role for macrophage scavenger receptors in atherosclerosis and susceptibility to infection. *Nature.* 1997;386(6622):292-296.

215. Areschoug T, Waldemarsson J, Gordon S. Evasion of macrophage scavenger receptor A-mediated recognition by pathogenic streptococci. *Eur J Immunol.* 2008;38(11):3068-3079.

216. Greaves DR, Gordon S. The macrophage scavenger receptor at 30 years of age: current knowledge and future challenges. *J Lipid Res.* 2009;50 Suppl:S282-286.

217. Gordon S. Pattern recognition receptors: doubling up for the innate immune response. *Cell.* 2002;111(7):927-930.

218. Kunjathoor VV, Febbraio M, Podrez EA, Moore KJ, Andersson L, Koehn S, Rhee JS, Silverstein R, Hoff HF, Freeman MW. Scavenger receptors class A-I/II and CD36 are the principal receptors responsible for the uptake of modified low density lipoprotein leading to lipid loading in macrophages. *J Biol Chem.* 2002;277(51):49982-49988.

219. Kuchibhotla S, Vanegas D, Kennedy DJ, Guy E, Nimako G, Morton RE, Febbraio M. Absence of CD36 protects against atherosclerosis in ApoE knock-out mice with no additional protection provided by absence of scavenger receptor A I/II. *Cardiovasc Res.* 2008;78(1):185-196.

220. Kanke M, Simmons GH, Weiss DL, Bivins BA, DeLuca PP. Clearance of 141C3-labeled microspheres from blood and distribution in specific organs following intravenous and intraarterial administration in beagle dogs. *J Pharm Sci.* 1980;69(7):755-762.

221. Dunn SE, Brindley A, Davis SS, Davies MC, Illum L. Polystyrene-poly (ethylene glycol) (PS-PEG2000) particles as model systems for site specific drug delivery. 2. The effect of PEG surface density on the in vitro cell interaction and in vivo biodistribution. *Pharm Res.* 1994;11(7):1016-1022.

222. Ogawara K, Yoshida M, Higaki K, Kimura T, Shiraishi K, Nishikawa M, Takakura Y, Hashida M. Hepatic uptake of polystyrene microspheres in rats: effect of particle size on intrahepatic distribution. *J Control Release.* 1999;59(1):15-22.

223. Moghimi SM, Porter CJ, Muir IS, Illum L, Davis SS. Non-phagocytic uptake of intravenously injected microspheres in rat spleen: influence of particle size and hydrophilic coating. *Biochem Biophys Res Commun.* 1991;177(2):861-866.

224. Beningo KA, Wang Y-l. Fc-receptor-mediated phagocytosis is regulated by mechanical properties of the target. *J Cell Sci.* 2002;115(Pt 4):849-856.

225. Champion JA, Mitragotri S. Role of target geometry in phagocytosis. *Proc Natl Acad Sci USA.* 2006;103(13):4930-4934.

226. Bharadwaj D, Mold C, Markham E, Du Clos TW. Serum amyloid P component binds to Fc gamma receptors and opsonizes particles for phagocytosis. *J Immunol.* 2001;166(11):6735-6741.

227. Mold C, Gresham HD, Du Clos TW. Serum amyloid P component and C-reactive protein mediate phagocytosis through murine Fc gamma Rs. *J Immunol.* 2001;166(2):1200-1205.

228. Hamilton RF, Thakur SA, Mayfair JK, Holian A. MARCO mediates silica uptake and toxicity in alveolar macrophages from C57BL/6 mice. *J Biol Chem.* 2006;281(45):34218-34226.

229. McCarty DJ, Gatter RA. Recurrent acute inflammation associated with focal apatite crystal deposition. *Arthritis Rheum.* 1966;9(6):804-819.

230. Maurer KH, Schumacher HR. Hydroxyapatite phagocytosis by human polymorphonuclear leucocytes. *Annals of the Rheumatic Diseases.* 1979;38(1):84-88.

231. Denko CW, Petricevic M. Hydroxyapatite crystal-induced inflammation and prostaglandin E1. *J Rheumatol.* 1979;6(2):117-123.

232. Kandori K, Miyagawa K, Ishikawa T. Adsorption of immunogamma globulin onto various synthetic calcium hydroxyapatite particles. *J Colloid Interface Sci.* 2004;273(2):406-413.

233. Nadra I, Mason JC, Philippidis P, Florey O, Smythe CDW, McCarthy GM, Landis RC, Haskard DO. Proinflammatory activation of macrophages by basic calcium phosphate crystals via protein kinase C and MAP kinase pathways: a vicious cycle of inflammation and arterial calcification? *Circ Res.* 2005;96(12):1248-1256.

234. Grandjean-Laquerriere A, Tabary O, Jacquot J, Richard D, Frayssinet P, Guenounou M, Laurent-Maquin D, Laquerriere P, Gangloff S. Involvement of toll-like receptor 4 in the inflammatory reaction induced by hydroxyapatite particles. *Biomaterials.* 2007;28(3):400-404.

235. Fellah BH, Josselin N, Chappard D, Weiss P, Layrolle P. Inflammatory reaction in rats muscle after implantation of biphasic calcium phosphate micro particles. *J Mater Sci Mater Med.* 2007;18(2):287-294.

236. Nadra I, Boccaccini AR, Philippidis P, Whelan LC, McCarthy GM, Haskard DO, Landis RC. Effect of particle size on hydroxyapatite crystal-induced tumor necrosis factor alpha secretion by macrophages. *Atherosclerosis.* 2008;196(1):98-105.

237. Pazár B, Ea H-K, Narayan S, Kolly L, Bagnoud N, Chobaz V, Roger T, Lioté F, So A, Busso N. Basic Calcium Phosphate Crystals Induce Monocyte/Macrophage IL-1{beta} Secretion through the NLRP3 Inflammasome In Vitro. *The Journal of Immunology.* 2011;186(4):2495-2502.

238. In vivo imaging of calcified lesions. Patent. WO002012022486A1

239. Gentleman RC, Carey VJ, Bates DM, Bolstad B, Dettling M, Dudoit S, Ellis B, Gautier L, Ge Y, Gentry J, Hornik K, Hothorn T, Huber W, Iacus S, Irizarry R, Leisch F, Li C, Maechler M, Rossini AJ, Sawitzki G, Smith C, Smyth G, Tierney L, Yang JYH, Zhang J. Bioconductor: open software development for computational biology and bioinformatics. *Genome Biol.* 2004;5(10):R80.

240. Gautier L, Cope L, Bolstad BM, Irizarry RA. affy--analysis of Affymetrix GeneChip data at the probe level. *Bioinformatics.* 2004;20(3):307-315.

241. Kauffmann A, Gentleman R, Huber W. arrayQualityMetrics--a bioconductor package for quality assessment of microarray data. *Bioinformatics.* 2009;25(3):415-416.

242. Gentleman R, Carey V, Huber W, Hahne F. Genefilter: methods for filtering genes from microarray experiments. *R package version 1.24.2.*

243. Pollard K, Gilbert H, Ge Y, Taylor S, Dudoit S. Multtest: Resampling-based multiple hypothesis testing. *R package version 2.1.1.* 2009.

244. Smith C. Annaffy: Annotation tools for Affymetrix biological metadata. *R package version 1.16.0.* 2008.

245. Gentleman R. Annotate: Annotation for microarrays. *R package version 1.22.0.*

246. Carlson M, Falcon S, Pages H, Li N. Mouse4302.db: Affymetrix Mouse Genome 430 2.0 Array annotation data (chip mouse4302). *R package version 2.2.11.*

247. Morgan M, Falcon S, Gentleman R. GSEABase: Gene set enrichment data structures and methods. *R package version 1.6.1.*

248. Laemmli UK. Cleavage of structural proteins during the assembly of the head of bacteriophage T4. *Nature.* 1970;227(5259):680-685.

249. Perkins DN, Pappin DJ, Creasy DM, Cottrell JS. Probability-based protein identification by searching sequence databases using mass spectrometry data. *Electrophoresis.* 1999;20(18):3551-3567.

250. Ishihama Y, Oda Y, Tabata T, Sato T, Nagasu T, Rappsilber J, Mann M. Exponentially modified protein abundance index (emPAI) for estimation of absolute protein amount in proteomics by the number of sequenced peptides per protein. *Mol Cell Proteomics.* 2005;4(9):1265-1272.

251. Rasband W. ImageJ. *U. S. National Institutes of Health, Bethesda, Maryland, USA*.http://rsb.info.nih.gov/ij/:1997-2009.

252. Frey B, Schildkopf P, Rödel F, Weiss E-M, Munoz LE, Herrmann M, Fietkau R, Gaipl US. AnnexinA5 renders dead tumor cells immunogenic--implications for multimodal cancer therapies. *J Immunotoxicol.* 2009;6(4):209-216.

253. Grewal T, Heeren J, Mewawala D, Schnitgerhans T, Wendt D, Salomon G, Enrich C, Beisiegel U, Jäckle S. Annexin VI stimulates endocytosis and is involved in the trafficking of low density lipoprotein to the prelysosomal compartment. *J Biol Chem.* 2000;275(43):33806-33813.

254. Drummond RA, Saijo S, Iwakura Y, Brown GD. The role of Syk/CARD9 coupled C-type lectins in antifungal immunity. *Eur J Immunol.* 2011;41(2):276-281.

255. Barrionuevo P, Beigier-Bompadre M, Ilarregui JM, Toscano MA, Bianco GA, Isturiz MA, Rabinovich GA. A novel function for galectin-1 at the crossroad of innate and adaptive immunity: galectin-1 regulates monocyte/macrophage physiology through a nonapoptotic ERK-dependent pathway. *J Immunol.* 2007;178(1):436-445.

256. Karlsson A, Christenson K, Matlak M, Björstad A, Brown KL, Telemo E, Salomonsson E, Leffler H, Bylund J. Galectin-3 functions as an opsonin and enhances the macrophage clearance of apoptotic neutrophils. *Glycobiology.* 2009;19(1):16-20.

257. Kinkeldey A, Gremse F, Herrmann M, Schaefer C, Kiessling F, Jahnen-Dechent W. Fetuin-A based in vivo imaging of calcified lesions. *Bone.* 2011;48:S236-S236.

258. Jahnen-Dechent W, Schäfer C, Ketteler M, McKee MD. Mineral chaperones: a role for fetuin-A and osteopontin in the inhibition and regression of pathologic calcification. *J Mol Med.* 2008;86(4):379-389.

259. Hull D. The structure and function of brown adipose tissue. *Br Med Bull.* 1966;22(1):92-96.

260. De Heller-Milev M, Huber M, Panizzon R, Hohl D. Expression of small proline rich proteins in neoplastic and inflammatory skin diseases. *Br J Dermatol.* 2000;143(4):733-740.

261. Zimmermann N, Doepker MP, Witte DP, Stringer KF, Fulkerson PC, Pope SM, Brandt EB, Mishra A, King NE, Nikolaidis NM, Wills-Karp M, Finkelman FD, Rothenberg ME. Expression and regulation of small proline-rich protein 2 in allergic inflammation. *Am J Respir Cell Mol Biol.* 2005;32(5):428-435.

262. Zheng L, Zhou Z, Lin L, Alber S, Watkins S, Kaminski N, Choi AMK, Morse D. Carbon monoxide modulates alpha-smooth muscle actin and small proline rich-1a expression in fibrosis. *American Journal of Respiratory Cell and Molecular Biology.* 2009;41(1):85-92.

263. Pradervand S, Yasukawa H, Muller OG, Kjekshus H, Nakamura T, St Amand TR, Yajima T, Matsumura K, Duplain H, Iwatate M, Woodard S, Pedrazzini T, Ross J, Firsov D, Rossier BC, Hoshijima M, Chien KR. Small proline-rich protein 1A is a gp130 pathway- and stress-inducible cardioprotective protein. *EMBO J.* 2004;23(22):4517-4525.

264. Herrmann M. Pathologie der ektopischen Kalzifizierung in Fetuin-A Defizienten Mäusen. 2007.

265. Shanahan CM, Cary NR, Metcalfe JC, Weissberg PL. High expression of genes for calcification-regulating proteins in human atherosclerotic plaques. *J Clin Invest.* 1994;93(6):2393-2402.

266. Paulsen IT, Skurray RA. The POT family of transport proteins. *Trends Biochem Sci.* 1994;19(10):404.

267. Liu W, Liang R, Ramamoorthy S, Fei YJ, Ganapathy ME, Hediger MA, Ganapathy V, Leibach FH. Molecular cloning of PEPT 2, a new member of the H+/peptide cotransporter family, from human kidney. *Biochim Biophys Acta.* 1995;1235(2):461-466.

268. Rubio-Aliaga I, Boll M, Daniel H. Cloning and characterization of the gene encoding the mouse peptide transporter PEPT2. *Biochem Biophys Res Commun.* 2000;276(2):734-741.

269. Denecke B, Gräber S, Schäfer C, Heiss A, Wöltje M, Jahnen-Dechent W. Tissue distribution and activity testing suggest a similar but not identical function of fetuin-B and fetuin-A. *Biochem J.* 2003;376(Pt 1):135-145.

270. Flo TH, Smith KD, Sato S, Rodriguez DJ, Holmes MA, Strong RK, Akira S, Aderem A. Lipocalin 2 mediates an innate immune response to bacterial infection by sequestrating iron. *Nature.* 2004;432(7019):917-921.

271. Kushner I. The phenomenon of the acute phase response. *Ann N Y Acad Sci.* 1982;389:39-48.

272. Baranova IN, Bocharov AV, Vishnyakova TG, Kurlander R, Chen Z, Fu D, Arias IM, Csako G, Patterson AP, Eggerman TL. CD36 is a novel serum amyloid A (SAA) receptor mediating SAA binding and SAA-induced signaling in human and rodent cells. *J Biol Chem.* 2010;285(11):8492-8506.

273. Tolleshaug H. Binding and internalization of asialo-glycoproteins by isolated rat hepatocytes. *Int J Biochem.* 1981;13(1):45-51.

274. Drevon CA, Tolleshaug H, Carlander B, Berg T. Metabolism of asialoglycoproteins in cultured rat hepatocytes: evidence for receptor mediated uptake and degradation which is not feed-back regulated. *Int J Biochem.* 1983;15(6):827-833.

275. Peters T. Serum albumin. *Adv Protein Chem.* 1985;37:161-245.

276. Martinez-Pomares L, Platt N, McKnight AJ, da Silva RP, Gordon S. Macrophage membrane molecules: markers of tissue differentiation and heterogeneity. *Immunobiology.* 1996;195(4-5):407-416.

277. Kraal G, Mebius R. New insights into the cell biology of the marginal zone of the spleen. *Int Rev Cytol.* 2006;250:175-215.

278. Mócsai A, Ruland J, Tybulewicz VLJ. The SYK tyrosine kinase: a crucial player in diverse biological functions. *Nat Rev Immunol.* 2010;10(6):387-402.

279. Oliver JM, Burg DL, Wilson BS, McLaughlin JL, Geahlen RL. Inhibition of mast cell Fc epsilon R1-mediated signaling and effector function by the Syk-selective inhibitor, piceatannol. *J Biol Chem.* 1994;269(47):29697-29703.

280. Kiefer F, Brumell J, Al-Alawi N, Latour S, Cheng A, Veillette A, Grinstein S, Pawson T. The Syk protein tyrosine kinase is essential for Fcgamma receptor signaling in macrophages and neutrophils. *Mol Cell Biol.* 1998;18(7):4209-4220.

281. Majeed M, Caveggion E, Lowell CA, Berton G. Role of Src kinases and Syk in Fcgamma receptor-mediated phagocytosis and phagosome-lysosome fusion. *Journal of Leukocyte Biology.* 2001;70(5):801-811.

282. Law DA, Nannizzi-Alaimo L, Ministri K, Hughes PE, Forsyth J, Turner M, Shattil SJ, Ginsberg MH, Tybulewicz VL, Phillips DR. Genetic and pharmacological analyses of Syk function in alphaIIbbeta3 signaling in platelets. *Blood.* 1999;93(8):2645-2652.

283. Nimmerjahn F, Ravetch J. Fcgamma receptors as regulators of immune responses. *Nat Rev Immunol.* 2008;8(1):34-47.

284. Silverstein R, Febbraio M. CD36, a scavenger receptor involved in immunity, metabolism, angiogenesis, and behavior. *Science signaling.* 2009;2(72):re3.

285. Kundranda M, Ray S, Saria M, Friedman D, Matrisian L, Lukyanov P, Ochieng J. Annexins expressed on the cell surface serve as receptors for adhesion to immobilized fetuin-A. *Biochim Biophys Acta.* 2004;1693(2):111-123.

286. Leffler H, Carlsson S, Hedlund M, Qian Y, Poirier F. Introduction to galectins. *Glycoconj J.* 2004;19(7-9):433-440.

287. Liu F-T, Rabinovich GA. Galectins: regulators of acute and chronic inflammation. *Ann N Y Acad Sci.* 2010;1183:158-182.

288. Li Y, Komai-Koma M, Gilchrist DS, Hsu DK, Liu F-T, Springall T, Xu D. Galectin-3 is a negative regulator of lipopolysaccharide-mediated inflammation. *J Immunol.* 2008;181(4):2781-2789.

289. Green CB, Takahashi JS. Xenobiotic metabolism in the fourth dimension: PARtners in time. *Cell Metabolism.* 2006;4(1):3-4.

290. St-Arnaud R, Arabian A, Travers R, Barletta F, Raval-Pandya M, Chapin K, Depovere J, Mathieu C, Christakos S, Demay MB, Glorieux FH. Deficient mineralization of intramembranous bone in vitamin D-24-hydroxylase-ablated mice is due to elevated 1,25-dihydroxyvitamin D and not to the absence of 24,25-dihydroxyvitamin D. *Endocrinology.* 2000;141(7):2658-2666.

291. Vergnes L, Phan J, Stolz A, Reue K. A cluster of eight hydroxysteroid dehydrogenase genes belonging to the aldo-keto reductase supergene family on mouse chromosome 13. *J Lipid Res.* 2003;44(3):503-511.

292. Zaidi N, Hermann C, Herrmann T, Kalbacher H. Emerging functional roles of cathepsin E. *Biochem Biophys Res Commun.* 2008;377(2):327-330.

293. Lee C, Weaver DR, Reppert SM. Direct association between mouse PERIOD and CKIepsilon is critical for a functioning circadian clock. *Mol Cell Biol.* 2004;24(2):584-594.

294. Hayasaka N, Aoki K, Kinoshita S, Yamaguchi S, Wakefield JK, Tsuji-Kawahara S, Horikawa K, Ikegami H, Wakana S, Murakami T, Ramabhadran R, Miyazawa M, Shibata S. Attenuated food anticipatory activity and abnormal circadian locomotor rhythms in Rgs16 knockdown mice. *PLoS ONE.* 2011;6(3):e17655.

295. Maeda N, Doi K, Mitsuoka T. Development of heart and aortic lesions in DBA/2NCrj mice. *Lab Anim.* 1986;20(1):5-8.

296. Van Vleet JF, Ferrans VJ. Ultrastructural changes in inherited cardiac calcinosis of DBA/2 mice. *Am J Vet Res.* 1987;48(2):255-261.

297. Itagaki S, Maeda N, Doi K, Mitsuoka T. Ultrastructure of spontaneous cardiac calcification in DBA/2NCrj mice. *Vet Pathol.* 1988;25(5):393-395.

298. Yamate J, Tajima M, Maruyama Y, Kudow S. Observations on soft tissue calcification in DBA/2NCrj mice in comparison with CRJ:CD-1 mice. *Lab Anim.* 1987;21(4):289-298.

299. Ryall R. The future of stone research: rummagings in the attic, Randall's plaque, nanobacteria, and lessons from phylogeny. *Urol Res.* 2008;36(2):77-97.

300. Ghadially FN. As you like it, Part 3: A critique and historical review of calcification as seen with the electron microscope. *Ultrastruct Pathol.* 2001;25(3):243-267.

301. Herrmann M, Schaefer C, Kinkeldey A, Jahnen-Dechent W. Ectopic calcification in fetuin-A deficient mice starts in the microvasculature. *Bone.* 2011;48:S241-S241.

302. Fitzpatrick LA, Severson A, Edwards WD, Ingram RT. Diffuse calcification in human coronary arteries. Association of osteopontin with atherosclerosis. *J Clin Invest.* 1994;94(4):1597-1604.

303. Scatena M, Liaw L, Giachelli CM. Osteopontin: A Multifunctional Molecule Regulating Chronic Inflammation and Vascular Disease. *Arteriosclerosis, Thrombosis, and Vascular Biology.* 2007;27(11):2302-2309.

304. Dean RA, Cox JH, Bellac CL, Doucet A, Starr AE, Overall CM. Macrophage-specific metalloelastase (MMP-12) truncates and inactivates ELR+ CXC chemokines and generates CCL2, -7, -8, and -13 antagonists: potential role of the macrophage in terminating polymorphonuclear leukocyte influx. *Blood.* 2008;112(8):3455-3464.

305. Kim KM. Calcification of matrix vesicles in human aortic valve and aortic media. *Fed Proc.* 1976;35(2):156-162.

306. Tanimura A, McGregor DH, Anderson HC. Calcification in atherosclerosis. I. Human studies. *J Exp Pathol.* 1986;2(4):261-273.

307. Kockx MM, Muhring J, Bortier H, De Meyer GR, Jacob W. Biotin- or digoxigenin-conjugated nucleotides bind to matrix vesicles in atherosclerotic plaques. *Am J Pathol.* 1996;148(6):1771-1777.

308. Boström K, Watson KE, Stanford WP, Demer LL. Atherosclerotic calcification: relation to developmental osteogenesis. *Am J Cardiol.* 1995;75(6):88B-91B.

309. Kaden JJ, Bickelhaupt S, Grobholz R, Haase KK, Sarikoç A, Kiliç R, Brueckmann M, Lang S, Zahn I, Vahl C, Hagl S, Dempfle CE, Borggrefe M. Receptor activator of nuclear factor kappaB ligand and osteoprotegerin regulate aortic valve calcification. *J Mol Cell Cardiol.* 2004;36(1):57-66.

310. Anger T, Carson W, Weyand M, Daniel WG, Hoeher M, Garlichs CD. Atherosclerotic inflammation triggers osteogenic bone transformation in calcified and stenotic human aortic valves: still a matter of debate. *Exp Mol Pathol.* 2009;86(1):10-17.

311. Villa-Bellosta R, Millan A, Sorribas V. Role of calcium-phosphate deposition in vascular smooth muscle cell calcification. *Am J Physiol, Cell Physiol.* 2011;300(1):C210-220.

312. Alves RDAM, Koedam M, van de Peppel J, Eijken M, van Leeuwen JPTM. Gene expression analysis of osteoblasts and calcifying vascular cells: Similar cell types or similar mechanisms? *Bone.* 2011;48:S119-S119.

313. Heiss A, Pipich V, Jahnen-Dechent W, Schwahn D. Fetuin-A Is a Mineral Carrier Protein: Small Angle Neutron Scattering Provides New Insight on Fetuin-A Controlled Calcification Inhibition. *Biophys J.* 2010;99(12):3986-3995.

314. Coetzee GA, Strachan AF, van der Westhuyzen DR, Hoppe HC, Jeenah MS, de Beer FC. Serum amyloid A-containing human high density lipoprotein 3. Density, size, and apolipoprotein composition. *J Biol Chem.* 1986;261(21):9644-9651.

315. Pavlidis P, Li Q, Noble WS. The effect of replication on gene expression microarray experiments. *Bioinformatics.* 2003;19(13):1620-1627.

316. Wu C-Y, Martel J, Young D, Young JD. Fetuin-A/albumin-mineral complexes resembling serum calcium granules and putative nanobacteria: demonstration of a dual inhibition-seeding concept. *PLoS ONE.* 2009;4(11):e8058.

317. Yuste J, Botto M, Bottoms SE, Brown JS. Serum amyloid P aids complement-mediated immunity to Streptococcus pneumoniae. *PLoS Pathog.* 2007;3(9):1208-1219.

318. Li X, Hatanaka K, Ishibashi-Ueda H, Yutani C, Yamamoto A. Characterization of serum amyloid P component from human aortic atherosclerotic lesions. *Arterioscler Thromb Vasc Biol.* 1995;15(2):252-257.

319. Song Z, Cai L, Guo L, Tsukamoto Y, Yutani C, Li X-A. Accumulation and expression of serum amyloid P component in human atherosclerotic lesions. *Atherosclerosis.* 2010;211(1):90-95.

320. Hall GE, Kenny AD. Role of carbonic anhydrase in bone resorption: effect of acetazolamide on basal and parathyroid hormone-induced bone metabolism. *Calcif Tissue Int.* 1987;40(4):212-218.

321. Whyte MP. Carbonic anhydrase II deficiency. *Clin Orthop Relat Res.* 1993(294):52-63.

322. Kim G, Lee T-H, Wetzel P, Geers C, Robinson MA, Myers TG, Owens JW, Wehr NB, Eckhaus MW, Gros G, Wynshaw-Boris A, Levine RL. Carbonic anhydrase III is not required in the mouse for normal growth, development, and life span. *Mol Cell Biol.* 2004;24(22):9942-9947.

323. Spiess M. The asialoglycoprotein receptor: a model for endocytic transport receptors. *Biochemistry.* 1990;29:10009-10018.

324. Tolleshaug H, Berg T. Uptake and degradation of asialo-fetuin by isolated rat hepatocytes. *Acta Biol Med Ger.* 1977;36(11-12):1753-1762.

325. Henson P, Hume D. Apoptotic cell removal in development and tissue homeostasis. *Trends Immunol.* 2006;27(5):244-250.

326. De Jong W, Hagens W, Krystek P, Burger M, Sips A, Geertsma R. Particle size-dependent organ distribution of gold nanoparticles after intravenous administration. *Biomaterials.* 2008;29(12):1912-1919.

327. Tanaka T, Decuzzi P, Cristofanilli M, Sakamoto J, Tasciotti E, Robertson F, Ferrari M. Nanotechnology for breast cancer therapy. *Biomed Microdevices.* 2009;11(1):49-63.

328. Jansen RW, Molema G, Harms G, Kruijt JK, van Berkel TJ, Hardonk MJ, Meijer DK. Formaldehyde treated albumin contains monomeric and polymeric forms that are differently cleared by endothelial and Kupffer cells of the liver: evidence for scavenger receptor heterogeneity. *Biochem Biophys Res Commun.* 1991;180(1):23-32.

329. Hughes D, Fraser I, Gordon S. Murine macrophage scavenger receptor: in vivo expression and function as receptor for macrophage adhesion in lymphoid and non-lymphoid organs. *Eur J Immunol.* 1995;25(2):466-473.

330. Blomhoff R, Eskild W, Berg T. Endocytosis of formaldehyde-treated serum albumin via scavenger pathway in liver endothelial cells. *Biochem J.* 1984;218(1):81-86.

331. Mebius RE, Kraal G. Structure and function of the spleen. *Nat Rev Immunol.* 2005;5(8):606-616.

332. Elliott M, Ravichandran K. Clearance of apoptotic cells: implications in health and disease. *J Cell Biol.* 2010;189(7):1059-1070.

333. John T, Vogel S, Tiruppathi C, Malik A, Minshall R. Quantitative analysis of albumin uptake and transport in the rat microvessel endothelial monolayer. *Am J Physiol Lung Cell Mol Physiol.* 2003;284(1):L187-196.

334. Neyen C, Plüddemann A, Roversi P, Thomas B, Cai L, Van Der Westhuyzen DR, Sim RB, Gordon S. Macrophage scavenger receptor A mediates adhesion to apolipoproteins A-I and E. *Biochemistry.* 2009;48(50):11858-11871.

335. Kraal G, van der Laan LJ, Elomaa O, Tryggvason K. The macrophage receptor MARCO. *Microbes Infect.* 2000;2(3):313-316.

336. Mortensen RF, Osmand AP, Lint TF, Gewurz H. Interaction of C-reactive protein with lymphocytes and monocytes: complement-dependent adherence and phagocytosis. *J Immunol.* 1976;117(3):774-781.

337. Bharadwaj D, Stein MP, Volzer M, Mold C, Du Clos TW. The major receptor for C-reactive protein on leukocytes is fcgamma receptor II. *J Exp Med.* 1999;190(4):585-590.

338. Stein MP, Mold C, Du Clos TW. C-reactive protein binding to murine leukocytes requires Fc gamma receptors. *J Immunol.* 2000;164(3):1514-1520.

339. Goodridge HS, Shimada T, Wolf AJ, Hsu Y-MS, Becker CA, Lin X, Underhill DM. Differential use of CARD9 by dectin-1 in macrophages and dendritic cells. *J Immunol.* 2009;182(2):1146-1154.

340. Lin J-S, Huang J-H, Hung L-Y, Wu S-Y, Wu-Hsieh BA. Distinct roles of complement receptor 3, Dectin-1, and sialic acids in murine macrophage interaction with Histoplasma yeast. *Journal of Leukocyte Biology.* 2010;88(1):95-106.

341. Keeley FW, Sitarz EE. Identification and quantitation of alpha 2-HS-glycoprotein in the mineralized matrix of calcified plaques of atherosclerotic human aorta. *Atherosclerosis.* 1985;55(1):63-69.

342. Moe S, Neal C, O'Neill K, Brown K, Westenfeld R, Jahnen-Dechent W, Ketteler M. Fetuin-A and matrix gla protein (MGP) arc important inhibitors of vascular calcification in CKD. *J Am Soc Nephrol.* 2003;14:692A-692A.

343. Emoto M, Mori K, Lee E, Kawano N, Yamazaki Y, Tsuchikura S, Morioka T, Koyama H, Shoji T, Inaba M, Nishizawa Y. Fetuin-A and atherosclerotic calcified plaque in patients with type 2 diabetes mellitus. *Metabolism.* 2010;59(6):873-878.

344. Block GA, Raggi P, Bellasi A, Kooienga L, Spiegel DM. Mortality effect of coronary calcification and phosphate binder choice in incident hemodialysis patients. *Kidney Int.* 2007;71(5):438-441.

345. Colinayo VV, Qiao J-H, Demant P, Krass K, Lusis AJ, Drake TA. Genetic characterization of the Dyscalc locus. *Mamm Genome.* 2002;13(6):283-288.

346. Korff S, Riechert N, Schoensiegel F, Weichenhan D, Autschbach F, Katus HA, Ivandic BT. Calcification of myocardial necrosis is common in mice. *Virchows Arch.* 2006;448(5):630-638.

347. Daugherty A, Whitman SC, Block AE, Rateri DL. Polymorphism of class A scavenger receptors in C57BL/6 mice. *J Lipid Res.* 2000;41(10):1568-1577.

348. Yan D, Willett TL, Gu X, Martinez-Mier EA, Sardone L, McShane L, Grynpas M, Everett ET. Phenotypic Variation of Fluoride Responses between Inbred Strains of Mice. *Cells, tissues, organs.* 2011.

349. Fadini GP, Albiero M, Menegazzo L, Boscaro E, Vigili de Kreutzenberg S, Agostini C, Cabrelle A, Binotto G, Rattazzi M, Bertacco E, Bertorelle R, Biasini L, Mion M, Plebani M, Ceolotto G, Angelini A, Castellani C, Menegolo M, Grego F, Dimmeler S, Seeger F, Zeiher A, Tiengo A, Avogaro A. Widespread increase in myeloid calcifying cells contributes to ectopic vascular calcification in type 2 diabetes. *Circ Res.* 2011;108(9):1112-1121.

350. Spiro RG. Studies on fetuin, a glycoprotein of fetal serum. I. Isolation, chemical composition, and physiochemical properties. *J Biol Chem.* 1960;235(10):2860-2869.

351. Murray AC, Oikawa K, Kay CM. Circular dichroism studies on native fetuin and some of its derivatives. *Biochim Biophys Acta.* 1969;175(2):331-338.

Abbreviations

24-OHase	25-hydroxyvitamin D-24-hydroxylase
Abbc6	ATP-binding cassette sub-family C member 6
Ace2	angiotensin 1 converting enzyme 2
acLDL	acetylated low density lipoprotein
Ahsg	α_2-Heremans-Schmid-glycoprotein
ApoA1	apolipoprotein A1
ApoE	apolipoprotein E
AsF	asialofetuin
ASGP-R	asialoglycoprotein receptor
B6	C57BL/6N mouse strain
B6D2	offspring (F1) of C57BL/6N x DBA/2N matings
BAT	brown adipose tissue
bp	base pairs
BCP	basic calcium phosphate
BMM	bone marrow derived macrophage
BMP	bone morphogenic protein
BSA	bovine serum albumin
C9	complement component 9
Ca3	carbonic anhydrase 3
Cbfa1	core-binding factor subunit alpha-1
CDS	coding sequences
CKD	chronic kidney disease
cM	centi Morgan
CPP	calciprotein particle
CR	complement receptor
CTDL	C-type lectin carbohydrate-binding domain
CUA	calcific uremic arteriolopathy
Cyp24a1	cytochrome P450, family 24, subfamily a, polypeptide 1
D	domain
D2	DBA/2N mouse strain
Dbp	D site albumin promoter binding protein
DC	dendritic cells
Dpp4	dipeptidyltransferase 4
EDTA	ethylenediaminetetraacetic acid
EMP-3	epithelial membrane protein 3

ESRD	end-stage renal disease
FBS	fetal bovine serum
FcγR	Fcγ receptor
FETUB	fetuin-B
FGF-23	fibroblast growth factor 23
Gapdh	Glycerinaldehyd-3-phosphat-dehydrogenase
Glt25d2	glycosyltransferase 25 domain containing 2
Gpi	glycosylphosphatidylinositol
HAP	hydroxyapatite
HL	hepatic lectin
Hrc	histidine rich calcium binding protein
HRG	histidine rich gycoprotein
IgG	immunoglobulin G
Il-1β	interleukin-1beta
i.v.	*intravenous*
Kb	kilo bases
KEGG	Kyoto encyclopedia of genes and genomes
KNG	kininogen
KO	knockout
LAMP	lysosomal-associated membrane protein
LCM	L929 cell conditioned medium
LDL	low density lipoprotein
log10p	logarithm to base 10
LOX-1	lectin-like oxidized low density lipoprotein receptor 1
LPS	lipopolysaccharide
Mal	myelin and lymphocyte protein, T-cell differentiation protein
MARCO	macrophage receptor with collagenous structure
Mbp	mega base pairs
M-CSF	macrophage colony-stimulating factor
MetS	metabolic syndrome
MGP	matrix gla protein
MMM	marginal metallophilic macrophages
Mmp12	macrophage-specific metalloelastase 12
MOMA-1	antibody recognizing marginal metallophilic macrophages in the mouse spleen
MPS	mononuclear phagocyte system
MS	mass spectrometry

MZ	marginal zone
MZM	marginal zone macrophage
NCBI	national center for biotechnology information
NFκB	nuclear factor kappa-light-chain-enhancer of activated B cells
NK	natural killer
ns	not significant
OPN	osteopontin
PAMP	pathogen-associated molecular pattern
PBMC	peripheral blood mononuclear cell
PBS	phosphate buffered saline
PCR	polymerase chain reaction
Per3	period homolog 3
PEPT2	peptide transporter 2
PI3K	phosphoinositole-3-kinase
Poly-I	polyinosinic acid
POT	proton oligopetide transporter
PP	pyrophosphat
pp63	phosphorylated N-glycoprotein
PRR	pattern recognition receptor
PTH	parathyroid hormone
PXE	pseudoxanthoma elasticum
QTL	quantitative trait locus
RES	reticuloendothelial system
RP	red pulp
Runx2	runt-related transcription factor 2
SAP	serum-amyloid P
SDS	sodium dodecyl sulfate
SDS-PAGE	SDS polyacrylamid gel electrophoresis
Slc15a2	solute carrier family 15, member 2
SOP	standard operation procedure
Spp1	secreted phosphoprotein 1, equivalent to OPN
Sprr	small proline rich
SR-A	scavenger receptor A
SRCR	scavenger receptor cysteine-rich domain
SYK	spleen tyrosin kinase
TEM	transmission electron microscopy
TGF-β	transforming growth factor-beta

TLR	toll-like receptor
Tmprss2	transmembrane protease, serine 2
TNF	tumor necrosis factor
TRAP	tatrate-resitant acid phosphatase
Tris	Tris base (2-Amino-2-hydroxymethyl-propane-1,3-diol)
VSMC	vascular smooth muscle cell
WP	white pulp
WT	wildtype

List of Figures

List of Tables

Supplement

Supplemental Figures

Supplemental Figure 1. Organ distribution and kinetics of fetuin-A and asialofetiun containing CPPs.
Mice were injected with CPPs i.v., sacrificed 10, 30, 60 and 180 minutes afterwards and organs were harvested. The tissue protein extracts were analyzed by SDS-PAGE and the content of the fluorescence-label in the tissues was evaluated by densitometry. The values shown were quantified relative to an internal standard of 10 ng labeled fetuin-A co-separated on each gel. The protein content is given as the absolute protein amount per 100 mg fresh organ weight. The dotted lines indicate the mean signal of all organs after the subtraction of the brain values considered as negative control because of the blood-brain barrier and excluding bone because of the considerably lower values. Fetuin-A (F-A) containing CPPs (A) and asialofetuin containing CPPs (B) showed the same organ distribution. Compared to the average protein content of all organs increased levels of labeled protein were found in liver and spleen. (At least three animals per group were investigated at each time point).

Supplemental Tables

Supplemental Table 1. Differential expression in adipose tissue of D2 fetuin-A deficient mice.

probe set	p-value	log-ratio
upregulation		
RIKEN cDNA 1110032A04 gene	0.004	-6.977
small proline-rich protein 1A	0.005	-6.021
small proline-rich protein 2A	0.005	-5.495
small proline-rich protein 2A	0.009	-4.683
RIKEN cDNA 1110032A04 gene	0.003	-4.369
myelin and lymphocyte protein, T-cell differentiation protein	0.001	-4.316
matrix metallopeptidase 12	0.001	-4.315
transmembrane protease, serine 2	0.008	-4.157
secreted phosphoprotein 1	0.024	-4.116
uroplakin 3A	0.014	-3.949
lymphocyte antigen 6 complex, locus D	0.002	-3.845
sorting nexin 31	0.008	-3.728
forkhead box A1	0.001	-3.628
myelin protein zero	0.001	-3.525
Purkinje cell protein 4	0.001	-3.493
prostate stem cell antigen	0.008	-3.436
carnitine palmitoyltransferase 1b, muscle	0.006	-3.390
WAP four-disulfide core domain 2	0.022	-3.351
cadherin 1	0.007	-3.256
claudin 4	0.002	-3.185
pyridoxal-dependent decarboxylase domain containing 1	< 0.001	-3.159
myelin basic protein	0.001	-3.148
forkhead box Q1	0.001	-3.137
involucrin	0.005	-3.078
transmembrane protease, serine 2	0.016	-3.063
FXYD domain-containing ion transport regulator 3	0.001	-3.056
keratin 18	0.002	-3.046
chloride channel calcium activated 2	0.001	-2.976
small proline-rich protein 2F	0.001	-2.969
myelin basic protein	0.001	-2.943
gasdermin C2	0.028	-2.917
chloride channel calcium activated 2	0.010	-2.904
regulator of G-protein signaling 1	0.043	-2.862
grainyhead-like 2 (Drosophila)	0.001	-2.799
transmembrane protease, serine 2	0.008	-2.798
ring finger protein 128	0.020	-2.792
myelin basic protein	0.003	-2.785
otopetrin 1	0.043	-2.784
keratin 20	0.001	-2.775
ring finger protein 128	0.011	-2.772
GATA binding protein 3	< 0.001	-2.743
myelin basic protein	0.001	-2.702
cytochrome c oxidase, subunit VIIa 1	0.030	-2.699
myelin basic protein	0.003	-2.654
keratin 7	0.027	-2.652
uroplakin 1A	0.010	-2.623
sonic hedgehog	0.012	-2.619
epiphycan	0.001	-2.600
pyruvate dehydrogenase kinase, isoenzyme 4	0.005	-2.597
calponin 1	0.005	-2.535
RIKEN cDNA 1600029D21 gene	0.047	-2.506
keratin 5	0.001	-2.504
steroid 5 alpha-reductase 1	0.002	-2.504
forkhead box Q1	0.005	-2.497
SH3-binding domain glutamic acid-rich protein	0.007	-2.492
SH3-domain GRB2-like 2	0.001	-2.454
RIKEN cDNA 1600029D21 gene	0.006	-2.451
myosin, heavy polypeptide 11, smooth muscle	0.003	-2.416

aquaporin 3	0.009	-2.409
SH3-domain GRB2-like 2	0.001	-2.406
PERP, TP53 apoptosis effector	0.029	-2.340
shisa homolog 3 (Xenopus laevis)	0.001	-2.324
aquaporin 3	0.010	-2.311
aquaporin 3	0.008	-2.290
interleukin 1 receptor antagonist	0.033	-2.255
RIKEN cDNA 2200001I15 gene	0.007	-2.222
cathepsin E	0.001	-2.203
tetraspanin 8	0.011	-2.185
claudin 7	0.005	-2.178
interferon regulatory factor 6	0.044	-2.177
apolipoprotein D	0.005	-2.159
transmembrane protein 30B	0.012	-2.158
myelin basic protein	0.005	-2.140
vesicle amine transport protein 1 homolog-like (T. californica)	0.001	-2.137
serine protease inhibitor, Kunitz type 1	0.033	-2.132
myocardin	0.010	-2.110
regulating synaptic membrane exocytosis 1	0.003	-2.087
steroid 5 alpha-reductase 1	0.002	-2.070
actin, gamma 2, smooth muscle, enteric	0.009	-2.057
claudin 23	0.005	-2.044
flavin containing monooxygenase 5	0.013	-2.030
cell death-inducing DNA fragmentation factor, alpha subunit-like effector A	0.009	-2.022
deiodinase, iodothyronine, type II	0.022	-2.015
RIKEN cDNA 4930550L11 gene	0.006	-2.011
integrin alpha X	0.030	-1.985
myelin and lymphocyte protein, T-cell differentiation protein	0.011	-1.971
estrogen-related receptor gamma	0.044	-1.941
keratin 8	0.014	-1.936
ATPase, H+ transporting, lysosomal V0 subunit D2	0.047	-1.934
thrombospondin 4	0.003	-1.927
oncoprotein induced transcript 1	0.001	-1.916
ladinin	0.050	-1.882
myosin, light polypeptide kinase	0.046	-1.879
Kruppel-like factor 5	0.001	-1.873
acyl-CoA synthetase short-chain family member 1	0.010	-1.872
RAB27b, member RAS oncogene family	0.007	-1.866
tropomyosin 2, beta	0.006	-1.855
prominin 2	0.005	-1.845
grainyhead-like 3 (Drosophila)	0.013	-1.843
uroplakin 2	0.011	-1.835
carboxypeptidase X 2 (M14 family)	0.028	-1.809
chloride channel calcium activated 1	0.003	-1.805
solute carrier family 14 (urea transporter), member 1	0.008	-1.792
transformation related protein 63	0.004	-1.790
keratin 8	0.017	-1.787
CDP-diacylglycerol synthase 1	0.005	-1.786
transgelin	0.007	-1.782
tumor-associated calcium signal transducer 2	0.011	-1.770
CAP, adenylate cyclase-associated protein, 2 (yeast)	0.009	-1.755
Purkinje cell protein 4-like 1	0.037	-1.725
potassium channel tetramerisation domain containing 1	0.008	-1.719
actin, alpha 2, smooth muscle, aorta	0.003	-1.706
syndecan 1	0.010	-1.704
aldehyde dehydrogenase family 3, subfamily A1	0.009	-1.681
serine protease inhibitor, Kunitz type 2	0.009	-1.667
corneodesmosin	0.041	-1.663
chemokine (C-X-C motif) ligand 14	0.010	-1.660
mast cell protease 2	0.028	-1.657
RIKEN cDNA 2310076L09 gene	0.013	-1.638
predicted gene, 100043005	0.030	-1.633
oligodendrocyte transcription factor 1	0.038	-1.620
Ly6/Plaur domain containing 3	0.023	-1.614

keratin 8	0.024	-1.603
RIKEN cDNA A330049M08 gene	0.010	-1.599
tenascin C	0.030	-1.589
chemokine (C-C motif) ligand 3	0.047	-1.582
tropomyosin 2, beta	0.007	-1.564
RAB27b, member RAS oncogene family	0.031	-1.545
neurotrophic tyrosine kinase, receptor, type 3	0.047	-1.538
regulator of G-protein signaling 2	0.029	-1.535
serine incorporator 2	0.005	-1.530
mast cell protease 4	0.013	-1.522
myosin, light polypeptide kinase	0.003	-1.517
syndecan 1	0.047	-1.517
myosin, light polypeptide kinase	0.003	-1.509
stratifin	0.013	-1.497
chemokine (C-X-C motif) ligand 14	0.046	-1.488
SH3 domain binding glutamic acid-rich protein like 2	0.005	-1.482
RIKEN cDNA 2310076L09 gene	0.022	-1.471
RIKEN cDNA 6330546B05 gene	0.020	-1.468
estrogen-related receptor gamma	0.025	-1.462
shisa homolog 3 (Xenopus laevis)	0.016	-1.460
periaxin	0.008	-1.458
SH3-domain GRB2-like 2	0.005	-1.455
cortexin 1	0.003	-1.447
RNA binding motif protein 24	0.021	-1.427
syndecan 1	0.008	-1.425
potassium intermediate/small conductance calcium-activated channel, subfamily N, member 4	0.011	-1.416
myosin, light polypeptide 9, regulatory	0.008	-1.408
RNA binding motif protein 4B	0.016	-1.389
chymase 1, mast cell	0.008	-1.384
cyclin-dependent kinase inhibitor 1A (P21)	0.020	-1.383
RNA binding motif protein 35A	0.033	-1.370
eyes absent 4 homolog (Drosophila)	0.041	-1.350
matrix Gla protein	0.047	-1.345
cadherin 2	0.036	-1.340
V-set and immunoglobulin domain containing 2	0.007	-1.339
smoothelin	0.008	-1.337
oxysterol binding protein-like 3	0.004	-1.336
carboxypeptidase A3, mast cell	0.028	-1.334
enabled homolog (Drosophila)	0.017	-1.333
filamin binding LIM protein 1	0.047	-1.325
melanoregulin	0.024	-1.321
RAB27b, member RAS oncogene family	0.032	-1.319
transmembrane protease, serine 13	0.017	-1.318
peripheral myelin protein 2	0.047	-1.311
RNA binding motif protein 35b	0.033	-1.308
CDP-diacylglycerol synthase 1	0.015	-1.304
regulating synaptic membrane exocytosis 1	0.024	-1.300
syndecan 1	0.010	-1.296
T-box 2	0.010	-1.286
fatty acid 2-hydroxylase	0.008	-1.278
synaptopodin 2	0.008	-1.271
L1 cell adhesion molecule	0.022	-1.264
Jun-B oncogene	0.030	-1.264
growth arrest and DNA-damage-inducible 45 gamma	0.047	-1.262
acetyl-Coenzyme A acyltransferase 2 (mitochondrial 3-oxoacyl-Coenzyme A thiolase)	0.028	-1.259
potassium voltage-gated channel, shaker-related subfamily, member 1	0.027	-1.257
steroid 5 alpha-reductase 1	0.008	-1.247
uroplakin 1B	0.033	-1.234
proteolipid protein (myelin) 1	0.030	-1.233
ankyrin repeat domain 9	0.008	-1.231
CCAAT/enhancer binding protein (C/EBP), beta	0.004	-1.229
acetyl-Coenzyme A acyltransferase 2 (mitochondrial 3-oxoacyl-Coenzyme A thiolase)	0.030	-1.221
RIKEN cDNA 2810432L12 gene	0.019	-1.204
S100 protein, beta polypeptide, neural	0.022	-1.204

metallothionein 1	0.022	-1.192
beta-site APP-cleaving enzyme 2	0.030	-1.188
KH domain containing, RNA binding, signal transduction associated 3	0.040	-1.188
ATP-binding cassette, sub-family C (CFTR/MRP), member 4	0.015	-1.182
tripartite motif-containing 29	0.008	-1.173
secreted frizzled-related protein 1	0.008	-1.173
CCAAT/enhancer binding protein (C/EBP), beta	0.007	-1.163
expressed sequence AA986860	0.028	-1.159
glutathione S-transferase, mu 1	0.004	-1.154
expressed sequence AI452195	0.022	-1.148
serine protease inhibitor, Kunitz type 2	0.016	-1.132
solute carrier family 14 (urea transporter), member 1	0.022	-1.131
pleckstrin homology domain containing, family B (evectins) member 1	0.048	-1.129
glutathione S-transferase, mu 1	0.006	-1.122
acetyl-Coenzyme A acyltransferase 2 (mitochondrial 3-oxoacyl-Coenzyme A thiolase)	0.024	-1.114
dickkopf homolog 2 (Xenopus laevis)	0.010	-1.094
inhibitor of DNA binding 4	0.020	-1.090
NIPA-like domain containing 2	0.018	-1.079
calpain 13	0.008	-1.074
cell division cycle associated 2	0.007	-1.069
PCTAIRE-motif protein kinase 3	0.008	-1.069
cytochrome c oxidase, subunit VIIIb	0.044	-1.061
DNA segment, Chr 14, ERATO Doi 449, expressed	0.009	-1.059
potassium intermediate/small conductance calcium-activated channel, subfamily N, member 4	0.043	-1.057
neuropilin 2	0.048	-1.053
protein tyrosine phosphatase, receptor type, F	0.047	-1.052
potassium voltage-gated channel, shaker-related subfamily, member 1	0.024	-1.048
phosphoglucomutase 5	0.010	-1.047
major facilitator superfamily domain containing 4	0.047	-1.046
RAB25, member RAS oncogene family	0.049	-1.041
chloride channel calcium activated 1	0.024	-1.026
glutathione S-transferase, mu 1	0.010	-1.013
transmembrane protein 20	0.033	-1.010
double homeobox B-like	0.036	-0.999
protein kinase N1	0.022	-0.997
adrenergic receptor, beta 2	0.048	-0.997
high mobility group AT-hook 1	0.040	-0.989
testis derived transcript	0.044	-0.989
protein phosphatase 1, regulatory (inhibitor) subunit 12A	0.049	-0.988
similar to apolipoprotein D	0.022	-0.985
CD24a antigen	0.041	-0.984
transmembrane protein 40	0.043	-0.961
transformation related protein 53 inducible protein 11	0.021	-0.954
desmin	0.047	-0.949
solute carrier family 6 (neurotransmitter transporter, creatine), member 8	0.016	-0.944
glutathione S-transferase, alpha 4	0.015	-0.940
latent transforming growth factor beta binding protein 2	0.022	-0.937
protein phosphatase 1, regulatory (inhibitor) subunit 12A	0.048	-0.935
transmembrane channel-like gene family 4	0.041	-0.934
calpain 5	0.048	-0.932
ADP-ribosylation factor-like 4C	0.044	-0.931
placenta specific 9	0.023	-0.908
cDNA sequence X99384	0.049	-0.903
RIKEN cDNA 9230104K21 gene	0.043	-0.892
dystonin	0.012	-0.886
cyclin J-like	0.047	-0.873
EMI domain containing 1	0.026	-0.872
protein kinase C, eta	0.042	-0.869
pleckstrin homology domain containing, family H (with MyTH4 domain) member 1	0.035	-0.849
calpain 1	0.048	-0.834
pyridoxal-dependent decarboxylase domain containing 1	0.022	-0.831
huntingtin interacting protein 1 related	0.048	-0.820
integrin beta 4	0.026	-0.817
E26 avian leukemia oncogene 2, 3' domain	0.044	-0.815

cysteine rich protein 2	0.033	-0.805
MARVEL (membrane-associating) domain containing 1	0.038	-0.795
serine (or cysteine) peptidase inhibitor, clade B, member 5	0.047	-0.790
secreted frizzled-related protein 1	0.046	-0.733
beta-site APP-cleaving enzyme 2	0.043	-0.714
tsukushin	0.046	-0.701
huntingtin interacting protein 1 related	0.047	-0.683
guanine nucleotide binding protein, alpha 12	0.049	-0.674

downregulation

pyridoxal-dependent decarboxylase domain containing 1	< 0.001	4.111
cytochrome b reductase 1	< 0.001	3.119
penta-EF hand domain containing 1	< 0.001	3.108
basonuclin 1	0.004	2.587
glycoprotein m6a	0.005	2.483
mesothelin	0.008	2.460
glycoprotein m6a	0.023	2.355
fibroblast growth factor 1	0.007	2.091
plakophilin 2	0.028	2.011
ISL1 transcription factor, LIM/homeodomain	0.019	1.954
catechol-O-methyltransferase 1	0.002	1.874
suprabasin	0.047	1.818
R-spondin homolog (Xenopus laevis)	0.014	1.781
ribosomal protein L17	0.001	1.778
dermokine	0.028	1.757
mucin 16	0.001	1.755
gremlin 2 homolog, cysteine knot superfamily (Xenopus laevis)	0.010	1.702
chordin-like 1	0.001	1.659
fibroblast growth factor 1	0.011	1.624
oligonucleotide/oligosaccharide-binding fold containing 2A	0.003	1.604
uroplakin 3B	0.011	1.565
uroplakin 3B	0.011	1.552
spectrin beta 3	0.021	1.544
orosomucoid 2	0.008	1.505
epidermal growth factor-containing fibulin-like extracellular matrix protein 1	0.046	1.499
chordin-like 1	0.003	1.487
dipeptidylpeptidase 4	0.007	1.480
UDP-Gal:betaGlcNAc beta 1,3-galactosyltransferase, polypeptide 2	0.024	1.475
chordin-like 1	0.009	1.469
phosphorylase kinase gamma 1	0.024	1.423
secretory leukocyte peptidase inhibitor	0.015	1.417
rhophilin, Rho GTPase binding protein 2	0.027	1.406
succinate receptor 1	0.030	1.405
dipeptidylpeptidase 4	0.003	1.400
UDP-Gal:betaGlcNAc beta 1,3-galactosyltransferase, polypeptide 2	0.028	1.379
solute carrier family 39 (metal ion transporter), member 8	0.013	1.355
immunoglobulin-like domain containing receptor 2	0.049	1.349
G protein-coupled receptor 34	0.049	1.347
solute carrier family 39 (metal ion transporter), member 8	0.043	1.340
kelch-like 2, Mayven (Drosophila)	0.023	1.337
macrophage activation 2 like	0.024	1.312
T-cell specific GTPase	0.048	1.305
estrogen receptor 1 (alpha)	0.025	1.299
GULP, engulfment adaptor PTB domain containing 1	0.021	1.299
dipeptidylpeptidase 4	0.028	1.279
stanniocalcin 2	0.010	1.278
kelch-like 2, Mayven (Drosophila)	0.016	1.277
complement component 2 (within H-2S)	0.006	1.273
angiotensinogen (serpin peptidase inhibitor, clade A, member 8)	0.044	1.270
RIKEN cDNA 9330159F19 gene	0.022	1.262
GULP, engulfment adaptor PTB domain containing 1	0.007	1.260
Na+/K+ transporting ATPase interacting 4	0.047	1.230
UDP-Gal:betaGlcNAc beta 1,3-galactosyltransferase, polypeptide 2	0.036	1.195
coiled-coil domain containing 80	0.042	1.192

cache domain containing 1	0.007	1.183
complement component 2 (within H-2S)	0.008	1.166
oligonucleotide/oligosaccharide-binding fold containing 2A	0.005	1.141
orosomucoid 1	0.030	1.136
solute carrier family 16 (monocarboxylic acid transporters), member 7	0.035	1.131
insulin-like growth factor 1	0.028	1.123
complement component 2 (within H-2S)	0.008	1.114
intersectin 1 (SH3 domain protein 1A)	0.048	1.114
avian musculoaponeurotic fibrosarcoma (v-maf) AS42 oncogene homolog	0.039	1.112
androgen receptor	0.009	1.106
histone cluster 1, H4h	0.030	1.101
GULP, engulfment adaptor PTB domain containing 1	0.038	1.100
macrophage galactose N-acetyl-galactosamine specific lectin 2	0.030	1.087
chemokine (C-X-C motif) ligand 9	0.049	1.085
fibroblast growth factor binding protein 1	0.026	1.084
homeo box C8	0.016	1.084
immunoglobulin-like domain containing receptor 2	0.026	1.083
ATP-binding cassette, sub-family D (ALD), member 2	0.011	1.062
activin A receptor, type IC	0.047	1.058
ATP-binding cassette, sub-family D (ALD), member 2	0.006	1.055
somatostatin receptor 4	0.024	1.054
insulin-like growth factor 1	0.047	1.051
predicted gene, 100039706	0.021	1.047
guanine nucleotide binding protein (G protein), alpha inhibiting 1	0.005	1.042
RIKEN cDNA 2610019F03 gene	0.029	1.040
RAB30, member RAS oncogene family	0.045	1.039
RIKEN cDNA 1110059G02 gene	0.019	1.021
ISL1 transcription factor, LIM/homeodomain	0.030	1.017
oligonucleotide/oligosaccharide-binding fold containing 2A	0.021	1.012
synaptopodin 2	0.049	1.010
suppressor of cytokine signaling 2	0.047	0.987
zinc finger protein 503	0.019	0.986
ubiquitin specific peptidase 15	0.047	0.981
hect domain and RLD 5	0.047	0.973
SLIT and NTRK-like family, member 4	0.049	0.964
Rho GTPase activating protein 29	0.010	0.964
RAS p21 protein activator 2	0.047	0.961
histone cluster 1, H2bc	0.028	0.955
growth hormone receptor	0.017	0.953
RIKEN cDNA 1110059G02 gene	0.038	0.947
dopachrome tautomerase	0.022	0.932
DnaJ (Hsp40) homolog, subfamily A, member 1	0.037	0.929
X-box binding protein 1	0.025	0.926
growth hormone receptor	0.011	0.922
oligonucleotide/oligosaccharide-binding fold containing 2A	0.024	0.920
ubiquitin specific peptidase 15	0.019	0.914
cytochrome P450, family 2, subfamily s, polypeptide 1	0.038	0.912
cache domain containing 1	0.027	0.903
activin A receptor, type IC	0.028	0.903
RIKEN cDNA 9030425E11 gene	0.022	0.902
polycystic kidney disease 2-like 2	0.028	0.896
butyrylcholinesterase	0.011	0.886
RIKEN cDNA 1110059G02 gene	0.025	0.877
guanine nucleotide binding protein (G protein), alpha inhibiting 1	0.022	0.877
solute carrier family 9 (sodium/hydrogen exchanger), member 6	0.030	0.874
exonuclease 3'-5' domain-like 1	0.041	0.866
integrin beta 1 binding protein 1	0.027	0.865
RIKEN cDNA 9330159F19 gene	0.044	0.856
guanine nucleotide binding protein (G protein), alpha inhibiting 1	0.026	0.853
eukaryotic translation initiation factor 4E binding protein 1	0.028	0.850
ring finger protein 41	0.016	0.840
predicted gene, 100042856	0.044	0.837
butyrylcholinesterase	0.025	0.836
DNA segment, Chr 3, ERATO Doi 751, expressed	0.047	0.827

phosphoribosyl pyrophosphate synthetase 1	0.028	0.827
androgen receptor	0.024	0.822
hypothetical protein LOC621549	0.049	0.820
F-box protein 4	0.043	0.807
ST3 beta-galactoside alpha-2,3-sialyltransferase 1	0.022	0.805
3-ketodihydrosphingosine reductase	0.035	0.804
fibronectin type III and SPRY domain containing 2	0.027	0.804
RAD51-like 1 (S. cerevisiae)	0.047	0.794
cDNA sequence BC034902	0.049	0.787
phosphoribosyl pyrophosphate synthetase 1	0.030	0.785
ATP-binding cassette, sub-family D (ALD), member 2	0.039	0.763
X-box binding protein 1	0.046	0.747
asparagine synthetase	0.042	0.740
estrogen receptor 1 (alpha)	0.046	0.711
X-box binding protein 1	0.047	0.691
DNA segment, Chr 3, ERATO Doi 751, expressed	0.047	0.689
amylase 1, salivary	0.049	0.685
histone cluster 1, H1e	0.047	0.681
UDP-Gal:betaGlcNAc beta 1,3-galactosyltransferase, polypeptide 1	0.050	0.662

The table shows probe sets, which were significantly (p-value < 0.05) differentially expressed in adipose tissue dissected from 6-week-old DBA/2 wildtype (n=4) and fetuin-A deficient mice (n=6). Bayesian statistics was used for calculation of probabilities (p-value) and log-ratio, negative log-ratio encode upregulation of the particular probe-set in fetuin-A deficient mice, positive values denote downregulation. Note that gene names are given for each probe set, double entries may occur in case of genes which are represented by several probe sets encoding different regions or splice variants of the gene.

Supplemental Table 2. Differential expression in liver from fetuin-A deficient D2 mice.

probe set	p-value	log-ratio
upregulation		
sulfotransferase family 3A, member 1	0.012	-6.695
RIKEN cDNA C730007P19 gene	0.032	-5.665
sulfotransferase family 1E, member 1	0.009	-4.002
lipocalin 2	0.004	-3.820
serum amyloid A 2	0.042	-2.890
solute carrier family 15 (H+/peptide transporter), member 2	< 0.001	-2.817
ribonucleotide reductase M2	0.005	-2.810
DNA segment, Chr 17, human D6S56E 5	0.024	-2.744
baculoviral IAP repeat-containing 5	0.014	-2.721
cyclin B2	0.038	-2.670
serum amyloid A 1	0.043	-2.575
pyridoxal-dependent decarboxylase domain containing 1	< 0.001	-2.551
cDNA sequence AB056442	0.008	-2.517
minichromosome maintenance deficient 6 (MIS5 homolog, S. pombe) (S. cerevisiae)	0.007	-2.516
minichromosome maintenance deficient 6 (MIS5 homolog, S. pombe) (S. cerevisiae)	0.016	-2.474
regulator of calcineurin 2	0.002	-2.470
ribonucleotide reductase M2	0.017	-2.411
SPARC related modular calcium binding 2	0.004	-2.247
PDZ binding kinase	0.046	-2.204
SPARC related modular calcium binding 2	0.008	-2.148
cell division cycle associated 8	0.025	-2.131
CD36 antigen	0.015	-2.059
minichromosome maintenance deficient 5, cell division cycle 46 (S. cerevisiae)	0.013	-2.043
histone cluster 1, H2ae	0.016	-2.039
cell division cycle associated 3	0.046	-2.011
suppressor of cytokine signaling 2	0.019	-1.988
cytochrome P450, family 17, subfamily a, polypeptide 1	0.008	-1.953
aldo-keto reductase family 1, member C18	0.032	-1.897
stathmin 1	0.041	-1.887
aldo-keto reductase family 1, member B7	0.002	-1.830
hypothetical protein LOC215866	0.038	-1.742
cDNA sequence AB056442	0.032	-1.682
transcription factor 19	0.019	-1.639
insulin-like growth factor binding protein 1	0.007	-1.601
solute carrier family 25 (mitochondrial carrier, adenine nucleotide translocator),	0.004	-1.600

member 4		
basic helix-loop-helix domain containing, class B9	0.015	-1.591
neuregulin 4	0.027	-1.560
nicotinamide N-methyltransferase	0.024	-1.559
RAD51-like 1 (S. cerevisiae)	0.043	-1.478
solute carrier family 25 (mitochondrial carrier, adenine nucleotide translocator), member 4	0.002	-1.455
solute carrier family 25 (mitochondrial carrier, adenine nucleotide translocator), member 4	0.002	-1.450
MAD2 mitotic arrest deficient-like 1 (yeast)	0.019	-1.448
family with sequence similarity 19, member A2	0.013	-1.401
fibrinogen-like protein 1	0.043	-1.367
stearoyl-Coenzyme A desaturase 2	0.032	-1.358
DNA primase, p49 subunit	0.016	-1.334
pituitary tumor-transforming gene 1	0.004	-1.324
ribosomal protein S4, Y-linked 2	0.013	-1.323
centromere protein A	0.045	-1.320
RIKEN cDNA 2610305J24 gene	0.043	-1.288
nucleolar and spindle associated protein 1	0.044	-1.281
transmembrane protein 48	0.012	-1.253
CDC28 protein kinase 1b	0.008	-1.218
growth factor receptor bound protein 10	0.038	-1.207
S100 calcium binding protein A8 (calgranulin A)	0.037	-1.190
proliferating cell nuclear antigen	0.046	-1.182
pantothenate kinase 2 (Hallervorden-Spatz syndrome)	0.010	-1.178
S100 calcium binding protein A9 (calgranulin B)	0.045	-1.177
thyroid hormone receptor interactor 13	0.019	-1.168
transmembrane protein 98	0.003	-1.167
RIKEN cDNA 2700094K13 gene	0.038	-1.127
solute carrier family 41, member 2	0.037	-1.126
prostaglandin reductase 1	0.018	-1.118
uracil DNA glycosylase	0.007	-1.108
ligase I, DNA, ATP-dependent	0.045	-1.094
neuregulin 4	0.038	-1.073
RIKEN cDNA D630004K10 gene	0.037	-1.044
cyclin-dependent kinase inhibitor 2C (p18, inhibits CDK4)	0.033	-1.038
carbonic anhydrase 2	0.019	-1.034
six transmembrane epithelial antigen of prostate 2	0.041	-1.031
geminin	0.032	-0.988
thioredoxin 2	0.034	-0.987
deoxythymidylate kinase	0.041	-0.973
insulin-like growth factor 2 mRNA binding protein 3	0.038	-0.939
peroxisome proliferator activated receptor gamma	0.027	-0.915
lectin, galactose binding, soluble 1	0.046	-0.911
GINS complex subunit 1 (Psf1 homolog)	0.044	-0.807
retinol binding protein 1, cellular	0.032	-0.779
protein tyrosine phosphatase-like (proline instead of catalytic arginine), member b	0.046	-0.770
downregulation		
alpha-2-HS-glycoprotein	< 0.001	8.631
pyridoxal-dependent decarboxylase domain containing 1	< 0.001	4.762
cytochrome P450, family 4, subfamily a, polypeptide 12a	0.041	4.635
solute carrier organic anion transporter family, member 1a1	0.017	3.712
elongation of very long chain fatty acids (FEN1/Elo2, SUR4/Elo3, yeast)-like 3	0.016	3.522
hydroxy-delta-5-steroid dehydrogenase, 3 beta- and steroid delta-isomerase 5	0.008	3.275
kidney androgen regulated protein	0.001	3.193
RIKEN cDNA 2610016E04 gene	0.011	3.181
GRAM domain containing 3	< 0.001	2.651
hydroxy-delta-5-steroid dehydrogenase, 3 beta- and steroid delta-isomerase 2	0.002	2.593
cytochrome P450, family 7, subfamily b, polypeptide 1	0.001	2.252
cytochrome P450, family 7, subfamily b, polypeptide 1	0.002	2.244
GRAM domain containing 3	< 0.001	2.190
major urinary protein 3	0.001	2.125
NADPH oxidase 4	0.006	2.039
neurotrophic tyrosine kinase, receptor, type 2	0.001	1.997

ribosomal protein L17	< 0.001	1.927
aminolevulinic acid synthase 2, erythroid	0.019	1.886
UDP glycosyltransferases 3 family, polypeptide A1	0.001	1.863
RIKEN cDNA 9130221J18 gene	0.014	1.813
glutathione peroxidase 3	0.001	1.771
4short chain dehydrogenase/reductase family 9C, member 7	< 0.001	1.705
uromodulin	0.001	1.631
4short chain dehydrogenase/reductase family 9C, member 7	< 0.001	1.595
complement component 6	0.010	1.533
serine (or cysteine) peptidase inhibitor, clade A, member 4, pseudogene 1	0.041	1.518
UDP glycosyltransferases 3 family, polypeptide A1	0.009	1.488
polypyrimidine tract binding protein 1	0.005	1.468
guanine nucleotide binding protein, alpha 14	0.003	1.430
predicted gene, OTTMUSG00000007486	0.009	1.397
N-myc downstream regulated gene 1	0.008	1.382
RIKEN cDNA 2810416A17 gene	0.041	1.359
aldehyde oxidase 3	0.002	1.344
cleavage and polyadenylation specific factor 6	0.043	1.332
RIKEN cDNA 2310043N10 gene	0.007	1.316
catechol-O-methyltransferase 1	0.002	1.235
radical S-adenosyl methionine domain containing 2	0.045	1.223
interferon regulatory factor 2 binding protein 2	0.007	1.216
serine (or cysteine) peptidase inhibitor, clade A, member 4, pseudogene 1	0.019	1.208
predicted gene, ENSMUSG00000074917	0.002	1.201
elastase 1, pancreatic	0.009	1.164
splA/ryanodine receptor domain and SOCS box containing 4	0.006	1.080
cytoplasmic polyadenylation element binding protein 2	0.046	1.077
guanine nucleotide binding protein, alpha 14	0.002	1.054
major urinary protein 3	0.041	1.046
meningioma 1	0.012	1.043
frizzled homolog 5 (Drosophila)	0.007	1.012
glucokinase	0.013	1.007
avian musculoaponeurotic fibrosarcoma (v-maf) AS42 oncogene homolog	0.017	1.007
UDP glucuronosyltransferase 2 family, polypeptide B5	0.016	0.976
glucokinase	0.043	0.931
cadherin, EGF LAG seven-pass G-type receptor 1 (flamingo homolog, Drosophila)	0.046	0.931
RIKEN cDNA 6430527G18 gene	0.046	0.928
fetuin beta	0.013	0.883
glyoxalase 1	0.013	0.875
deleted in lymphocytic leukemia, 2	0.019	0.861
histocompatibility 2, K1, K region	0.021	0.836
neurotrophic tyrosine kinase, receptor, type 2	0.041	0.825
interferon regulatory factor 2	0.045	0.820
2'-5' oligoadenylate synthetase-like 1	0.046	0.812
gelsolin	0.043	0.780
histocompatibility 2, D region	0.029	0.760
Ras association (RalGDS/AF-6) domain family member 3	0.043	0.751

The table shows probe sets, which were significant (p-value < 0.05) differentially expressed in liver dissected from 5-weeks-old DBA/2 wildtype (n=3) and fetuin-A deficient mice (n=5). Bayesian statistics was used for calculation of probabilities (p-value) and log-ratio, negative log-ratio encode upregulation of the particular probe-set in fetuin-A deficient mice, positive values denote downregulation. Note that gene names are given for each probe set, double entries may occur in case of genes which are represented by several probe sets encoding different regions or splice variants of the gene.

Supplemental Table 3. Differential expression in kidney of B6 fetuin-A deficient mice.

probe set	p-value	log-ratio
upregulation		
D site albumin promoter binding protein	< 0.001	-3.169
cytochrome P450, family 24, subfamily a, polypeptide 1	0.003	-2.987
D site albumin promoter binding protein	< 0.001	-2.890
RIKEN cDNA 4933439C20 gene	0.001	-2.366
RIKEN cDNA 4933439C20 gene	< 0.001	-2.010
RIKEN cDNA 4933439C20 gene	< 0.001	-1.979
cytochrome P450, family 24, subfamily a, polypeptide 1	0.030	-1.796
peptidase M20 domain containing 1	< 0.001	-1.688
solute carrier family 7, (cationic amino acid transporter, y+ system) member 13	< 0.001	-1.679
period homolog 3 (Drosophila)	< 0.001	-1.634
peptidase M20 domain containing 1	< 0.001	-1.531
camello-like 3	< 0.001	-1.494
period homolog 2 (Drosophila)	0.003	-1.174
period homolog 3 (Drosophila)	0.002	-1.120
nuclear receptor subfamily 1, group D, member 2	0.006	-1.096
similar to Zinc finger BED domain containing protein 4	0.004	-1.014
nuclear receptor subfamily 1, group D, member 2	0.013	-0.943
cytoplasmic polyadenylation element binding protein 3	0.001	-0.936
uridine phosphorylase 2	0.016	-0.870
thyrotroph embryonic factor	0.010	-0.833
cytoplasmic polyadenylation element binding protein 3	0.034	-0.818
period homolog 3 (Drosophila)	0.018	-0.789
cytoplasmic polyadenylation element binding protein 3	0.030	-0.775
camello-like 3	0.030	-0.757
downregulation		
aldo-keto reductase family 1, member C14	< 0.001	2.928
aldo-keto reductase family 1, member C18	0.001	2.519
alpha-2-HS-glycoprotein	< 0.001	2.466
lymphocyte antigen 6 complex, locus F	< 0.001	2.387
RIKEN cDNA 9130221J18 gene	0.001	2.017
suppressor of cytokine signaling 2	0.008	1.972
solute carrier family 22 (organic anion transporter), member 7	< 0.001	1.968
nuclear factor, interleukin 3, regulated	< 0.001	1.938
major urinary protein 3	0.010	1.852
RIKEN cDNA 1110069O07 gene	< 0.001	1.755
major urinary protein 1	0.027	1.700
dipeptidylpeptidase 4	< 0.001	1.696
neuronal PAS domain protein 2	< 0.001	1.673
dipeptidylpeptidase 4	< 0.001	1.654
suppressor of cytokine signaling 2	0.017	1.626
phosphatidylinositol-specific phospholipase C, X domain containing 2	0.002	1.582
dipeptidylpeptidase 4	< 0.001	1.517
RIKEN cDNA 1110069O07 gene	< 0.001	1.505
RIKEN cDNA A630005I04 gene	< 0.001	1.481
solute carrier family 9 (sodium/hydrogen exchanger), member 8	0.001	1.467
phosphatidylinositol-specific phospholipase C, X domain containing 2	0.013	1.412
complement component 8, alpha polypeptide	0.002	1.349
3-hydroxy-3-methylglutaryl-Coenzyme A reductase	0.042	1.320
solute carrier family 10, member 2	0.017	1.277
myosin VA	0.017	1.228
carbonic anhydrase 8	0.001	1.224
sorting nexin 29	0.001	1.222
solute carrier family 16 (monocarboxylic acid transporters), member 1	< 0.001	1.210
solute carrier family 17 (sodium phosphate), member 2	0.045	1.114
SH3-domain binding protein 2	0.044	1.081
yippee-like 2 (Drosophila)	0.015	1.051
RIKEN cDNA 2200001I15 gene	0.001	1.038
Rho-related BTB domain containing 1	0.040	1.033
aryl hydrocarbon receptor nuclear translocator-like	0.008	1.020

ATP-binding cassette, sub-family C (CFTR/MRP), member 3	0.010	1.000
RIKEN cDNA 1300002K09 gene	0.008	0.987
RIKEN cDNA 5730559C18 gene	0.027	0.986
forkhead box Q1	0.050	0.951
SEC16 homolog B (S. cerevisiae)	0.021	0.928
family with sequence similarity 107, member A	0.009	0.920
arylsulfatase G	0.009	0.919
family with sequence similarity 129, member A	0.010	0.919
RIKEN cDNA 1700112E06 gene	0.013	0.874
transmembrane protein 68	0.028	0.869
family with sequence similarity 107, member A	0.030	0.862
histidine decarboxylase	0.016	0.860
guanylate binding protein 3	0.028	0.859
solute carrier family 17 (sodium phosphate), member 3	0.042	0.776
family with sequence similarity 129, member A	0.025	0.763
glycosyltransferase 25 domain containing 2	0.036	0.718

The table shows probe sets, which were significant (p-value < 0.05) differentially expressed in kidney dissected from 5-week-old B6 wildtype (n=4) and fetuin-A deficient mice (n=6). Bayesian statistics was used for calculation of probabilities (p-value) and log-ratio, negative log-ratio encode upregulation of the particular probe-set in fetuin-A deficient mice, positive values denote downregulation. Note that gene names are given for each probe set, double entries may occur in case of genes which are represented by several probe sets encoding different regions or splice variants of the gene.

Supplemental Table 4. Differential expression in liver of B6 fetuin-A deficient mice.

probe sets	p-value	log-ratio
upregulation		
D site albumin promoter binding protein	< 0.001	-4.823
cathepsin E	< 0.001	-3.768
D site albumin promoter binding protein	< 0.001	-3.676
H19 fetal liver mRNA	< 0.001	-2.980
period homolog 3 (Drosophila)	< 0.001	-2.882
renin 1 structural	< 0.001	-2.282
regulator of G-protein signaling 16	0.005	-2.084
period homolog 3 (Drosophila)	< 0.001	-2.070
uridine phosphorylase 2	< 0.001	-1.914
RIKEN cDNA 4933439C20 gene	< 0.001	-1.840
uridine phosphorylase 2	< 0.001	-1.819
ubiquitin specific peptidase 2	< 0.001	-1.791
period homolog 3 (Drosophila)	< 0.001	-1.612
cytochrome P450, family 3, subfamily a, polypeptide 16	0.003	-1.565
thyroid hormone responsive SPOT14 homolog (Rattus)	0.023	-1.485
nuclear receptor subfamily 1, group D, member 2	< 0.001	-1.471
thyrotroph embryonic factor	< 0.001	-1.440
regulator of G-protein signaling 16	0.001	-1.435
C-type lectin domain family 2, member h	0.002	-1.413
thyroid hormone responsive SPOT14 homolog (Rattus)	0.032	-1.409
ring finger protein 170	0.002	-1.399
tribbles homolog 3 (Drosophila)	0.002	-1.354
tribbles homolog 3 (Drosophila)	0.001	-1.330
serine (or cysteine) peptidase inhibitor, clade A (alpha-1 antiproteinase, antitrypsin), member 7	0.010	-1.326
regulator of G-protein signaling 16	0.020	-1.246
nuclear receptor subfamily 5, group A, member 2	0.002	-1.225
period homolog 2 (Drosophila)	0.004	-1.198
pigeon homolog (Drosophila)	< 0.001	-1.165
gene model 129, (NCBI)	< 0.001	-1.155
nuclear receptor subfamily 1, group D, member 1	0.001	-1.131
nuclear receptor subfamily 1, group D, member 2	< 0.001	-1.119
cytochrome P450, family 2, subfamily c, polypeptide 55	0.014	-1.116
nuclear factor, erythroid derived 2	0.001	-1.109
RIKEN cDNA 4933439C20 gene	< 0.001	-1.085
ATPase, H+ transporting, lysosomal V0 subunit D2	0.024	-1.084
basic helix-loop-helix family, member e40	0.039	-1.075
RIKEN cDNA 4933439C20 gene	< 0.001	-1.068

BTB and CNC homology 2	0.015	-1.068
PHD finger protein 17	0.011	-1.067
response to metastatic cancers 5	0.019	-1.024
BTB and CNC homology 2	0.005	-1.021
thyrotroph embryonic factor	0.010	-1.006
growth arrest and DNA-damage-inducible 45 alpha	0.001	-0.998
cytochrome P450, family 2, subfamily b, polypeptide 13	0.015	-0.993
ubiquitin specific peptidase 2	0.001	-0.991
thyrotroph embryonic factor	0.001	-0.988
SH3-binding kinase 1	0.001	-0.983
histocompatibility 2, class II antigen A, alpha	0.046	-0.964
transglutaminase 1, K polypeptide	0.011	-0.956
peroxisome proliferative activated receptor, gamma, coactivator 1 beta	0.001	-0.951
aldehyde dehydrogenase 1 family, member L1	0.018	-0.949
C-type lectin domain family 2, member h	0.006	-0.944
solute carrier family 16 (monocarboxylic acid transporters), member 5	0.012	-0.932
glutathione S-transferase, mu 3	0.044	-0.927
histocompatibility 2, class II antigen A, alpha	0.018	-0.927
ATPase, H+ transporting, lysosomal V0 subunit D2	0.010	-0.918
X-linked lymphocyte-regulated 3A	0.022	-0.918
RIKEN cDNA 6430706D22 gene	0.001	-0.912
collagen, type IV, alpha 5	0.009	-0.895
occludin	0.011	-0.870
tensin like C1 domain-containing phosphatase	< 0.001	-0.870
family with sequence similarity 134, member B	0.010	-0.867
serine peptidase inhibitor, Kazal type 3	0.034	-0.865
histocompatibility 2, class II antigen A, beta 1	0.034	-0.863
cytochrome P450, family 2, subfamily g, polypeptide 1	0.046	-0.861
CD24a antigen	0.009	-0.857
PHD finger protein 17	0.001	-0.857
glucosaminyl (N-acetyl) transferase 2, I-branching enzyme	0.005	-0.855
brain expressed gene 1	0.024	-0.854
peptidase M20 domain containing 1	0.002	-0.849
C-type lectin domain family 2, member h	0.009	-0.847
cyclin-dependent kinase inhibitor 3	0.024	-0.840
uridine phosphorylase 2	0.029	-0.838
oligodendrocyte transcription factor 1	0.007	-0.838
CD24a antigen	0.049	-0.836
X-linked myotubular myopathy gene 1	0.018	-0.835
family with sequence similarity 134, member B	0.028	-0.833
guanine nucleotide binding protein, alpha transducing 1	0.037	-0.832
CD74 antigen (invariant polypeptide of major histocompatibility complex, class II antigen-associated)	0.030	-0.826
ataxin 1	0.001	-0.820
tumor necrosis factor receptor superfamily, member 19	< 0.001	-0.811
cytochrome P450, family 26, subfamily b, polypeptide 1	0.039	-0.806
period homolog 3 (Drosophila)	0.010	-0.804
protease, serine, 8 (prostasin)	0.014	-0.802
ankyrin 3, epithelial	0.016	-0.800
RIKEN cDNA 6430706D22 gene	0.006	-0.787
ATP-binding cassette, sub-family C (CFTR/MRP), member 4	0.036	-0.785
mitogen-activated protein kinase kinase 6	0.015	-0.782
gremlin 2 homolog, cysteine knot superfamily (Xenopus laevis)	0.010	-0.776
doublecortin-like kinase 3	0.047	-0.762
retinoic acid receptor, beta	0.025	-0.744
ankyrin 3, epithelial	0.046	-0.744
cDNA sequence BC048546	0.001	-0.741
Ngfi-A binding protein 2	0.037	-0.740
peptidase M20 domain containing 1	0.016	-0.730
erythroid differentiation regulator 1	0.030	-0.728
WEE 1 homolog 1 (S. pombe)	0.016	-0.728
Ras association (RalGDS/AF-6) domain family member 5	0.010	-0.719
DNA segment, human D4S114	0.035	-0.709
BCL2 modifying factor	0.023	-0.709
DNA segment, human D4S114	0.038	-0.708

very low density lipoprotein receptor	0.022	-0.705
frizzled homolog 8 (Drosophila)	0.003	-0.704
period homolog 2 (Drosophila)	0.018	-0.703
myeloid cell leukemia sequence 1	0.031	-0.702
cryptochrome 2 (photolyase-like)	0.012	-0.700
RIKEN cDNA A930033H14 gene	0.029	-0.697
G protein-coupled receptor 146	0.002	-0.691
serum/glucocorticoid regulated kinase 2	0.007	-0.689
MAP kinase-interacting serine/threonine kinase 2	0.027	-0.685
zinc finger, FYVE domain containing 21	0.044	-0.677
RIKEN cDNA 2900026A02 gene	0.030	-0.666
CD24a antigen	0.046	-0.663
chemokine (C-X-C motif) ligand 1	0.042	-0.660
LIM domain containing 2	0.010	-0.659
G protein-coupled receptor 146	0.015	-0.655
MHC class I like protein GS10	0.037	-0.648
cytochrome P450, family 2, subfamily a, polypeptide 5	0.030	-0.642
transmembrane protein 146	0.030	-0.631
solute carrier family 20, member 1	0.018	-0.628
WEE 1 homolog 1 (S. pombe)	0.033	-0.618
very low density lipoprotein receptor	0.037	-0.617
dehydrogenase E1 and transketolase domain containing 1	0.012	-0.615
SRY-box containing gene 7	0.017	-0.612
folliculin	0.009	-0.607
immunoglobulin-like domain containing receptor 2	0.022	-0.592
immunoglobulin-like domain containing receptor 2	0.022	-0.590
DEAD (Asp-Glu-Ala-Asp) box polypeptide 59	0.016	-0.589
cytohesin 1	0.028	-0.565
von Willebrand factor C and EGF domains	0.040	-0.562
G protein-coupled receptor 146	0.049	-0.556
NAD(P)H dehydrogenase, quinone 1	0.040	-0.556
transcription factor Dp 2	0.031	-0.554
RIKEN cDNA 1810013L24 gene	0.014	-0.551
family with sequence similarity 81, member A	0.020	-0.548
spinster homolog 2 (Drosophila)	0.044	-0.544
annexin A13	0.027	-0.544
metastasis suppressor 1	0.033	-0.537
oxysterol binding protein-like 3	0.026	-0.530
serine (or cysteine) peptidase inhibitor, clade A, member 6	0.040	-0.530
frizzled homolog 8 (Drosophila)	0.024	-0.524
solute carrier family 38, member 3	0.030	-0.520
C-type lectin domain family 16, member A	0.023	-0.518
nuclear prelamin A recognition factor	0.022	-0.515
RIKEN cDNA 2610204M08 gene	0.037	-0.512
RIKEN cDNA 5730409N24 gene	0.050	-0.496
chromodomain helicase DNA binding protein 1-like	0.047	-0.490
metastasis suppressor 1	0.040	-0.489
zinc finger protein 217	0.044	-0.489
sirtuin 5 (silent mating type information regulation 2 homolog) 5 (S. cerevisiae)	0.041	-0.483
solute carrier family 39 (zinc transporter), member 14	0.047	-0.478
olfactomedin 1	0.045	-0.468
downregulation		
alpha-2-HS-glycoprotein	< 0.001	9.073
serine (or cysteine) peptidase inhibitor, clade A, member 4, pseudogene 1	0.005	2.826
serine (or cysteine) peptidase inhibitor, clade A, member 4, pseudogene 1	0.003	2.787
serine (or cysteine) peptidase inhibitor, clade A, member 4, pseudogene 1	0.008	2.513
dipeptidylpeptidase 4	< 0.001	2.454
RIKEN cDNA A630005I04 gene	< 0.001	2.254
dipeptidylpeptidase 4	< 0.001	2.222
caseinolytic peptidase X (E.coli)	< 0.001	1.968
elongation of very long chain fatty acids (FEN1/Elo2, SUR4/Elo3, yeast)-like 3	0.020	1.886
carbonic anhydrase 8	< 0.001	1.819
nuclear factor, interleukin 3, regulated	< 0.001	1.798

aryl hydrocarbon receptor nuclear translocator-like	< 0.001	1.723
hydroxy-delta-5-steroid dehydrogenase, 3 beta- and steroid delta-isomerase 5	0.011	1.715
solute carrier organic anion transporter family, member 1a1	0.004	1.698
choline kinase alpha	< 0.001	1.697
choline kinase alpha	< 0.001	1.694
RIKEN cDNA C730036E19 gene	< 0.001	1.636
dipeptidylpeptidase 4	< 0.001	1.624
heat shock protein 1	< 0.001	1.565
solute carrier organic anion transporter family, member 1a1	0.006	1.562
pyruvate dehydrogenase kinase, isoenzyme 4	< 0.001	1.543
5,10-methylenetetrahydrofolate reductase	< 0.001	1.530
solute carrier family 25, member 30	0.020	1.505
DNA segment, Chr 9, Wayne State University 90, expressed	0.019	1.495
ceruloplasmin	< 0.001	1.485
solute carrier family 25, member 30	0.013	1.470
solute carrier family 25, member 30	0.014	1.452
cyclin-dependent kinase inhibitor 1A (P21)	< 0.001	1.429
heat shock protein 1	< 0.001	1.314
LON peptidase N-terminal domain and ring finger 3	0.002	1.292
neuronal PAS domain protein 2	< 0.001	1.289
RIKEN cDNA 2610016E04 gene	0.016	1.269
carbonic anhydrase 8	< 0.001	1.247
regulatory factor X, 4 (influences HLA class II expression)	0.001	1.223
N-myc downstream regulated gene 1	< 0.001	1.219
AT hook containing transcription factor 1	< 0.001	1.206
acyl-CoA thioesterase 2	< 0.001	1.187
acyl-CoA thioesterase 1	< 0.001	1.177
choline kinase alpha	< 0.001	1.167
N-myc downstream regulated gene 1	< 0.001	1.164
cytochrome P450, family 4, subfamily a, polypeptide 12a	0.040	1.151
transmembrane protein 68	< 0.001	1.147
RIKEN cDNA 1110067D22 gene	0.001	1.120
E2F transcription factor 8	0.009	1.094
fetuin beta	< 0.001	1.065
RIKEN cDNA 1110067D22 gene	< 0.001	1.023
development and differentiation enhancing factor 2	< 0.001	1.021
caseinolytic peptidase X (E.coli)	< 0.001	0.998
RIKEN cDNA 6430573F11 gene	0.003	0.991
sulfotransferase family 5A, member 1	0.001	0.984
N-myc downstream regulated gene 1	< 0.001	0.942
cryptochrome 1 (photolyase-like)	0.007	0.941
insulin induced gene 2	< 0.001	0.931
solute carrier family 45, member 3	0.005	0.917
insulin induced gene 2	< 0.001	0.908
insulin induced gene 2	< 0.001	0.905
N-myc downstream regulated gene 1	0.001	0.895
S100 calcium binding protein A10 (calpactin)	< 0.001	0.890
predicted gene, 100040465	0.002	0.881
solute carrier family 45, member 3	0.011	0.857
3'-phosphoadenosine 5'-phosphosulfate synthase 1	0.001	0.856
SKI-like	0.001	0.852
circadian locomoter output cycles kaput	< 0.001	0.844
RAB30, member RAS oncogene family	0.025	0.828
neural precursor cell expressed, developmentally down-regulated gene 4-like	0.006	0.826
neuron navigator 1	0.002	0.821
protein phosphatase 1, regulatory (inhibitor) subunit 3B	0.014	0.819
solute carrier family 30, member 10	0.001	0.816
predicted gene, OTTMUSG00000007486	0.033	0.802
arginine vasopressin receptor 1A	0.020	0.779
LON peptidase N-terminal domain and ring finger 3	0.002	0.777
arginine vasopressin receptor 1A	0.018	0.776
apolipoprotein A-IV	0.004	0.762
trans-golgi network protein	0.004	0.741
cAMP responsive element modulator	0.040	0.741

RIKEN cDNA C730049O14 gene	0.010	0.735
predicted gene, 100039344	0.009	0.734
N-myc downstream regulated gene 1	0.003	0.730
RIKEN cDNA 9030425P06 gene	0.021	0.726
DNA methyltransferase 3B	0.004	0.726
cysteine-rich hydrophobic domain 1	0.017	0.724
ADP-ribosylation factor-like 4A	0.009	0.723
proline-rich nuclear receptor coactivator 1	0.002	0.714
lysyl oxidase-like 4	0.016	0.712
serine (or cysteine) peptidase inhibitor, clade A, member 3K	0.029	0.709
AT hook containing transcription factor 1	0.011	0.705
trans-golgi network protein	0.009	0.695
ring finger protein 125	0.023	0.688
major urinary protein 5	0.018	0.685
RIKEN cDNA C730029A08 gene	0.022	0.681
ADP-ribosylation factor-like 4A	0.046	0.675
hydroxysteroid dehydrogenase like 2	0.026	0.674
retinol saturase (all trans retinol 13,14 reductase)	0.028	0.662
nuclear receptor subfamily 0, group B, member 2	0.040	0.662
leucine-rich repeat, immunoglobulin-like and transmembrane domains 1	0.013	0.658
apolipoprotein A-IV	0.010	0.645
leucine rich repeat and fibronectin type III domain containing 3	0.009	0.642
solute carrier family 30, member 10	0.003	0.637
RAB interacting factor	0.016	0.625
steroid 5 alpha-reductase 1	0.014	0.624
SET binding factor 2	0.018	0.621
trans-golgi network protein	0.009	0.619
ring finger protein 144A	0.007	0.612
retinol saturase (all trans retinol 13,14 reductase)	0.015	0.612
trans-golgi network protein	0.010	0.603
carnitine acetyltransferase	0.028	0.602
adipose differentiation related protein	0.013	0.601
expressed sequence AI117581	0.045	0.597
SCO cytochrome oxidase deficient homolog 2 (yeast)	0.010	0.581
4short chain dehydrogenase/reductase family 9C, member 7	0.026	0.579
defensin related cryptdin, related sequence 7	0.027	0.561
ST3 beta-galactoside alpha-2,3-sialyltransferase 6	0.030	0.551
AT hook containing transcription factor 1	0.047	0.550
progestin and adipoQ receptor family member IX	0.048	0.546
DNA segment, Chr 5, Wayne State University 178, expressed	0.044	0.542
leptin receptor overlapping transcript-like 1	0.014	0.540
USP6 N-terminal like	0.037	0.540
mitogen-activated protein kinase kinase kinase 7 interacting protein 2	0.036	0.510
deltex 4 homolog (Drosophila)	0.031	0.504
hydroxysteroid dehydrogenase like 2	0.048	0.499
melanoregulin	0.034	0.497

The table shows probe sets, which were significant (p-value < 0.05) differentially expressed in liver dissected from 5-week-old B6 wildtype (n=4) and fetuin-A deficient mice (n=6). Bayesian statistics was used for calculation of probabilities (p-value) and log-ratio, negative log-ratio encode upregulation of the particular probe-set in fetuin-A deficient mice, positive values denote downregulation. Note that gene names are given for each probe set, double entries may occur in case of genes which are represented by several probe sets encoding different regions or splice variants of the gene.

Supplemental Protocols

SOP Purification of Fetuin-A

Column	Superdex 200 16/60 (run with a ÄKTA purifier system)
Fetuin-A	Sigma Cat. No. F-2379
Eluent	PBS (Biochrom Cat. No. L-182):

	NaCL	8.00 g/l
	KCL	0.20 g/l
	Na_2HPO_4	1.15 g/l
	KH_2PO_4	0.20 g/l

Flow rate	1 ml/min
Fraction size	3 ml
Concentration of fetuin-A	20 mg/ml
Volume	5 ml

Fractions	monomeric fetuin-A	21-27
	dimeric fetuin-A	18-20
	aggregrates	14-17

After chromatography fetuin-A is concentrated using Centriprep YM-30 (Millipore Cat. No. 4307).

Extinction Coefficient Fetuin-A: E1% = 4.1 (278 nm) [350]; E1% = 4.5 (27) [351]

SOP Formation of CPPs

Stock solutions:

purified fetuin-A
(SOP purification of fetuin-A)   > 2mg/ml
$CaCl_2$ 100 mM
Na_2HPO_4 60 mM
Tris-Cl pH 7,4   0,5 M
NaCl   5 M
PBS (Biochrom Cat. No. L-182)

Materials:

Centrisart 1, cut-off 300kDa, Sartorius Cat. No. 13279
Water bath 37°C
Centrifuge 4°C

Experimental procedure:
produce 1 ml reaction mixtures each; a rapid and complete mixture of all compounds is
crucial for CPP formation; when more CPPs are needed several 1 ml reaction mixtures have
to be prepared

prepare a reaction mixtures with final concentrations:

purified fetuin-A   1 mg/ml
Na_2HPO_4 6 mM
Tris PH 7,4   50 mM
NaCl   140 mM   vortex and add

$CaCl_2$ 10 mM   vortex immediately 10s

incubate: - 1 h at 37 °C (water bath)
               - 10 min on ice
               - combine all reaction mixtures

Concentration of CPPs:

all reagents and disposables have to be pre-cooled !

          - pipette CPPs in centrisarts, fill-up centrisarts with PBS to 2.5ml
          - centrifugation 15 min, 4 °C, 1500 x g
          - collect the filtrate in a falcon tube and fill-up again with PBS
          - centrifugation 15 min, 4 °C, 1500 x g
          - collect the filtrate in a falcon tube
          - centrifugation 15 min, 4 °C, 1500 x g
          - collect the filtrate in a falcon tube, determine the final volume of the CPP
          solution (the final volume depend on the number of CPP reaction mixtures
          started-with, approx. 1 ml for 6 x 1 ml, approx. 0.3 ml for 2 x 1 ml)
          - determine the protein content in both, the CPP and the filtrate

Acknowledgement

First of all, I would like to thank my supervisor Prof. Dr. Willi Jahnen-Dechent for this interesting project, stimulating scientific discussions, his ongoing support, critical reading of the thesis and for giving me the opportunity to attend international workshops and conferences.

Many thanks to Prof. Dr. Johannes Bohrmann who kindly agreed to be my second reviewer.

I would like to acknowledge several people who contributed to this thesis in different aspects: Special regards belong to Dr. Cora Schäfer who started the work on the clearance of calciprotein particles. In particular, I would like to thank her for supporting me during the starting period of my thesis. I thank Dr. Alexander Heiss for the basic work on calciprotein particles and scientific discussions. Prof. Dr. Siamon Gordon and Dr. Laura Helming supported this thesis with their in-depth knowledge in macrophage biology. I thank them for their interest, technical support and fruitful discussions. I thank Steffen Gräber for his technical assistance and providing purified fetuin-A. I thank Linda Schaub and Maren Hamann for technical assistance. I would also like to thank all internal and external collaborators.

I thank Anne Kinkeldey for her ongoing support, the perfect teamwork and her friendship. This friendship inspired me even in bad times and I'll never forget the special time we spent together in the lab, at conferences and beyond this.

Thanks to all my colleagues of the Bionterface Group and the IZKF Aachen for the pleasant working atmosphere.

I thank Sabine Mollus and Dr. Jörg Felder for proofreading of this manuscript.

This work was supported by the DFG Graduate School Grant 1035 Biointerface.

Finally, I would like to thank my family and friends for their support during my studies.

LEBENSLAUF

PERSÖNLICHE DATEN

Name	Herrmann
Vorname	Marietta Ariane
Geburtstag	14.07.1982
Geburtsort	Berlin
Staatsangehörigkeit	deutsch

QUALIFIKATIONEN

2001	Abitur am Gymnasium Moltkestraße, Gummersbach
2002-2007	Diplom-Studiengang Biologie an der RWTH Aachen
ab 2007	Promotion am Institut für Biomedizinische Technologien – Zell- und Molekularbiologie an Grenzflächen, RWTH Aachen